

# **An Evaluation of Direct Sample Analysis Time of Flight Mass Spectrometry for Forensic Analysis**

by

**Eliza Moule**

*Thesis  
Submitted to Flinders University  
for the degree of*

**Doctor of Philosophy**  
College of Science and Engineering  
April 2020

---



## Contents

.....	1
Table of Figures.....	v
Table of tables.....	xiv
Table of equations.....	xvii
Glossary.....	xviii
Summary.....	xxii
Declaration.....	xxiv
Conference publications.....	xxv
Acknowledgements.....	xxvi
1 Literature Review.....	1
1.1 Mass spectrometry in forensic science.....	1
1.2 Ionisation and mass analysers.....	1
1.2.1 Ionisation techniques and mechanisms.....	2
1.2.2 Mass analyser types and mechanisms.....	3
1.3 Chromatography and MS.....	4
1.4 Ambient ionisation mass spectrometry.....	5
1.4.1 Desorption electrospray ionisation (DESI).....	10
1.4.2 Direct analysis in real-time (DART).....	12
1.4.3 Direct Sample Analysis (DSA).....	13
1.5 Current applications of Direct Sample Analysis.....	15
1.6 Ambient ionisation in forensic science.....	17
1.6.1 Explosives.....	18
1.6.2 Drugs and toxicology.....	21
1.6.3 Chemical warfare agents (CWA).....	38

1.6.4	Inks and documents.....	39
1.6.5	Fingermarks.....	41
1.6.6	Lubricants.....	42
1.6.7	Gunshot residues.....	43
1.6.8	Broader ambient ionisation evaluation.....	45
1.7	Conclusions.....	46
1.8	Research overview.....	47
	Materials and methods.....	49
	Standards and solvents.....	49
	Preparation of drug solutions.....	49
	Plasma cleaning protocol.....	49
	Instrumentation.....	49
	Data extraction and analysis.....	50
2	Development of DSA-ToF method for the detection of MDMA, cocaine and THC.....	59
2.1	Introduction.....	59
2.2	Accurate mass identification.....	61
2.2.1	Accurate mass identification of THC, MDMA and cocaine.....	61
2.2.2	Sample positioning optimisation.....	67
2.2.3	Sample volume optimisation.....	69
2.2.4	Adjacent sample placement.....	72
2.3	Impact of atmospheric water on ionisation.....	74
2.4	Influence of syringe flow rate.....	76
2.5	Robustness.....	78
2.6	Cocaine peak reproducibility.....	78
2.7	External interferences: intensity cycling over time.....	80

2.8	Conclusions .....	88
3	Quantification of illicit drugs in water using DSA-ToF.....	89
3.1	Introduction.....	89
3.2	Illicit drug detection internal standard use.....	90
3.3	Quantification of MDMA, cocaine and THC in water.....	91
3.3.1	Collection of mesh background information .....	91
3.3.2	Plasma cleaning optimisation .....	95
3.3.3	Plasma cleaning summary.....	100
3.4	Determination of linear range .....	101
3.4.1	Large range calibration of cocaine on various mesh types .....	102
3.4.2	Low range calibration of cocaine on various mesh types.....	107
3.4.3	Large range calibration of THC on various mesh types .....	112
3.4.4	Low range calibration of THC on various mesh types.....	117
3.4.5	Large range calibration of MDMA on various mesh types.....	123
3.4.6	Low range calibration of MDMA on various mesh types .....	128
3.4.7	Summary of results – linear range .....	132
3.5	Inter- & intra- day consistency .....	133
3.6	Conclusions .....	140
4	Development of extraction methods for THC, MDMA and cocaine from saliva .....	142
4.1	Introduction.....	142
4.2	Materials and Methods .....	143
4.3	Solvent extraction of MDMA, THC and cocaine from spiked saliva .....	144
4.1	Timed interaction extraction of MDMA, THC and cocaine from spiked saliva.....	157
4.2	Conclusions .....	163
5	DSA-ToF for breath analysis of nicotine, pseudoephedrine and caffeine.....	165

5.1	Introduction.....	165
5.2	Materials and methods .....	172
5.2.1	Standards and solvents .....	172
5.2.2	Sample collection.....	172
5.3	Results and discussion .....	173
5.4	Detection caffeine, caffeine metabolites and pseudoephedrine in breath .....	175
5.5	Detection of nicotine from breath using Eppendorf collection and direct exhalation .....	178
5.6	Conclusions .....	181
6	Towards the combined detection of organic and inorganic gunshot residues .....	183
6.1	Introduction.....	183
6.2	Materials and methods .....	187
6.2.1	Standards and solvents .....	187
6.2.2	Sample collection.....	188
6.2.3	Equipment .....	189
6.2.4	Data analysis .....	189
6.3	Evaluation of DSA -ToF for detection of GSR compounds .....	190
6.4	Quantification of EC.....	191
6.5	Extraction and Analysis .....	192
6.6	SEM-EDS impacts on solvent recovery - organic GSR compound analysis.....	203
6.7	Solvent recovery impacts on SEM-EDS analysis - Inorganic GSR trace detection.....	207
6.8	Conclusions .....	210
7	Conclusions and Future Work.....	212
8	References.....	215

## Table of Figures

Figure 1: Web of science publication numbers (y-axis) for articles with 'ambient ionisation mass spectrometry' as a topic from 2004-2020 (x axis) .....	9
Figure 2: Web of science publication numbers (y-axis) for articles with 'desorption electrospray ionisation' or 'direct analysis in real time mass spectrometry' as a topic from 2004-2020 (x-axis).....	10
Figure 3: Schematic of DESI source. Reproduced from [27] .....	11
Figure 4: Schematic of DART ionisation source. Reproduced from [5].....	13
Figure 5: Schematic of Direct Sample Analysis-Time of Flight front end, showing solid sample capillary (inset, top) liquid sample analysis mesh (inset, bottom). Image provided by Perkin Elmer for training purposes.....	14
Figure 6: Total Ion Chromatogram for the deposition of a solution of 1000ng/mL cocaine in water on untreated mesh. X-axis is time (sec), y -axis is intensity (a.u). .....	63
Figure 7: Extracted Base Ion Chromatogram for m/z 304-305 for injection of a solution of 1000ng/mL cocaine in water on untreated mesh. X-axis is time (sec), y -axis is intensity (a.u).....	64
Figure 8: Representative mass spectrum of 200ng/mL solution of cocaine in water on mesh.....	65
Figure 9: Representative mass spectrum of 200ng/mL solution of MDMA in water on mesh .....	66
Figure 10: Representative mass spectrum of 200ng/mL solution of THC in water on mesh.....	67
Figure 11: Positions evaluated for optimisation of sample positions. From left: middle, top middle, bottom middle, left middle & right middle. ....	68
Figure 12: Comparison of molecular ion peak intensity (m/z 304.367) for alternative sample positions on mesh (n=3), error bars are 1SD.....	68
Figure 13: Comparison of 20ng/mL cocaine molecular ion peak intensity (m/z 304.367) for alternative sample volumes on mesh (n=3), error bars are 1SD .....	70
Figure 14: Comparison of 1000ng/mL cocaine molecular ion peak intensity (m/z 304.367) for alternative sample volumes on mesh (n=3), error bars are 1SD .....	71
Figure 15: Comparison of cocaine peak intensity (m/z 304.367) for six adjacent mounted samples (n=3), error bars are 1SD.....	73
Figure 16: Intensity variation across five subsequent acquisitions of 1000ng/mL cocaine solution in water	74
Figure 17: Representative mass spectrum of cocaine in EtOH, with D <sub>2</sub> O in calibrant solution and pipetted on top of the dried sample spot. ....	75

Figure 18: Representative mass spectrum of MDMA in EtOH, with D<sub>2</sub>O in calibrant solution and pipetted on top of the dried sample spot. .... 76

Figure 19: Comparison of amplitude (top) and signal to noise (bottom) for calibrant syringe flow rates of 10-40µL/min ..... 77

Figure 20: Distribution of cocaine (200ng/mL) amplitude and signal to noise over 50 consecutive injections. .... 79

Figure 21: Amplitude, area and width data (clockwise from top left) for calibrant acquisition over 30 minutes, for calibrant acquisition over 30 minutes using DSA-ToF ..... 81

Figure 22: Frequency analysis of amplitude data for calibrant peak m/z 622. Graphs are from the top down: frequency, cycle time, and amplitude (original data)..... 83

Figure 23: Comparison of amplitude data for 30 minute acquisition for capped flight tube only, capped flight tube and covered AC vent, and uncovered flight tube and AC vent (clockwise from top left) ..... 85

Figure 24: Calibrant peak data across 30 minutes using ESI source, with AC vents covered and flight tube capped..... 87

Figure 25: Intensity variation across five subsequent acquisitions of 1000ng/mL cocaine solution in water 90

Figure 26: Average spectra of un-treated mesh blank, across 30 second acquisition time, with calibration peaks labelled..... 91

Figure 27: Average spectra of un-treated mesh blank, across 30 second acquisition time, showing approximate areas where cocaine, MDMA and THC are likely to be identified..... 93

Figure 28: Comparison of neat mesh prior to instrument plasma exposure (green trace), and the same area of mesh after 30 seconds of instrument plasma exposure (blue trace)..... 94

Figure 29: Comparison of background between two minutes of argon plasma cleaning (blue trace) and two minutes of oxygen plasma cleaning (green trace), with calibrant peaks highlighted ..... 96

Figure 30: Comparison of background between three minutes of argon plasma cleaning (green trace) and oxygen plasma cleaning (blue trace), with calibrant peaks highlighted..... 97

Figure 31: Comparison of background between five minutes of argon plasma cleaning (green trace) and oxygen plasma cleaning (blue trace), with calibrant peaks highlighted..... 98

Figure 32: Comparison of background between 10 minutes of argon plasma cleaning (blue trace) and oxygen plasma cleaning (green trace), with calibrant peaks highlighted ..... 99

Figure 33: Comparison of background between instrument cleaned mesh with lab exposure after clean (blue trace) and no lab exposure after clean (green trace). Calibrant peaks are highlighted ..... 100

Figure 34: Quantification of cocaine in water on instrument-plasma treated mesh across a large range 20-1000ng/mL, n=5 and each error bar is equivalent to $\pm 1$ SD. $R^2= 0.9806$ .....	102
Figure 35: Residuals analysis of the linear regression of cocaine in water (20-1000ng/mL) on instrument plasma treated mesh .....	102
Figure 36: Comparison of cocaine peak (m/z 304) and D3- cocaine (m/z 307) for solution in water at equivalent concentrations (200ng/mL) on non-plasma treated mesh .....	103
Figure 37: Quantification of cocaine in water on argon plasma treated mesh across a large range 20-1000ng/mL, n=5 and each error bar is equivalent to $\pm 1$ SD. $R^2= 0.9841$ .....	104
Figure 38: Residuals analysis of the linear regression of cocaine in water (20-1000ng/mL) on argon plasma treated mesh.....	105
Figure 39: Quantification of cocaine in water on oxygen plasma treated mesh across a large range 20-1000ng/mL, n=5 and each error bar is equivalent to $\pm 1$ SD. $R^2=0.9689$ .....	106
Figure 40: Residuals analysis of the linear regression of cocaine in water (20-1000ng/mL) on oxygen plasma treated mesh .....	106
Figure 41: Quantification of cocaine in water on instrument-plasma treated mesh across a low working range 10-200ng/mL, n=5 and each error bar is equivalent to $\pm 1$ SD. $R^2=0.9880$ .....	108
Figure 42: Residuals analysis of the linear regression of cocaine in water (10-200ng/mL) on instrument plasma treated mesh. ....	108
Figure 43: Quantification of cocaine in water on argon treated mesh across a low working range 10-200ng/mL, n=5 and each error bar is equivalent to $\pm 1$ SD. $R^2=0.9928$ .....	109
Figure 44: Residuals analysis of the linear regression of cocaine in water (10-200ng/mL) on argon plasma treated mesh.....	110
Figure 45: Quantification of cocaine in water on oxygen treated mesh across a low working range 10-200ng/mL, n=5 and each error bar is equivalent to $\pm 1$ SD. $R^2=0.9237$ .....	111
Figure 46: Residuals analysis of the linear regression of cocaine in water (10-200ng/mL) on oxygen plasma treated mesh.....	111
Figure 47: Quantification of THC in water on instrument plasma treated mesh across a large range 20-1000ng/mL, n=5 and each error bar is equivalent to $\pm 1$ SD. $R^2=0.9445$ .....	112
Figure 48: Residuals analysis of the linear regression of THC in water (20-1000ng/mL) on instrument plasma treated mesh .....	113

Figure 49: Quantification of THC in water on argon plasma treated mesh across a large range 20-1000ng/mL, n=5 and each error bar is equivalent to $\pm 1$ SD. $R^2=0.9034$ .....	114
Figure 50: Residuals analysis of the linear regression of THC in water (20-1000ng/mL) on argon plasma treated mesh.....	115
Figure 51: Quantification of THC in water on oxygen plasma treated mesh across a large range 20-1000ng/mL, n=5 and each error bar is equivalent to $\pm 1$ SD. $R^2=0.8920$ .....	116
Figure 52: Residuals analysis of the linear regression of THC in water (20-1000ng/mL) on oxygen plasma treated mesh.....	116
Figure 53: Quantification of THC in water on instrument plasma treated mesh across a low working range 10-200ng/mL, n=5 and each error bar is equivalent to $\pm 1$ SD. $R^2=0.8723$ .....	118
Figure 54: Residuals analysis of the linear regression of THC in water (10-200ng/mL) on instrument plasma treated mesh.....	118
Figure 55: Quantification of THC in water on argon treated mesh across a low working range 10-200ng/mL, n=5 and each error bar is equivalent to $\pm 1$ SD. $R^2=0.7764$ .....	120
Figure 56: Residuals analysis of the linear regression of THC in water (10-200ng/mL) on argon plasma treated mesh.....	120
Figure 57: Quantification of THC in water on oxygen plasma treated mesh across a dynamic range 20-1000ng/mL, n=5 and each error bar is equivalent to $\pm 1$ SD. $R^2=0.8920$ .....	121
Figure 58: Residuals analysis of the linear regression of THC in water (10-200ng/mL) on oxygen plasma treated mesh.....	122
Figure 59: Quantification of MDMA in water on instrument plasma treated mesh across a large range 20-1000ng/mL, n=5 and each error bar is equivalent to $\pm 1$ SD. $R^2=0.9486$ .....	123
Figure 60: Residuals analysis of the linear regression of MDMA in water (20-1000ng/mL) on instrument plasma treated mesh .....	123
Figure 61: Quantification of MDMA in water on argon plasma treated mesh across a large range 20-1000ng/mL, n=5 and each error bar is equivalent to $\pm 1$ SD. $R^2=0.9858$ .....	125
Figure 62: Residuals analysis of the linear regression of MDMA in water (20-1000ng/mL) on argon plasma treated mesh.....	125
Figure 63: Quantification of MDMA in water on oxygen plasma treated mesh across a large range 20-1000ng/mL, n=5 and each error bar is equivalent to $\pm 1$ SD. $R^2=0.9187$ .....	126

Figure 64: Residuals analysis of the linear regression of MDMA in water (20-1000ng/mL) on oxygen plasma treated mesh..... 127

Figure 65: Quantification of MDMA in water on instrument plasma treated mesh across a low working range 10-200ng/mL, n=5 and each error bar is equivalent to  $\pm 1$  SD.  $R^2=0.9646$  ..... 128

Figure 66: Residuals analysis of the linear regression of MDMA in water (10-200 ng/mL) on instrument plasma treated mesh ..... 128

Figure 67: Quantification of MDMA in water on argon treated mesh across a low working range 10-200ng/mL, n=5 and each error bar is equivalent to  $\pm 1$  SD.  $R^2=0.9522$  ..... 129

Figure 68: Residuals analysis of the linear regression of MDMA in water (10-200 ng/mL) on argon plasma treated mesh..... 130

Figure 69: Quantification of MDMA in water on oxygen treated mesh across a low working range 10-200ng/mL, n=5 and each error bar is equivalent to  $\pm 1$  SD.  $R^2=0.9496$  ..... 131

Figure 70: Residuals analysis of the linear regression of MDMA in water (10-200 ng/mL) on oxygen plasma treated mesh..... 131

Figure 71: Comparison of calibration curves taken on day one for solutions of cocaine in water across 10-200 ng/mL (n=6), error bars are 1SD.  $R^2= 0.9723, 0.9944$  &  $0.9951$  for calibration 1, 2 & 3 respectively. 134

Figure 72: Comparison of calibration curves taken on day one for solutions of MDMA in water across 10-200 ng/mL (n=6), error bars are 1SD.  $R^2= 0.9884, 0.931$  &  $0.9408$  for calibration 1, 2 & 3 respectively. . 135

Figure 73: Comparison of calibration curves taken on day one for solutions of THC in water across 10-200 ng/mL (n=6), error bars are 1SD.  $R^2= 0.5839, 0.0185$  &  $0.1823$  for calibration 1, 2 & 3 respectively. .... 135

Figure 74: Comparison of calibration curves taken on day two for solutions of cocaine in water across 10-200 ng/mL (n=6), error bars are 1SD.  $R^2= 0.9776, 0.9899$  &  $0.9929$  for calibration 1, 2 & 3 respectively. 136

Figure 75: Calibration of MDMA in water on day two across 10-200 ng/mL (n=6), error bars are 1SD.  $R^2= 0.821$ ..... 136

Figure 76: Calibration of THC in water on day two across 10-200 ng/mL (n=6) error bars are 1SD.  $R^2= 0.5502$ ..... 137

Figure 77: Comparison of calibration curves taken on day three for solutions of cocaine in water across 10-200 ng/mL (n=6), error bars are 1SD.  $R^2= 0.9813, 0.9691$  &  $0.9565$  for calibration 1, 2 & 3 respectively. 138

Figure 78: Comparison of calibration curves taken on day three for solutions of MDMA in water across 10-200 ng/mL (n=6), error bars are 1SD.  $R^2= 0.803, 0.812$  &  $0.6902$  for calibration 1, 2 & 3 respectively. ... 138

Figure 79: Comparison of solvent type and saliva: solvent ratio for extraction of cocaine from spiked saliva, n=3, error bars are 1SD .....	145
Figure 80: Comparison of solvent type and saliva: solvent ratio for extraction of THC from spiked saliva, n=3, error bars are 1SD .....	146
Figure 81: Comparison of solvent type and saliva: solvent ratio for extraction of MDMA from spiked saliva, n=3, error bars are 1SD .....	146
Figure 82: Comparison of solvent type and saliva: solvent ratio for the extraction of THC from spiked saliva, n=3, error bars are 1SD .....	147
Figure 83: Comparison of centrifugation times (sec) for the chloroform extraction of THC, MDMA and cocaine from spiked saliva, n=3 and error bars are equal to 1SD .....	148
Figure 84: Comparison of solvent volumes ( $\mu$ L) onto non-plasma treated mesh for chloroform extraction of THC, MDMA and cocaine, n=3, error bars are 1SD .....	149
Figure 85: Comparison of buffer types for chloroform extraction of MDMA, cocaine and THC from spiked saliva, n=3, error bars are 1SD .....	150
Figure 86: Comparison of acidification types for borax buffered chloroform extraction of MDMA, THC and cocaine from spiked saliva, n=3, error bars are 1SD .....	151
Figure 87: Comparison of sample spot treatment with 0.1% TFA, FA and metal triflates with buffered chloroform extraction of 1ng/mL MDMA, THC and cocaine from spiked saliva, n=3 and error bars are 1SD .....	152
Figure 88: Comparison of sample spot treatment with 0.1% TFA, FA and metal triflates with buffered chloroform extraction of 10ng/mL MDMA, THC and cocaine from spiked saliva, n=3 and error bars are 1SD .....	153
Figure 89: Ratio of THC: ISTD for THC concentrations of 10-200ng/mL, using optimised chloroform extraction method. R2= 0.9, n=3 and error bars are 1SD .....	154
Figure 90: Ratio of cocaine: ISTD for cocaine concentrations of 10-200ng/mL, using optimised chloroform extraction method. R2= 0.9575, n=3 and error bars are 1SD .....	154
Figure 91: Ratio of MDMA: ISTD for MDMA concentrations of 10-200ng/mL, using optimised chloroform extraction method. R2= 0.9301, n=3 and error bars are 1SD .....	155
Figure 92: Ratio of THC: ISTD for THC concentrations of 10-200ng/mL, using heptane extraction method. R2= 0.9919, error bars are 1SD .....	156

Figure 93: Comparison of interaction time on non-plasma treated mesh for extraction of THC, MDMA and cocaine from spiked saliva, n=3, error bars are 1SD .....	157
Figure 94: Comparison of plasma cleaned mesh types for the extraction of THC from spiked saliva, n=3, error bars are 1SD .....	158
Figure 95: Comparison of plasma cleaned mesh types for the extraction of MDMA from spiked saliva, n=3, error bars are 1SD .....	159
Figure 96: Comparison of plasma cleaned mesh types for the extraction of cocaine from spiked saliva, n=3, error bars are 1SD .....	159
Figure 97: Comparison of buffered extraction (ammoniacal, borax and non-buffered) of THC, MDMA and cocaine from spiked saliva.....	160
Figure 98: Comparison of acidification methods for the timed interaction extraction (60 seconds) of THC, MDMA and cocaine from spiked saliva, n=3, error bars are 1SD .....	161
Figure 99: Ratio of THC: ISTD for THC concentrations of 10-200ng/mL in saliva, using optimised timed interaction extraction method, error bars are 1SD (n=3). R <sup>2</sup> =0.0029.....	161
Figure 100: Ratio of MDMA: ISTD for MDMA concentrations of 10-200ng/mL in saliva, using optimised timed interaction extraction method, error bars are 1SD (n=3) R <sup>2</sup> =0.0464 .....	162
Figure 101: Ratio of cocaine: ISTD for cocaine concentrations of 10-200ng/mL in saliva, using optimised timed interaction extraction method, error bars are 1SD (n=3). R <sup>2</sup> = 0.2798 .....	162
Figure 102: Off-line method for sampling breath. Reproduced from [167] .....	166
Figure 103: Representative spectrum of nicotine standard (10µg/mL) acquired by DSA-ToF analysis, showing nicotine detection at m/z 163 .....	173
Figure 104: Comparison of nicotine signal to noise for varying suspension volumes, using Eppendorf based method. Volumes investigated were 5, 10 & 20µL. Non-smoking comparison data collected with 5µL volume .....	174
Figure 105: Average S/N of caffeine (m/z 195) in exhaled breath of a volunteer from DSA-ToF analysis. Error bars represent one SD from n=3 .....	175
Figure 106: Average S/N (m/z 180) of caffeine metabolites in exhaled breath of a volunteer from DSA-ToF analysis. Error bars represent one SD from n=3.....	176
Figure 107: Average SN of pseudoephedrine in exhaled breath of a volunteer from DSA-ToF analysis. Error bars represent one SD from n=3 .....	177

Figure 108: Average S/N of nicotine in exhaled breath of a smoker from DSA-ToF analysis using Eppendorf sample collection method. Error bars represent one SD from n=3 ..... 178

Figure 109: Average SN of nicotine in exhaled breath of a smoker from DSA-ToF analysis using modified sample collection method. Error bars represent one SD , n=3 ..... 179

Figure 110: Representative spectrum of neat vape-liquid, provided by the volunteer. A nicotine peak can be seen at m/z 163. .... 181

Figure 111: Calibration curve for Ethyl Centralite, using Methyl Centralite as the internal standard. Response is given as the ratio between the molecular ion peaks of EC and MC, n=3 & error bars are 1SD (R<sup>2</sup>= 0.9577). ..... 191

Figure 112: Comparison of extraction solvents and methods for EC spiked onto an adhesive GSR stub . 194

Figure 113: 50µL solvent recovery (%) comparison for EC from adhesive GSR stubs..... 196

Figure 114: Comparison of MeOH volume for extraction of EC from GSR stubs..... 197

Figure 115: Representative spectra for 2:2:1 solvent recovery of mixed GSR surveillance standard from surface of SEM stub ..... 199

Figure 116: Reaction scheme for decomposition of N-NDPA (left) to dipheylamidogen (right)..... 199

Figure 117: Comparison of EC S/N for aged, field used stubs using MeOH extraction method ..... 201

Figure 118: Recovered EC (ng) across seven-day period for GSR stubs stored at room temperature ..... 203

Figure 119: Representative spectrum from right hand of volunteer, after discharge of a firearm, using 0.40 calibre ammunition. Inset shows peak at m/z 227. Dimethylphthalate is shown at m/z 195. .... 205

Figure 120: Extract of smokeless powder from 0.40 ammunition used in test firing, showing akardite at m/z 227 and deuterated N-NDPA standard at m/z 176 ..... 206

Figure 121: Comparison of analysis order based on the area response of peak with m/z 227 recovered from and 0.40 stubs ..... 207

Figure 122: Secondary electron image of 0.22 calibre ammunition sample stub, both pre-solvent (left) and post-solvent (right). Red circle indicates a slight visible change to the stub, attributable to solvent contact ..... 208

Figure 123: Secondary electron image of 0.40 calibre ammunition sample stub, both pre-solvent (left) and post-solvent (right)..... 208

Figure 124: Particle distribution map of sample stub from the shooter's left-hand following discharge of 6x 0.22LR rounds from a revolver. Pre-solvent (black) and Post-solvent (red, offset)..... 210

Figure 125: Particle distribution map of a sample stub from the shooter's left hand following discharge of 6x 0.22 calibre rounds from a revolver. Pre-solvent (black) and Post-solvent (red) are offset..... 210

## Table of tables

Table 1: Types of ambient ionisation techniques. Adapted from [7].....	8
Table 2: Summary of the DSA-ToF, DART-MS and DESI-MS applications for the drug detection and toxicology.....	26
Table 3: General DSA-ToF settings for analysis.....	50
Table 4: Composition, molecular formula, molecular weight and structure of compounds in the APCI tuning mix.....	52
Table 5: Molecular weights, protonated weights, structures and chemical formulae of MDMA, THC and cocaine.....	62
Table 6: Mass error associated with the accurate mass identification of cocaine, MDMA and THC.....	64
Table 7: Typical cocaine, MDMA & THC concentrations in bodily fluids for varying levels of intoxication. Reproduced from [151].....	89
Table 8: Molecular weights of protonated and non-protonated deuterated internal standards of THC, MDMA and cocaine.....	101
Table 9: Calculated %CV for cocaine in water over large range on instrument-plasma treated mesh.....	104
Table 10: Calculated %CV for cocaine in water across a large range on argon plasma treated mesh.....	105
Table 11: Calculated %CV for cocaine in water across a large range on oxygen plasma treated mesh....	107
Table 12: Calculated %CV for cocaine in water across a low working range on instrument-plasma treated mesh.....	109
Table 13: Calculated %CV for cocaine in water across a low working range on argon plasma treated mesh.....	110
Table 14: Calculated %CV for cocaine in water across a low working range on oxygen plasma treated mesh.....	112
Table 15: Calculated %CV for THC in water over dynamic range on instrument-plasma treated mesh....	114
Table 16: Calculated %CV for THC in water across a large range on argon plasma treated mesh.....	115
Table 17: Calculated %CV for THC in water across a large range on oxygen plasma treated mesh.....	117
Table 18: Calculated %CV for THC in water across a low working range on instrument-plasma treated mesh.....	119
Table 19: Calculated %CV for THC in water across a low working range on argon plasma treated mesh	121
Table 20: Calculated %CV for THC in water across a low range on oxygen plasma treated mesh.....	122
Table 21: Calculated %CV for MDMA in water over large range on instrument plasma treated mesh.....	124

Table 22: Calculated %CV for MDMA in water across a large range on argon plasma treated mesh .....	125
Table 23: Calculated %CV for MDMA in water across a large range on oxygen plasma treated mesh .....	127
Table 24: Calculated %CV for MDMA in water across a low working range on instrument plasma treated mesh.....	129
Table 25: Calculated %CV for MDMA in water across a low working range on argon plasma treated mesh .....	130
Table 26: Calculated %CV for MDMA in water across a low working range on oxygen plasma treated mesh .....	132
Table 27: Summary of LoD and LoQ data for THC across low range and large range, on varying mesh types.....	132
Table 28: Summary of LoD and LoQ data for cocaine across low range and large range, on varying mesh types.....	132
Table 29: Summary of LoD and LoQ data for MDMA across low range and large range, on varying mesh types.....	133
Table 30: Calculated limits of detection and quantification for cocaine, THC and MDMA for inter and intraday comparison. Where linearity was poor, values are recorded as 'N/A' in place of a negative number or zero. ....	139
Table 31: %RSD for LoD and LoQs calculated for cocaine, MDMA and THC for inter and intra-day comparison. Where values are recorded as 'N/A' no data was available. ....	140
Table 32: Limits of detection and quantification for buffered chloroform extraction of THC, MDMA and cocaine from spiked saliva.....	155
Table 33: Limits of detection and quantification for buffered heptane extraction of THC from spiked saliva .....	156
Table 34: Detectable drugs of abuse in the breath .....	170
Table 35: oGSR associated compounds contained in Accustandard GSR surveillance standard (Accustandard, New Haven, CT) .....	188
Table 36: Set-up and Operating Conditions for SEM-EDS analysis .....	189
Table 37: Accurate mass error (ppm) for targeted oGSR compounds (n=6) .....	190
Table 38: Comparison of solvent type for Ethyl Centralite recoveries from spiked SEM stub surface .....	195
Table 39: Deposition amounts (ng) for oGSR associated compounds in mixed GSR surveillance standard .....	198

Table 40: Pre- and post- solvent particle counts for 0.22 calibre ammunition from the dominant hand of the shooter..... 209

Table 41: Pre- and post- solvent particle counts for 0.40 calibre ammunition from the dominant hand of the shooter..... 209

## Table of equations

Equation 1: Generation of metastable gas ions in APCI .....	6
Equation 2: Generation of charged species from reaction with metastable helium gas ions generated from APCI .....	6
Equation 3: Generation of charged species from reaction with metastable nitrogen gas ions generated from APCI .....	6
Equation 4: Protonation of analyte (S) via charged water clusters.....	6

# Glossary

<b>%CV</b>	Percent Cross Validation
<b>%RSD</b>	Percent Relative Standard Deviation
<b>4-FMC</b>	4-fluoromethcathione
<b>4-MEC</b>	4-Methylethcathione
<b>6-MAM</b>	6-Monoacetyl morphine
<b>AC</b>	Air Conditioning
<b>AcCN</b>	Acetonitrile
<b>APCI</b>	Atmospheric Pressure Chemical Ionisation
<b>AP-MALDI</b>	Atmospheric Pressure Matrix Assisted Laser Desorption Ionisation
<b>APTDI</b>	Atmospheric Pressure Thermal Desorption Ionisation
<b>ASAP</b>	Ambient Solid Analysis Probe
<b>ASTM</b>	American Society for Testing and Materials
<b>BIC</b>	Base ion chromatogram
<b>CBD</b>	Cannabidiol
<b>CI</b>	Chemical Ionisation
<b>cm</b>	Centimetre
<b>CMV DART</b>	Capillary Microextraction of Volatiles Direct Analysis in Real Time Mass
<b>MS</b>	Spectrometry
<b>COPD</b>	chronic obstructive pulmonary disease
<b>CWA</b>	Chemical Warfare Agent
<b>Da</b>	Dalton
<b>DAPCI</b>	Desorption Atmospheric Pressure Chemical Ionisation
<b>DAPPI</b>	Desorption Atmospheric Pressure Photoionisation
<b>DART-MS</b>	Direct Analysis in Real Time Mass Spectrometry
<b>DBDI</b>	Dielectric Barrier Discharge Ionisation
<b>DESI-MS</b>	Desorption Electrospray Ionisation Mass Spectrometry
<b>DIMP</b>	Diisopropyl methylphosphonate
<b>DIOS</b>	Desorption ionisation on porous silicon
<b>DMMP</b>	Dimethyl methylphosphonate
<b>DNA</b>	Deoxyribonucleic Acid
<b>DNT</b>	dinitrotoluene
<b>DoA</b>	Drugs of abuse
<b>DPA</b>	Diphenylamine
<b>DSA</b>	Direct Sample Analysis
<b>DSA-ToF</b>	Direct Sample Analysis Time of Flight
<b>EASSI</b>	Easy Ambient Sonic-Spray Ionisation
<b>EC</b>	Ethyl Centralite
<b>EDDP</b>	2-ethylidene - 1,5 - dimethyl- 3,3- diphenylpyrrolidine
<b>EEOA</b>	Ethyl Ester of Oleic Acid
<b>EESI</b>	Extractive Electrospray Ionisation
<b>EI</b>	Electron Impact
<b>ELDI</b>	Electrospray Laser Desorption Ionisation

<b>ELF</b>	epithelial lining fluid
<b>EMPA</b>	Ethyl methylphosphoric acid
<b>ESI</b>	Electrospray Ionisation
<b>EtOH</b>	Ethanol
<b>FA</b>	Formic acid
<b>FAB</b>	Fast Atom Bombardment
<b>FD-ESI</b>	Fused-Droplet Electrospray Ionisation
<b>FSSA</b>	Forensic Science South Australia
<b>FTICR</b>	Fourier Transform Ion Cyclotron Resonance
<b>FTIR</b>	Fourier transform infrared spectroscopy
<b>GC</b>	Gas Chromatography
<b>GC-MS</b>	Gas Chromatography Mass Spectrometry
<b>GSR</b>	Gunshot Residues
<b>HAPGDI</b>	Helium Atmospheric Pressure Glow Discharge Ionisation
<b>HCA</b>	Hierarchical Clustering Analysis
<b>HMTD</b>	Hexamethylene Triperoxide Diamine
<b>HMX</b>	Octogen (High Melting Explosive)
<b>HPLC</b>	High pressure liquid chromatography
<b>HRMS</b>	High Resolution Mass Spectrometry
<b>ICP-MS</b>	Inductively coupled plasma mass spectrometry
<b>ICR</b>	Ion Cyclotron Resonance
<b>iGSR</b>	Inorganic Gunshot Residue
<b>IMPA</b>	isopropyl-methylphosphoric acid
<b>ISTD</b>	Internal Standard
<b>L</b>	Litre
<b>LAESI</b>	Laser-Ablation Electrospray Ionisation
<b>LC</b>	Liquid Chromatography
<b>LC-MS</b>	Liquid Chromatography Mass Spectrometry
<b>LDA</b>	Linear Discriminant Analysis
<b>LESA</b>	Liquid Extraction Surface Analysis
<b>LoD</b>	Limit of Detection
<b>LoQ</b>	Limit of Quantification
<b>LTP</b>	Low-Temperature Plasma
<b>m/z</b>	Mass to charge
<b>MA</b>	Methamphetamine
<b>MAAQ</b>	1- methylaminoanthraquinone
<b>MALDI</b>	Matrix Assisted Laser Desorption Ionisation
<b>MC</b>	Methyl Centralite
<b>MDMA</b>	Methylenedioxyamphetamine
<b>MDPBP</b>	3, 4 - methylenedioxy - $\alpha$ - pyrrolidinobutiophenone
<b>MDPV</b>	methylenedioxypropylvalerone
<b>MeOH</b>	Methanol
<b>min</b>	Minutes
<b>mL</b>	millilitre

<b>MP</b>	Mobile Phase
<b>MPA</b>	Methylphosphoric Acid
<b>MS</b>	Mass Spectrometry
<b>NATA</b>	National Association of Testing Authorities
<b>NC</b>	nitrocellulose
<b>ND-EESI</b>	Neutral Desorption Extractive Electrospray Ionisation
<b>ng</b>	nanogram
<b>NG</b>	Nitroglycerine
<b>N-NDPA</b>	N-nitrosodiphenylamine
<b>OA</b>	Oleic Acid
<b>oGSR</b>	Organic Gunshot Residue
<b>PADI</b>	Plasma-Assisted Desorption/Ionisation
<b>PCA</b>	Principal Component Analysis
<b>PDE 5</b>	Phosphodiesterase 5
<b>PEG</b>	Polyethylene Glycol
<b>PETN</b>	Pentaerythritol tetranitrate
<b>pg</b>	picogram
<b>PMMA</b>	polymethyl methacrylate
<b>ppb</b>	parts per billion
<b>ppm</b>	parts per million
<b>psi</b>	pounds per square inch
<b>PTFE</b>	Polytetrafluoroethylene
<b>PTR-MS</b>	Proton transfer reaction mass spectrometry
<b>QLD</b>	Queensland
<b>RDX</b>	Hexogen
<b>RF</b>	radio frequency
<b>rpm</b>	revolutions per minute
<b>S/N</b>	Signal to Noise
<b>SA</b>	South Australia
<b>SALDI</b>	Surface Assisted Laser Desorption Ionisation
<b>SD</b>	Standard Deviation
<b>SDME</b>	Single drop microextraction
<b>Sec</b>	Seconds
<b>SEM-EDS</b>	Scanning electron microscopy energy dispersive x-ray analysis
<b>SESI</b>	Secondary electrospray ionisation
<b>SIFT-MS</b>	Selected ion flow tube mass spectrometry
<b>SPE</b>	Solid Phase Extraction
<b>SPME</b>	Solid Phase Microextraction
<b>TATP</b>	Triacetone Triperoxide
<b>TD-CDI</b>	Thermal Desorption Corona Discharge Ionisation
<b>TD-DART-MS</b>	Thermal Desorption Direct Analysis in Real Time High Resolution Mass Spectrometry
<b>TDM</b>	therapeutic drug monitoring
<b>TFA</b>	Trifluoroacetic acid

<b>THC</b>	Tetrahydrocannabidol
<b>TIC</b>	Total ion chromatogram
<b>TLC</b>	Thin Layer Chromatography
<b>TNT</b>	Trinitrotoluene
<b>ToF</b>	Time of Flight
<b>UHPLC-MS</b>	Ultra high pressure liquid chromatography mass spectrometry
<b>UV-VIS</b>	
<b>MSP</b>	Ultra-violet/visible microspectrophotometry
<b>VOC</b>	volatile organic compound
<b><math>\alpha</math> - MPPP</b>	3 - methyl - $\alpha$ - pyrrolidinopropiophenone
<b><math>\alpha</math> - PVP</b>	$\alpha$ - pyrrolidinopentiophenone
<b><math>\mu</math>A</b>	microamp
<b><math>\mu</math>g</b>	microgram
<b><math>\mu</math>L</b>	Microlitre
<b><math>\mu</math>m</b>	micrometre

# Summary

The emergence of ambient ionisation mass spectrometry has been driven by a need for high-throughput, accurate and flexible methods for analysis of a broad range of compounds. There are a broad range of techniques already developed and explored, including (but not limited to) Desorption Electrospray Ionisation (DESI) and Direct Analysis in Real Time (DART). Direct Sample Analysis Time of Flight (DSA-ToF) has not been comprehensively evaluated or explored as a competing technique in the ambient ionisation space. This work sought to evaluate the DSA-ToF as a technique for use in forensic science.

Optimisation of a broad method for the identification of MDMA, THC and cocaine demonstrated that there are substantial reproducibility issues with the instrument. Environmental contributions to signal variability were identified, with humidity, airflow and temperature fluctuations being responsible for large sinusoidal cycling in the signal response. Plasma cleaning was identified as necessary to remove organic matter contaminating the provided mesh that convoluted the low mass range. Quantification of the three drugs was possible but is not recommended. Limits of detection and quantification were able to be established but were not consistent when compared intra- and inter-day. This inconsistency would compromise the validity of any quantitative results.

Two methods were developed for the detection of THC, MDMA and cocaine from saliva, one involving a solvent extraction and the other involving a timed physical interaction of the saliva with mesh. The solvent extraction method allowed both qualitative and quantitative detection of the three drugs, although quantitative is not recommended. The timed-interaction method was suitable for qualitative identification only.

A further two applications were developed, involving the detection of nicotine, caffeine, caffeine metabolites and pseudoephedrine in breath. Uptake and elimination curves for these drugs were mapped across 2 hours from the breath of two volunteers. The detection of organic GSR components was also demonstrated, using a solvent extraction from the surface of adhesive GSR stubs. This solvent extraction was shown to not disrupt the inorganic particles present, and is suitable for integration into the existing GSR detection protocol (SEM-EDS identification of inorganic components).

Evaluation of this instrument indicated that it is capable of high-throughput, accurate screening of a broad range of samples in complex matrices. Environmental variables should be controlled by limiting air flow,

temperature fluctuations, and humidity in the laboratory. Quantification can be performed but should not be relied upon as the only measure of content.

# Declaration

This thesis presents work carried out by myself and does not incorporate with acknowledgement any material previously submitted for a degree or diploma in any university; to the best of my knowledge it does not contain any materials previously published or written by another person except where due reference is made in the text; and all substantative contributions by other to the work presented are clearly acknowledged.



This document has been signed digitally

Eliza Moule

9<sup>th</sup> January 2020

## Conference publications

**'Analysis of butanediol, GHB & GHB-glucuronide to extend the scope of drug facilitated sexual assault urine analysis'** 2014, poster presented at the Australia and New Zealand Forensic Science Society 22<sup>nd</sup> International Symposium, Adelaide, Australia.

**'Lab-on-a-chip Mass Spectrometry tools for testing illicit drugs'** 2015, poster presented at the Royal Australian Chemical Institute Research and Development conference, Melbourne University, Australia.

**'Allied Spectroscopic and Surface Assisted Lased Desorption Ionisation (SALDI) techniques for the detection of forensically relevant molecules'** 2016, oral presented at the Australia and New Zealand Forensic Science 23<sup>rd</sup> International Symposium, Auckland, New Zealand.

**'Rapid detection of THC, MDMA and cocaine in saliva via Direct Analysis Time of Flight Mass Spectrometry (DSA-ToF)'** 2017, oral presented at the Australian and New Zealand Society of Mass Spectrometry 26<sup>th</sup> biannual conference, Adelaide Australia.

**'Towards combined detection of organic and inorganic gun shot residue via Direct Sample Analysis Time of Flight mass spectrometry'** 2018, oral presented at the Australia and New Zealand 24<sup>th</sup> International Symposium, Perth, Australia.

**'Rapid detection of nicotine from breath using Direct Sample Time of Flight mass spectrometry'** 2018, poster presented at the Australian and New Zealand Forensic Science 24<sup>th</sup> International Symposium, Perth, Australia.

## Acknowledgements

Completing my PhD has been the hardest, most rewarding thing I have done so far. It would not have been possible without a great number of people who I will do my best to thank below.

Paul, your unwavering optimism and support for me over the last 5 years has been totally invaluable. There is no possible way I could have done this without you. Your guidance and kind words kept me on track when I thought (quite often) that everything was falling apart around me.

To Jason from Flinders Analytical, your stories and chats were a delight over the hours and hours spent in front of a very belligerent instrument. Thank you for your advice and for being so hands on when I needed any help at all.

Thanks to Taryn for taking me under your wing for three years. You were patient, kind and helpful at all times and I couldn't have asked for a better mentor.

To Nick and Kelsey... Where do I even start? Thank you for all the days, nights, weekends and all other units of time we spent together. Our own weird and dark brand of optimism made our office my favourite place to be. You are wonderful friends, and I am so happy that somehow, we have all ended up finishing together and with jobs in the same (approximate place). Looks like we are stuck with each other for a long time to come.

Ruby, you are an angel. Your never-ending optimism and willingness to share that with me have kept me going long since I left Adelaide (and you) behind. I've never met someone so willing to drop everything and listen, and even when your advice isn't what I want to hear at the time, it is *always* right. Long-distance is not the best but we have made it work over and over again, and until you agree to move to Canberra with me, it will have to do.

My newest friends Grace and Jenitta, who took me in when I was sad and lonely in a new city. You are a blessing, and I am so fortunate to know you.

Thanks, of course, to my family for their patience and for giving me everything I needed to get where I am today. To Greg and Virginia for taking me into their home when I moved to Canberra. I would not have been able to finish this without your help and encouragement. Special thanks to Greg for writing the program that shaved hours off my processing times.

To Harper, because you have been with me for almost my entire time at university. You have seen me at my best and at my worst, and have given me all the love and cuddles I needed to get through it.

The final and biggest thanks is reserved for Alex. You've barely known me without my PhD being the third wheel, and you've been nothing but supportive the entire time. For all the meals you have made me, all the pep-talks, all the times you have had to talk me down from quitting: thank you. For all the joy you have given me and the patience you have shown: thank you. I cannot fully express my gratitude to you.

I also wish to acknowledge the financial support given by the Australian Government Research Training Scholarship, and the Ross Vining Memorial Award.

I would also like to acknowledge the facilities, and the scientific and technical assistance of the Australian Microscopy & Microanalysis Research Facility at the College of Science and Engineering, Flinders University. This work was also performed in part at the Melbourne Centre for Nanofabrication (MCN) in the Victorian Node of the Australian National Fabrication Facility (ANFF).

# 1 Literature Review

## 1.1 Mass spectrometry in forensic science

The nature of forensic science demands that a rigorous and highly critical eye be turned to all analysis techniques employed in this field. Results produced and reported in court must be infallible and scrutable, to ensure the appropriate outcomes are achieved within the justice system. These methods, when shown to be effective, often remain in place for years after their inception, with advancements in analytical techniques sometimes gaining little traction until such a time that a full validation has been achieved. For this reason, many of the techniques employed in forensic science today are considered among practitioners to be the 'gold-standard' of analysis. Of particular interest to this thesis is the use of mass spectrometry for the identification and quantification of a large range of analytes. Research in both the applications of mass spectrometry and innovations in instrumentation continue to grow, despite the high cost and skill barriers in place.

The reason for the intense interest in the applications of mass spectrometry is clear: there is no other analytical technique that offers such discrete discriminatory powers for compound identification, particularly when combined with a chromatographic technique. Only nuclear magnetic resonance can compete, but requires mg quantities of analyte and is not typically in-line with chromatography. There already exists an extensive collection of literature on the forensic applications of gas chromatography-mass spectrometry (GC-MS) and liquid chromatography-mass spectrometry (LC-MS), and the purpose of this literature review is not to go into detail in this area. Rather, this review will discuss ambient ionisation mass spectrometry as high-throughput, simple techniques with the potential for field deployment. More specifically Direct Analysis in Real Time MS (DART-MS), Desorption Electrospray Ionisation MS (DESI-MS) and Direct Sample Analysis Time of Flight MS (DSA-ToF) and their applications to forensic science will be discussed.

## 1.2 Ionisation and mass analysers

At its core, mass spectrometry is a powerful analytical tool to determine mass of molecules in mixtures, based on a molecule's mass and charge acquired over an ionisation process[1]. The process whereby the ions are separated depends on the type of MS employed, and can offer multiple different approaches to the identification of known and unknown compounds. The process of mass spectrometric analysis can be separated into three distinct stages: ionisation, mass separation, and detection. For the purposes of this review, the ionisation and separation mechanisms will be discussed only.

### 1.2.1 Ionisation techniques and mechanisms

Ionisation is the first stage of the process; wherein a neutral molecule is converted into a charged one through the removal or addition of a charged moiety [2]. The type of charged particle formed depends on the ionisation technique utilised, and can be anything from the addition or removal of one mass unit through protonation and de-protonation, to the addition of small molecules or ions to drastically alter the mass and charge of a compound (i.e., formation of an adduct) [2].

The type of ionisation used directly affects the type of spectra produced and will differ depending on the type of chromatography used. For Liquid chromatography the types of ionisation most commonly encountered are electrospray ionisation (ESI), matrix assisted laser desorption ionisation (MALDI) and atmospheric pressure chemical ionisation (APCI) [2]. These techniques have largely superseded older methods such as fast atom bombardment (FAB) and electron impact ionisation (EI), due to their propensity to form molecular ions rather than fragments. For gas chromatography, EI remains the most popular ionisation technique, with Chemical Ionisation (CI) the most popular alternative. Although more ionisation methods exist than those five mentioned, most are variations on ESI, APCI and MALDI.

During ESI, a high voltage is applied across a flow of liquid at atmospheric pressure [2]. This charged spray is directed into the mass spectrometer inlet where it is de-solvated into a charged gas using heat under vacuum. Voltages are applied to the spray to eject ions present and direct them into the mass spectrometer for detection. This ionisation method is highly sensitive and allows the formation of a wide range of adducts and charged species, even allowing for the formation of multiple charged ions for the detection of high molecular weight compounds [2].

In contrast, MALDI takes place under vacuum with ionisation being initiated by targeted bombardment with a laser [2]. A matrix (applied with the sample) absorbs the energy from the laser, and transfers that energy through a secondary process to the analyte of interest. This process is termed 'soft ionisation', as it once again preferentially forms protonated molecular ions for detection via mass spectrometry [2]. Unlike ESI, MALDI doesn't typically form multiple charged ions, but does allow the formation of adducts.

APCI under atmospheric conditions involves a similar ionisation source to ESI, but the voltage is applied to a corona needle instead of to the spray itself [2-4]. A corona discharge is formed, which creates a spray of protonated water clusters, into which the sample is introduced. A heated gas is also present, which causes the sample to vaporise and facilitates proton transfer from the water clusters to the sample molecules (termed 'declustering') [4, 5]. Finally, the ions are transferred into the mass spectrometer. APCI has the advantage of being faster than other ionisation techniques thanks to the higher collision frequencies experienced under atmospheric pressure. When compared to MALDI

specifically, APCI is more suited to the ionisation of low molecular weight compounds, which can be lost in convoluted low mass ranges when the matrix itself is ionised, desorbed and detected [2]. Unlike ESI, APCI does not require any special conditions for ionisation (such as pH alterations or the addition of solvents), as the ionisation process is facilitated by the presence of water molecules. That is, positive and negative ionisation using an ESI source typically involve the addition of acidic or basic components to a mobile phase to assist in the addition or removal of a proton during the ionisation.

It is not surprising then, that many modern analytical processes are turning to APCI as the preferred ionisation method. Soft ionisation under APCI conditions allows for similar sensitivity to MALDI to be achieved that doesn't suffer from the same low mass deficits. When combined with an appropriate mass analyser the applications of APCI are vast and varied.

### 1.2.2 Mass analyser types and mechanisms

Mass analysers are used to separate the ionised masses by their mass to charge ( $m/z$ ) ratio, which are then sent to the detector for conversion into a digital output. Mass analyser types are characterised based on the mechanisms by which they separate the ions. The varieties to be discussed within are: quadrupole, quadrupole ion trap, time of flight (ToF), magnetic sector, electrostatic sector, and ion cyclotron resonance (ICR) (including orbitrap).

Ion trap and quadrupole mass analysers employ either a series of oscillating electrostatic fields across a metal rod-incorporating design (either four rods in parallel or the topological equivalent described below) to concentrate (trap) or disperse ions of a particular  $m/z$  ratio [1]. At a particular setting the electrostatic fields on opposing pairs of rods in a quadrupole mass analyser causes ions of a particular  $m/z$  value to spiral in the direction of travel to the detector, ions of higher or lower  $m/z$  have unstable trajectories and do not reach the detector. In full-scan duty the electric field settings are scanned to sequentially allow ions of different  $m/z$  to reach the detector to be counted. Ion trap mass analysers use electric fields for the same purpose, where ions of a certain  $m/z$  ratio are forced to orbit in the space within the ion trap [1]. Ion trap designs are not limited to rods in quadrupole formation. Topological equivalents exist that utilise two of the rods joined to form a ring, and the other two shortened rods to form end caps. This allows for multiple ions to be monitored easily and can also facilitate the further fragmentation of ions of interest. These fragmentation patterns can be used to differentiate between ions of similar  $m/z$  ratios, offering increased discrimination power [1].

Time of Flight MS (ToF-MS) determines the mass to charge ratio of ions based on the time taken to move through a drift region, after application of kinetic energy. ToF-MS is regarded as a high resolution technique, in that it offers accurate mass information about the compounds being separated [1]. The

ions' path along the flight tube is so long that compounds with subtle differences in mass and charge are able to be separated. This technique is suitable for high and low mass compounds, as the length of the flight tube can be increased with the addition of a reflectron. This increased path length allows separation of very high mass compounds, and increases the resolution of instrument by focussing fast and slow ions of the same mass to charge ratio.

Like ToF-MS, a magnetic sector analyser uses a 'flight tube', but disperses the ions in space rather than time using a magnetic field. Similar ions will be deflected by the field in the same way if the voltage and magnetic field strength are held constant [1]. Ions of a particular mass to charge ( $m/z$ ) ratio can be selected by manipulating these parameters, so that only those ions are permitted to pass through a slit into the detector. An electrostatic sector mass analyser operates in a similar manner, but uses an electric field rather than a magnetic one. Ions of a particular kinetic energy can be selected and concentrated by altering the potential across two curved plates of opposite charge [1].

Ion Cyclotron Resonance (ICR) mass analysers collect ions of a targeted mass range and trap them into orbit using a magnetic field. Ions are not separated, but are assigned a  $m/z$  value based on their angular velocity as a varying electric field is applied. The higher the angular velocity, the lower the  $m/z$ , and vice versa. Ions of the same mass but opposite charge have equivalent angular velocity values, but orbit in opposite directions [1]. The orbitrap mass analyser uses a similar concept, but employs an electric field rather than a magnetic field, allowing a reduction in instrument size. [6]. For both of these mass analysers, a Fourier transform is used to correlate the angular frequency to the  $m/z$ . Both of these are considered to be high resolution mass spectrometry (HRMS) methods.

High resolution mass spectrometry (HRMS) is the term used to describe accurate mass separations where the ions are separated by a 4<sup>th</sup>-5<sup>th</sup> decimal place in  $m/z$ . HRMS analysers include Fourier Transform ICR, orbitrap and ToF, offering highly discriminating mass data. These are favoured techniques for testing samples where the matrix is complicated, as the high-resolution data produced can increase the sensitivity of methods, and increase the chance of identifying compounds that may otherwise remain un-identified for integer mass techniques.

### **1.3 Chromatography and MS**

When combined with chromatography, the discriminatory powers of MS are enhanced significantly. Compounds can be pre-separated on columns so complex mixtures are not entering the spectrometer, convoluting spectra produced and increasing data processing time for the analyst. Additionally, the retention times on column for the compounds during the initial separation can add further evidence for the identification of a compound. Indeed, many identification procedures rely both on the retention time

and the spectrum produced by a compound to provide a positive identification. Not only this, but parameters in this initial separation can be tweaked to improve separation between isomers and diastereoisomers, which cannot be separated or identified with MS alone (ion mobility, fragmentation, or chromatography would need to be included in the analysis). Additives to the mobile phases (MP) employed in chromatography may also aid in the ionisation of compounds in MS too, with acidic MP additives increasing ionisation in positive mode through the provision of additional protons, and basic additives aiding in the removal of protons. Furthermore, the formation of adducts in MS can be facilitated through the presence of ions and compounds such as sodium, potassium and ammonia in the MP, offering another avenue for ionisation of protonation or de-protonation is difficult, to improve the stability of a compound during ionisation.

Despite these advantages, GC-MS and LC-MS remain high cost analysis techniques, from a number of perspectives. From a purely financial perspective, the initial outlay and ongoing maintenance costs of this equipment can be prohibitive for many labs. The consumables; solvents, gasses, columns and ongoing maintenance only add to this cost, increasing over the life of the instrument. Analysis on a GC- or LC-MS is also costly from an analyst time perspective. Adjustments and optimisation of methods, particularly for validation purposes can take months of an analyst's time. Once the method is ready for use, the analysis time is highly dependent on the sample type itself, with complex and 'dirty' sample matrices often requiring pre-analysis clean-up and concentration. The analysis itself can take anywhere from a few minutes to a few hours, depending on the compounds. For unknown compounds, data processing involves analysing and comparing retention times and spectra produced, which can add hours of time to an analysis depending on the compound and the skill of the analyst themselves.

#### **1.4 Ambient ionisation mass spectrometry**

It is clear then, that despite the obvious advantages to GC- or LC-MS analysis, there is a push to move away from chromatography-based systems and use direct mass spectrometry. As described above the use of chromatography can lead to increased analysis times, sample preparation, complicated method development and validation, high consumable consumption, and increased analyst time spent deciphering chromatograms and their associated mass spectra for compound identification. This step of the analysis process is the most time consuming, with ionisation and mass detection taking a fraction of the time. It stands to reason that removal of this process would substantially decrease the analysis time, both for analysis and method development.

Most recently, there has been a great deal of interest in the development of direct MS that utilizes ambient ionisation, particularly for forensic science [7, 8]. These methods involve only ionisation and

mass detection steps, with ionisation occurring at atmospheric pressures. Electrospray ionisation (ESI) and atmospheric pressure chemical ionisation (APCI) are the two most common ionisation techniques encountered in direct MS, and are those utilised in DART, DESI and DSA (the three techniques discussed in this review). Atmospheric ionisation MS generally results in the generation of molecular ions ( $[M+H]^+$ ) [8], making it a soft ionisation technique. This is true for both APCI and ESI, with fragmentation of ions unusual. Depending on the mass analysed used, this can drastically increase the chances of identifying compounds through accurate mass.

In APCI positive ions are formed by proton transfer and negative ions are formed by either proton abstraction or adduction with an anionic species. Gas flow (either nitrogen or helium, depending on the technique) passes through a corona needle where an electric potential is applied to generate a glow discharge (plasma). This plasma contains excited metastable gas ions ( $M^*$ ) that then react with atmospheric gas and water molecules (Equation 1), according to the following equations for helium (Equation 2) and nitrogen plasma ionisation (Equation 3) [9].

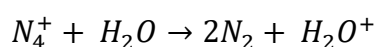
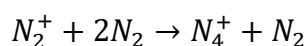
Equation 1: Generation of metastable gas ions in APCI



Equation 2: Generation of charged species from reaction with metastable helium gas ions generated from APCI

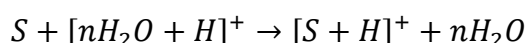


Equation 3: Generation of charged species from reaction with metastable nitrogen gas ions generated from APCI



The charged water clusters formed act as a secondary ionising species according to the following equation (Equation 4) [9].

Equation 4: Protonation of analyte (S) via charged water clusters



Ionisation under these circumstances requires little to no sample preparation, and to maximize time-saving and detection limit benefits applications have been examined that do not involve clean-up of the sample prior to ionisation. Since the inception of this idea, there has been an explosion of literature

surrounding the application and development of new instrument and ionisation types [7]. A selection of these techniques and their associated mechanisms are highlighted in Table 1.

Table 1: Types of ambient ionisation techniques. Adapted from [7]

<b>Technique name</b>	<b>Ionisation agent</b>	<b>Ionisation mechanism</b>	<b>Acronym</b>
Ambient solid analysis probe	Heated gas flow	Chemical ionisation	ASAP [10]
Atmospheric pressure thermal desorption ionisation	Heated gas flow	Chemical ionisation	APTDI [11]
Desorption atmospheric pressure chemical ionisation	Heated gas flow	Chemical ionisation	DAPCI [12]
Desorption atmospheric pressure photoionisation	Heated gas flow	Photoionisation	DAPPI [13]
Desorption electrospray ionisation	Droplet projectiles	Electrospray ionisation	DESI [14]
Easy ambient sonic-spray ionisation	Droplet projectiles	Electrospray ionisation	EASI [15]
Dielectric discharge barrier ionisation	Plasma ionisation	Chemical ionisation	DBDI [16]
Direct analysis in real time	Heated gas flow	Chemical ionisation	DART [17]
Electrospray laser desorption/ionisation	Laser	Electrospray ionisation	ELDI [18]
Extractive electrospray ionisation	Gas flow	Electrospray ionisation	EESI [19]
Fused-droplet electrospray ionisation	Droplet projectiles	Electrospray ionisation	FD-ESI [20]
Helium atmospheric pressure glow discharge ionisation	Gas flow	Chemical ionisation	HAPGDI [21]
Laser-ablation electrospray ionisation	Laser	Electrospray ionisation	LAESI [22]
Low-temperature plasma ionisation	Plasma ionisation	Chemical ionisation	LTP [23]
Neutral desorption extractive electrospray ionisation	Gas flow	Electrospray ionisation	ND-EESI [24]
Plasma-assisted desorption/ionisation	Heated gas flow	Chemical ionisation	PADI [25]

Ambient ionisation generally requires a two step process: desorption and ionisation, which can occur in sequence or in the same stage. The desorption process involves a change of phase, and the mechanism depends on the ionisation agent used. The ionisation then transfers the required energy to those desorbed neutral analytes. The types of ambient ionisation listed in Table 1 vary in the combination of desorption and ionisation mechanism, which gives rise to the large (and growing) number of these methods. Web of Science citation data demonstrates the strong interest in the development and uptake of this suite of techniques, with papers published in 2019 numbering 212 (Figure 1).

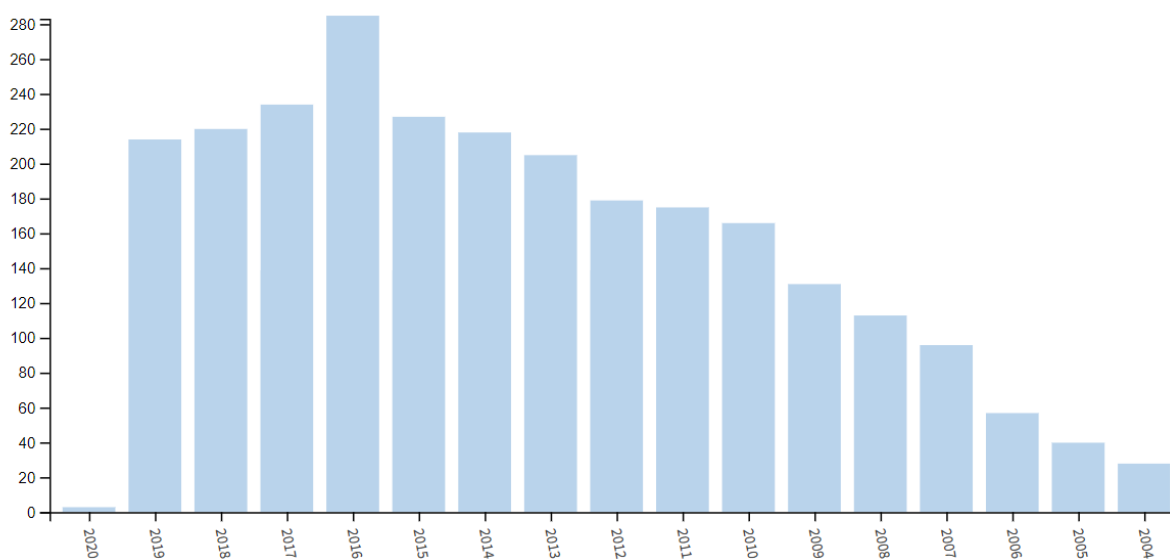


Figure 1: Web of science publication numbers (y-axis) for articles with 'ambient ionisation mass spectrometry' as a topic from 2004-2020 (x axis)

DESI and DART were first reported in 2004 [17] and 2005 [14] respectively, and were a catalyst for the explosion of ambient mass spectrometry, which can be visualised in the number of papers published with 'DESI' or 'DART' as a topic (Figure 2).

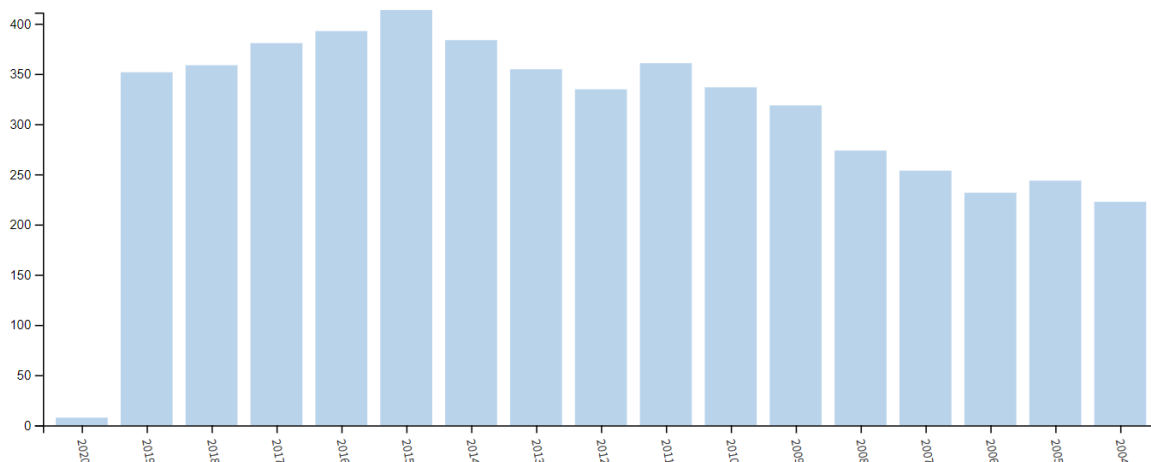


Figure 2: Web of science publication numbers (y-axis) for articles with 'desorption electrospray ionisation' or 'direct analysis in real time mass spectrometry' as a topic from 2004-2020 (x-axis)

These numbers steadily increased since the initial publications, and appear to have tapered off in recent years perhaps due to the development of newer techniques.

#### 1.4.1 Desorption electrospray ionisation (DESI)

The process of DESI involves the directional spray of charged solvent droplets onto a surface, and the subsequent desorption of ionised analyte towards to MS inlet [14, 26]. The ionisation mechanism takes place on the surface of the sample, where molecules are desorbed into the gas phase and subsequently ionised. Those ionised molecules are then transported to the MS inlet, where heat and vacuum then remove any solvent. All of these ionisation processes rely on liquid-phase interactions, with ions formed by protonation, de-protonation, or adduct formation [14, 26]. Ionisation occurs under ambient conditions, in an open system (Figure 3)

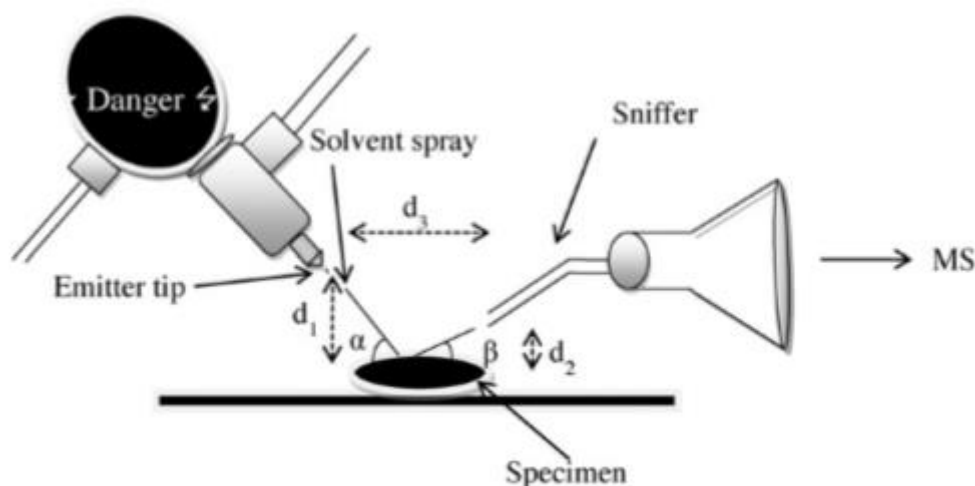


Figure 3: Schematic of DESI source. Reproduced from [27]

The sample is mounted on the sample stage, which has x, y & z ranges of motion, allowing for manual control of sample positioning. In theory, this allows for the sampling area to be controlled based on its proximity to the solvent spray source and the MS inlet. In reality, this instrument configuration results in the signal observed being highly dependent on variable and (mostly) controllable geometric parameters [28]. These include the incident angle ( $\alpha$ ), the collection angle ( $\beta$ ), the emitter tip-to-surface distance ( $d_1$ ), the inlet-to-surface distance ( $d_2$ ), and the emitter-to-inlet distance ( $d_3$ ) [28]. One of the biggest challenges when using DESI is to keep these parameters consistent across measurements of the same sample, and between samples. Changing sample shape and topography can alter the signal observed through subtle changes in the positioning and angles of the sample in relation to the emitter and MS inlet. The angles of incidence and collection are particularly important, as these dictate the amount and direction in which the solvent is applied to the sample and then desorbed [14]. Forensic specimens tend to be variable in size, shape and composition, resulting in these parameters being particularly vulnerable to alterations when used for this purpose. The solvent choice and flow rate can also alter the efficiency of ionisation, but to a much lesser extent.

Solvent choice effects can be mitigated (to a point) by the use of adulterants in the solvent to initiate reactions in the ionisation process that improve ionisation efficiency. This DESI variation is termed 'reactive DESI' and can improve the selectivity and sensitivity of DESI significantly [3]. Adulteration can be as simple as the addition of surfactants to increase the surface tension of the solvent-analyte droplets on their journey to the MS inlet. Increasing the organic component (or replacing non-organic solvents altogether) can decrease the LoD of an analyte through more efficient removal of the solvent prior to MS detection, as the solvent becomes more volatile [3].

Further alterations to the DESI apparatus have involved removing the geometric movement of the sample stage, fixing it in place within a pressure tight enclosure [29]. This is termed 'geometry-independent DESI', and was designed with the view to improve the repeatability of DESI measurements, by reducing/removing sample stage movement that might alter the angles of incidence and collection. In this configuration, changes in sample shape and topography may still influence the MS signal, but the emitter tip and MS inlet positions are fixed [29].

Transmission DESI utilises a mesh between the emitter tip and MS inlet to completely remove the influence of these geometric parameters [30]. Samples are suspended on the mesh and the solvent spray passes directly through, carrying the analyte into the MS inlet with it. Required solvation of the sample also has the benefit of homogenising the sample. Solvent spray onto the surface of a sample (particularly a forensic specimen) reveals composition of the area the solvent spray interacts with. Spatial data is required to determine if this composition reflects the entire specimen, and could result in false negatives if the wrong area of the sample is targeted [30].

#### 1.4.2 Direct analysis in real-time (DART)

The first paper on the development of DART was published shortly after the introduction of DESI [17]. Where DESI involves the use of a 'wet' solvents spray to desorb and ionise, DART ionisation is facilitated by charged particles in the gas phase [9]. A schematic of a DART source can be seen below (Figure 4). The first step in the process is the movement of helium gas into the ionising chamber. Electric potential is applied to the gas to form a plasma [9, 31]. Excited helium ions have a very high internal energy, which would exceed the ionisation energy of most analytes and environmental molecules. The metastable gas then flows into the heating chamber where the temperature is controlled by the analyst, and can be altered to improve the ionisation of target analytes based on their thermal stability [17].

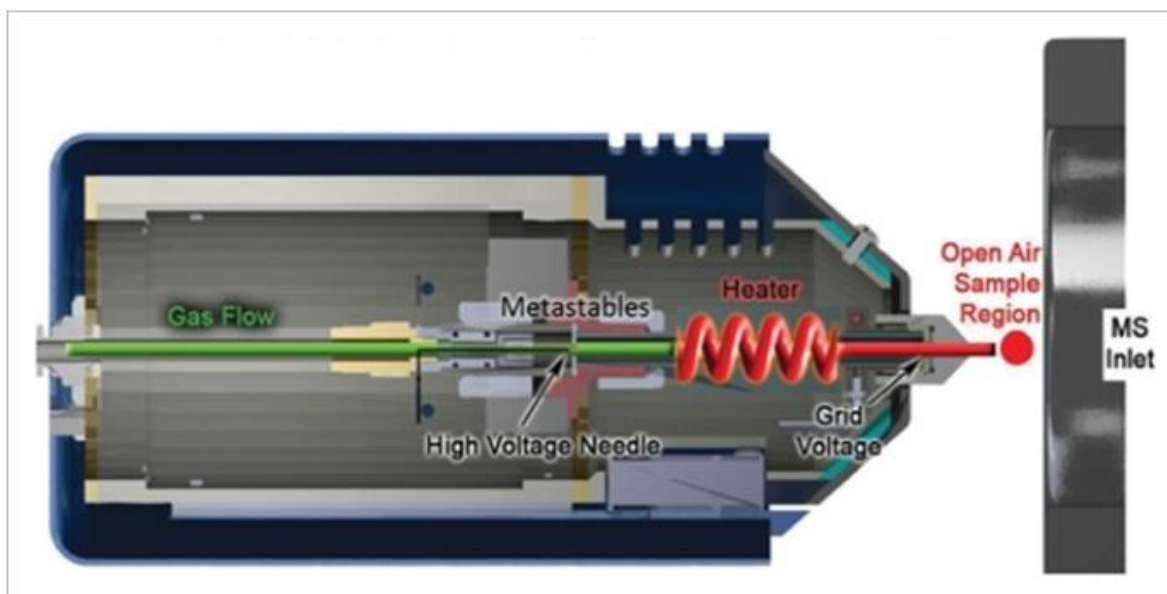


Figure 4: Schematic of DART ionisation source. Reproduced from [5]

The heated plasma is then moved out of the DART source where it interacts with molecules in the atmosphere to ionise analyte molecules by one of two processes [5]. The first, Penning ionisation, is the direct transfer of ionisation energy to the analyte ions through the loss of an electron [32]. The second is the formation of charged water clusters, which then transfer protons to eventually form  $[M+H]^+$  ions. This mechanism results in the protonated molecular ion being formed as the most commonly observed species [5]. This does not mean that other adducts (positive or negative) cannot be formed, just that they are far less common [5].

DART-MS does not have as many parameters for optimisation when compared to DESI, most obviously that there is generally no sample stage. For heat sensitive samples a reflection stage can be used to reduce sample degradation [33]. For samples to be analysed directly without preparation, they must be manually suspended between the source and the MS inlet. In fact, the only adjustable parameters are the helium gas temperature and the ion polarity. The original instrument had adjustable gas flow, ionising voltage, and gas temperature. These had a negative impact on the reproducibility of results, and more recent iterations of the instrument have made the gas flow constant to avoid these reproducibility issues [5].

#### 1.4.3 Direct Sample Analysis (DSA)

Direct Sample Analysis (DSA) is a proprietary ambient ionisation instrument developed by Perkin Elmer. The ionisation mechanism is most similar to DART but using nitrogen in place of helium. The use of nitrogen instead of helium removes the need for helium to indirectly ionise nitrogen (Equation 2). Additionally, the DSA apparatus cannot be used with non-Perkin Elmer mass spectrometers, limiting

the use of the instrument to those who already own or have the capacity to purchase a full system. A schematic of a DSA-ToF can be seen in Figure 5

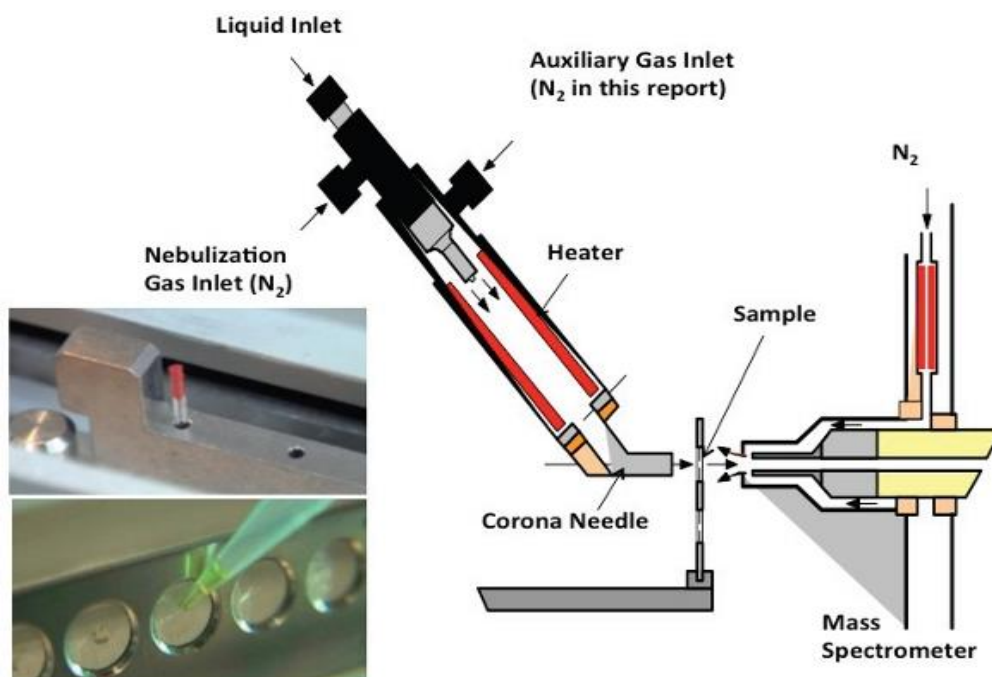


Figure 5: Schematic of Direct Sample Analysis-Time of Flight front end, showing solid sample capillary (inset, top) liquid sample analysis mesh (inset, bottom). Image provided by Perkin Elmer for training purposes.

The corona needle is embedded in the source, directly in the path of the nitrogen gas, and as a high voltage passes through the needle, reagent ions are formed, which are then directed towards the sample. Molecular ions from the sample are formed through the transfer of protons from water clusters (formed from atmospheric water available) to the analyte (Equation 4) [4]. Thus, the amount of ionisation achieved is directly related to the amount of water present in the system. The sample is ionised when contact between the water clusters and the sample is made, freeing the ions to move towards the mass analyser in a steady stream. This APCI system creates minimal ion suppression and creates molecular ions to allow for quick and simple identification of the analyte. Additional benefits to this system include lower contamination and carry-over levels. This is due to the presence of interchangeable and disposable sample holders, and a fully enclosed housing for the sample holders, which also reduces background noise. Another thing to consider regarding this instrument is that there exists a corresponding AxION ToF mass analyser that must be used with this ionisation source, although the ToF does not have to be used with the DSA. That is, the ToF is multifunctional with regards to the type of ionisation system, and can be used with GC or LC systems, but the DSA front end cannot be attached and used with any other spectrometer.

There has been work performed in an attempt to characterise the DSA source, as the ionisation mechanism is not well enough understood at this point in time. The work performed by Winter et al. [4] showed that one of the major flaws in the DSA design is that the area in which ionisation takes place (where the plasma hits the mesh) is too large to ensure that no atmospheric contamination is occurring from external sources, and that efficient ionisation is taking place. With large amounts of ionisation occurring, as is the case for an open system like the DSA, there is always the potential for ion suppression to occur via competitive ionisation. Efforts were made to reduce this area through application of cones to the source in order to improve the selectivity of the area being ionised.

## **1.5 Current applications of Direct Sample Analysis**

Current literature surrounding the use of DSA-ToF is minimal. Much of it being in the form of application notes published by Perkin Elmer themselves, due to the newness of the technique. At the time this thesis was completed there were a small number of applications for DSA-ToF described, these are discussed both in the current section of this review and section 1.6.

It was shown, in two different application notes, that DSA-ToF was able to differentiate natural vanilla from artificial vanilla flavourings (vanillin). The substitution of vanillin for natural vanilla is a problem in the industry, due to the highly labour intensive process required to plant, grow, harvest and extract the natural flavours from the vanilla beans [34]. The high costs for natural flavours when compared to the artificial flavour results in economically motivated fraud through adulteration and substitution of natural flavour. The compound 4-hydroxybenzaldehyde, which is present in natural flavourings only, was used as a marker ion for the differentiation of natural and artificial flavours. The samples were able to be directly pipetted onto the DSA sample mesh, and analysis time was 15 seconds, showing the presence of the marker ion in natural samples only [35]. Furthermore, the presence of benzoic acid in the artificial samples (as a preservative) interfered with the marker ion in the same spectral range, but fragmentation of this marker ion was able to be observed, which allowed further confirmation of natural vanilla flavour due to the presence of characteristic fragments from the chosen marker ion. Building on this work, further analysis of adulterated vanilla bean samples was undertaken, to determine if the quality of a vanilla sample could be assessed using DSA-ToF. A common adulterant in the vanilla industry is Tonka bean extract, which smells and tastes like vanilla due to the presence of a compound called coumarin [36]. The natural vanilla bean samples were adulterated with various levels of Tonka bean extract and pipetted directly onto the DSA mesh. Analysis time was 15 seconds, and the results clearly showed no coumarin peak for the non-adulterated vanilla samples, with an increasing response at the coumarin peak for increasing percentage presence of coumarin in the vanilla samples [34].

Two case studies involving milk have also been performed utilising the DSA-ToF instrument. The first of these focussed on milk adulteration, specifically the addition of melamine to milk to give a consistent protein reading while allowing further dilution of the milk. As melamine is toxic to humans above a certain dosage level, it is imperative that a method for the identification and quantification of melamine in milk exists. This case study showed that DSA-ToF could be used to identify the presence of melamine in both powdered and liquid samples, and with the addition of a melamine standard into the milk samples, could give an approximate quantitative value [37]. Although this is no substitution for LC or GC in an accredited food lab, the addition of DSA-ToF along the supply chain was highlighted as a possible real-time screening process to assess the quality of the milk. The second case study entailed the use of DSA-ToF to differentiate between organic and non-organic milks. The growing interest in organic milk has been, in part, fuelled by the public's increasing concern about additives (such as melamine) in milk, with the sales of organic milk steadily increasing. Unfortunately, a price difference comes with the label 'organic' with these milks costing anywhere from 25% -100% more than non-organic milk [38], due to demand far outstripping supply capabilities. The compound chosen as a marker for the differentiation was hippuric acid, as this has been shown to be in higher concentration in organic milk, due to the grazing habits of the milking animals [39, 40]. Protein precipitation was carried out on both the organic and non-organic milk samples, and an aliquot of this precipitate was pipetted directly onto the DSA mesh. Analysis time was 30 seconds, with detection of hippuric acid in the organic sample only [38]. The addition of a deuterated internal standard allowed for the approximation of hippuric acid concentration within the samples, without the need for a calibration curve. Although further research into the levels of hippuric acid would need to be undertaken to assess the validity of DSA-ToF to this application, the results suggest that the technique would be sufficient to differentiate between the two milks [38].

Detection of olive oil adulteration has also been investigated as a possible application of DSA-ToF. The addition of soybean oil [41], olive pomace oil [42] and seed oils [43] are all common methods for the dilution of olive oils to fetch a higher price for a lower quality product. In all three cases of adulteration, the unadulterated olive oils were compared to those oils that are commonly added to reduce the product quality. Although triglycerides are present in all oils, the majority triglyceride constituent for each oil varies. For olive oil it was determined to be triolein and for both corn and soybean oil the main triglyceride present was trilinolein [41, 43]. The relative response for the two triglycerides could be used to determine the presence of and levels of adulteration in the olive oil, with a baseline level of trilinolein in olive oil naturally being established, and anything over this baseline being considered adulteration. In the case of adulteration with olive pomace oil, it has been shown in the past that high levels of ethyl

ester of oleic acid (EEOA) are present in pomace oil when compared to olive oil [44]. The levels of EEOA were shown to markedly higher in the pomace oil when analysed with DSA-ToF, with the response ratio of EEOA to oleic acid (OA) increasing for percentage increase of adulteration with pomace oil in olive oil [42]. It is important to note that for all work performed on the olive oils and associated adulterants, there was no sample preparation performed, with all oils being analysed straight from the bottle into capillary tubes in the DSA sampling area. All analysis was performed within 30 seconds of the sample being introduced to the instrument [41-43]. Previously, results such as these have been obtained via LC-MS or GC-MS, which would have required hours of sample preparation, method development and analysis run time.

Most recently, the use of DSA-ToF for the detection of degradation products of methyldiethanolamine, a natural gas sweetener. These by-products can cause foaming and corrosion in gas cylinders which can weaken the metal and cause a safety risk. The method developed in this work allowed rapid identification and quantification of these compounds, improving the safety of the use of these chemicals.

Forensic applications of DSA-ToF have been described, but these are discussed in the relevant sections below.

## **1.6 Ambient ionisation in forensic science**

The use of ambient ionisation in forensic science has been well explored to date, although the methods developed have remained in the research labs, few have been applied to genuine evidential artefacts. In general, the applications explored highlight the potential for ambient ionisation MS in the screening space, where high-throughput analysis is essential. The body of work is unanimous in describing difficulties in the application of these techniques to the generation of evidence in a forensic context, due to issues with specificity, sensitivity and reproducibility. One of the greatest potential benefits to ambient ionisation, due to speed and simplicity of the techniques, is if they can be field deployable to crime scenes or roadsides. The application of ambient MS to in-lab screening would allow for immunoassays to be augmented or totally replaced, increasing the efficiency of these in-lab processes. Once the difficulties described above are overcome, it is reasonable to expect that these methods will find use with most forensic and police departments to more reliably inform and direct further testing of forensic exhibits from crime scenes or roadsides.

As previously highlighted, DART and DESI remain the primary methods of choice in this space, the remainder of this review will address the development of applications across explosives, drugs & toxicology, chemical warfare agents, inks & documents, fingermarks, and gunshot residues.

### 1.6.1 Explosives

The rapid detection of trace explosives in various matrices is of high interest and importance for the forensic community. The application of DESI and DART-MS have been heavily explored in this area, in fact the first publication that mentioned DESI was centred around the detection of explosive residues from the clothing of someone who had been in proximity to a controlled explosion [45]. Since that paper there have been a great deal of publications dealing with the detection of explosive residues on glass, paper, plastic and metal surfaces. Years later this capability was extended to the detection of those same residues on human skin and fabric.

One of the first papers after the initial publication detailed the detection of hexogen (RDX), trinitrotoluene (TNT), pentaerythritol tetranitrate (PETN) and octogen (HMX) on a variety of surfaces using reactive DESI-MS [46]. These surfaces included glass slides, plastic, floppy disks, computer hard drives, metal, swabs, nitrile gloves, paper, and Teflon. This was the first in a series of papers that used a combination of positive and negative ion mode to detect a range of analytes, and in this particular example RDX was detected in both modes. This was the first DESI based paper that demonstrated the detection of exogenous RDX residues on fingerprints, with no pre-treatment applied [46]. Detection of the same analytes was also achieved on paper and metal using non-reactive DESI [12]. In the years following, reactive DESI was applied to the detection of organic peroxide explosives such as hexamethylene triperoxide diamine (HMTD) [47] and triacetone triperoxide (TATP) [47, 48] on paper, metal and brick, as well as RDX and PETN spiked frosted glass slides in negative mode [49].

Shortly after this, reactive DESI was applied to the non-proximate detection of TATP, RDX, HMX, and PETN on paper, plastic (a laptop computer) and metal surfaces [50]. As with other non-proximate detection methods discussed in this review, the sensitivity of the method suffered as a result of the transfer line, with the reduction in sensitivity being linked to the length of the line itself. That is, the longer the line became, the less sensitive the method became. Despite this loss of sensitivity, the ability to detect explosive residues from a potentially dangerous piece of evidence at a distance is something that many forensic practitioners are keen to develop, and attempts to do so continue to surface in publications.

Forensic exhibits are, by nature, often quite chemically complex. Matrices may interfere with analysis, or there may be trace levels of compounds of interest that are heavily masked by other artefacts in the vicinity. This is complicated enough when applying the commonly used analytical techniques such as LC-MS or GC-MS, where sample clean-up is typically performed, and chromatographic separation on column further separates potentially interfering compounds from one another. When using ambient

ionisation techniques such as DESI-MS, interfering compounds must be anticipated and ideally simulated in the laboratory before the technique is applied to case work samples. In 2008, a reactive DESI-MS paper examined exactly this issue [51]. Different fabric types were spiked with TNT, PETN, RDX, and HMX, and analysed in negative ion mode. Interfering compounds including urine, insect repellent and lotion were applied to the 'samples', to determine the impact on sensitivity. In this case, the lotion did reduce sensitivity, but only until the top layers were removed by the solvent application occurring during DESI. All other 'interfering' mixtures did not impact the detection of the explosive residues. In fact, other studies showed that the limits of detection for explosive residues in the presence of interfering compounds were comparable to those without [46]. Work involving the detection of organic peroxide explosives TATP, tetraacetone tetraperoxide and HMTD showed detection of these compounds in the presence of organic (diesel) and aqueous (vinegar) solvents [47, 48]. Given the need to detect these residues rapidly and accurately in many situations, the ability to do so in complicated matrices represents a vital step forward for DESI.

In more recent years, the focus has been on portable MS technology for in field screening of samples, and the application of these developed methods to more complicated sample types. The first paper to examine portable MS technology coupled to DESI looked to detect RDX on paper using non-reactive DESI [52]. Nanogram limits of detection were achieved for RDX in positive mode with negative mode also achievable on the instrument used, which would allow for a greater number of analytes to be detected. Microgram limits of detection were achieved for TNT, HMX and 2,4,6- trinitrophenyl-N-methylnitramine (tetryl) using another model of portable MS [53]. Despite the leap forward that the use of portable MS and ambient ionisation would represent for forensic science, the two studies reporting this so far showed a loss of sensitivity (much like non-proximate detection) that simply isn't feasible to incorporate into regular forensic practice.

There has also been an interest in the incorporation of solid phase microextraction probes directly into the DESI interface, with Bianchi et al. demonstrating detection of explosives in soil using this method. Homemade cartridges were exposed to spiked soil, and TNT, cyclotrimethylene-trinitramine, cyclotrimethylene-tetranitramine, pentaerythritol tetranitrate and trinitrophenylmethylnitramine were able to be detected in the ng/kg range [54]. This method outperformed straight spiking onto PTFE slides, with DESI-HRMS detection, demonstrating the benefits of solid phase microextraction (SPME) sample concentration for trace amounts of analytes.

DART-MS has not been as heavily explored as DESI-MS in this field. Much like DESI, the initial DART publication demonstrated the detection of explosives on the necktie of a man who had been in the

vicinity of a rock blasting operation. The technique was also used to detect TNT in muddy water, and some inorganic explosive residues such as ammonium nitrate and sodium azide [17]. Again, in a manner similar to DESI, the use of DART for the detection of explosives has been achieved through the use of positive and negative ion modes, and in some cases can only be achieved through the addition of dopants, in order to form adducts for detection [55]. Nitro organic compounds, for example, tend to ionise poorly unless doped with chlorine, readily forming chloride adducts. Nilles et al. set the precedent for the use of DART for explosive detection, showing the peroxide compounds (such as TATP, HMTD) form positive ions, and all other classes of explosives form either negative ions or adducts. Detection of nitroglycerins, glycols, nitrotoluenes and nitrobenzenes was successfully achieved on a variety of surfaces, including glass, foam, wood, steel and asphalt [56].

It wasn't until 2013 that the optimisation of DART processes for the detection of all categories of explosive was performed [57]. In general the four groups of explosives (nitroaromatics, straight chain nitrate esters, cyclic nitro compounds and peroxides) were ionised more effectively at higher temperatures, although this was dependent on the size and thermal stability of the molecule in question. This work also touched on one of the major limitations of ambient ionisation methods, the difficulty discriminating between compounds with identical masses and fragmentation patterns. The use of chromatographic separation allows for both the retention time and mass spectrum of a compound to be determined, which is more diagnostic of identity than mass spectrometry alone. Indeed, in many cases similar compounds cannot be differentiated between one another. Where screening is the aim, this is less of an issue, as classes of compounds (such as explosives) can be identified, and further testing can confirm the identity.

Further work to improve the method coupled DART with an accuToF, to allow high resolution mass spectrometry analysis of analyte in solution and deposited onto surfaces. This work was notable due to the observation of positive adduct formation for a number of straight chain and cyclic nitroaromatic compounds, which had previously been thought to only form negative ions or adducts. Analysis was performed at 350°C [58], significantly higher than the initial published work, which showed negative ion formation at 225°C [57]. Humidity was also shown to have significant influence over the type and abundance of ions formed. Newsome et al. [59] showed that positive molecular ion formation for HMTD was far enhanced by an increase in humidity. The abundance of this ion increased as humidity increased, with a significant reduction in fragmentation. Increased molecular ion abundance improves the likelihood of successful identification of a compound, reducing confusion caused by the presence of identical fragmentation patterns for similar compounds.

More specific applications of DART were shown to detect explosive residues in fingermarks, using microextraction techniques, as well as the detection of explosive precursors in bulk. A study comparing surface assisted laser desorption ionisation (SALDI) and DART for the detection of explosive residues in fingermarks showed DART out-performing SALDI where no pre-treatment was applied. That is, for SALDI to be most effective, a powder coating on the ridges of the fingermark was required. SALDI outperformed DART where tape lifts were used, with DART failing to detect any residues from the tape [60]. Clemons et al. [61] pre-concentrated samples using direct analyte-probed nanoextraction to remove single particles of RDX and TNT from surfaces. Results were in agreement with previous work, with regards to limits of detection (LoDs), without the matrix effects often encountered [57]. Sugar alcohol precursors to explosive manufacture were successfully detected with detection limits between picograms to hundreds of nanograms, across a variety of substrates. Of particular interest was erythritol, precursor to erythritol tertranitrate, which was detected to sub-nanogram limits on Teflon [62]. Detection of precursor compounds is vital for the prevention of crime, and detection down to such low limits shows promise for the application of this technique to screen quickly and accurately for these compounds when required.

Of particular interest, and mentioned in several publications, is the application of ambient ionisation methods such as DESI and DART to the detection of explosive compounds and precursors in airports. Current ion mobility spectroscopy methods suffer from low resolution, despite being relative fast and accurate. Ambient ionisation could vastly improve the analytical capability of high traffic screening, and its capability to detect those compounds of great national interest has been demonstrated capably and continuously.

### 1.6.2 Drugs and toxicology

If DART and DESI have been explored thoroughly for the detection of explosive residues, they have been exhaustively mined for applications for the drug detection and toxicology. Drugs and their metabolites are a high value target for ambient mass spectrometry techniques, owing to the vast number of drugs, samples, and the range of sample types these exhibits can take. Drug detection alone can fall into two vast categories: illicit and pharmaceutical (over the counter) drugs. Illicit drug investigation may involve analysis of an unknown active constituent in seized exhibits, or from counterfeit pills.

DESI-MS has been investigated as a method for application to tablets, solutions, ointments, creams & gels, skin patches, capsules and herbal materials. Where drug formulations are concerned, excipients can cause issues for selectivity, and contribute matrix effects. Surface material choice has been shown

to increase selectivity to distinguish between excipients and actives in complex mixtures using DESI-MS [63]. Of arguably even more value is the ability to map the distribution of an active compound over the surface of a tablet (or similar), with impressive spatial resolution being achieved [64, 65]. One other major benefit to the use of ambient mass spectrometry for drug analysis is the ability to directly analyse herbal material. Typically, the analysis of active compounds from herbal material (such as cannabis) requires a number of extraction, clean-up and concentration steps, as herbal matrices are often complicated and make spectral interpretation extremely time-consuming for the analyst. DESI-MS has been shown to directly detect cannabidiol,  $\Delta^9$ -THC, cannabidiol (CBD) or cannabichromene from the leaves of the cannabis plant [66]. The disadvantage to not performing chromatography on cannabis plant matter is that many of the compounds of interest have the same molar mass (THC, CBD and cannabichromene), and therefore cannot be discriminated on that basis alone [67]. For illicit samples this is less of a concern, as the identification of cannabis is the primary concern, and this can certainly be done using DESI-MS. However, the legalisation of medicinal cannabis and the subsequent requirement for regulation still require information relating to the ratio of the active compounds in commercially grown cannabis crops. Without the ability to discriminate between active ingredients DESI-MS (and indeed other ambient MS techniques) cannot be used in this space. The use of non-proximate detection for drug detection has also been demonstrated for the detection of drugs using DESI-MS. Single drugs (cocaine) and mixtures (cocaine, methamphetamine (MA), diacetylmorphine) were detected directly from human skin, with a transfer line of up to 3m being used. It was found that the analyte ions travelled the full length of the tube, but much of the background contribution was lost during the transfer, resulting in cleaner and less convoluted mass spectra, despite the reduction in signal [68].

DART-MS has been shown to detect many of the same compounds as DESI-MS for drug detection and toxicological analysis. The initial DART publication demonstrated both the detection of cocaine from currency [17] (also later performed by DESI, using a portable MS [69]), and the application to pharmaceutical analysis (interrogating the tablets and creams directly) [17]. DART has been used to analyse bulk seizures, demonstrated in Switzerland, where 10 ecstasy tablets were interrogated. The results showed methylenedioxymethamphetamine (MDMA) as the major component, and also allowed the identification of excipients in the tablets including N-methyl-1-(1,3-benzodioxol-5-yl)-2-butanamine, amphetamine, 4-methylthioamphetamine, and caffeine. This work has also been completed using DESI-MS, showing protonated MDMA as the major constituent of 5 seized ecstasy tablets, as well as MA as a minor component [66]. DART has also been used for the identification and classification of new and novel drugs, including cathionics ('bath salts') and synthetic cannabinoids. This is of great

interest, as the market in which drugs are bought and sold is continuously changing and innovation and adjustments to chromatographic methods are required to ensure detection of these compounds. DART-MS has found mainstream acceptance as a screening technology, with the Virginia Department of Forensic Science utilising it for screening all drug samples. A library of over 3200 positive ion spectra from over 800 samples has been established, and is available for the forensic community to access and add to when required [5].

From a toxicological standpoint, DESI-MS has been shown on a great number of occasions to be suitable for the detection of parent drugs, degradants and metabolites from complex biological matrices such as skin, hair and urine. The nature of these samples means that many of the methods developed and demonstrated involve a sample pre-treatment step. Many reported methods use solid-phase extraction cartridges [70], which pre-concentrate the sample and minimise matrix suppression effects. Morelato et al. discuss that this defeats the purpose of using techniques such as DESI, where the advantage is that there is no sample preparation to be done [27]. Nonetheless, these extraction protocols have allowed the detection of cocaine [51, 71], cannabis [71], opiates [71], benzodiazepines [71], and glucuronic acid conjugates of various pharmaceuticals [71] in urine. The detection of anabolic steroids in urine has been achieved through reactive DESI using derivatisation with hydroxylamine [72]. Steroids have also been detected in hair, using an ultrasonic liquid extraction [73], opening the door to hair analysis for other compounds of interest. The analysis of drugs in hair offers a timeline of ingestion, over time periods far exceeding those offered by blood, oral fluid and urine.

From a forensic standpoint, there has been some exploration of the application of DSA-ToF to the detection of drug compounds. The current methods for drug detection often rely on the use of reference standards (in the case of chromatographic based methods), or rely on method development that cannot easily adapt to the changes in illicit drug trends. Perkin Elmer presented a case study wherein they analysed 369 unknown drugs from seized pills, vials, powders and urine samples [74]. This compared the analysis of the drugs using both traditional methods (LC-MS, GC-MS) and the DSA-ToF instrument. DSA-ToF identification of the compounds was done by identifying exact monoisotopic masses of the compounds of interest, and their major fragments. Analysis time was below 25 seconds for all samples, and including run and post-analysis time took approximately 2.5 hours. For the majority of samples, although some crushing and a small number of methanol (MeOH) extractions were required, but even with the addition of these steps, total analysis time was 4 hours. When compared to the preparation and lengthy run times of the chromatographic methods (20-60 minutes per run) [74], these results suggest that ambient mass spectrometry techniques like this have a potential use in the analysis of illicit drug related samples.

Recent work described a method for the detection of opioids in methanol, which was then applied to a number of seized drug samples. Moore et al. were able to detect 18 opioids, including multiple fentanyl analogues. This method was then applied to 81 seized drugs, which had already been analysed using GC-MS. The DSA-ToF results were in agreement with the GC-MS results in 80 of the 81 samples, demonstrating the utility of this instrument in forensic laboratories.

DSA-ToF analysis has also been applied to the analysis of synthetic drugs, a rapidly growing problem. A particular problem is the use and distribution of a group of drugs called cathinones, known as 'bath salts' on the streets. These synthetics are used as legal substitutes for illicit drugs such as cocaine and methamphetamine, however the composition of these drugs are continuously changing [75, 76]. This makes it difficult both to legislate against the synthetic drugs, and to detect them, as conventional detection methods involved extensive method development, and to add new compounds to the mix may require additional method development and validation. The DSA-ToF was used to detect the presence of these cathinones in a number of 'bath salt' samples. The entire mass range was monitored to ensure that any and all masses of interest were captured. Minimal sample preparation was required, with the bath salt samples themselves being analysed as solids, and the cathinone standards being dissolved in MeOH. By determining the molecular ion and fragmentation patterns of eleven cathinone standards initially, the DSA-ToF instrument was able to detect and identify a wide range of cathinone drugs within the bath salt samples [35]. Analysis time was below 15 seconds for all bath salt samples, with no sample preparation required.

Herbal supplements are also a growing concern for law enforcement, with adulteration of the natural herbs being observed frequently. The typical additions include synthetic prescription drugs, where analogues of these prescription drugs and drugs have been removed from the market for safety reasons. The adulteration is performed to enhance the properties of the supplement, and often increase the price. The work involving the DSA-ToF instrument was undertaken to assess the viability of this technique for the detection of phosphodiesterase 5 (PDE 5) inhibitors in a complex herbal matrix. The analysis was successful, with the molecular ion peaks for PDE 5 inhibitors spiked into the herb sample being detected within an acceptable accurate mass range (2ppm) of the expected peak [77]. Again, sample preparation was minimal, and analysis time was below 20 seconds. DSA-ToF use for the analysis of complex herbal profiles in complementary and alternative medicines has been further explored by Crighton et al., who demonstrated the detection of 21 ubiquitous herbal compounds in a number of multivitamins and complementary medicines [78]. Samples were prepared using a methanol extract, with a total reported analysis time of under one minute. The lab reporting these results performed 'untargeted' analysis, as is typical for DSA-ToF, which then had an in-house library applied

to the data This transition from untargeted to targeted analysis can improve the interpretation of the complicated mass spectra associated with herbal compounds (and other forensic samples).

Further benefits of DSA-ToF are highlighted in a study of the South African street drug 'Nyaope' [79]. This drug is extremely cheap, and is highly addictive. The ingredients of this drug are not clear, and vary between sellers. Typically, the drug is cut with sand, soil or cement powder and has been shown to contain ingredients such as: opiates, benzodiazepines, antibiotics, antiretrovirals and stimulants. The powder is rolled in marijuana leaves and smoked. The heterogeneity and changes in formula make treating overdose and withdrawal extremely difficult. This study examined 40 samples from 12 different areas of South Africa, and compared results obtained from DSA-ToF and GC-MS. All samples were analysed by DSA-ToF, and a wide variety of compounds were detected, from a number of drug classes, often within the same sample. The presence of these compounds were confirmed by GC-MS in almost all the samples (where sufficient sample was available) [79]. The results provided by the DSA-ToF enabled rapid, accurate identification of drug composition, even where that composition is unknown and inconsistent between samples.

Also of relevance is a recent conference paper where the use of the DSA-ToF was described for the analysis of a number of seized pills. The author of this work noted that despite the benefits that a screening system such as DSA-ToF would have in the laboratory, the instrument itself did not perform as expected, and in some cases actually increased the analysis time of the samples [80]. The authors had attempted to replicate the application note in which Perkin Elmer described the direct analysis of pills, without sample preparation. Rather than rapid and accurate detection of drug compounds in the pill matrices, the authors experienced high levels of contamination and carry-over. These issues often resulted in significant delays in analysis time, as the instrument often required substantial cleaning steps. As a work-around, dilution of the samples was attempted, however without an understanding of the original analyte concentrations and distribution in the sample this often resulted in the samples being too concentrated or too dilute. Samples that were too concentrated caused the instrument to suffer from carry-over, and samples that were not detected by the instrument. In most cases, the established chromatographic methods in place were superior in both data provision and analysis time.

A summary of the drugs successfully detected by DSA-ToF, DESI-MS and DART-MS, the formulation type tested, the surface tested on (if applicable) and any pre-treatments required can be found in Table 2.

Table 2: Summary of the DSA-ToF, DART-MS and DESI-MS applications for the drug detection and toxicology

Compounds detected	Methods	Mode	Matrix analysed	Pre-treatment	Reference
Caffeine, acetaminophen, meconin, methadone, papverine, dimenoxitol, dextromethorphan, codeine & metabolites, morphine & metabolites, heroin, amphetamine, methamphetamine & metabolites, cathine, citroflex A, duracaine, lidocaine, zidovudine, thiofentanyl, benzitramide, benzodiazepines, phenobarbitone, pipradol, moramide narcotics, fenethylline	DSA-ToF	Positive	Powder sample	Not specified	[79]
Methadone, etorphine, methyl-desmorphine, dihydromorphine, hydromorphinol, morphine, oxycodone, codeine, dihydrocodeine, 6-MAM, EDDP, testosterone propionate,	DSA-ToF	Positive	Liquid & solid samples, urine	Liquid samples analysed without treatment, solid samples analysed without pre-treatment or dissolving in MeOH, urine diluted	[74]

<p>testosterone decanoate,  nandrolone decanoate,  stanozolol, boldenone  undecylenate,  methandrostenolone,  testosterone enanthate,  mesterolone, trenbolone,  nandrolone phenylpropionate,  trenbolone enanthate, 4-  methoxyamphetamine,  fluoromethamphetamine, TCP,  parahexyl, MDMA, N-  ethylamphetamine, THC,  caffeine, NRG-2, phenmetrazine,  mephedrone, MDPV,  diethylcathionine, 4-FMC, cocaine,  benzoylecgonine, pentobarbital,  tadalafil, carbamazepine,  amitriptyline, sibutramine,  sildenafil, risperidone, quinine,  zolpidem, clenbutrol, diazepam,</p>				<p>20:1 in 50:50  MeOH:water</p>	
---	--	--	--	--------------------------------------	--

ketamine, lidocaine, benzocaine					
Butylone, methylone, naphyrone, mephedrone, ethcathione, 4-fluoromethcathione (4-FMC), 4-methylethcathione (4-MEC), 3,4-methylenedioxy- $\alpha$ -pyrrolidinobutiophenone (MDPBP), $\alpha$ -pyrrolidinopentiophenone ( $\alpha$ -PVP), 3-methyl- $\alpha$ -pyrrolidinopropiophenone ( $\alpha$ -MPPP), methylenedioxypropylone (MDPV)	DSA-ToF	Positive	Solid samples and standards (powder)	Standards were analysed as powder on mesh with MeOH droplet. Samples were analysed as powders on the solid sample holder	[35]
Sildenafil, tadalafil, vardenafil	DSA-ToF	Positive	Mint leaves (herbal preparation analogue)	MeOH extraction	[77]
Caffeine, catechin, epicatechin, epigallocatechin. Gallic acid, gallocatechin, theanine, pantothenic acid, pyridoxine hydrochloride, isorhamnetin,	DSA-ToF	Positive	MeOH extract	MeOH extraction	[78]

kaempferol, quercetin, calcium pantothenate, nicotinamide, ginkgo biloba					
Heroin, 6-MAM, morphine buprenorphine, norbuprenorphine, fentanyl, norfentanyl, acetylfentanyl, $\beta$ -hydroxythiofentanyl, butyrylfentanyl, furanylfentanyl, valerylfentanyl, AH-7921, U-47700, desomorphine MT-45, W-18, W-15, cocaine, oxycodone, ethylone	DSA-ToF	Positive	MeOH standards	N/A	[81]
Claritin, paracetamol, aspirin, Excedrin, centrum Ketoconazole, clotrimazole (ointment), alanine (eyedrops)	DESI-MS	Positive/negative	Tablet, cream, filter paper	No	[82]
Flunitrazepam, clonazepam	DESI-MS	Positive	Chromatography paper	No	[83]
Methylamphetamine	DESI-MS	Positive	Single droplet microextraction (SDME) syringe	SDME	[84]

Aspirin, paracetamol, caffeine	DESI-MS	Positive	Thin Layer chromatography (TLC) plate	Separation by TLC	[85]
Propranolol, testosterone, dobutamine, verapamil, chloramphenicol, ibuprofen, diazepam, roxithromycin, carbamazepine, acetylcholine, PG, angiotensin	DESI-MS	Positive/negative	Polymethylmethacrylate (PMMA), polytetrafluoroethylene (PTFE) -printed, porous PTFE, PTFE sheets	No	[86]
Ranitidine, paracetamol, codeine, nicotine (skin-patch), chlorhexidine gluconate, anastrozole, bradykinin	DESI-MS	Positive	Tablet, skin-patch, cellulose nitrate filter membrane	No	[63]
Loratidine, verapamil	DESI-MS	Positive	Tablet, Teflon surface	Neat, dissolved and dried on Teflon	[87]
Bradykinin (peptide)	DESI-MS	Positive	Teflon	Dissolved and dried on Teflon	[87]
Caffeine, nicotine, allicin, propanethial-S-oxide, glycol monosalicylate, methyl nicotinate, capsicum oleoresin,	DESI-MS	Positive	Tablets, glass slides, swabs	Film-coated tablets were scraped, creams deposited on glass slides, Swab	[25]

phenylephedrine HCl, guaifenesin, aspirin, ibuprofen, mefenamic acid, paracetamol					
Oseltamivir	Reactive DESI-MS (crown ethers, alkali metal cations)	Positive	PTFE, capsules	Capsules were pressed (KBr press)	[88]
Alprazolam, amfepramone, atenolol, clomipramine, cortisone, dexchlorpheniramine, ethambutol, fluvoxamine, ibuprofen, indomethacin, lamotrigine, metoclopramide, mianserine, nefazodone, paracetamol, olanzapine, propafenone, sertraline, tramadol, reboxetine, tamoxifen, zolpidem, MDMA tablets	DESI-MS	Positive/negative	Tablet	Film-coated tablets were scraped, capsules were pressed (KBr press)	[64]
Loratidine, paracetamol, aspirin, caffeine, naproxen, ibuprofen, cocaine, methylamphetamine, diacetylmorphine, bradykinin	Reactive DESI-MS (NaCl, NH <sub>4</sub> AOC)	Positive/negative	Tablet, skin, Teflon	No	[68]

Hydrocodone bitartrate, paracetamol, alprazolam, MDMA tablets, cannabis leaves (THC)	DESI-MS	Positive	Tablet, plant material	No	[66]
Sildenafil, oxycontin, hydrocodone bitartrate, paracetamol, alprazolam, MDMA tablets, cannabis leaves (THC), morphine, codeine, thebaine, papaverine, noscapine, gamma hydroxybutyrate/gamma butyrolactone	DESI-MS	Positive	Tablets, breath mints (THC), chocolate-coated opium bars, liquid on glass slide	No	[89]
Cocaine, heroin, methylamphetamine	Reactive DESI-MS (NaCl)	Positive	Urine on polyester, cotton fabrics	No	[51]
Cannabis (THC), codeine, morphine, oxymorphone, amphetamine, temazepam, oxazepam, desmethyldiazepam, parahydroxytemazepam	DESI-MS	Positive/negative	Urine on PTFE, Teflon	Solvent extraction	[71]
Dobutamine, paracetamol, dehydroepiandrosterone, $\beta$ -estradiol (and glucuronide	Reactive DESI-MS (NaCl, NH <sub>4</sub> OH, NH <sub>4</sub> AOC, TFA)	Positive/negative	Urine on PMMA, glass slide, stainless steel, envelope paper, Teflon	No	[90]

conjugates)					
Clenbuterol	DESI-MS	Positive/negative	Urine on PMMA	Solid-phase extraction	[70]
Androstadienedione, androsterone hemisuccinate, stigmastadienone, epitestosterone, 6-dehydrocholestenone, androsterone, 5 $\alpha$ -androstan-3 $\beta$ , 17 $\beta$ -diol-16-one	Reactive DESI-MS (hydroxylamine)	Positive	Urine on polished & ground glass, filter paper, porous PTFE	No	[72]
Estradiol benzoate, testosterone cypionate, testosterone decanoate	DESI-MS	Positive	Solution on glass, PTFE, hair	Ultrasonic liquid extraction	[73]
Artesunate (counterfeit)	Reactive DESI-MS (dodecylamine)	Positive/negative	Tablet	No	[65]
Amphetamine, methylamphetamine, MDMA, dimethoxyamphetamine, paramethoxyamphetamine, paramethoxy-N-methylamphetamine, benzylpiperazine,	DESI-MS	Positive	Semi-porous PTFE or Teflon sheets	Dissolved in MeOH	[91]

trifluoromethylphenylpiperazine, meta-chlorophenylpiperazine, para-methoxyphenylpiperazine					
4-methylmethcathione (mephedrone), caffeine, methamphetamine, cathione, paracetamol	DESI-MS	Positive	PTFE surface	No	[92]
Cocaine, benzoylecgonine, ecgonine methyl ester	DESI-MS	Positive	Fingermarks	No	[93]
Cocaine, caffeine, procaine, levamisole, lignocaine, paracetamol, atrophine, truxillines	DESI-MS	Positive	PTFE	Dissolved in MeOH	[94]
Methyl phenidate, venlafaxine, barbituric acid, alprazolam, 3- methyl-morphine, propranolol, methyl salicylate, paracetamol, dextromethorphan, doxylamine	Reactive DESI-MS (NaCl)	Positive/Negative	Tablets, cream formulations, liquids	No	[95]
Cathione 'bath salts' mixtures (2- ethylethcathione, diethylcathione, isopentadrone, 3- methylethcathione, 2-	DART-MS	Positive	Powders	No	[75]

methylethcathione, 2-fluoromethcathione, 2-fluoroethcathione)					
Synthetic cannabinoids (AM-2201, JHW-122, JHW-203, JWH-210, RCS-4)	Collision-induced dissociation DART-MS	Positive	Liquid standards, plant material	No	[96]
Synthetic cannabinoids (JHW-015, AM-251)	DART-MS	Positive	Doped plant material	No	[97]
Synthetic cannabinoid (JWH-018)	DART-MS	Positive	Plant material	No	[98]
Sibutramine hydrochloride	DART-MS/MS	Positive	Capsules and content	No	[99]
$\Delta^9$ -THC	DART-MS	Positive	Hair	Washed with dichloromethane (tested before and after)	[100]
Duquenois-levine chromophore	DART-MS	Positive	Extracted marijuana solution treated with Duquenois-levine reagent	Separated from bulk solution with TLC	[101]
Synthetic cannabinoids (AM-2201, JWH-122, JWH-203, JWH-210, RCS-4)	DART-MS	Positive	Plant material	No	[102]

Metformin, nateglinide, gliclazide, rosiglitazone, glipizide, glibenclamide, gliquidone	DART-MS	Positive	Capsules	Extraction in MeOH	[103]
Mitragynine, epicatechin	Collision induced dissociation DART-MS	Positive	Plant material	No	[104]
Oxycodone, paracetamol, methadone, morphine, zolpidem, alprazolam, celecoxib, oxymorphone, amphetamine, methyl phenidate, meperidine, diazepam, tizanidine, clonazepam, hydrocodone, aspirin, caffeine, lorazepam, buprenorphine, naloxone, lidexamphetamine, codeine, ibuprofen	DART-MS	Positive	Tablets and capsules	Dry-extraction	[105]
3,4-dimethylcathione, 2,3-methylenedioxy-methcathione, 3,4-methylenedioxy-N-benzylcathione	DART-MS	Positive	Solid material	No	[106]
Nicotine	DART-MS	Positive	Fabric, paper, coffee	No	[107]

			cup		
Monoacetylmorphine, heroin, methadone, nicotine, noscapine	DART-MS	Positive	Fingerprint lifting tape, ceramic tile	Powder dusting with silicon-CB particles	[108]
Diazepam, cocaine	DART-MS	Positive	Pre-coated and conditioned mesh	Mesh is dipped in sample and rinsed prior to the testing	[109]
Dimethylamine	DART-MS	Positive	Powders, tablets, capsules, urine	No	[110]
3,4-dimethylmethcathion (3,4-DMMC), 4-Ethylmethcathion, 2-methylmethcathion, 3,4-DMMC metabolite, pentedrone metabolite, mephedrone metabolite	DART-MS	Positive	Spiked urine on sample cards	No	[76]

### 1.6.3 Chemical warfare agents (CWA)

The security threats posed by chemical and biological warfare agents are of high importance, techniques used in this space must be rapid, accurate and able to analyse samples that vary in size, shape and composition. Ambient mass spectrometry is ideal for this purpose, and indeed the first DART article envisioned this as a potential application of this technology. The first paper detailing the use of DART for quantitative analysis of CWAs showed the detection of sulfur mustard, tabun, and sarin. All the compounds formed positive adducts (including  $[M+OH]^+$  and  $[M+NH_4]^+$ ), and were detected with LoDs of 5ppb when coupled to an AccuToF mass spectrometer [111]. DART has also been used to assay the toxicity of ricin when interacting with DNA, demonstrating the ability of DART for more than just screening and quantitative work in this space [112]. DESI-MS for direct analysis of SPME fibres has allowed detection of tabun [113, 114], sarin [113, 114], cyclohexyl methylphosphonofluoridate [113], soman [113], triethyl phosphate [113, 114], and sulfur mustard [114]. Detection was achieved on a variety of surfaces the compounds were spiked onto, including textiles, paper and plastic. Direct SPME fiber detection of tabun using DESI has also been demonstrated from spiked 'office-like' surfaces such as carpet, fabrics, photocopy paper, and sampling swabs typically used for collection of this material from surfaces [113, 114]. Other compounds including ethyl tetramethylphosphorodiamidate, diethyl dimethylphosphoroamidate, ethyl isopropyl dimethylphosphoroamidate, diisopropyl dimethylphosphoroamidate and triisopropyl phosphate, soman, and sarin were detected. Results were compared with an LC-MS method and it was found that the DESI-MS/SPME method was more efficient for extraction of these compounds.

The experiments discussed above are unusual in that they use the CWAs themselves. Far more research concerning CWA analogues are used due to their diminished toxicity yet similar analytical characteristics. Nerve agent simulants such as dimethyl methylphosphonate (DMMP) (a sarin analogue) has been used in a number of DART and DESI studies. DMMP and a related compound, diisopropyl methylphosphonate (DIMP) were detected by DART coupled to a Fourier Transform-ion cyclotron mass spectrometer to determine the chemical signatures of the two compounds [115]. The same compound was used for an experiment to discern the optimal spatial and temperature parameters for increased ion abundance in DART-MS [116]. The same compound was analysed using drift-tube ion mobility spectrometry, where it was found that in the optimised configuration DMMP was detected 95% of the time at a concentration of 0.28%v/v [117].

For DESI analysis, most work has involved the use of SPME fibres, with 'direct' detection from the fibres themselves [27]. Using these methods, DESI has been involved in the detection of DMMP [50, 52, 68], malathion [118], dichrotophos [118], methylphosphoric acid (MPA) [119], ethyl-

methylphosphoric acid (EMPA) [119], and isopropyl-methylphosphoric acid (IMPA) [119]. DMMP detection using headspace SPME was demonstrated using filter paper and a stainless steel capillary, with the potential for in-situ analysis with the use of portable MS [52]. Non-proximate detection of DMMP on paper, plastic (laptop computer) and metal was also demonstrated [50, 68], using the same set-up as that discussed for the detection of explosive compounds. This is one of the biggest advantages of using an instrument such as DESI, the potential to detect multiple compound classes (illicit drugs, CWAs and explosive residues) on the same surface, with no sample preparation [50]. Organophosphate pesticides malathion and dichrotophos (considered appropriate analogues for many low volatility CWAs) were detected from glass, PTFE, and paper with an LoD as low as 100pg [118]. Although less utilised in the analysis of CWA, reactive DESI has been shown to enhance the selectivity of MPA, EMPA and IMPA analysis from Teflon and glass surfaces [119]. In most studies presented here, DART/DESI were less sensitive than most GC/LC-MS methods, but offer the advantage of speed and minimal sample prep, which is vital for these analyses, where analysis is so often urgent.

#### 1.6.4 Inks and documents

The forensic analysis of inks and documents can determine the presence of alterations, common origin of documents, and in some cases, the age of the document [120]. Common methods for ink analysis include Raman, FTIR, ultra-violet/visible microspectrophotometry (UV-VIS MSP), and thin layer chromatography (TLC). TLC in particular is a destructive method that separates ink components for comparison to a potential source [121]. Ambient MS analysis of inks offers both chemical and spatial information, with component mapping having been demonstrated a number of times. DESI-MS in particular has been used for the provision of molecular and spatial information. Ifa et al. have demonstrated the use of DESI-MS imaging to identify amendments to a date made with a different ink to the original markings [121]. If a large surface area of an exhibit is rastered, post-processing can produce maps of specific ions to show areas of alteration. Typical resolution for these DESI-MS experiments falls between 150-300 $\mu$ m [7], which is more than enough for the spatial information typically required for forensic applications. This spatial approach has also been demonstrated for the identification of ink components pre-separated on TLC plates [122].

Molecular information has been used to differentiate between a large number of ballpoint, gel and fluid inks [123]. The deposited inks were of different ages, having been made between 7 weeks and 16 months prior to analysis. The surface on which the marks were made and the chemical composition of the inks themselves were found to impact the ion abundance, however sufficient differences were observed to allow for the differentiation of almost all the inks. A follow-up study investigated whether the paper on which the ink is deposited affects the MS, the evolution of the MS of a mark over time, and the

classification of an ink according to a spectral library [124]. The results showed that the surface onto which the ink was deposited had little impact on the MS, but that the MS of the ink changed rapidly over the initial lifetime of the mark. Results indicated that the MS results stabilised after approximately one year, but that the period prior to that stabilisation involved a great deal of change in the spectra produced. Finally, the spectral library allowed identification of most of the inks, with the majority of the spectra in the library being related to ballpoint pen inks. DART-MS has been directly compared to another ambient ionisation technique, DSA-ToF, for the detection of ink components [125].

Recent work has demonstrated the potential of DART-MS for the analysis of inkjet inks from printers, and the differentiation of ink brands [126]. TLC methods typically are not able to differentiate between black inkjet ink brands, however DART-MS was shown to offer sufficient spectral information to allow for the differentiation of seven ink brands, based on the manufacturer.

DART-MS has been used to detect and identify the presence of 1- methylaminoanthraquinone (MAAQ), the dye used in exploding security packs contained within banknotes [55, 61, 127]. The exploding packs contain both the dye and tear gas (CS), which is designed to incapacitate the alleged perpetrator, and the combination of these two compounds is considered unique as being from an exploding pack [127]. Limits of detection were reported as 5ppm, with MAAQ also being detected on fabric. Direct analyte-probed nanoextraction used in combination with DART (the same instrument configuration reported for the analysis of explosive residues [61]) detected MAAQ both neat and when deposited as part of a fingerprint on a glass slide [61]. The authors reported successful detection of MAAQ from both the neat deposition and when recovered from the fingerprint. Much like the lubricant example [128], the ability to detect these compounds from fingerprints allows suspect-exhibit connections to be made.

The DSA-ToF has also been used in the analysis of writing inks recently, with the technique being compared directly with DART-MS for this application [125]. The pre-amble to the work details an experiment in which the authors compared DSA-ToF to LC-MS and GC-MS, and found that DSA-ToF detected more compounds than LC-MS but in a much shorter timeframe. This is the only reference to this work within the paper, with the remainder focussing on the comparison between DSA-ToF and DART-MS. The authors highlight that the advantage to DSA-ToF over DART-MS lies in its closed system, where sample introduction is through the sample holder that is held constantly in the stream of nitrogen plasma, minimising ambient air flow into the instrument. One of the drawbacks for using DART is that the sensitivity is reduced by the exposure to the lab atmosphere. This can reduce signal to noise values for analytes of interest, and may result in a reduction in reproducibility between experiments as

the lab conditions change. For this work, a customised sampling train was built to allow the use of the DSA sample holder in the DART source, minimising variability in sampling. Ballpoint pens with different stroke numbers were analysed to determine the limits of the techniques, and to establish a linear range. Following this, samples from the United States Secret Service were obtained to demonstrate the application of DART-MS and DSA-ToF in the analysis of ink on paper. The results for the ballpoint pens showed some overlap between the two methods in terms of the inks they were able to detect, however DART-MS was able to detect two additional inks that DSA-ToF was not able to, and DSA-ToF was able to detect a further four inks than DART-MS. The most important difference between the two instruments was shown to be the ability to visualise the sample as it enters the gas stream. As the DSA source is housed in a closed system, it is very difficult to align the sample with the source and sensitivity suffers as a result. This was seen in the detection of leucocystal violet, where DART-MS was able to detect this compound at 1mm stroke widths, and DSA-ToF was not able to do so until 3 mm was reached. This issue was also seen to impact the repeatability of the DSA-ToF analysis, with sample movement from the middle of the mesh not able to be monitored in the closed system.

Although DESI and DART are less destructive than TLC when it comes to ink analysis, the exhibits are compromised to an extent. The extent of these changes are totally reliant on the solvents used, the flow rate of the solvent (for DESI) and the amount of time that the exhibit is exposed to the ionising material [27]. It has been noted in at least one paper that the position of the paper relative to the source impacts the spectra produced [129], and this must also be taken into account.

#### 1.6.5 Fingermarks

The examination of fingermarks in forensic science is well established as an identification tool. More recent years have seen growth in the research surrounding the other information these exhibits can hold. The oils and other endogenous compounds contained within the ridges of a deposited fingerprint have been shown to contain information about the gender, ethnicity and age of the person who left it behind [8, 130]. DESI-MS has been used to classify volunteer age, ethnicity and gender based on the ratio of lipids taken from the forehead, which was thought to be representative of those compounds that may be found on a fingerprint. Classification based on those ratios was found to be accurate to 89.2% (gender), 82.4% (ethnicity), and 84.3% (age). This method was also applied to overlapping fingermarks deposited by two volunteers of different ages, genders and ethnicities. DESI-MS imaging allowed the differentiation of these two marks using ion maps based on different ratios [130].

Aside from endogenous compounds, the presence of exogenous analytes can give information about what an individual has touched or consumed. Parent compounds are readily transferred in fingerprints

[131], and can either be detected directly from the ridges or used to map the fingerprints. Ifa et al. report resolution of 150  $\mu\text{m}$  for imaging of endogenous compounds and a variety of exogenous compounds (cocaine,  $\Delta^9\text{-THC}$ , & RDX) [132]. This resolution is sufficient to discern ridge detail [131] and could therefore be considered a two-fold source of information: both for identification of an individual and for information about the activities undertaken by that individual prior to fingerprint deposition. These fingerprints were detected on a number of surfaces including paper, plastic and glass [132], demonstrating the applicability of this method to forensic exhibits. Explosive compounds have also been detected on the ridges of fingermarks, with TNT, RDX, HMX and PETN detected on the skin itself, using a chlorine dopant [133]. TNT and oxycodone have been directly detected from doped fingermarks [55], showing that diverse compound classes can be detected using the same instrument from a single exhibit.

Proof of consumption can be achieved through the detection of metabolites on fingermarks, excreted by sweat. Bailey et al. demonstrated the detection of cocaine and its major metabolite, benzoylecgonine from fingermarks [93]. This has also been demonstrated by the detection of loratidine from finger skin after consumption of Claratine [14]. The presence of metabolites on the skin (the sweat of an individual) offers the potential of action based associations to be made, in that the metabolites of an illicit compound are very unlikely to be found on the fingerprint ridges and on the skin of an individual who has not consumed the substance.

Overall, the field of fingerprint imaging and detection using ambient MS methods has the potential to offer a broad range of information. This includes the likely age, ethnicity and gender of an offender, as well as information about where they have been, what they have touched and potentially what they have consumed.

#### 1.6.6 Lubricants

Sexual assault cases often rely on the presence of DNA evidence for the perpetrator to be identified and prosecuted. As assailants become more educated, they are using condoms to avoid leaving this crucial piece of evidence behind, which is further complicating the prosecution of such incidences. The identification and classification of personal lubricants is a rapidly growing field of enquiry, with DART-MS being heavily involved.

Much of the work has involved the development of classification schemes based on common ingredients of the lubricants. Water-based lubricants were classified with 100% accuracy using principal component analysis (PCA) and linear discriminant analysis (LDA). Six groupings related to additives such as anaesthetics, sensation enhancers and flavours were categorised, from a sample pool of 33

lubricants [134]. Similar results have been achieved with silicon-based lubricants, with 37 samples being sorted into eleven classes based on results from DART-MS in both negative and positive ion mode. Multivariate statistics were then used to classify a series of known test samples and a number of 'blind' samples, with a classification accuracy of approximately 92% [135]. Maric et al. have also been involved in building the framework for a lubricant classification database, with further work combining classification of water-based, silicon-based and condom lubricants. In this study, 90 samples were grouped into twelve sub-groups using hierarchical clustering analysis (HCA), PCA and LDA [136]. This work aims to develop a database accessible to forensic practitioners for the identification of lubricant evidence in sexual assault cases. Further work has demonstrated the importance of analysis temperature in the detection of lubricant components. Bridge & Maric compared a low-temperature, high-temperature and thermal desorption/pyrolysis method for the classification of 33 water-based lubricants. The results showed that the low temperature method out-performed the high-temperature method in the desorption and identification of flavour and fragrance additives. The thermal desorption/pyrolysis method was found to offer enhanced differentiation between the samples, owing to the fine control of the temperature and provision of a gradient [137].

The application of these lubricant detection methods have recently been used to detect traces of lubricant in samples mixed with biological matrices. Proni et al. have detected the spermicide nonoxynol-9 mixed with vaginal fluid pre and post coitus [138]. DART was used to directly analyse the swabs and glass rods used to collect the evidence, indicating that contact with lubricants and spermicides can be detected in complex matrices, with no sample preparation. DART was also used to detect and identify lubricant traces in a fingermark deposited on a condom wrapper following condom handling. Three condom brands were purchased and analysed, with chemical compositions of each differing sufficiently to correctly identify the condom handled by the volunteer prior to fingermark deposition [128]. This work suggests that it may be possible to make linkages between victims of sexual assault, lubricants or condoms used in the assault and any residues remaining on an alleged perpetrator.

#### 1.6.7 Gunshot residues

The detection of gunshot residues (GSR) is closely related to the detection of explosive residues, with many of the compounds being of similar structure and class composition. The use of mass spectrometry for the detection of GSR is mostly limited to the detection of the organic components (termed organic gunshot residue, oGSR). Current methods for the detection of these residues are highlighted in the introduction to Chapter Seven and for the purposes of this initial review, only ambient mass spectrometry (DESI and DART) applications for oGSR detection will be discussed here.

Morelato et al. demonstrated the use of DESI-MS for the detection of oGSR components ethyl centralite (EC), methyl centralite (MC) and diphenylamine (DPA) spiked on carbon tape from GSR stubs used on skin [28]. These experiments took place on the same stubs that inorganic GSR is analysed on, without disrupting those analyses, but only EC was detected on the 'real-life' stubs.

Further studies demonstrated EC and MC detection without pre-treatment, using a homemade DESI source. Surfaces interrogated included glass, rubber gloves, leather gloves, human skin, towels, medical gauze, absorbent cotton, and human hair [139]. LoDs of as low as 5pg/cm<sup>2</sup> were achieved (on glass). Additional studies have shown the detection of nitro-DPA compounds arising from propellant degradation, which can assist in the dating of propellant, and in the detection of DPA itself, which can degrade at high temperatures [140]. Double-based smokeless powders were analysed using DESI-MS, where nitroglycerine was detected in positive ion mode as an NO<sub>3</sub> adduct. Nitrocellulose was not detected in positive ion mode, although several non-explosive additives were. The author of that work indicated that these additives may provide a chemical fingerprint to identify smokeless powders and differentiate between them [141].

In more recent years, smokeless powders have been characterised by PCA, HCA and LDA to allow classification and grouping, for identification [142, 143]. The ability to link GSR residues with a brand of ammunition would be of great benefit to forensic science, with current techniques offering not a great deal more than confirmation of GSR presence. Lennert et al. report the use of DART-MS to classify 34 smokeless powders, with results comparable to GC-MS in a fraction of the time [142]. Importantly, they report the detection of N-nitrosodiphenylamine [142], which typically degrades under GC-MS conditions [141]. Further work by the same team applied thermal desorption high resolution DART-MS (TD-DART-HRMS) to smokeless powders, and again compared the results directly to TD-DART. Comparison between DART and DART-HRMS showed that DART-HRMS was the most robust of the two techniques [143]. These studies demonstrate the potential of DART-MS for the screening of GSR.

Williamson et al. describe the coupling of capillary microextraction of volatiles to DART MS (CMV DART MS) for the detection of oGSR compounds in the air surrounding human skin [144]. Targeted compounds (nitroglycerine, diphenylamine, ethyl centralite, dinitrotoluene, methyl centralite, trinitrotoluene, nitrosoDPA, nitroDPA, diethyl phthalate and dibutyl phthalate) were detected at concentrations of 15ng in 2.5L of air [144]. The experiment was designed to simulate the sampling of air around the hand of an alleged shooter, and with portable MS technologies may allow for in field, non-invasive screening for GSR residues.

### 1.6.8 Broader ambient ionisation evaluation

A recent paper by the British Mass Spectrometry Society summarised the results of two interlaboratory studies on ambient mass spectrometry, confirming a number of the issues discussed earlier [145]. It was the first paper of its kind, assessing the limitations and capabilities of a number of ambient ionisation techniques. The first study assessed the quantitative and qualitative capabilities, the second investigated the repeatability and robustness of the methods. For the first study, data were recorded from five types of ionisation techniques: ASAP, DART, atmospheric pressure MALDI, thermal desorption corona discharge ionisation (TD-CDI), and automated nanospray (Nanomate, as a substitute for liquid extraction surface analysis, LESA). These instruments were located in nineteen laboratories, based both within the UK (14) and externally (5). Ten samples were sent to each lab, containing analytes such as paracetamol, TNT, HMX, cholesterol, aldrin, PEG 1500, diesel 0.1% in isooctane, and cough syrup. Two of the samples were calibration sets of paracetamol and TNT. The samples submitted to the labs for study one were designed to cover a broad range of chemistries, polarities and matrices in order to truly test the capabilities of the techniques in use. Study two involved 24 laboratories across four countries, and seven different ambient ionisation techniques: ASAP, DART, DESI, LESA, Secondary electrospray ionisation (SESI), TD-CDI, AP-MALDI, and paperspray. For this work, two samples were sent to each lab, with eight components in each sample. The two samples contained the same components at the same concentration, but in different matrices: one in acetonitrile, the other in Surine (a synthetic urine, acting as a complex matrix in this study). For both studies, the protocols were kept deliberately vague, with instructions to only analyse as the lab typically would, using the ambient ionisation technique of choice.

The results from study one showed that only three of the labs involved were able to detect all analytes submitted. General trends indicate that the polar compounds were detected more consistently than the nonpolar, compounds analysed in negative ion mode were not detected as well as those in positive ion mode, and finally that PEG 1500 detection was variable in nature across a number of the labs involved. What this work showed was that the results obtained from ambient ionisation, regardless of the instrument used, will vary based on the analyst performing the work, the methods used and the environment in which the work is performed.

This was further confirmed based on the results from study two, where it was shown that typical repeatability was greater than 50%, based on peak area alone. This was greatly improved with the inclusion of a matched internal standard (ISTD), which gave the best repeatability. Use of a non-matched internal standard improved the repeatability relative to the peak response alone, but not to the degree of a matched ISTD. That is to say, use of peak response alone cannot be relied upon for

quantification, but use of a ratio to an internal standard (matched or not, depending on availability) can improve results substantially. Study two also demonstrated that there is a deleterious effect on the detection, peak response and ratio precision, arising from the range of instruments (and associated ionisation mechanisms) and sampling techniques across the participating laboratories, and the inclusion of a matrix. These issues severely reduced the repeatability of the analyses. A number of labs countered the matrix effects by introducing temperature ramps or altering their sampling techniques through inclusion of a clean-up step (SPME or similar). Ultimately, the use of ambient ionisation (regardless of the instrument) was shown to be highly reliant on the instrument, and the analyst performing the work.

## **1.7 Conclusions**

This review has demonstrated that the use and potential use of ambient mass spectrometry for forensic purposes is extensive and wide-reaching. However, for the techniques to be integrated into regular use, there are some serious deficiencies that need to be addressed.

The first is the high backgrounds that many of these techniques suffer from. The presence of a large amount of background noise arising from atmospheric background, chemical noise from any matrices, and instrumental noise complicates the identification and detection of unknown compounds. These instrument types are often touted as a fantastic method for the detection of unknown compounds, as they don't require finicky fine-tuning of separation methods often required for chromatographic based methods. So, without the ability to accurately and simply detect and identify unknown compounds (due to these high backgrounds), this 'benefit' is not much of a benefit at all.

In addition to high background issues, ambient ionisation methods do not have the ability to resolve isobaric compounds, which are typically separated by chromatography prior to detection in more commonly used LC and GC methods. High resolution mass spectrometry may assist in the identification of isobaric compounds, but this calibre of instrument can be financially prohibitive to some labs, which may reap more benefits from a less sensitive mass spectrometer with chromatography on the front end.

These complicating factors may limit the use of ambient mass spectrometry to qualitative applications only, with some limited quantification ability where matched internal standards are available. Even in these cases, the results of the interlaboratory study [145] indicate that the methods used must be meticulously consistent with all factors concerned to reduce repeatability errors. Without consistency between analysts, sampling methods, instrument settings, and environmental factors the results of any quantitative measurements may not be reproducible.

Opting to use instruments for qualitative purposes could offer benefits to a lab in terms of screening efficiency, particularly for targeted analysis. However, screening samples that are of unknown concentration and origin offers an alternate set of challenges. As reported by Queensland (QLD) Health, testing samples without sample preparation may lead to contamination of the instrument, causing carry-over. In these cases, sample prep and clean-up would be required, further increasing the time of analysis.

Overall though, should these issues be resolved sufficiently to allow routine use in forensic laboratories, the benefits will be immense. The extreme rapidity of ambient ionisation, combined with the possibilities for fully comprehensive analysis of complicated samples in matrices make investigated and combatting the issues discussed above a priority. Compounds analysed in this manner will not experience being stuck on a column, suffer from poor resolution or retention and will not influence detection based on the polarity of the molecules themselves.

Ultimately, ambient ionisation should (and will continue to) be investigated thoroughly to bring these techniques to the forefront of analytical chemistry. Despite the challenges that exist for those already established instruments, new ways of working with the technology and new methods are emerging constantly. Emerging technologies should be evaluated to determine if they suffer the same shortcomings as those more well-known methods (DART, DESI). The earlier described instrument, DSA-ToF, is one such instrument that has not been explored fully. Therefore, there is a need to determine the instruments strengths, weaknesses and potential applications in order to complement the already existing suite of knowledge about ambient ionisation.

## 1.8 Research overview

This work aims to evaluate the potential of the Perkin Elmer Direct Sample Analysis ionisation platform, coupled with the AxION 2 Time of Flight Mass Spectrometer (also by Perkin Elmer) for its application to forensic science. This thesis will focus on illicit drugs and toxicology and gunshot residues, with a small investigation into the use of this platform for the detection of compounds in exhaled breath.

**Chapter two** will detail the initial establishment of optimal parameters for operation of the instrument, including physical and chemical alterations to the sampling platform. **Chapter three** investigates the detection of illicit drugs in solution, from a quantitative and qualitative standpoint. **Chapter four** extends this work to the detection of these same drugs in saliva, testing the ability of the instrument to detect small molecules in complex matrices. **Chapter five** demonstrates the ability of DSA-ToF to detect and profile the uptake and elimination of exogenous compounds from exhaled breath. Finally, **chapter six**

details the development of a method for the detection of organic gunshot residues that seamlessly integrates into the current analysis protocols.

The combination of this work will demonstrate that DSA-ToF is a suitable analysis technique for a number of forensic applications. The initial chapters will highlight a number of issues with the method that should be addressed in order for the technique to be fully suitable. The latter chapters demonstrate applications of the technique despite not having fully addressed these issues, which further proves that the technique would be highly beneficial once these are addressed.

## Materials and methods

The information below is true for all analysis within this thesis. Sample preparation and more specific information relating to individual chapters are included within the relevant chapters themselves.

### Standards and solvents

All drug standards and internal standards were all provided by Forensic Science South Australia (Adelaide, South Australia). Ethanol (EtOH), methanol (MeOH) and acetonitrile (AcCN) were provided by Sigma Aldrich (Sigma-Aldrich, Castle Hill, NSW). MilliQ was obtained from a Synergy water purification system (Merck, Darmstadt Germany).

### Preparation of drug solutions

Drug solutions were made up using a 100 $\mu$ g/mL stock (FSSA, Adelaide, SA). Working solutions were prepared to a final volume of 500 $\mu$ L in EtOH, and stored at 4°C for no longer than two weeks. Subsequent dilutions were performed on the day of analysis in milliQ water. Deuterated internal standard working solutions were prepared from 100 $\mu$ g/mL solutions (FSSA, Adelaide, SA). ISTD stocks were prepared by diluting to 10 $\mu$ g/mL in EtOH and were stored at 4°C. Subsequent dilutions were performed on the day of analysis to 200ng/mL, in the same solutions as the corresponding parent drugs.

### Plasma cleaning protocol

Plasma cleaning of DSA-ToF mesh provided by Perkin Elmer was performed using a Plasma Etch 25 series plasma system (Plasma Etch, Carson City, Nevada). Plasma cleaning times were between 2-10 minutes, with gas flow rates of 10cc/min into the instrument. Plasmas were generated at RF powers of 100 watts, with five full size mesh samples being etched at one time. Argon and oxygen gas for plasma cleaning purposes were purchased from BOC (NSW, Australia).

Instrumental plasma cleans were performed in the DSA-ToF, with 30 second nitrogen plasma exposure times per sample position. Nitrogen gas for use in the instrument was purchased from BOC (NSW, Australia). Analysis, unless otherwise specified was performed on instrument-plasma cleaned mesh.

### Instrumentation

DSA-ToF MS analysis was performed on an AxION DSA (Perkin Elmer, Waltham, MA), coupled with an AxION 2 Time of Flight Mass Spectrometer (Perkin Elmer), operating at a resolution of approximately 8,000 at  $m/z$  622.0290. The mass spectrometer scanned across a range of  $m/z$  100-1000 in positive ion mode, with a spectral acquisition rate of 1 spectrum/second. DSA heater was set at 350°C, with a nitrogen gas pressure of 90psi. Calibrant masses of  $m/z$  121.05087, 322.0500, 622.0300 and 922.0100 were utilised for external calibration, sourced from an APCI tuning mix, diluted 1:10 in acetonitrile fresh on the day of analysis (Agilent Technologies, Santa Clara, CA). Calibrant peaks of  $m/z$  121.05087 and 322.05000 were used for lockmass calibration, which

was performed on Perkin Elmer ToF MS Driver software (Perkin Elmer). Sample analysis time was approximately 30 seconds per sample, with each measurement stored in a single file, rather than multiple samples per file, and performed in triplicate where sample volume allowed.

DSA gas flow and heaters were turned on for one hour prior to the analysis to improve instrument stability. Nitrogen gas was sourced from the nitrogen boil-off from liquid nitrogen contained in a Dewar vessel (BOC Adelaide, South Australia). APCI tuning mix was run through the system for the entire duration of analysis, at a flow rate of 10uL/min. Instrument parameters are defined in Table 3

Table 3: General DSA-ToF settings for analysis

Parameter	Setting
Corona voltage	4.0µA
Endplate voltage	-200 volts
Capillary entrance	-800 volts
Drying gas flow	3.0 L/min
Drying gas heater	25°C
Nebulizer gas	90 psi
Auxiliary gas	4.0 L/min
APCI heater	350°C

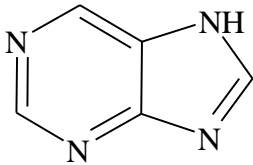
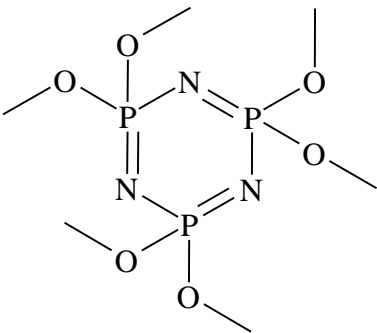
## Data extraction and analysis

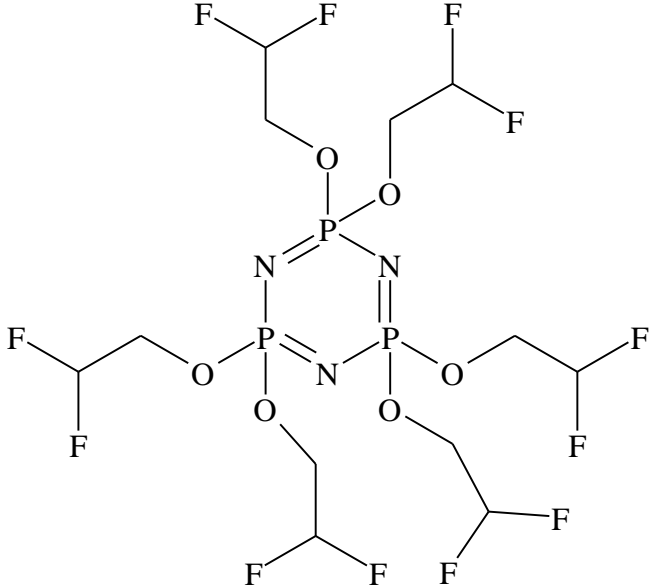
Mass spectra were extracted from the raw data using the Perkin Elmer ToF Driver program. Although there is no 'chromatogram' in the typical sense of the word, there is a profile of ions detected over time. This can have the appearance of a chromatogram and can even function in a similar way when specific ions are being sought. That is, a profile of the detection activity over the time of acquisition is produced following the acquisition process. If the analyst is searching for a particular ion, this can be searched for, producing a graph of that ion's intensity over the time of acquisition, showing when the analyte was desorbed and detected. Once the time frame of maximum ion intensity is known, the mass spectra at this point can be extracted by either clicking on the apex of the peak, or by clicking and dragging across the base of the peak. Clicking on the apex of the peak gives the mass spectra at the maximum intensity, giving a higher signal to noise ratio for the peak of interest. Clicking and dragging across the base of the peak averages the spectra for that entire time, which can give a higher peak intensity, but also may result in a lower signal to noise value (as the noise is also being averaged).

For the analysis discussed herein, the base ion chromatogram (BIC) was extracted from the total ion chromatogram (TIC), to give a clearer indication of when the analyte of interest was taken into the mass spectrometer, and therefore where the intensity of the ion would be highest. The mass spectra were obtained by manual averaging of the spectra across the BIC peak, and determination of the intensity of the ion peaks was performed in the ToF Driver program.

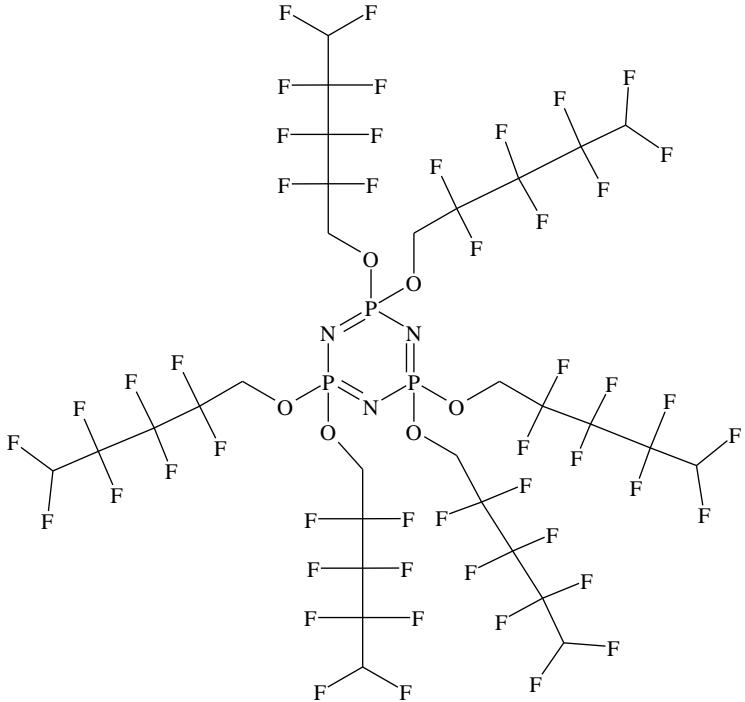
Mass lock calibration was performed by selecting two of the calibrant peaks on either side of the target mass, with peak masses within that range shifting based on the divergence of those two calibrant masses from their expected mass. The calibrant masses, formula and structures in the APCI-ToF tuning mix (Agilent Technologies, Santa Clara, CA) can be found in Table 4.

Table 4: Composition, molecular formula, molecular weight and structure of compounds in the APCI tuning mix

Compound name	Molecular formula	Protonated molecular weight	Structure
Purine	$C_5H_4N_4$	121.05	 <p>The structure of purine is a fused bicyclic system consisting of a six-membered imidazole ring fused to a five-membered imidazole ring. It features two nitrogen atoms in the six-membered ring and one nitrogen atom in the five-membered ring, with a hydrogen atom attached to the latter.</p>
Hexamethoxyphosphazine	$C_6H_{18}N_3O_6P_3$	322.05	 <p>The structure of hexamethoxyphosphazine is a six-membered ring containing three phosphorus (P) and three nitrogen (N) atoms in an alternating arrangement. Each phosphorus atom is bonded to two methoxy groups (-OCH<sub>3</sub>), and each nitrogen atom is bonded to one methoxy group. The ring is formed by alternating P=N and N=P double bonds.</p>

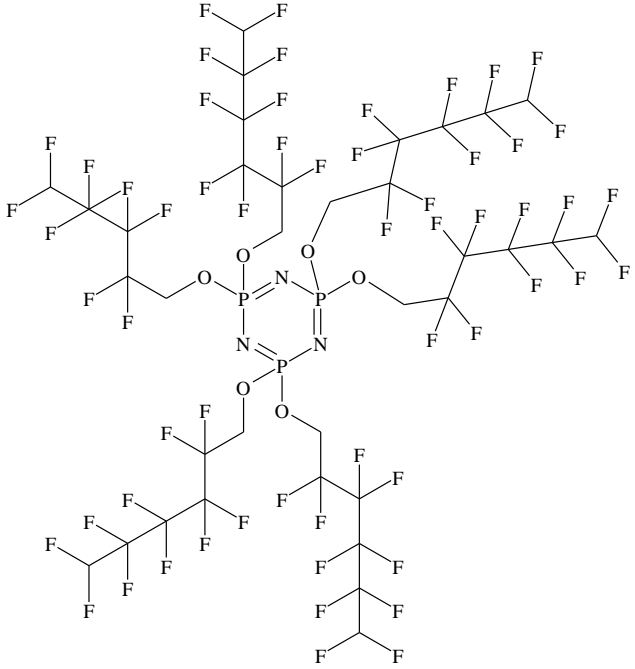
<p>Hexakis(2,2-difluoroethoxy)phosphazine</p>	<p><math>C_{12}H_{18}F_{12}N_3O_6P_3</math></p>	<p>622.03</p>	 <p>The image shows the chemical structure of Hexakis(2,2-difluoroethoxy)phosphazine. It features a central phosphazine ring consisting of three phosphorus (P) and three nitrogen (N) atoms in a six-membered ring. Each phosphorus atom is double-bonded to a nitrogen atom and single-bonded to two oxygen atoms. Each nitrogen atom is double-bonded to a phosphorus atom and single-bonded to one oxygen atom. The six oxygen atoms are further bonded to six 2,2-difluoroethyl groups, each represented as a -CH<sub>2</sub>-CF<sub>2</sub> group.</p>
---	---	---------------	---

<p>Hexakis (1H, 1H, 3H-tetrafluoropropoxy)phosphazine</p>	<p><math>C_{18}H_{18}F_{24}N_3O_6P_3</math></p>	<p>922.01</p>	
---	---	---------------	--

<p>Hexakis (1H, 1H, 5H- octafluoropentoxy) phosphazine</p>	<p><math>C_{30}H_{18}F_{48}N_3O_6P_3</math></p>	<p>1521.97</p>	
--	---	----------------	---

<p>Hexakis (1H, 1H, 7H-dodecafluoroheptoxy) phosphazine</p>	<p><math>C_{42}H_{18}F_{72}N_3O_6P_3</math></p>	<p>2121.93</p>	
---	---	----------------	--

<p>Hexakis (1H, 1H, 4H-n hexafluorobutyloxy) phosphazine</p>	<p><math>C_{24}H_{18}F_{36}N_3O_6P_3</math></p>	<p>1221.99</p>	
--	---	----------------	--

<p>Hexakis (1H, 1H, 6H-decafluorohexyloxy) phosphazine</p>	<p><math>C_{36}H_{18}F_{60}N_3O_6P_3</math></p>	<p>1821.95</p>	
--	---	----------------	---

## 2 Development of DSA-ToF method for the detection of MDMA, cocaine and THC

### 2.1 Introduction

Direct sample analysis time of flight mass spectrometry (DSA-ToF) has many advantages over traditional mass spectrometry techniques employed in typical forensic laboratories, notably over chromatography-based methods such as liquid and gas chromatography. These methods involve a great deal of labour for the analysts working on the analysis, as well as the consumption of solvents and gas during the analysis. These methods also typically are time-consuming from a further two perspectives. The first being that the analysis itself; with the separation of compounds on the column taking a considerable amount of time, depending on the complexity of the matrix and the amount of sample preparation undertaken prior to analysis. These sample clean-up steps must be performed in order to reduce the time spent on the columns for chromatographic analysis, and overall time spent on the analysis. The second problem to consider with column separation-based methods is that there is a great deal of method development to perform, both when starting to construct the method and when considering the addition of any other analytes to the mix. When unknown or new compounds are encountered, the separation method must be evaluated at the very least and altered to improve separation if necessary. These alterations can have impacts on the retention time, resolution and peak shape of other compounds, which can cause additional problems for the analyst.

For these reasons, the DSA-ToF could be considered as a simpler and faster instrument for use in similar analysis types. As DSA is an APCI method, there is no column and therefore no separation. This reduces the complexity and time for method development substantially, while also reducing the total analysis time. Data are obtained within 30 seconds of introduction into the instrument, with any data processing contributing little to the total time from sample introduction to results obtained. The lack of chromatograms means there is no peak integration or retention time to be calculated, further reducing complicated data analysis and time for review.

On top of this, no solvents are consumed in the use of the instrument, with the samples being pushed into the instrument by the nitrogen plasma. As there is no column, there is also no need for extensive sample clean-up procedures, with the only reason to clean up the sample being the concentrate the analyte and produce a less convoluted mass spectrum.

The DSA system on the front end of the instrument has not yet experienced widespread usage, and as such, there were few methods available to utilize as a base for any of the methods developed in this work. Although the appeal of the DSA-ToF lies in the ease of method development, there are still external conditions that may contribute to reductions in ionisation and sensitivity. For forensic purposes, this is particularly important, as the need for sensitivity is paramount. The very nature of the DSA-ToF, being that it ionises at atmospheric pressure, relatively open to the air, opens it up to outside interferences. Not only that, the sample delivery system itself is not designed to be as controlled as the non APCI techniques (chromatography-based techniques). For chromatography-based techniques, the delivery of the sample into the mass spectrometer is controlled, and through a small opening, which ensures that the entirety of the sample is delivered into the system. The DSA system, however, has a larger sample introduction area, where the sample is ionised, and then delivered into the mass spectrometer by the nitrogen plasma stream. However, the diameter of the nitrogen stream is smaller than that of the sample platform, meaning the entire surface of the mesh is not hit by the nitrogen plasma during exposure [4]. The benefit of this is that there is less chance that there will be contamination and carry-over from previous samples (as the sample holder is re-used consistently). The biggest drawback though, is that the sample spot loaded onto the mesh must be in the correct position during the ionisation, otherwise the sensitivity of the method is reduced substantially. In addition, there have been experiments that show other atmospheric pressure-based instruments (such as DESI) are subject to outside interference and contamination from atmospheric contaminants. The DSA in particular is vulnerable to outside interferences, not necessarily from contaminants, but from water in the atmosphere, as well as in the external calibrant solution being run through the system during analysis. Furthermore, the movement of the sample stage from the load or home position to the plasma stream can often result in the movement of the sample droplet, and result in a loss of sensitivity and carryover to the sample that will be placed on that spot in further analysis.

Other issues to consider include the heating of the mesh, which is integral to the ionisation process. The mesh itself is one continuous piece, that when exposed to the 350°C temperatures achieved by the plasma heats up a great deal. This leads to adjacent heating of samples, which may result in the premature ionisation and removal of sample from the samples yet to be exposed to the plasma, and the potential degradation of temperature sensitive analytes. This would also result in a reduction in sensitivity and opens the system up to contamination issues. The software itself also does not allow for the individual analysis of sample spots beyond the first one in the sample holder. In order to analyse samples on spot 2-13, the instrument passes the plasma over each of the sample spots for approximately 2 seconds. This contributes

to both the adjacent heating and the carry-over problem, particularly when working with samples of high concentrations or those with dirty and complex matrices.

Other problems to consider are the presence of contaminant peaks in the mass spectra from the calibrant solution, particularly when acetonitrile is used as the solvent. The calibrant also contributes to variability in the signal intensities produced by the analytes of interest, through inconsistencies in the pumping over the period in which the syringe pump is starting up. The syringe pump is an external piece of software, not integrated into the DSA system, which is another source of variability. It follows that the flow rate of the calibrant is also something that must be considered when creating a method, as faster flow rates push more calibrant through the system. Higher calibrant flow rate delivers more water, potentially increasing the number of water clusters formed, which may lead to an increase in ionisation potential for the analytes being measured.

Although there are a great deal of external parameters that need to be considered, the ease of use of the instrument, and versatility of analyte detection still result in an instrument and method that meet the requirements initially laid out: rapid, high-throughput, accurate and sensitive. This chapter details the method development for the detection of THC, MDMA and cocaine, with the aim to result in a method that can be utilised for a variety of analytes of forensic interest.

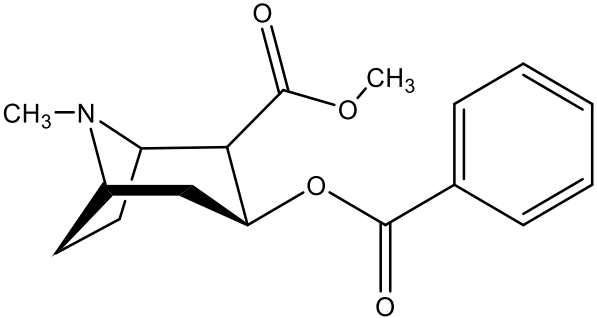
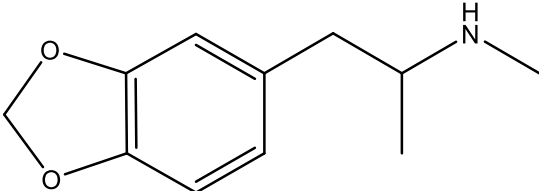
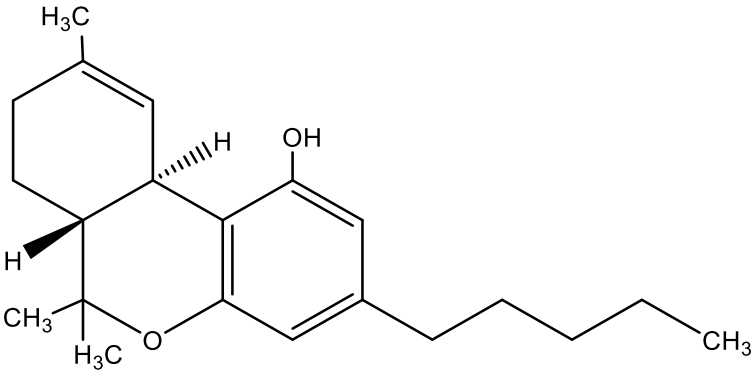
## **2.2 Accurate mass identification**

The three illicit drugs chosen for this analysis were THC, MDMA, and cocaine, as these are three of the more commonly analysed drugs in routine testing [146-148], either by typical toxicology methods such as LC/GC-MS or by the roadside drug testing apparatus. In the case of the roadside apparatus, THC, MDMA and methamphetamine are currently tested for, using their immunoassay devices [149].

### **2.2.1 Accurate mass identification of THC, MDMA and cocaine**

10 $\mu$ L of 200ng/mL MDMA, THC and cocaine were analysed in triplicate using the DSA-ToF. Formula matching software via the ToF Driver software was used to search the PubMed database, using the molecular ion peak and two additional isotopes. Error was determined through comparison of observed masses and intensities of the molecular ion peaks and related isotopic peaks and that which was expected based on the database, expressed as ppm. The calculated parent drug and molecular ion weights, alongside the structures of the drugs of interest can be found in Table 5.

Table 5: Molecular weights, protonated weights, structures and chemical formulae of MDMA, THC and cocaine

Drug name and formula	Molecular weight	Molecular ion weight	Structure
Cocaine $C_{17}H_{21}NO_4$	303.1471	304.36704	
MDMA $C_{11}H_{15}NO_2$	193.1103	194.25432	
THC $C_{21}H_{30}O_2$	314.2246	315.47767	

The total ion chromatograms (TIC) for the analysis of these simple drug solutions in water presented a new problem with the use of this instrument. The TIC shows two points at which ions are moving from the mesh into the mass spectrometer, which indicates there is a split in the total number of ions (Figure 6).

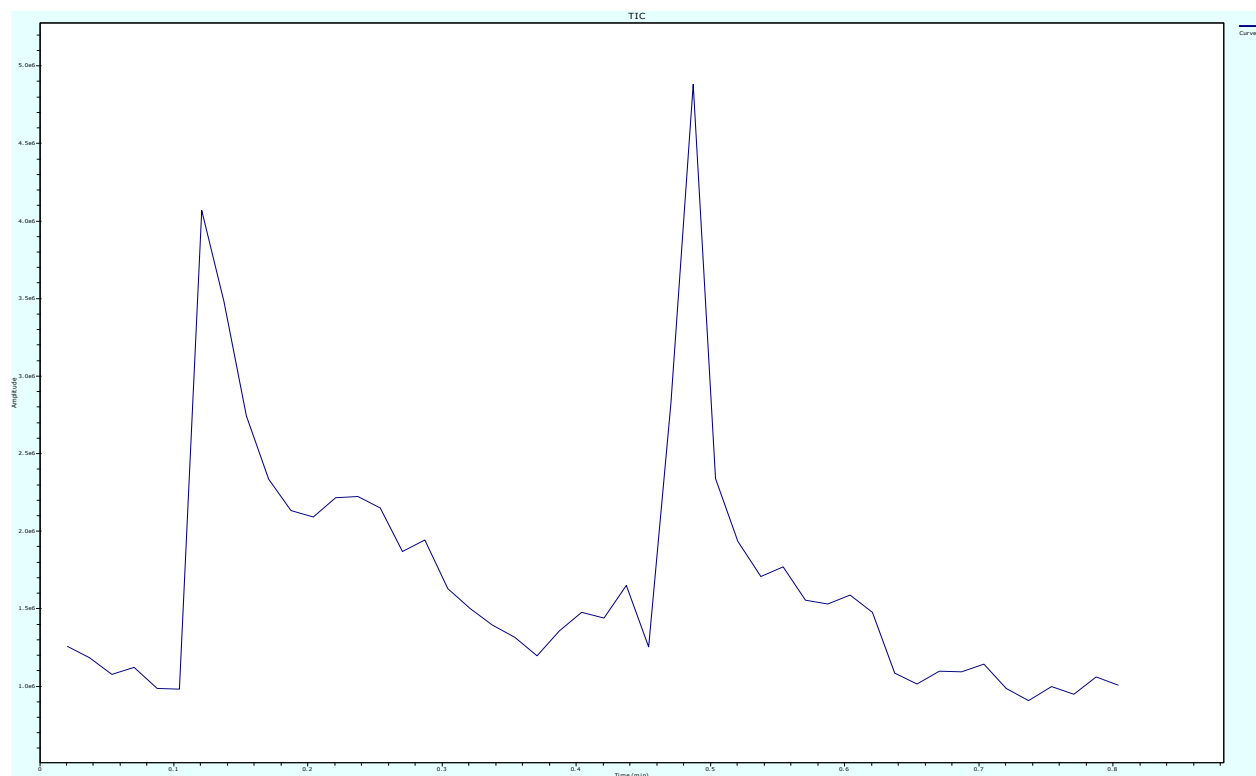


Figure 6: Total Ion Chromatogram for the deposition of a solution of 1000ng/mL cocaine in water on untreated mesh. X-axis is time (sec), y-axis is intensity (a.u).

In order to determine when the ions of interest are entering the mass spectrometer, the Base Ion Chromatogram (BIC) needs to be extracted. This isolates the peak at which the molecular ion of interest (in this case, cocaine) is located with the highest signal intensity (Figure 7).

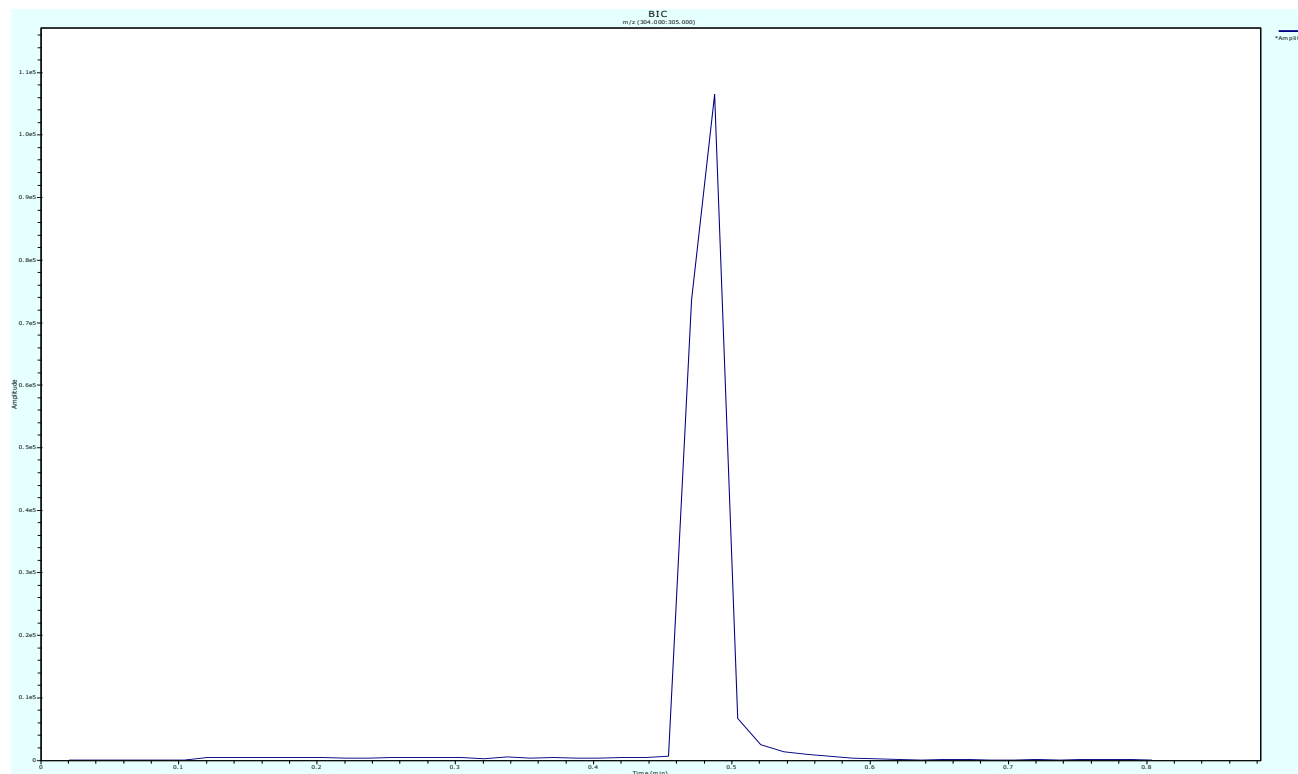


Figure 7: Extracted Base Ion Chromatogram for m/z 304-305 for injection of a solution of 1000ng/mL cocaine in water on untreated mesh. X-axis is time (sec), y-axis is intensity (a.u).

From here, a mass spectrum can be extracted from the BIC ion peak by averaging across the base of the peak. This method of analysis ensures that the maximum amount of analyte is identified through the extracted mass spectrum, by averaging the spectra from all points across the peak.

Using the DSA-ToF, the three analytes of interest were identified with mass errors of less than  $\pm 10$ ppm. The ppm errors associated with each of the drugs are outlined in Table 6.

Table 6: Mass error associated with the accurate mass identification of cocaine, MDMA and THC

Drug name	Average error (ppm)
Cocaine	+1.19
MDMA	+6.77
THC	+5.22

The spectra of the identified drugs can be seen in Figure 8 Figure 9, & Figure 10, for cocaine, MDMA and THC respectively, showing the molecular ion for each drug, and the two isotopes used for identification purposes.

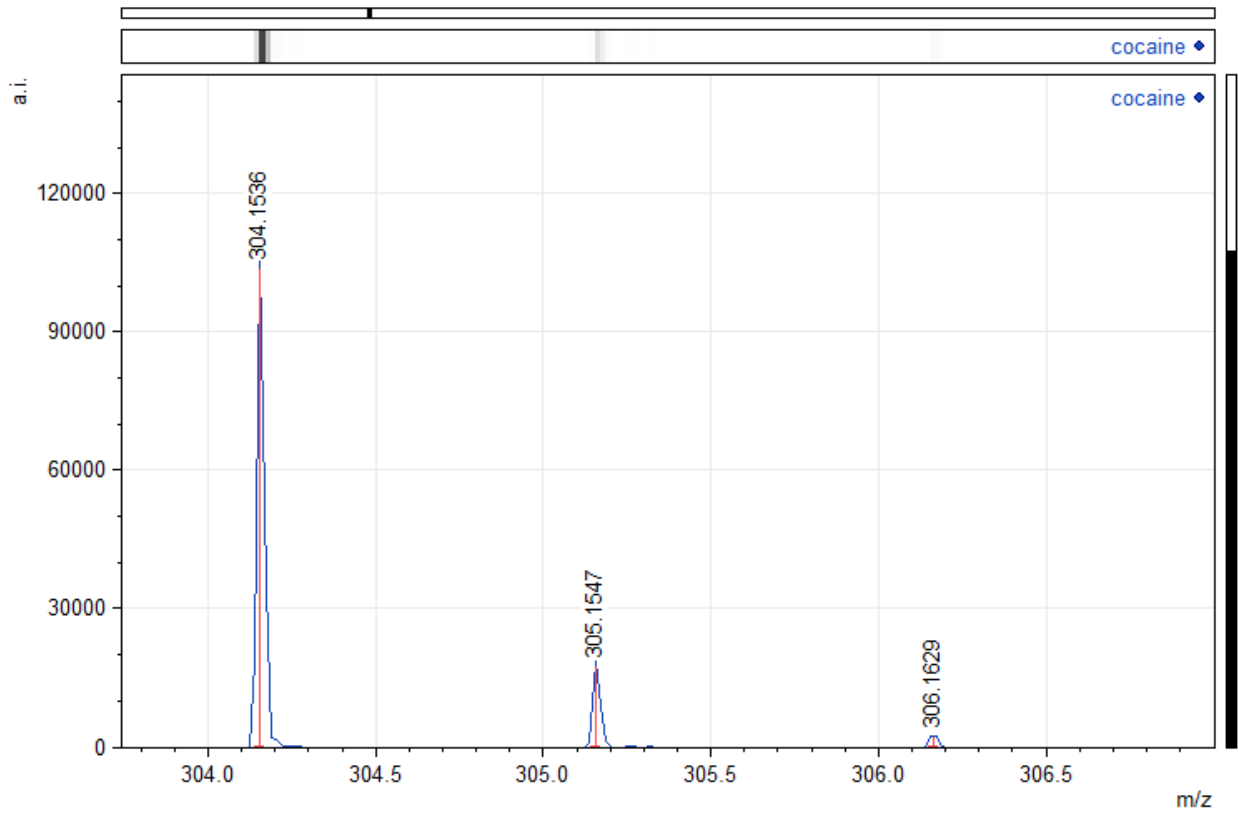


Figure 8: Representative mass spectrum of 200ng/mL solution of cocaine in water on mesh

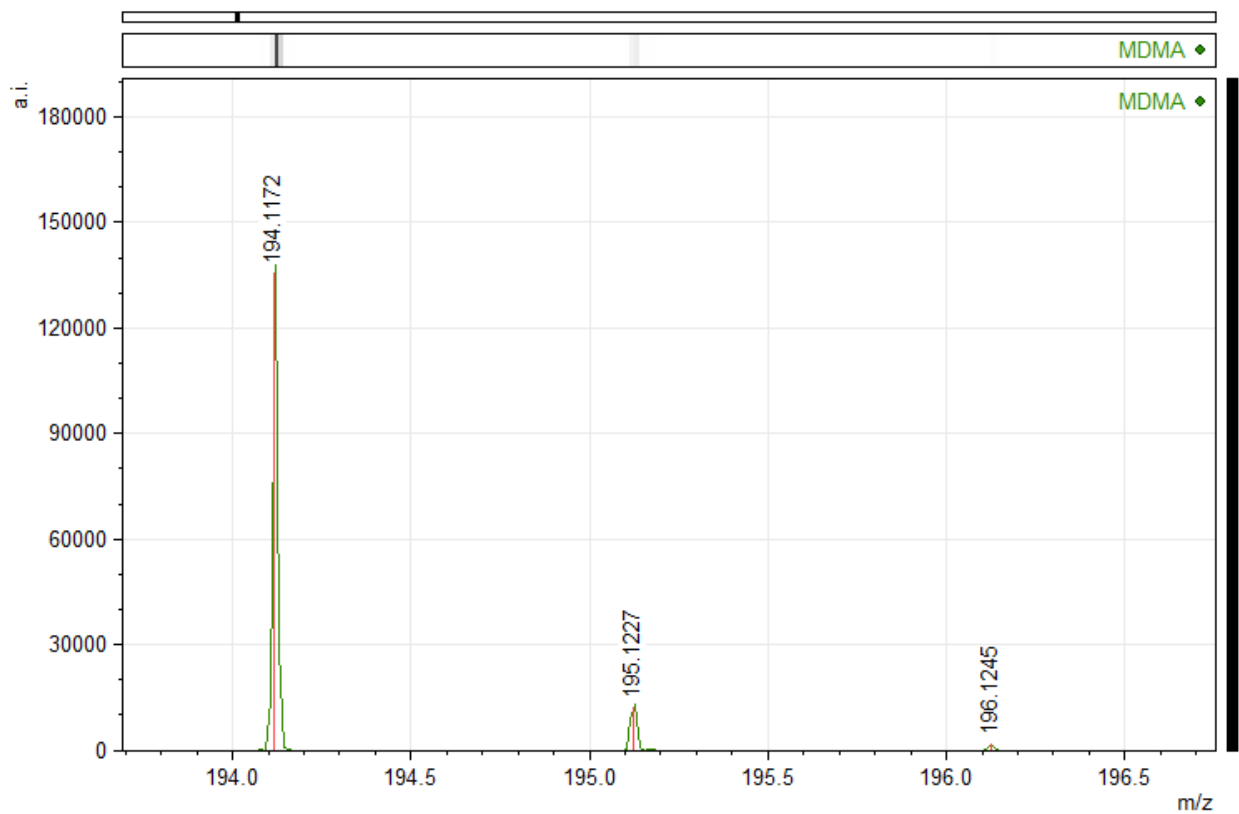


Figure 9: Representative mass spectrum of 200ng/mL solution of MDMA in water on mesh

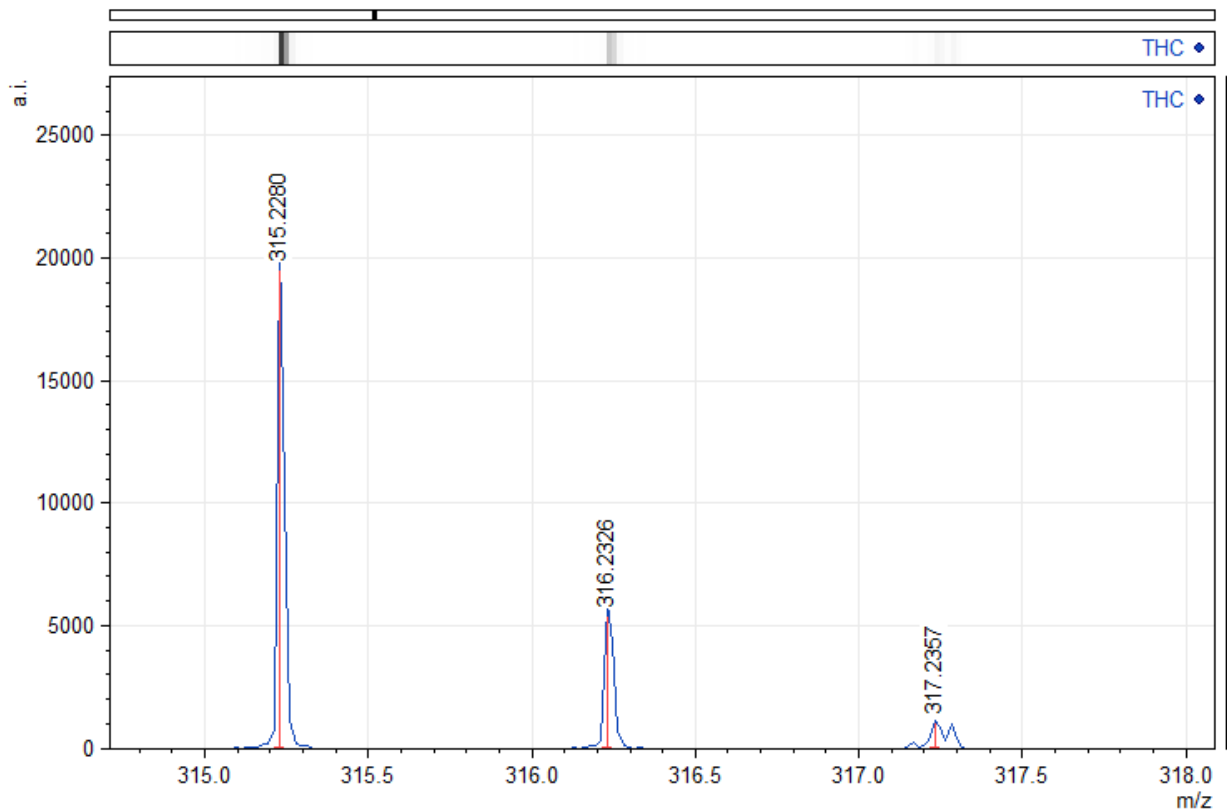


Figure 10: Representative mass spectrum of 200ng/mL solution of THC in water on mesh

### 2.2.2 Sample positioning optimisation

For sample loading into the DSA-ToF, sample volumes must be pipetted onto an approximately 0.5cm diameter circle of stainless-steel mesh. This mesh is part of a continuous 17cm long piece that is fitted into a sample holder with 13 sample positions. The corona needle that feeds the nitrogen plasma through the mesh and carries the analytes into the mass spectrometer is lined up with the centre of the mesh contained within the sample position. Therefore, if the sample itself is not lined up with the corona needle, there is a danger that there will be loss of sensitivity, through tailing of the peak, as the analyte desorbs from the mesh over a longer period of time. In order to determine the optimal position of the sample on the mesh, 10  $\mu$ L of a 1000ng/mL cocaine solution was pipetted in five different locations on the mesh: middle, top middle, bottom middle, left middle and right middle.

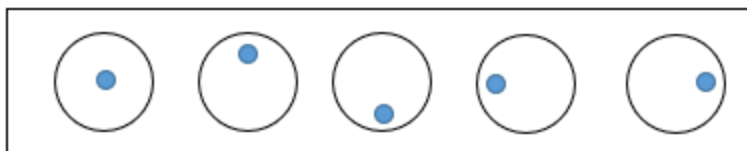


Figure 11: Positions evaluated for optimisation of sample positions. From left: middle, top middle, bottom middle, left middle & right middle.

Analysis was performed in triplicate, with the intensity of the cocaine peak (approximately  $m/z$  304.367) being measured as an indication of the strength of a molecular ion peak in response to mesh position. The results (Figure 12) indicate that top middle or middle produce the optimal cocaine signal, although the variability in the intensity is highest for these two positions also.

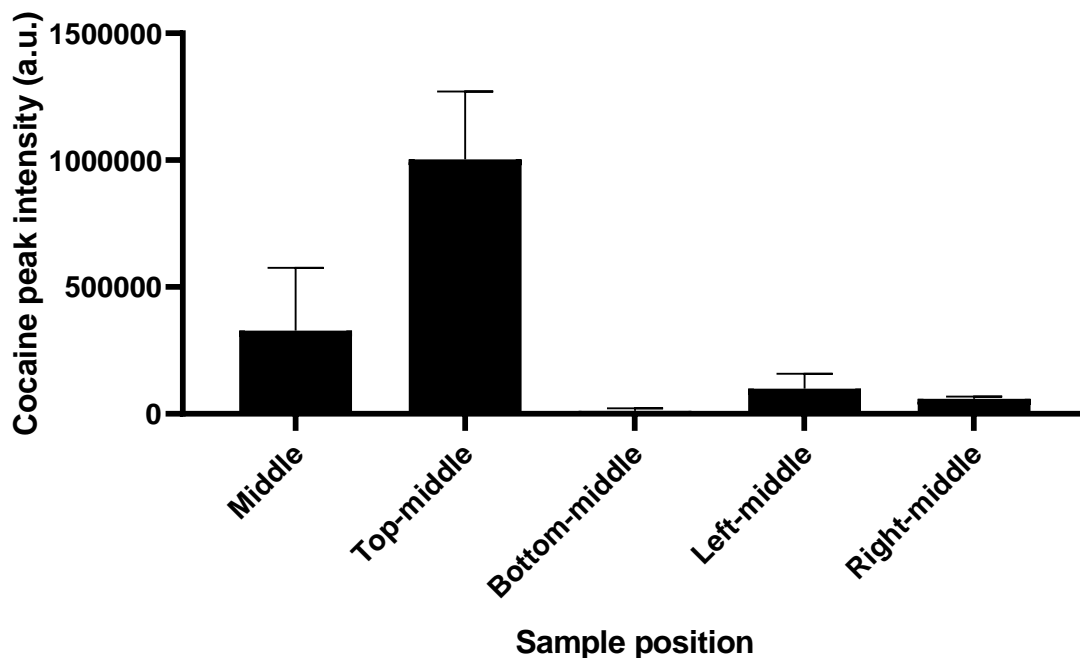


Figure 12: Comparison of molecular ion peak intensity ( $m/z$  304.367) for alternative sample positions on mesh ( $n=3$ ), error bars are 1SD

The direct comparison of middle and top-middle positioning indicate that the top-middle position is the optimal placement. Ten  $\mu\text{L}$  of sample is a large enough volume that movement of the sample holder will shift the position of the droplet slightly from the initial placement (investigation of this phenomenon follows). This is further compounded by the method with which the samples must be placed on the mesh and the holder installed into the instrument. In order for the sample droplet to be positioned exactly, the easiest

method with which to place the samples is by removing the entire holder from the instrument and pipetting them while the holder is horizontal on a bench or similar. The sample holder is then moved to a vertical position and installed back into the instrument, via alignment of holes in the instrument with pegs on the base of the holder. This movement can cause further movement of the sample droplets, and in the case of the top-middle samples, movement to the middle position on the mesh. Care should be taken when pipetting the sample on the mesh to avoid placing it to the left or right of the middle position, and certainly not in the bottom-middle position. Care should be taken when re-installing the sample holder into the DSA-ToF in order to avoid jolting the droplet out of the original position and reducing the sensitivity of the analysis.

### 2.2.3 Sample volume optimisation

Typical chromatography-based analysis runs via injection of a known volume (and therefore total amount) of sample into the instrument for analysis. The DSA-ToF sample delivery system is nowhere near as accurate as these injection-based systems, with the total amount of sample delivery into the mass spectrometer inlet not being exact each time a sample is ionised. Therefore, it is necessary to deliver the maximum amount of sample into the mass spectrometer in order to maximize the sensitivity of the analysis. Total sample volume is one method to control this sample amount and must therefore be optimised to ensure that the maximum amount of sample is delivered without compromising the analysis by overloading the instrument or contributing to sample spot movement during analysis.

In order to determine the optimal volume of sample, high (1000ng/mL) and low (20ng/mL) concentration cocaine solutions were pipetted onto the mesh in volumes of 5, 10, 15 and 20  $\mu$ L. Samples were pipetted onto the top middle position of the mesh, as per the optimal position determined in 2.2.2. Response was measured using the intensity of the cocaine molecular ion peak ( $m/z$  304.367) for the varying volumes. Optimal volume is that which produces the highest intensity peak of cocaine, with an acceptable variability.

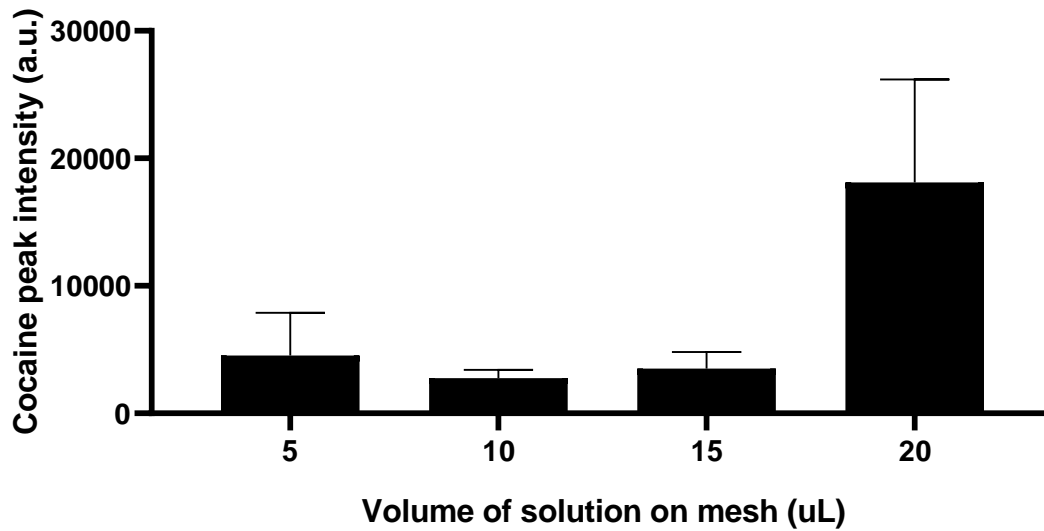


Figure 13: Comparison of 20ng/mL cocaine molecular ion peak intensity ( $m/z$  304.367) for alternative sample volumes on mesh ( $n=3$ ), error bars are 1SD

For the lower concentration of cocaine, there doesn't appear to be a large difference in the cocaine molecular ion peak intensities, with the variability of the intensity being relatively small. The highest signal intensity came about from the 20 $\mu$ L sample volume, although the variability of the intensity is large, with the error bars displayed in Figure 13 being only one standard deviation. The variability is likely due to the movement that the sample droplet undertakes on the mesh during and prior to analysis. Optimisation of the sample position showed that placement of the sample at the top-middle was the prime position for maximum sample throughput into the mass spectrometer (Figure 12). When performing the sample volume experiments, it was observed that the lower the sample volume, the more accurate the placement on the mesh. The highest variability in placement came from the 20 $\mu$ L sample volume, where despite the placement into the top-middle of the mesh initially, there was movement from that position as the sample holder was moved and re-positioned inside the instrument. This movement may account for the variability in the signal intensity of the cocaine molecular ion peak as seen in Figure 13. For position consistency reasons, the optimal sample volume was determined to be 10 $\mu$ L, as it delivers a comparable signal intensity to 15 $\mu$ L, but was not seen to move and had less S/N variation. There is also the consideration of sample preservation in a forensic context, where the sample available isn't always of a large volume and may require multiple tests for analysis.

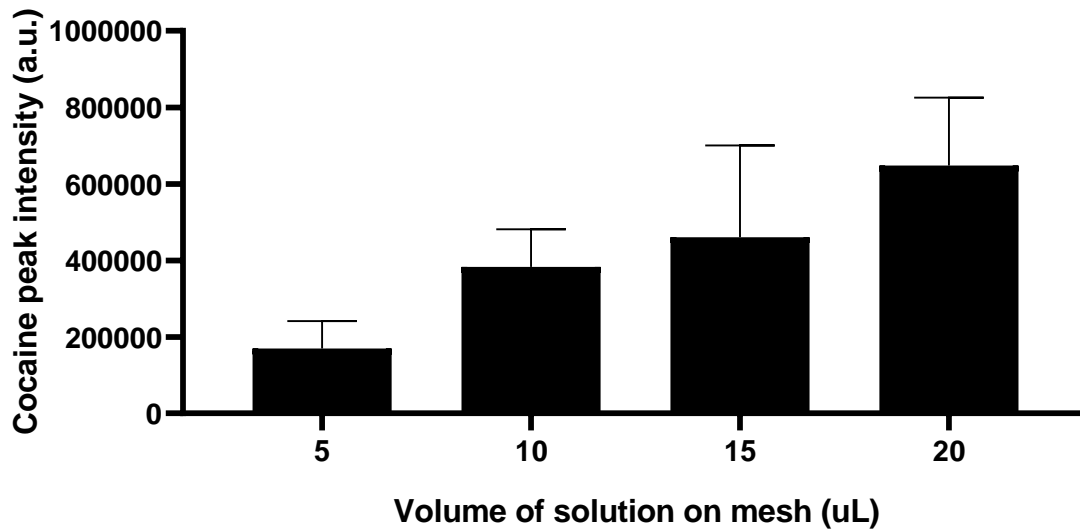


Figure 14: Comparison of 1000ng/mL cocaine molecular ion peak intensity ( $m/z$  304.367) for alternative sample volumes on mesh ( $n=3$ ), error bars are 1SD

For the higher concentration of cocaine (1000ng/mL), the volume of sample is directly correlated with the molecular ion intensity of cocaine (Figure 14). As would be expected, the higher the volume of sample deposited on the mesh, the higher the peak intensity of the molecular ion. Based on the results of this experiment, the optimal volume of sample onto the mesh is 20uL. Ultimately this was not carried through for a number of reasons. The first is that such a large volume weakens the adhesive forces between the droplet and the mesh. The movement of the sample stage from the position at which the sample is deposited onto the mesh to the position where it is exposed to the plasma is not smooth. Weakened adhesive forces owing to the larger volume can result in the movement of the droplet from the deposition position. In some cases, it was observed that the droplet moved all the way from the top middle position to rest on the sample holder itself. In this position, the sample is not exposed to the plasma, reducing the signal and potentially giving a false negative result. This is particularly pertinent as the mesh is difficult to observe once it moves from the sample deposition position, and the potential movement of the sample would be difficult or impossible to observe, further increasing the risk of a false negative result. The second reason the 20uL sample volume was not chosen was the potential for carryover when too much analyte is pushed into the system. This was observed by QLD Health who noted that high concentration samples tended to leave a residue on the MS inlet, causing carryover and requiring cleaning [80]. Although this was not observed in this experiment, it is a worthwhile consideration moving forward in that volumes of sample that would deliver a large amount into the MS inlet should be avoided.

The 15uL sample volume also moved from the deposition position when the sample holder was moved, although for a reduced number of occurrences. Again, this movement was difficult to observe once the sample was in the instrument, potentially resulting in false negatives where little to no sample is ionised.

Ultimately, 10uL was chosen as the optimal volume moving forward, as the droplets remained where they were deposited throughout the movement from deposition to ionisation. This consistency in placement means that the sample is continuously in the optimal position for ionisation. This lower volume also ensures that for most samples replicate analysis will be possible.

#### 2.2.4 Adjacent sample placement

The ionisation method used by the DSA-ToF relies heavily on heating of the samples to assist with the ionisation and movement of the sample into the mass spectrometer. This heating, as outlined in the materials and methods chapter, is up to 350°C. As the sample analysis time is approximately 30 seconds per sample, the mesh itself and the sample holder gets hot during and after the analysis. There are a number of problems with this, particularly when considering the sensitivity of the analysis, and especially from a forensic perspective. The sample holder includes space for 13 samples, which are to be used for analysing 13 samples in the one batch, to save individual pipetting onto the mesh areas, which would decrease the through-put of the instrument. When considering that the mesh is 17 cm of continuous metal (stainless steel), the heat travels through the length of the mesh and heats the adjacent sample spaces. As mentioned initially, the heat is an important component of the ionisation method, so if the adjacent samples are being heated, there is the possibility of loss of sample through this heating, prior to analysis. For sensitivity and cross-contamination reasons, this must be avoided.

To determine the extent of this adjacent heating problem, a 500ng/mL solution of cocaine in water was analysed on six adjacent sample spots on mesh. Each sample was analysed for 30 seconds, which was the approximate time required for the secondary peak in the TIC to be visualized. The S/N of the cocaine molecular ion peak was recorded and compared for each of the sample positions (Figure 15)

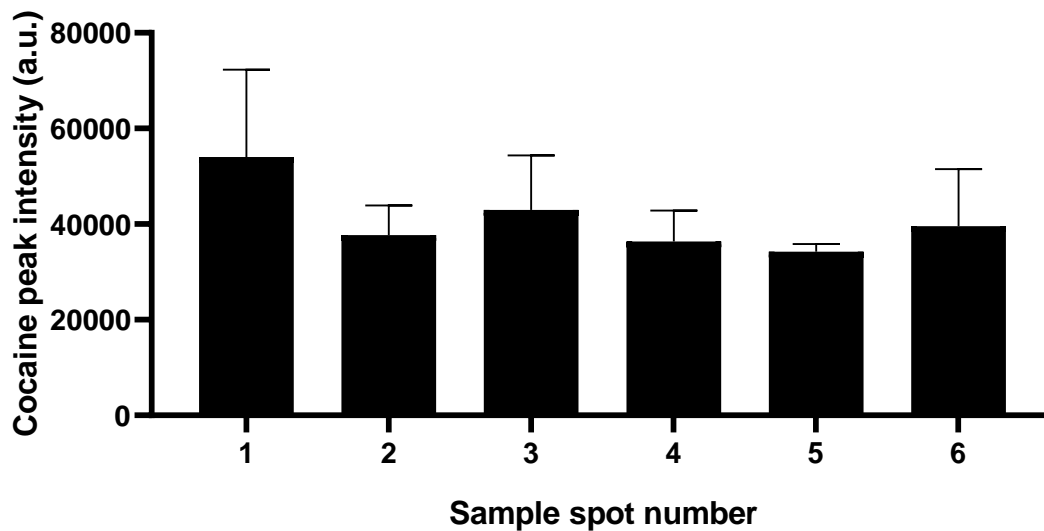


Figure 15: Comparison of cocaine peak intensity ( $m/z$  304.367) for six adjacent mounted samples ( $n=3$ ), error bars are 1SD

The comparison of the peak intensity alone for each of the adjacent samples does not show any trend across the positions. If there had been some early ionisation and desorption from the mesh due to adjacent heating, this would have manifested itself as a decrease in the signal intensity of the cocaine peak for each advancing spot position. Instead, the signal intensity appears variable in a random way. To investigate this further, a 1000ng/mL solution of cocaine in water was analysed five times in succession on the same mesh position (with cooling time between analyses). This was to determine whether the peak response for the analyte was consistent when the sample, spot position and temperature of the mesh remained constant.

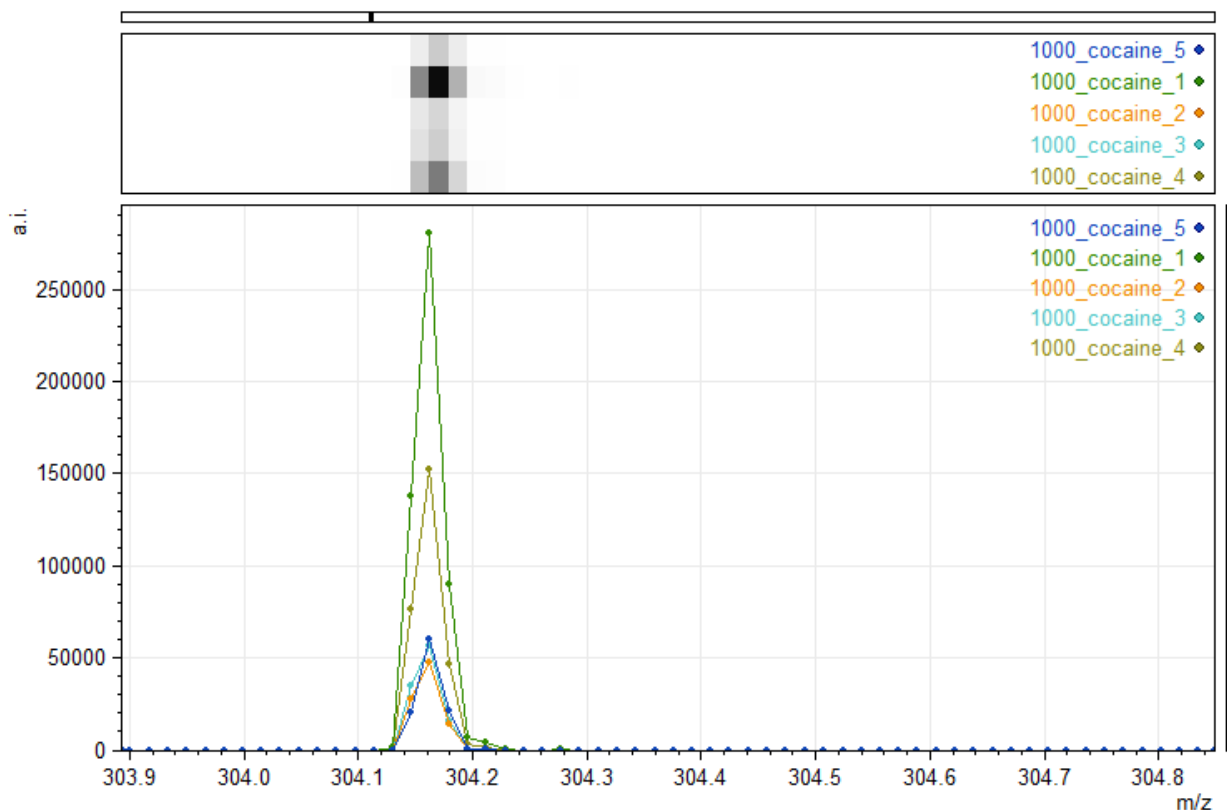


Figure 16: Intensity variation across five subsequent acquisitions of 1000ng/mL cocaine solution in water

The comparison of peaks for each acquisition shows a serious lack of consistency in the peak response (Figure 16). This was totally random, suggesting that the peak response is not consistent and more importantly, that this inconsistency cannot be predicted by any of the variables tested so far. This inconsistency in the peak response is in agreement with a recent paper investigating the repeatability of ambient ionisation mass spectrometry results [145]. Results from the study indicated that for consistency in quantitative results to be achieved the samples need to be analysed with a matched internal standard, with the ratio of the response being a more appropriate measure. For all quantitation in the remainder of this work a deuterated internal standard was used. Where peak response itself is required for method optimisation the signal to noise of the peak, rather than the peak area or intensity is used, to maximise the consistency of response where possible.

### 2.3 Impact of atmospheric water on ionisation

The ionisation mechanism employed in DSA-ToF makes use of water clusters to protonate the analytes [4]. The extent to which atmospheric water influences this ionisation was investigated by replacing as much of the water in the system as possible with D<sub>2</sub>O, to shift the molecular ion mass. For these experiments,

solutions of MDMA and cocaine (200ng/mL) in EtOH were deposited onto the mesh (instrument plasma cleaned). Once the EtOH had evaporated 10uL of D<sub>2</sub>O was placed over the dried spot. Typically the calibrant is diluted 1:10 in water, for these experiments the calibrant was diluted in D<sub>2</sub>O. Finally, the calibrant lines and syringe were rinsed with AcCN. The mass spectra were extracted by averaging across the 'peak' without extracting the BIC, ensuring that all ions present in the mixture would be shown in the mass spectrum.

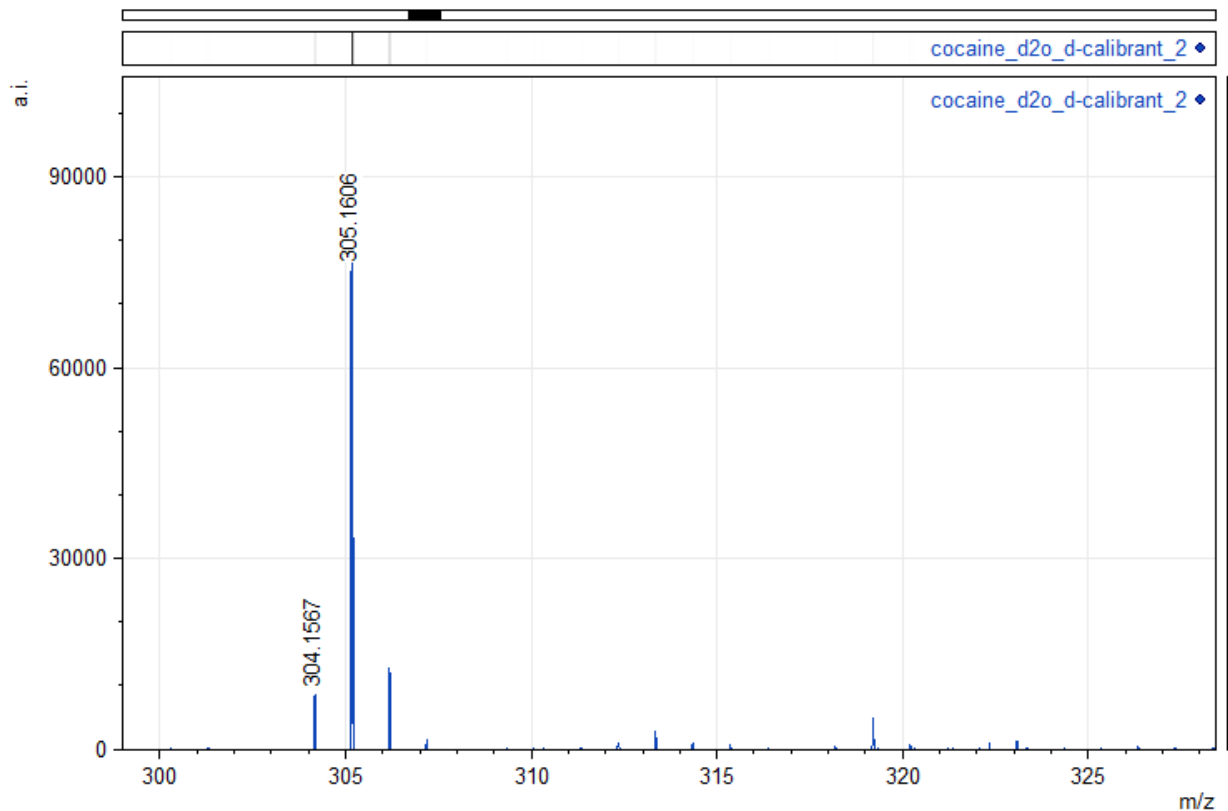


Figure 17: Representative mass spectrum of cocaine in EtOH, with D<sub>2</sub>O in calibrant solution and pipetted on top of the dried sample spot.

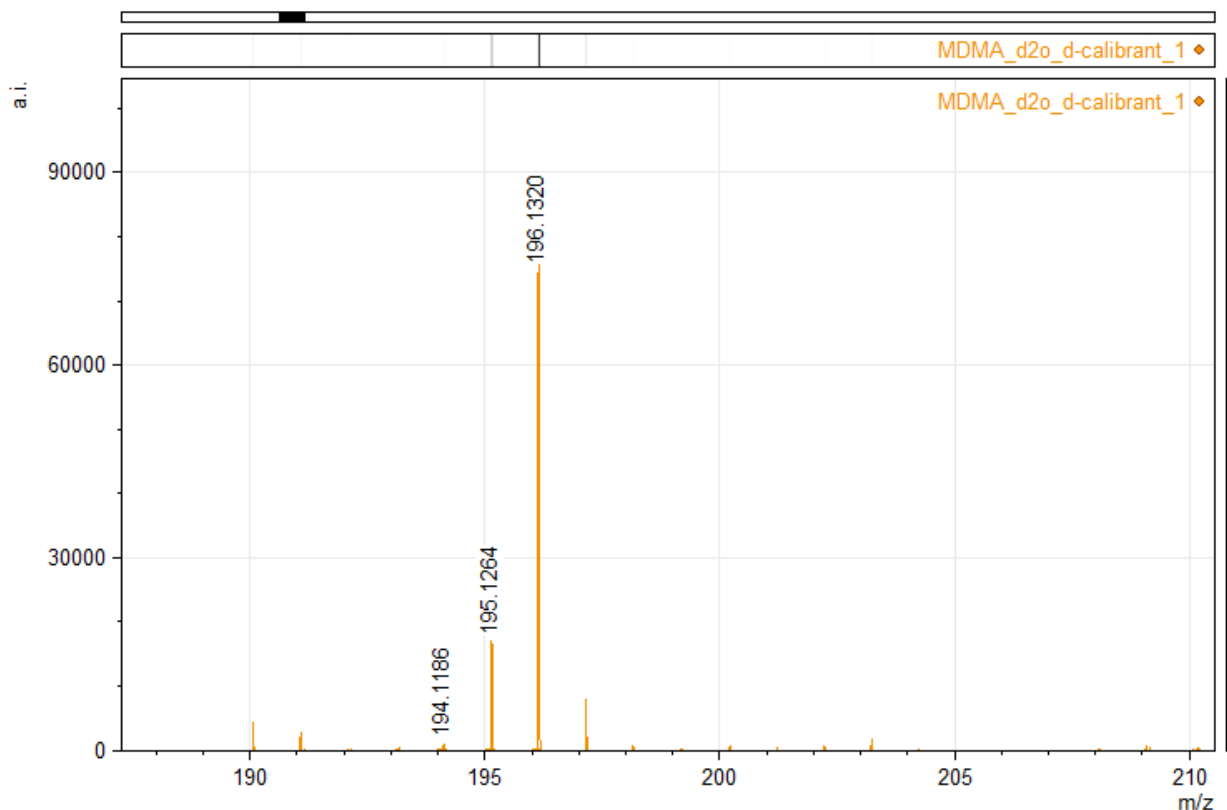


Figure 18: Representative mass spectrum of MDMA in EtOH, with D<sub>2</sub>O in calibrant solution and pipetted on top of the dried sample spot.

For both cocaine and MDMA the molecular ion peak moved 1-2 mass units up from the dominant molecular ion when no D<sub>2</sub>O is present (Figure 17 & Figure 18). This indicates that the water supplied to the system from the calibrant and the addition to the mesh does influence the molecular ion formation. In actuality, the shift of the dominant peak to the higher mass indicates that these sources of water have a huge impact on the ionisation. The presence of the original molecular ion peak (304 & 194 for cocaine and MDMA respectively) does indicate that the atmospheric water still has some influence over the ionisation. This has implications for the reproducibility of results, as atmospheric humidity is difficult to control in an open laboratory environment. Because of this, it is likely that on days of high humidity in the laboratory the ionisation will be improved, and conversely on days of low humidity the ionisation will be negatively impacted. For this particular instrument, the position of the instrument underneath the air-conditioning vent may have resulted in reduced ionisation owing to the dehumidifying effects of the AC system [150].

## 2.4 Influence of syringe flow rate

The ability of water present in the calibrant to influence ionisation led to the need to optimise the syringe flow for calibrant delivery. An increase in the calibrant flow rate may result in more water being present and

available to enhance analyte protonation. The original setting of 10 $\mu$ L/min was used on the recommendation of Perkin Elmer, but an increase in molecular ion response was observed after an engineer visit where the syringe flow rate was set to 40 $\mu$ L/min. A solution of cocaine (200ng/mL) was used as a measure of the response across the varied flow rates, with amplitude and signal to noise being compared.

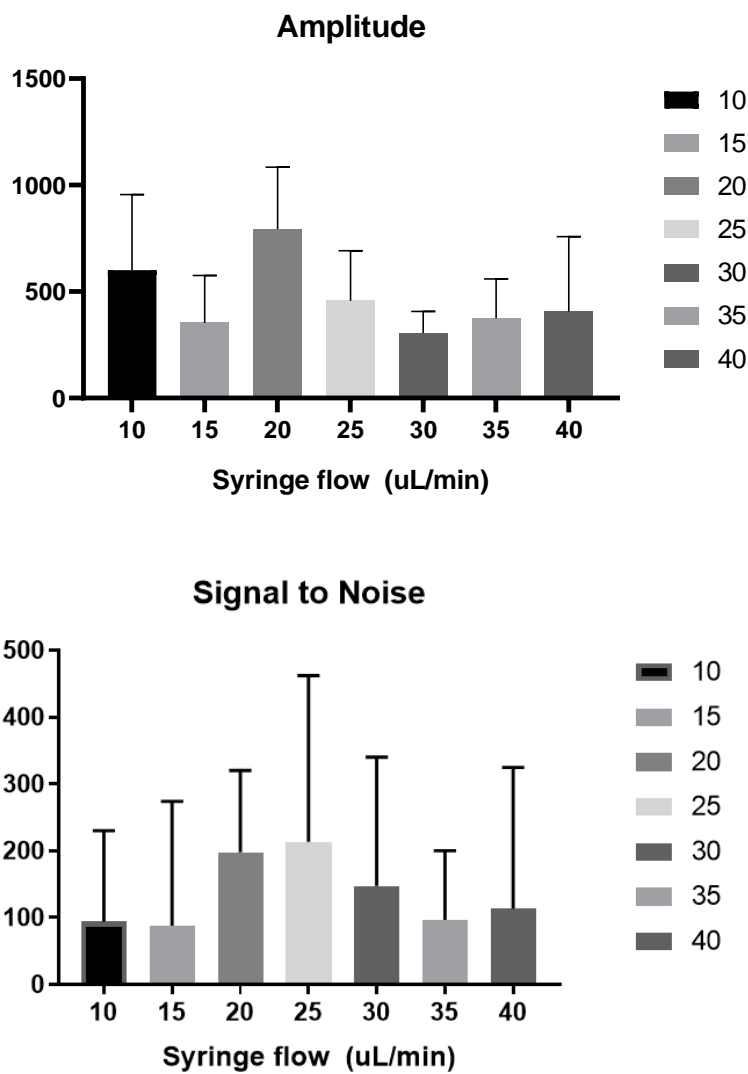


Figure 19: Comparison of amplitude (top) and signal to noise (bottom) for calibrant syringe flow rates of 10-40 $\mu$ L/min

The amplitude showed higher responses for the lower flow rates, with the highest response for the 20 $\mu$ L/min, with the original 10 $\mu$ L/min the next highest value (Figure 19). Signal to noise showed a more obvious trend, with the responses increasing from 10-25 $\mu$ L/min to a maxima and reducing again to 40 $\mu$ L/min (Figure 19). These results were contrary to the observation that triggered this experiment (the increase in S/N for 40 $\mu$ L/min flow rate), indicating that this increase may have been a random event. For the remainder of the analyses 10 $\mu$ L/min was maintained, although it was noted that for low concentration samples this flow rate may be increased to improve S/N where required.

## **2.5 Robustness**

Robustness of an analytical method is defined as the ability of that method to remain unaffected by small and deliberate variations in the method (mobile phase, temperature, pH etc.). However, in the context of this work, the robustness of the DSA-ToF drug detection methodology will be defined by the ability of the method to withstand uncontrolled environmental changes, which have been shown to impact the signal reproducibility.

To assess the robustness of this method, two approaches were investigated. Initially, a solution of cocaine (200ng/mL) was analysed 50 times in a row, without re-using the sample mesh. The amplitude, and signal to noise of the peak were assessed. This experiment was performed without an internal standard with the cocaine response alone being used as the measure. The second approach, consistency in LoD and LoQ, is discussed in 3.5, after the limits have been established.

## **2.6 Cocaine peak reproducibility**

A cocaine solution was prepared to 200ng/mL, and 2 $\mu$ L aliquots of this solution were analysed (50 replicates). Acquisition times were 30 seconds, and mass spectra were extracted by manually averaging across the base of the peak for the BIC of m/z 304-305. The amplitude and signal to noise were evaluated, to determine the deviation from the mean, and the magnitude of any variations. Although the work in this chapter so far has shown that there is some variation in the peak response (whichever parameter is chosen as the peak response measurement), this experiment was conducted to determine the magnitude of this variation.

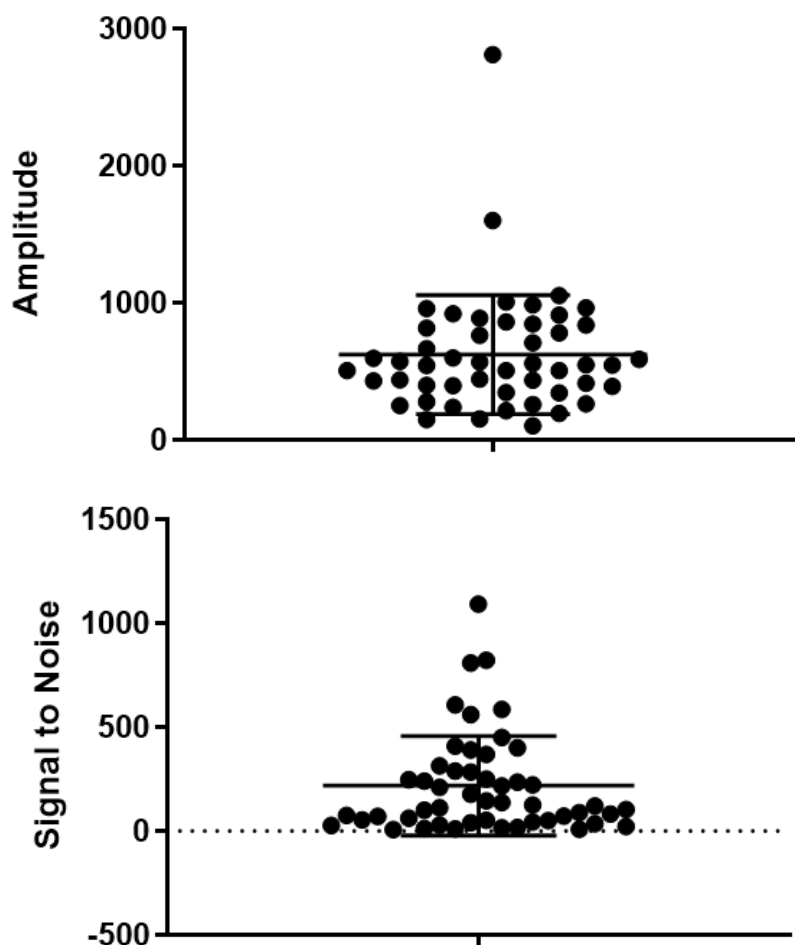


Figure 20: Distribution of cocaine (200ng/mL) amplitude and signal to noise over 50 consecutive injections.

The amplitude has a narrow distribution around the mean and two outliers at very high values (Figure 20). The signal to noise is the most interesting. Running the same solution over and over again, it would be expected that the signal to noise would remain relatively consistent for most instruments. For this instrument, there are quite a lot of values close to zero, and a large amount of variation from that position (Figure 20). What this indicates is that there is a significant amount of noise that influences this value, and that this noise is fluid. That is, the amplitude data from this experiment is consistent enough that the signal to noise should follow a similar trend. This S/N distribution shows that the amount of noise from the background deviates enough that the molecular ion peak is being lost in that background. Although disappointing, this has been documented in ambient mass spectrometry instruments previously [145], where detection of known and unknown compounds can be seriously hampered by the presence of background noise from the laboratory environment.

## **2.7 External interferences: intensity cycling over time**

Instability and irreproducibility were consistently observed in the results from the instrument, for all molecules. This was contributing to poor sensitivity for low concentration analytes. Although a reduction in sensitivity is expected from atmospheric ionisation mass spectrometry relative to other ionisation types, this was beyond what would be expected. In order for appropriate sensitivity to be achieved this needed to be addressed. The stability of the calibrant is particularly important, as the presence or absence of calibrant peaks can impact the ability of the analyst to determine the accurate mass of compounds. The calibrant is a good measure of the stability of the instrument, as it is a solution of constant concentration, being pushed into the instrument at a constant flow rate by an external syringe pump. To determine the extent of the problem, calibrant was run through the instrument for 30 minutes, with data acquired across this timeframe. The area, amplitude and width (at baseline) data were recorded for each calibrant peak across this entire timeframe. The responses for each parameter were plotted against time.

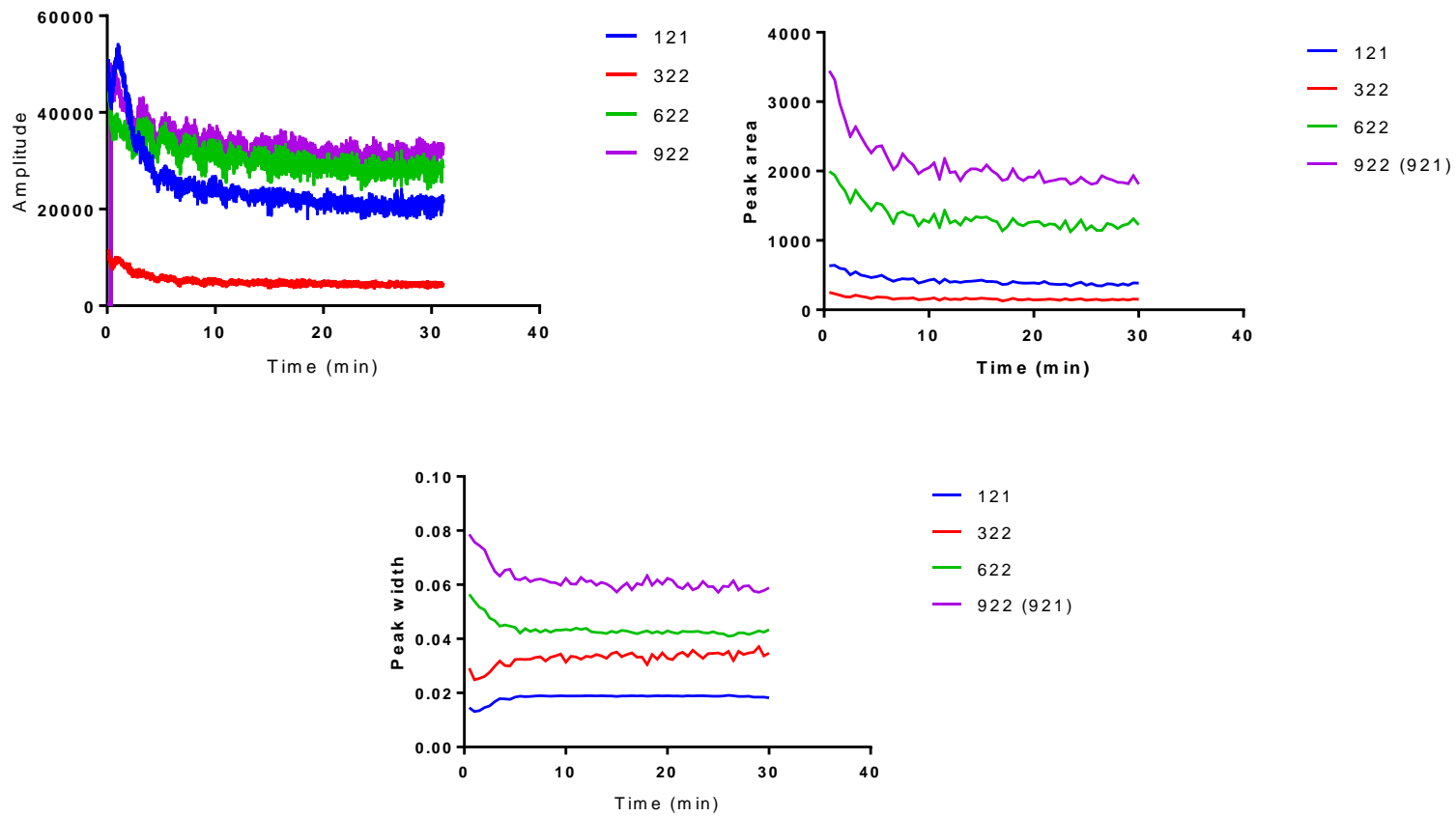


Figure 21: Amplitude, area and width data (clockwise from top left) for calibrant acquisition over 30 minutes, for calibrant acquisition over 30 minutes using DSA-ToF

These data show that there is a cycling problem. Both the amplitude and the area show some cycling, which is expected as the amplitude and width parameters are correlated with the area. An adjustment period over the first 10 minutes of acquisition can be seen, where the response drops significantly (Figure 21). This drop in signal suggests that the instrument requires a warming up period, and that if quantitation is required an assessment of instrument stability should be carried out using the calibrant to ensure that the drop does not take place during sample acquisition. The cycling, however, was present for the entire acquisition period. For the amplitude response, the cycling problem is two-fold. There is a short term frequency causing the thickened trace (Figure 21). There is a secondary cycling frequency observed in both the amplitude and area trace, that appears more severe at the start of the acquisition.

Frequency analysis was carried out on this data to establish the time frame over which the cycling occurs. A Fourier transformation was applied to the amplitude data for the above acquisition. This was done to identify if there was any consistent periodic amplitude variation, which would confirm a systematic issue rather than a random one.

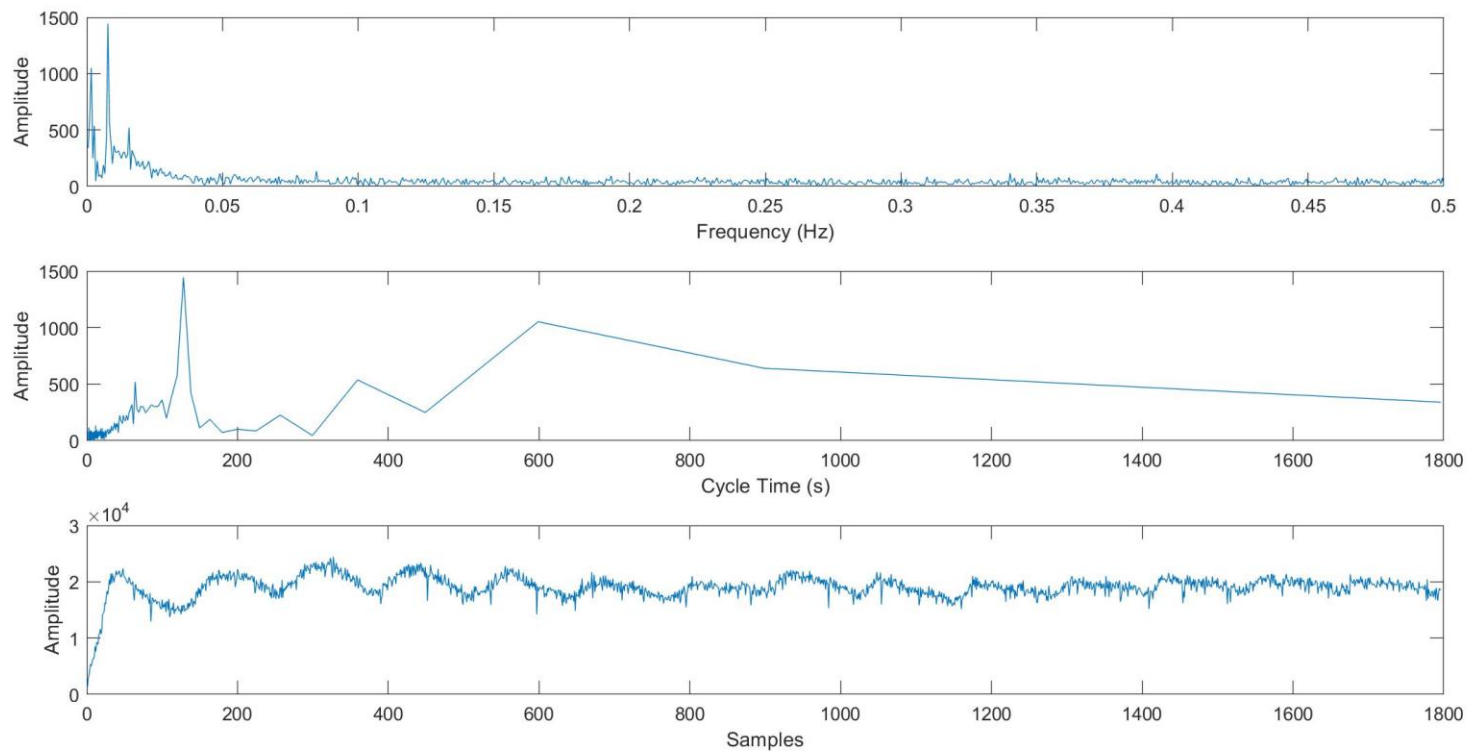


Figure 22: Frequency analysis of amplitude data for calibrant peak  $m/z$  622. Graphs are from the top down: frequency, cycle time, and amplitude (original data)

The frequency graph indicates that there are two stacked frequencies, one very small one, and one larger (Figure 22). These two frequencies can be seen in the cycle time graph, with the frequency of higher amplitude having an oscillation period of approximately 3 minutes. This is the frequency responsible for the sine wave-like cycling, which is the most concerning for future analyses. A consistent and periodic oscillation like this can have serious implications for sensitivity, in that measurements of samples taken at the peak or trough of this cycle will have very different responses. Typical analysis using the DSA-ToF is under 30 seconds, so a cycling time of 3 minutes could involve the analysis of 5-6 samples, along this curve. In order to determine if the frequencies were instrument or environmental based, further experiments were conducted to identify external sources of cycling.

The position of the instrument was underneath the air-conditioning vent in the laboratory. The flight tube used in ToF-MS is very sensitive to temperature fluctuations, which causes the flight tube to expand and contract. This movement increases and decreases the length of the drift region, causing changes in the masses determined by the detector. In order to identify if the air-conditioning was the cause of the sinusoidal cycling the same calibrant solution was run through the instrument for three separate 30 minute intervals. The first with the flight tube capped with a cardboard box (to insulate the flight tube, and maintain a consistent temperature), the second with the flight tube capped and the air-conditioning vent covered, and the third with both the vent and flight tube uncovered. The amplitude for these three experiments was compared to visualize any differences in the cycling.

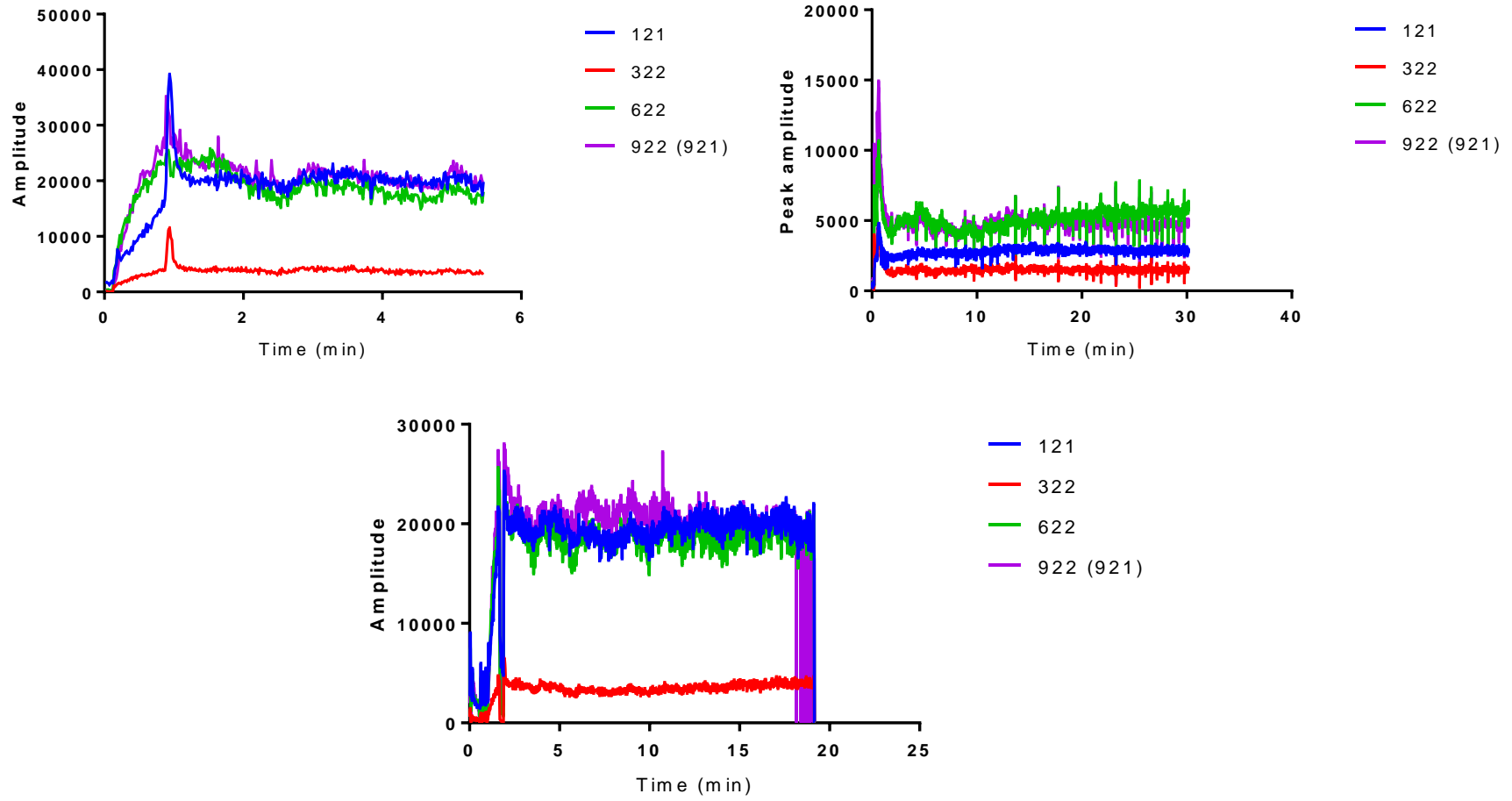


Figure 23: Comparison of amplitude data for 30 minute acquisition for capped flight tube only, capped flight tube and covered AC vent, and uncovered flight tube and AC vent (clockwise from top left)

The capped flight tube alone showed a reduction in the large sinusoidal cycling seen in the original data (Figure 23). These data alone might suggest that the air-conditioning was the problem, and that this simple fix was sufficient to fix it. The data acquired with both the AC vent covered and the flight tube capped showed the same oscillation patterns, but not the same as the original sinusoidal pattern (Figure 21). This further confirms that the temperature fluctuations are causing the cycling, and impact the results obtained using the instrument. The drop off at the end of the acquisition for the  $m/z$  922 (Figure 23) is due to a mass shift, where the mass of the peak recorded for that calibrant fell outside the range entered to extract the XIC. This is also a symptom of the temperature fluctuations, where accurate mass is affected so much that it falls outside the ranges specified by the calibration. Other parameters were explored in this set of experiments, including the influence of background DSA controller software, calibration, and instrument repairs. None of these influenced the cycling any further.

Despite the improvement in the cycling, there were still some fluctuations observed in the data where the temperature cycling was reduced. In order to determine whether there was an instrumental factor involved, the source was switched across to ESI. Therefore, if the ionisation source was a part of the problem, the fluctuations would be reduced or changed in some way. All other parameters remained the same.

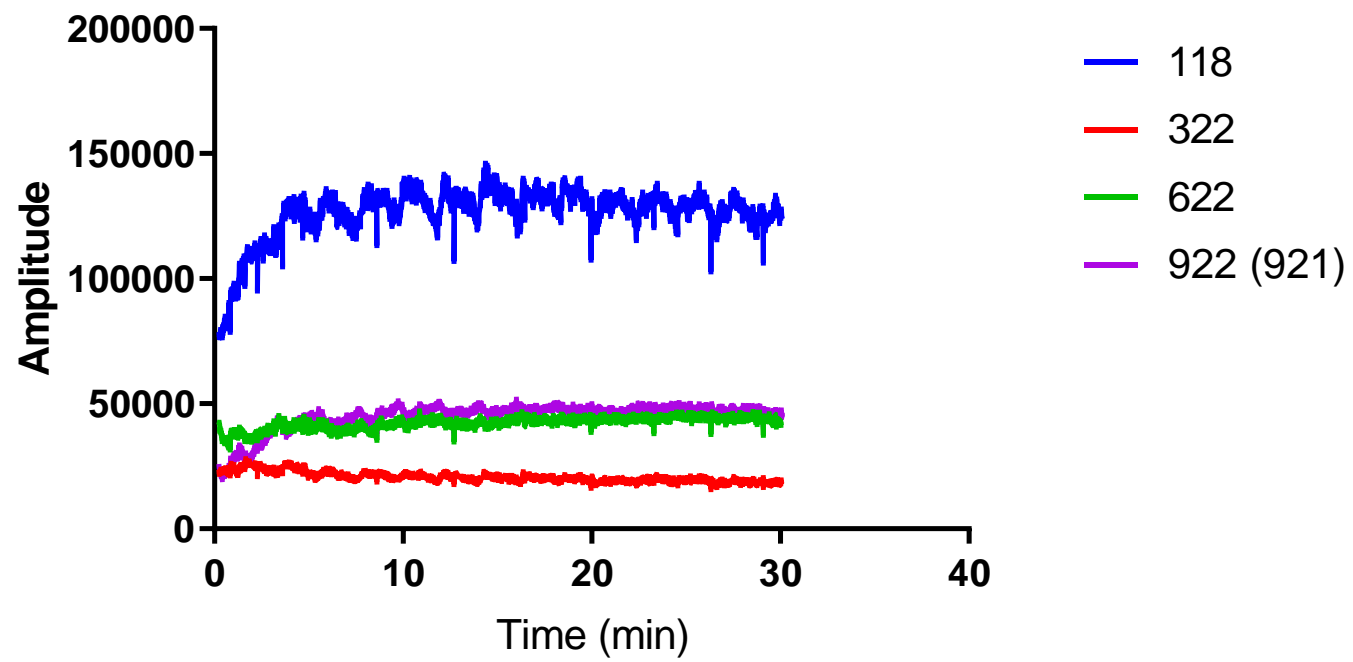


Figure 24: Calibrant peak data across 30 minutes using ESI source, with AC vents covered and flight tube capped.

The ESI data show the same small cycling as the DSA-ToF data under identical conditions (Figure 24). This suggests one of two things: that there is an alternate instrumental parameter that is causing the smaller fluctuations, or that there is another external condition causing the problems. Without a greater understanding of these variables, the best that can be done to minimize these fluctuations is to keep the temperature as stable as possible, and to allow the instrument sufficient warm-up time. Where sensitivity is required, the instrument should be assessed for stability by running calibrant through the system and assessing the cycling on a case by case basis.

After investigation of all potential controlled variables to improve the consistency of the DSA-ToF, it is clear that there are problems beyond the control of the analyst and the environment. In order to maximise the sensitivity and reproducibility of the results, the instrument must be calibrated prior to use, and placed in an area of the lab with minimal air flow and temperature fluctuations. If this is not possible, the air flow and temperature around the flight tube should be controlled as best as possible. These steps reduce variability in the amplitude, but will not reduce the occurrence and severity of random fluctuations. It is best that the analyst view any attempt at quantitative data acquisition and analysis with caution, and stability checks. Any comparative analysis must be run on the same day, and across multiple replicates, to smooth the effects of these fluctuations as much as possible. Overall, the sensitivity of the instrument is called into question by these experiments, as environmental and atmospheric influences have a great deal of impact on the quality of the results generated.

## **2.8 Conclusions**

This work has demonstrated that DSA-ToF has the capabilities to accurately and quickly perform qualitative data analysis on single drug solutions of MDMA, THC and cocaine. The analysis must be performed by placing a sample volume of 10 $\mu$ L into the top middle of the sample holder (onto the mesh). Care must be taken to avoid jostling the sample droplet from its position, as there are severe reductions in signal intensity when movement from this position is observed. For accurate mass identification of these compounds (and compounds like them in the future), a simple method is described within this section, which will provide identification of compounds within acceptable error ( $\pm$  7ppm), and theoretically be applicable to a broad range of substances.

### 3 Quantification of illicit drugs in water using DSA-ToF

#### 3.1 Introduction

The ability to identify and quantify illicit drugs in solution is of vital importance for forensic analysis. The need stems from both a toxicological and chemistry standpoint. In toxicology, sensitivity is paramount, with low concentrations of the drugs of interest being found in bodily fluids. Typically, for toxicological analysis, the range in which one would expect to find the analytes of interest is 0.05-468mg/L [151], which varies depending on the drug of interest and the fluid analysed (Table 7).

Table 7: Typical cocaine, MDMA & THC concentrations in bodily fluids for varying levels of intoxication. Reproduced from [151]

Drug	Source	Therapeutic/ non-toxic	Toxic	Lethal
Cocaine	Blood	0.1-0.3mg/L	0.4-5mg/L	0.1-330mg/L
	Urine			0.05-402mg/L
	Bile			2-468mg/L
MDMA	Blood	0.1-0.25mg/L	0.3-0.5mg/L	0.4-11mg/L
	Urine			14-141mg/L
	Bile			14-73mg/L
THC	Blood	0.05-0.27mg/L	0.18mg/L	
	Urine	0.003-0.05mg/L		

Additionally, there are difficulties when considering the matrix in which the analytes are found, with classical methods such as liquid or gas chromatography requiring sample clean-up before analysis can occur. This additional clean-up expends time, solvents and money, although it delivers the sensitivity required for toxicology. There is also a need to identify any physical powders or pills that may be present as well, which requires analysis of compounds that may be of a high concentration, but also in a complicated matrix that may or may not include several types of drugs. From a chemistry perspective, the sensitivity is less important than the selectivity, where specific analytes must be detected and quantified in the same matrix. Additionally, forensic analysis is often required quickly, and the typical methods involving chromatography can be time consuming, leading to a delay in results being delivered, or a backlog in evidence that requires

processing. When considering methods for the detection of illicit drugs in complex matrices, the need for sensitivity, selectivity and the time pressure component must be considered.

This chapter details a method for the detection of three common illicit drugs (MDMA, THC and cocaine) at high and low concentrations, while allowing for accurate quantitation, with analysis times of under one minute per sample. This method provides rapid, accurate screening and quantitative analysis of single drugs in solution, with detection limits suitable for use with biological forensic samples.

### 3.2 Illicit drug detection internal standard use

The previous chapter (Chapter 2) established that the area response of a peak is not consistent enough to use as a quantitative measure. Figure 25, below, shows the response of a cocaine 1000ng/mL solution acquired five times. The peak response difference between the highest area value and the lowest value is 200 000, demonstrating the need for normalization of the peak response for any non-qualitative purposes.

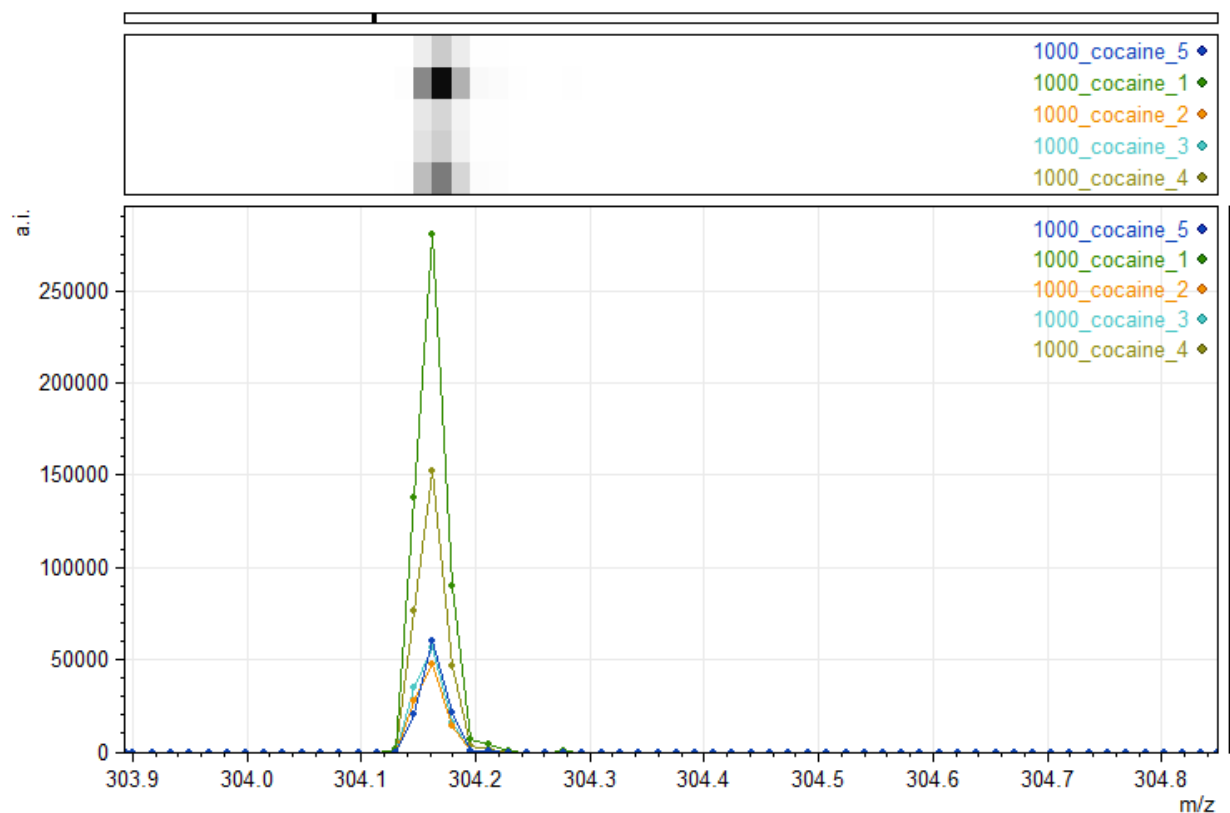


Figure 25: Intensity variation across five subsequent acquisitions of 1000ng/mL cocaine solution in water

To compensate for this variation in peak area and height, analyses using the DSA-ToF must be carried out using an internal standard (ISTD). The measured response is then not the intensity of the molecular ion

peak, but the ratio of peak intensity of the drug to the intensity of the internal standard. This is particularly relevant for the work in this chapter, where quantification is demonstrated.

### 3.3 Quantification of MDMA, cocaine and THC in water

#### 3.3.1 Collection of mesh background information

The mesh provided by Perkin Elmer is factory produced and was found to have a large amount of background noise. Background noise can interfere with limits of detection and sensitivity, which can result in compounds being present but not detected if this noise is sufficiently high. This high background noise is also a particular problem for ambient mass spectrometry, which is prone to high background from contaminants in the ambient atmosphere. Removal of these background compounds on the mesh would potentially improve the sensitivity of the instrument. An initial assessment of the neat mesh was performed, to determine if the regions of interest (where the drugs of interest are located) suffer from significant amounts of noise. Figure 26 (below) clearly shows a large amount of noise in the low mass regions, where the three targeted compounds are found. Excessive noise in these regions may lead to low signal to noise ratios and general difficulty in determining the presence or absence of a peak of interest.

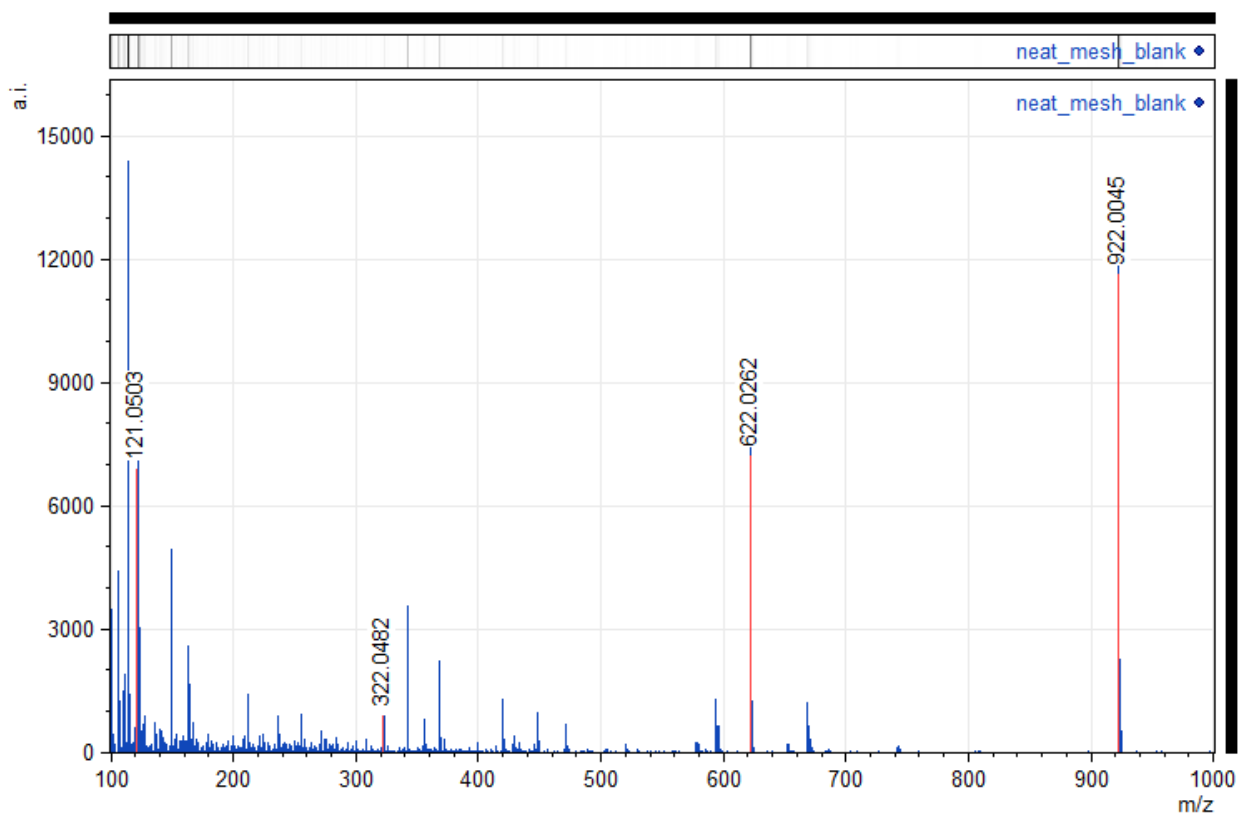


Figure 26: Average spectra of un-treated mesh blank, across 30 second acquisition time, with calibration peaks labelled.

There is some background, primarily in the areas of low molecular weight (<350) (Figure 26), where it is likely to interfere with detection of the drugs of interest discussed in this chapter. These areas of interest are magnified in Figure 27, below.

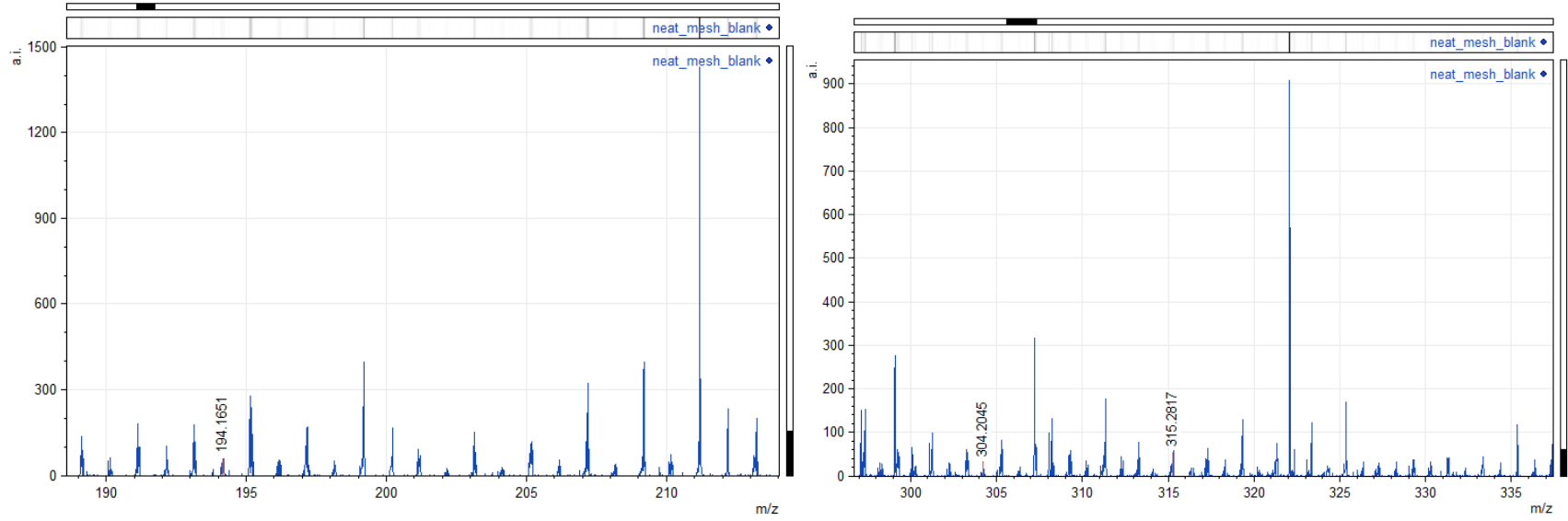


Figure 27: Average spectra of un-treated mesh blank, across 30 second acquisition time, showing approximate areas where cocaine, MDMA and THC are likely to be identified

Although the amount of noise in these areas is less likely to interfere with the qualitative identification of MDMA, cocaine or THC, their quantitative analysis may be impaired. The presence of peaks of close mass to the analyte can cause split peaks, and poor integration of unresolved masses, which would under or overestimate the peak. In order to remove any exogenous organic compounds on the mesh causing this noise, plasma cleaning was investigated. Both 'bulk' plasma cleaning and instrument-based cleans (as recommended by Perkin Elmer and described below) were investigated for this purpose. Bulk plasma cleaning involved the simultaneous cleans of no less than 5 mesh strips at one time under the same conditions.

As the recommended protocol from Perkin Elmer, the instrument-based mesh clean was investigated first. For this, neat mesh was loaded into the sample holder, and each sampling 'area' was then exposed to the nitrogen plasma (under normal operating conditions as outlined in the Methods and Materials chapter) for 30 seconds. For comparison, data was acquired for the first five seconds of a clean, and for five seconds following the 30 second exposure.

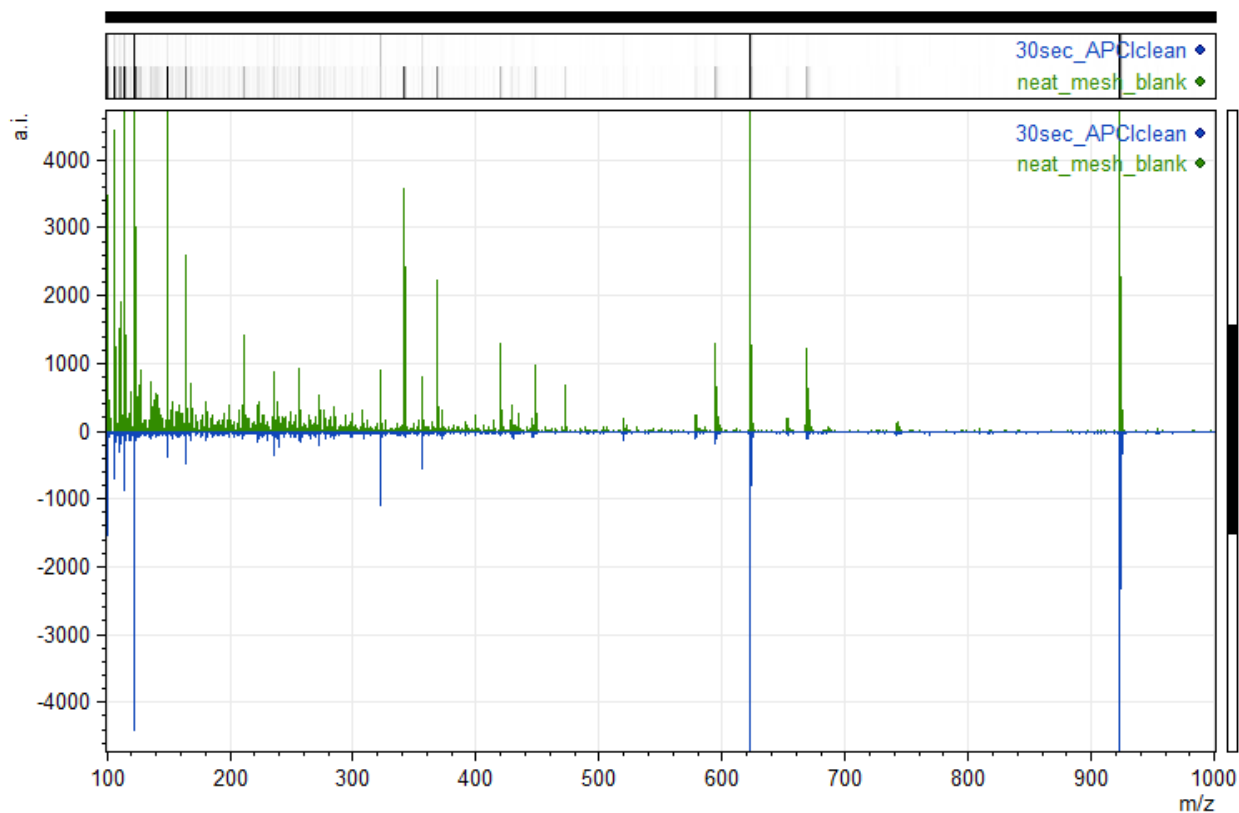


Figure 28: Comparison of neat mesh prior to instrument plasma exposure (green trace), and the same area of mesh after 30 seconds of instrument plasma exposure (blue trace)

Comparison of the neat mesh with the instrument cleaned mesh shows a marked decrease in the noise across the entire range (Figure 28). In particular, the areas below  $m/z$  350 where the noise was of most immediate concern show substantial improvement.

### 3.3.2 Plasma cleaning optimisation

Despite the success in applying instrument plasma mesh cleans to neat mesh, this process was time consuming, with each mesh strip taking no less than six minutes to clean. Where large amounts of testing are performed, many of these mesh strips will be used, and a six-minute cleaning time for each would substantially increase the time required for testing. Bulk plasma cleaning is able to treat multiple mesh strips at one time, with the only limiting factor being the size of the plasma chamber. This process involves the transformation of a gas into plasma, inside a vacuum chamber, by applying a current. This has been shown to burn away organic compounds [152], leaving behind a cleaner mesh, and therefore a cleaner background spectrum. The degree of cleanliness is dictated by the amount of time the mesh is cleaned for, therefore this must be optimised, and a compromise between the time taken for preparation and the sensitivity pay-off reached. Argon and oxygen plasma were chosen for the optimisation. Each of the plasma types were compared, along with cleaning times of 2, 3, 5 and 10 minutes, for argon and oxygen. Instrument based cleans were compared with the argon and oxygen plasma treatments as well.

For the purposes of comparison, the neat mesh spectrum in Figure 26 is considered representative of all neat mesh provided by the manufacturer and should be the baseline against which all plasma cleans in this section are compared.

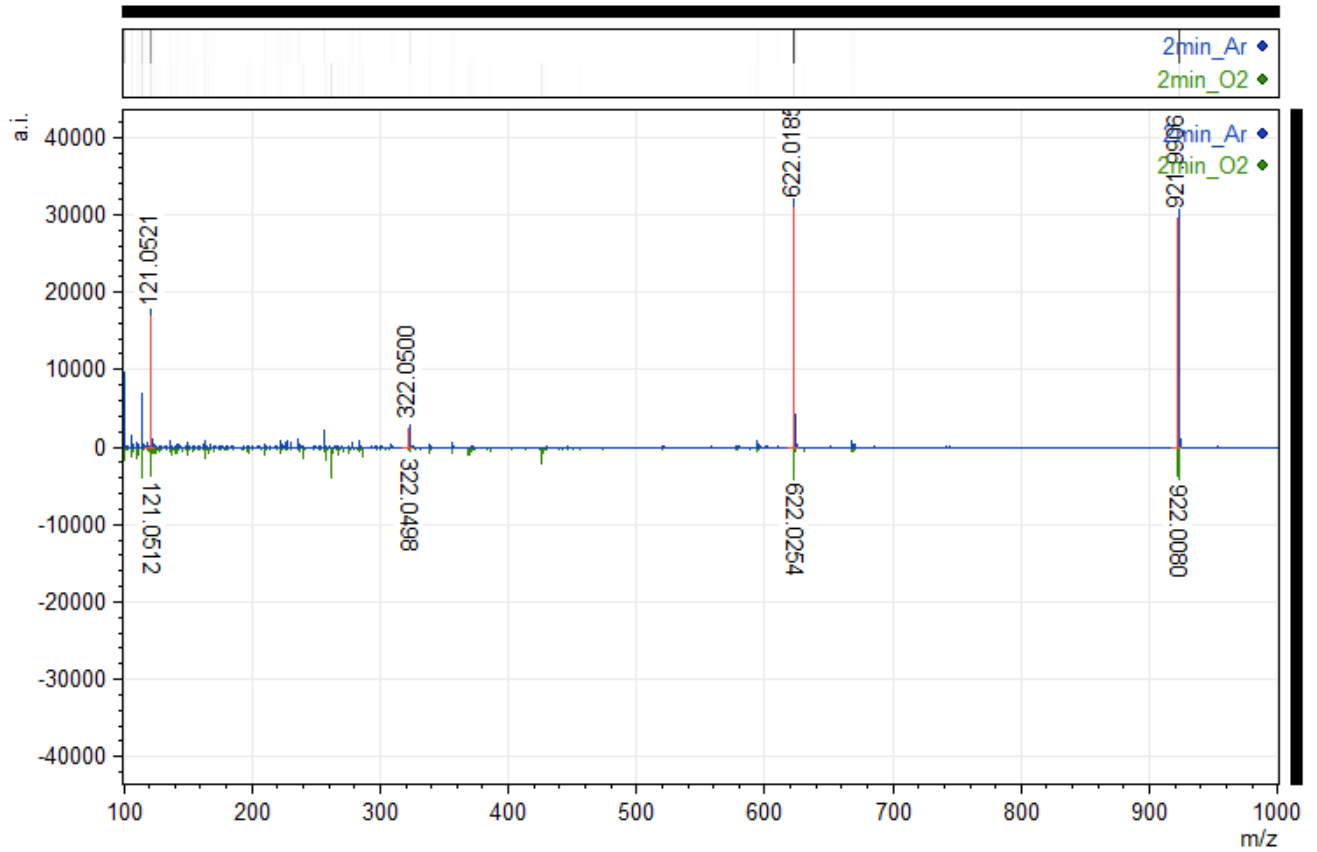


Figure 29: Comparison of background between two minutes of argon plasma cleaning (blue trace) and two minutes of oxygen plasma cleaning (green trace), with calibrant peaks highlighted

The comparison of the two plasma types for the two-minute clean shows that there isn't a significant difference between them in terms of total noise. The oxygen plasma (green trace) appears to have a few extra peaks in the low mass region, whereas the argon plasma (blue trace) appears to have a few extra peaks in the higher mass range (Figure 29).

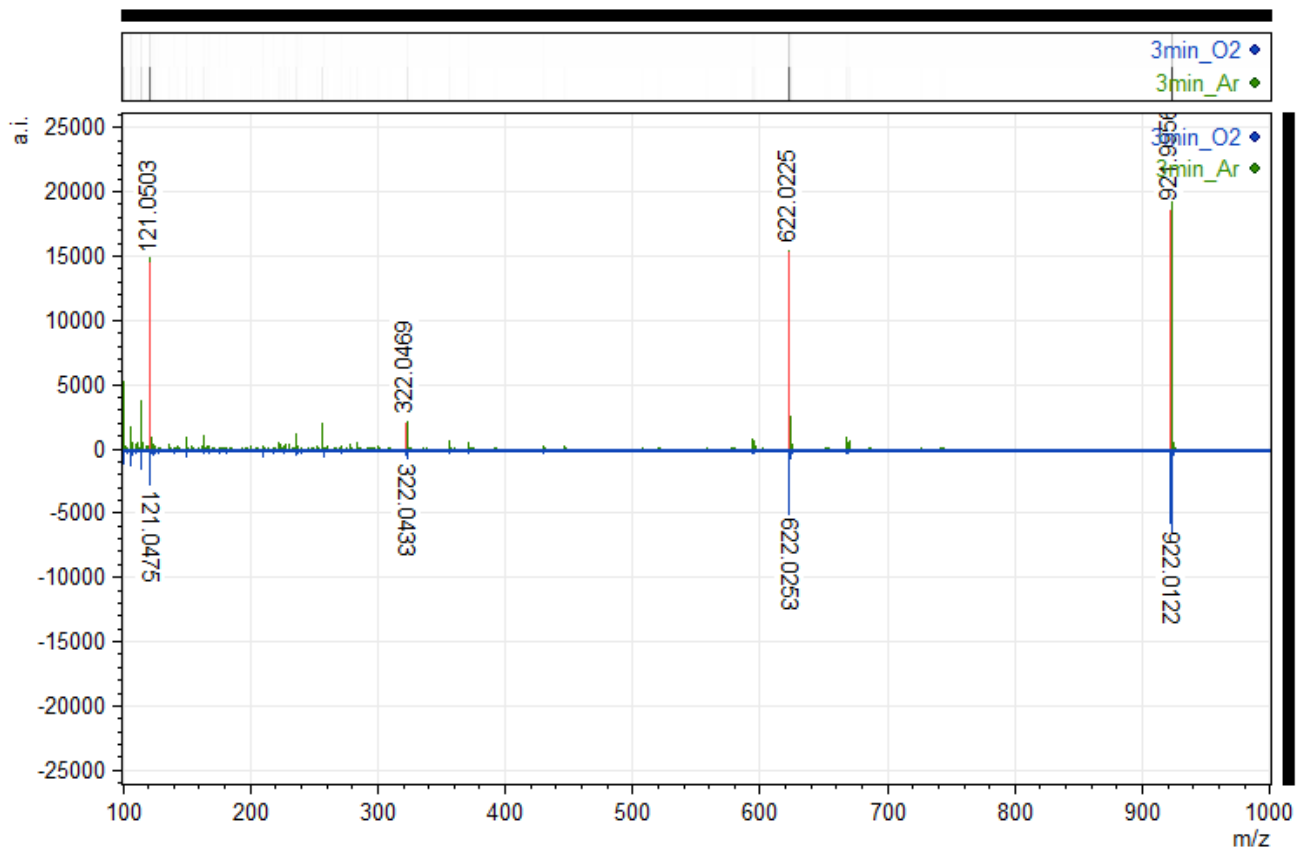


Figure 30: Comparison of background between three minutes of argon plasma cleaning (green trace) and oxygen plasma cleaning (blue trace), with calibrant peaks highlighted

Increasing the plasma cleaning time to three minutes reduced the total number of peaks, and the intensity of all peaks across the spectrum for both oxygen (blue trace) and argon (green trace) (Figure 30). The oxygen plasma has a smaller number of peaks overall in this background spectrum, although in the areas of interest (<350) there are significantly less peaks for both plasma types.

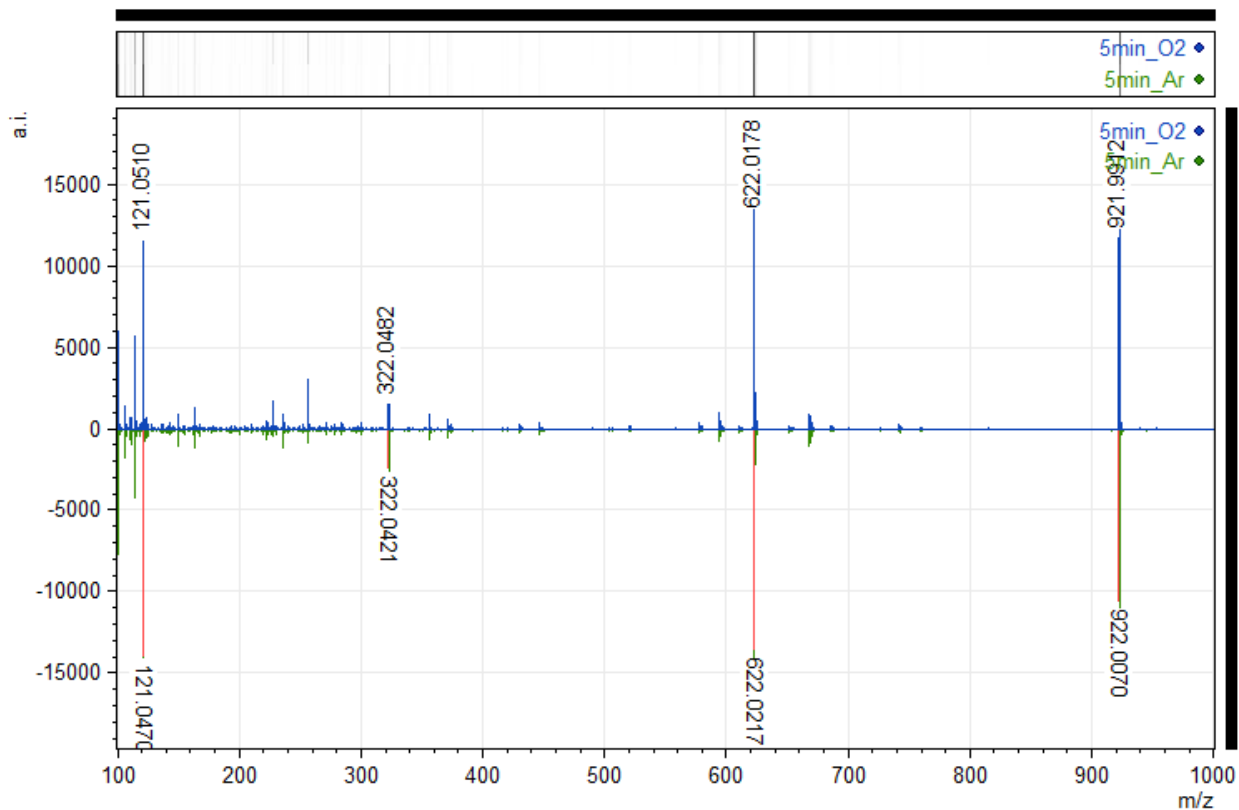


Figure 31: Comparison of background between five minutes of argon plasma cleaning (green trace) and oxygen plasma cleaning (blue trace), with calibrant peaks highlighted

An increase of the plasma cleaning time to five minutes shows a decrease in the total number of peaks in the argon treated plasma (green trace), in both number and intensity (Figure 31). The oxygen cleaned plasma shows what appears to be an increase in the number of peaks from the previous plasma clean, although this may be due to the movement and time delay between the plasma chamber and the DSA-ToF. The oxygen plasma deposits free radicals on the surface of the mesh, which can react with the air and other surfaces [153]. It is therefore reasonable to expect that longer oxygen plasma exposure would result in more free radicals deposited, and more subsequent fouling of the mesh through increased reactivity during this time delay between cleaning and use for acquisition.

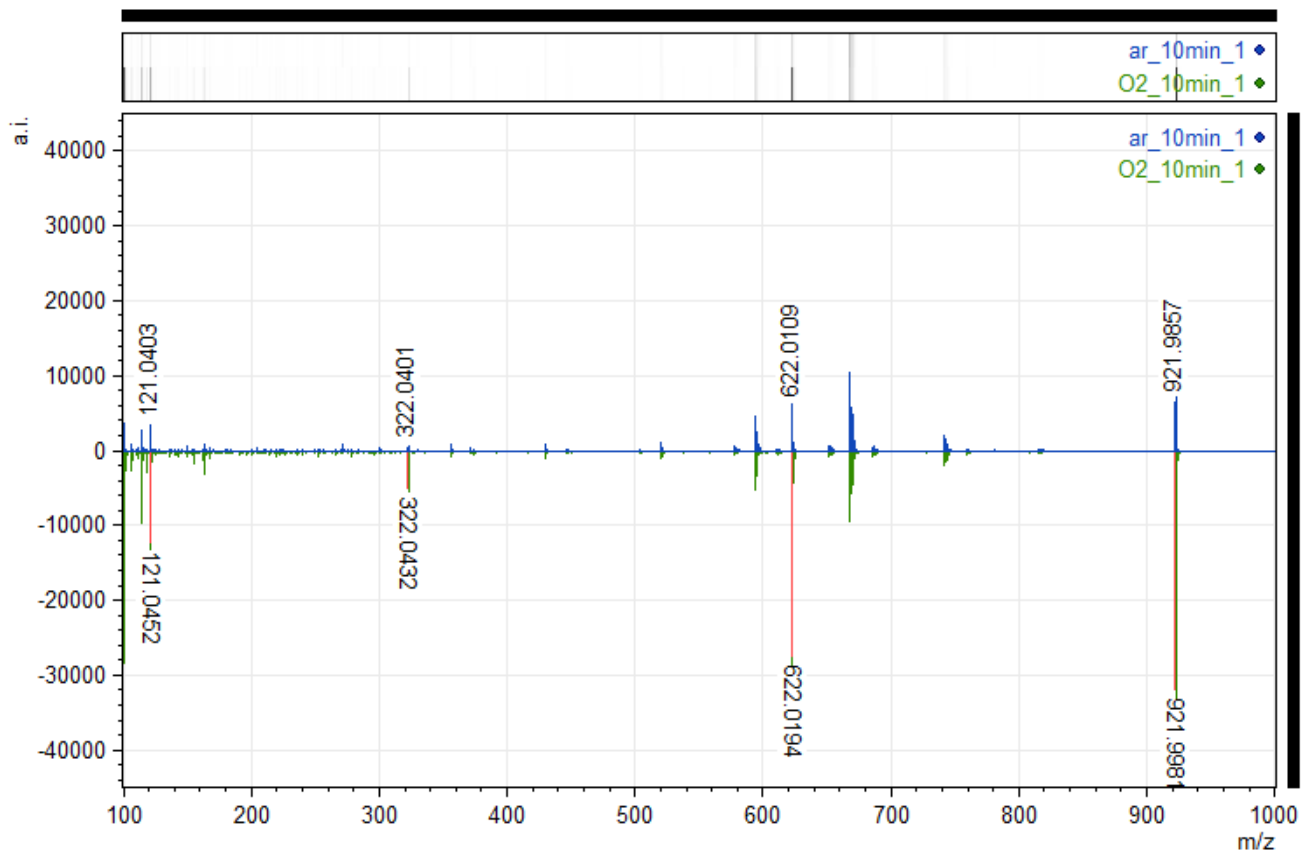


Figure 32: Comparison of background between 10 minutes of argon plasma cleaning (blue trace) and oxygen plasma cleaning (green trace), with calibrant peaks highlighted

The ten-minute plasma clean reduced the background peaks to a level where they are hardly visible at all in both the argon (blue trace) and the oxygen (green trace) plasma cleaned mesh (Figure 32). There are still some peaks present in the  $m/z$  600-700 region, which are due to polysiloxanes [154], common contaminants from the manufacturing processes and handling, or from the instrument itself. Regardless of their origin, these peaks are not in the areas of interest for this work and will not interfere with the analysis of the targeted compounds.

The initial testing of the instrument plasma clean was conducted without movement of the mesh from the instrument. That is, the clean and subsequent acquisition were performed on the same sample spot without a time delay. A small experiment to determine if instrument plasma cleaning increased mesh fouling through increase reactivity was carried out. For this, a sample spot was cleaned for 30 seconds in the instrument, removed from the instrument and replaced. A second acquisition was then carried out on the

same sample spot. The background from this spectrum was then compared to another sample position on the same mesh that was cleaned and tested without being removed from the instrument.

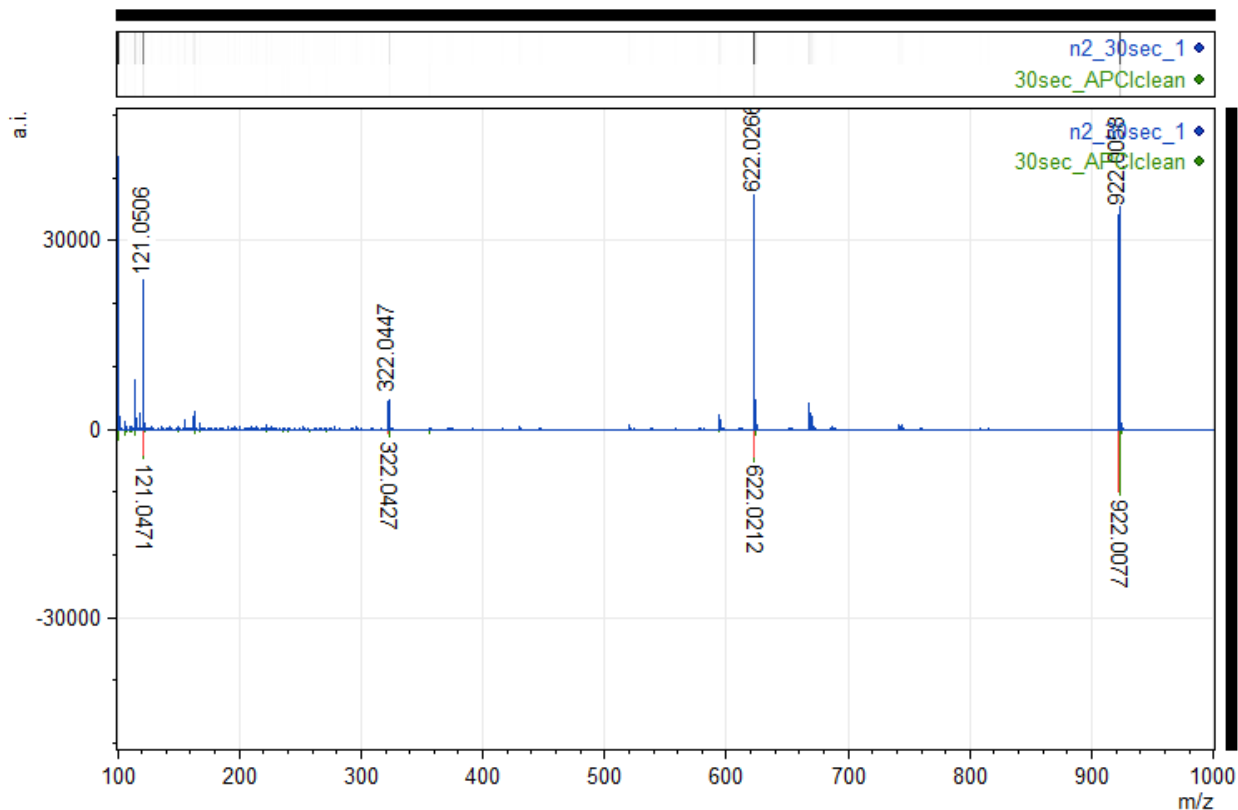


Figure 33: Comparison of background between instrument cleaned mesh with lab exposure after clean (blue trace) and no lab exposure after clean (green trace). Calibrant peaks are highlighted

A number of extra peaks are visible in the spectrum of the mesh with lab exposure after cleaning. These data indicate that there is some fouling of the mesh surface following lab exposure after the instrument plasma cleaning (Figure 33). The implications here are that the mesh should be moved and handled as little as possible after plasma exposure, regardless of the type of plasma cleaning regime used.

### 3.3.3 Plasma cleaning summary

These cleaning protocols clearly reduce the amount of organic matter on the mesh, reducing the background noise. Without appropriate care after cleaning, the noise may be increased by exposure and reaction with free radicals remaining on the mesh surface. For this reason, bulk plasma cleaning may only be appropriate when large numbers of mesh are required and the time constraints of instrument based cleans are unrealistic. For cases where a small number of tests are being carried out, instrument-based cleaning is more appropriate, as there is reduced potential for post-clean fouling through movement and

handling of the mesh. Where bulk plasma treatment is required, argon plasma reduces the background contamination and shows less post-clean fouling than the oxygen plasma treated mesh.

### 3.4 Determination of linear range

For the determination of linear range, two ranges of drug concentrations were analysed: A larger range of 20-1000ng/mL over eight points (20, 50, 100, 200, 300, 400, 500, 1000 ng/mL), and a lower range of 10-200ng/mL over seven points (10, 20, 50, 100, 120, 150, 200 ng/mL). All three of the drugs were analysed on three mesh types: argon plasma cleaned, oxygen plasma cleaned and instrument plasma cleaned mesh (instrument treated). Each solution was made up with an ISTD concentration of 200ng/mL for the larger range, and 100ng/mL for the low range. Solutions of 0ng/mL concentration for each of the drugs, with their ISTD were also made up, to determine the limits of detection and quantification for each of the mesh types and range. The ratio of the intensity of the parent drug to the ISTD was used as a measure of the response. Internal standard molecular weights and protonated molecular weights are highlighted in Table 8.

Table 8: Molecular weights of protonated and non-protonated deuterated internal standards of THC, MDMA and cocaine

	<b>Molecular weight (Da)</b>	<b>Protonated molecular weight (Da)</b>
D <sup>3</sup> -THC	317.48	318.2588
D <sup>5</sup> -MDMA	198.27	199.1585
D <sup>3</sup> - cocaine	306.37	307.1749

Limits of detection and quantification were calculated according to the NATA guidelines for Validation and Verification of Quantitative and Qualitative Test Methods [155]. Limits of detection (LoD) were calculated as the mean response of the blank plus three standard deviations of the blank. Limits of quantification (LoQ) were calculated as the mean response of the blank plus 10 standard deviations of the blank.

Cross-validation (%CV) of results was calculated by comparing the calculated concentration of each point of the calibration (using the linear regression) to the expected concentration at that point. These values are reported as percent deviations from the expected value.

Based on the results for the plasma cleaning optimisation, it was thought that determining the LoD and LoQ of each drug on mesh treated with different plasma types may improve these calculated limits based where noise is reduced. Evaluation of both a large and a small range for quantification was performed to identify the optimum working range for each drug where content can reliably be calculated.

As each mesh type was to be compared to one another within each of the two calibration ranges, all single drug data across either of the ranges on each mesh type was acquired on the same day. This was done to reduce the impact of inter-day environmental variation and the variations this can induce in the instrument response (as established in Chapter 2).

### 3.4.1 Large range calibration of cocaine on various mesh types

Initial testing for cocaine was done on instrument plasma treated mesh. Each mesh strip was cleaned immediately prior to use and was discarded once all sample spots were used.

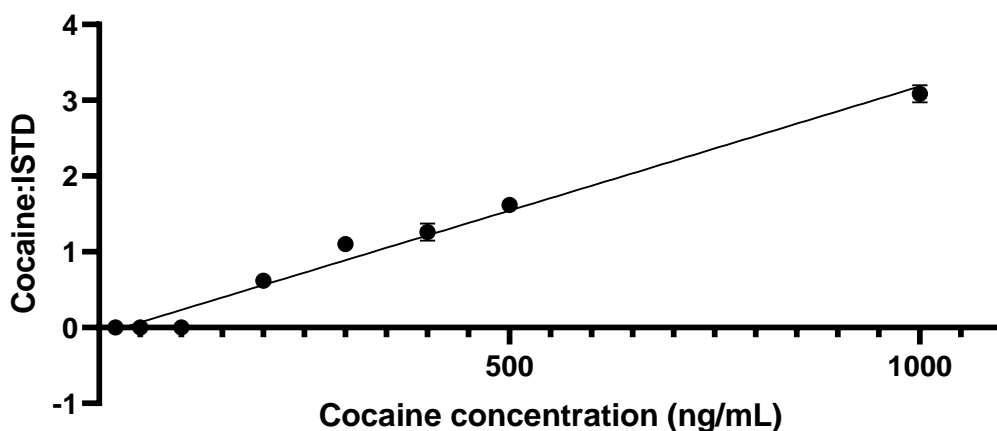


Figure 34: Quantification of cocaine in water on instrument-plasma treated mesh across a large range 20-1000ng/mL, n=5 and each error bar is equivalent to  $\pm 1$  SD.  $R^2= 0.9806$

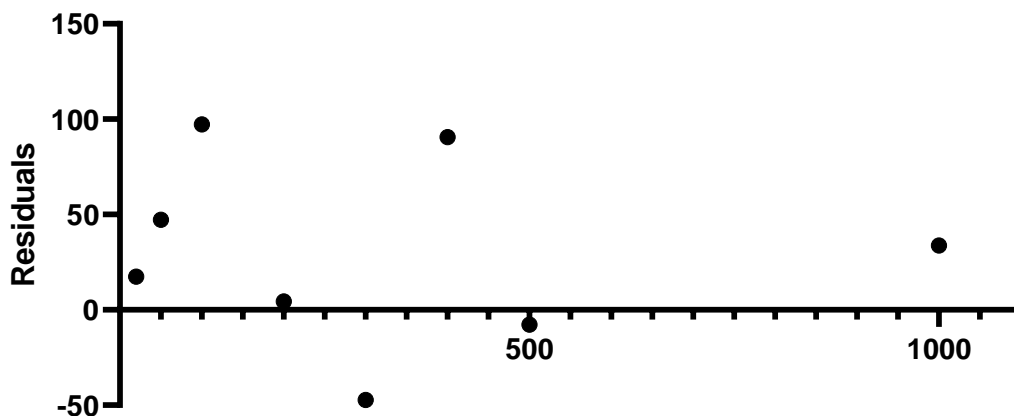


Figure 35: Residuals analysis of the linear regression of cocaine in water (20-1000ng/mL) on instrument plasma treated mesh

For cocaine in water across this range on this mesh type (Figure 34) the trend appears linear for concentrations above 200ng/mL. Residuals analysis is unbiased and homoscedastic, with mostly positive values. This indicates that the predicted values at these points are being underestimated.

This analysis also revealed that the deuterated ISTD of cocaine had a higher response than the cocaine molecular ion at the same concentration (Figure 36).

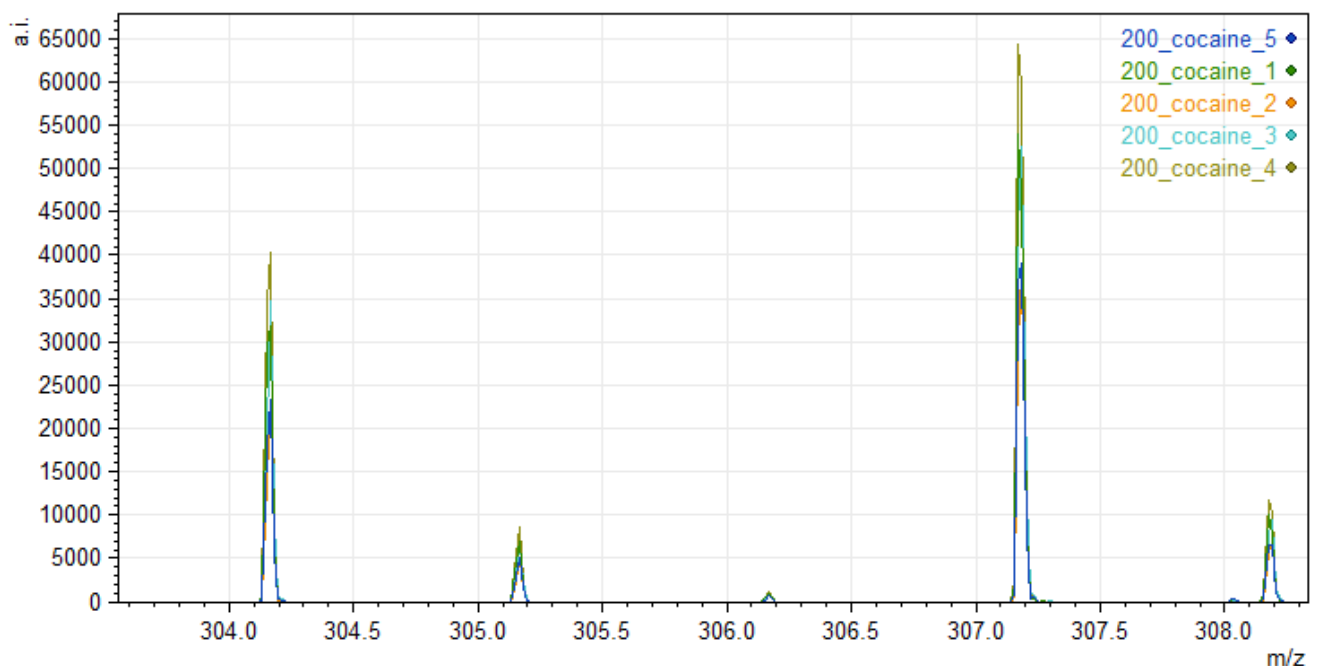


Figure 36: Comparison of cocaine peak (m/z 304) and D3- cocaine (m/z 307) for solution in water at equivalent concentrations (200ng/mL) on non-plasma treated mesh

Typically, the two peaks would be equivalent, with a ratio of approximately 1.0, which is true for both THC and MDMA. However, for cocaine, this ratio has an average of 0.62, which confirms a higher peak intensity of ISTD at this concentration. This is unusual, as the isotopologue should behave chemically identically to the target analyte, which includes ionisation behaviour. Despite this unusual response, the behaviour is consistent for all analyses, and therefore does not impact the results at all.

The calculated LoD for cocaine across this range on this mesh type, was 30ng/mL, and the LoQ was determined to be 32ng/mL.

The %CV for cocaine in this range are recorded in Table 9, where the results also indicate an accurate quantitation across this range for cocaine, with all values (with the exception of 100ng/mL) falling within an acceptable range.

Table 9: Calculated %CV for cocaine in water over large range on instrument-plasma treated mesh

Expected concentration (ng/mL)	Calculated concentration (ng/mL)	% CV
20	19	7
50	44	13
100	57	43
200	196	2
300	347	-16
400	397	0.8
500	508	-2
1000	966	3

These %CV values show that the under estimation of the lower points in the calibration is quite significant. Consistent underestimation of concentration can mean that the regression is weighted towards the higher points in the calibration, and that calibration across this range may not be appropriate for accurate quantification.

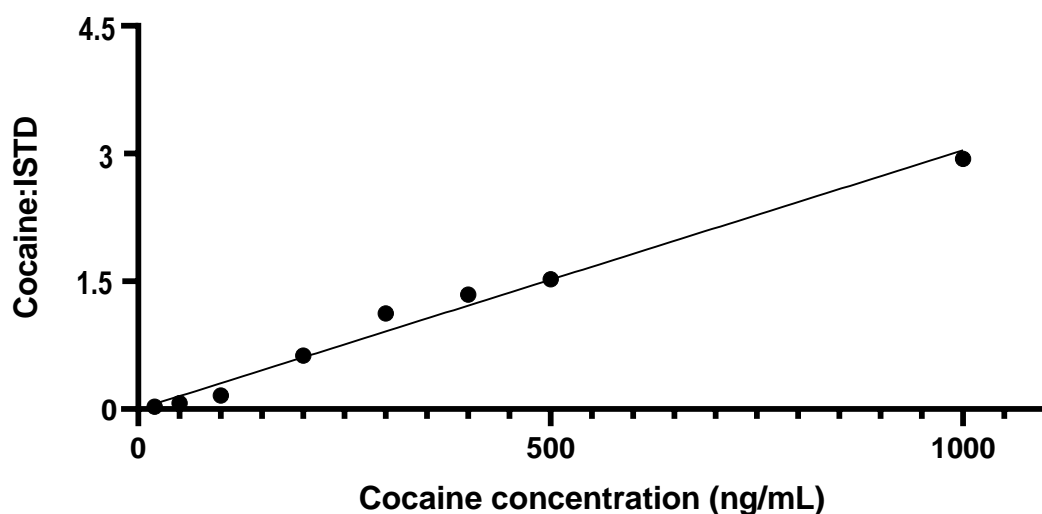


Figure 37: Quantification of cocaine in water on argon plasma treated mesh across a large range 20-1000ng/mL, n=5 and each error bar is equivalent to  $\pm 1$  SD.  $R^2= 0.9841$

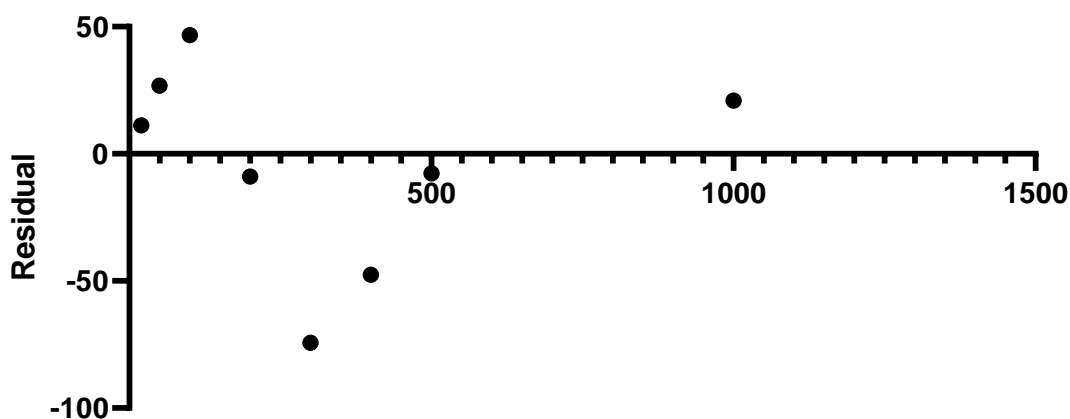


Figure 38: Residuals analysis of the linear regression of cocaine in water (20-1000ng/mL) on argon plasma treated mesh

For the argon plasma treated mesh (Figure 37), comparison to the instrument-plasma cleaned mesh (Figure 34) would indicate that the linearity has increased for cocaine in this range, based on the correlation coefficient alone. The data on argon plasma treated mesh certainly appears to be more linear, and very consistent (small SD values). Residuals analysis is unbiased and homoscedastic, with the random distribution indicating that the predicted values are not being consistently over or under estimated.

The LoD and LoQ for cocaine in this range on mesh were unable to be determined, due to poor linearity. The calculated %CV for cocaine are recorded in Table 10.

Table 10: Calculated %CV for cocaine in water across a large range on argon plasma treated mesh

Expected concentration (ng/mL)	Calculated concentration (ng/mL)	% CV
20	9	56
50	23	54
100	53	47
200	209	-5
300	374	-25
400	448	-12
500	508	-2
1000	979	2

Despite the linearity observed, and the high correlation coefficient, the predicted values for the lower points in the calibration are underestimated quite significantly. This indicates that a calibration range this wide is

not acceptable for quantification of cocaine on argon plasma treated mesh.

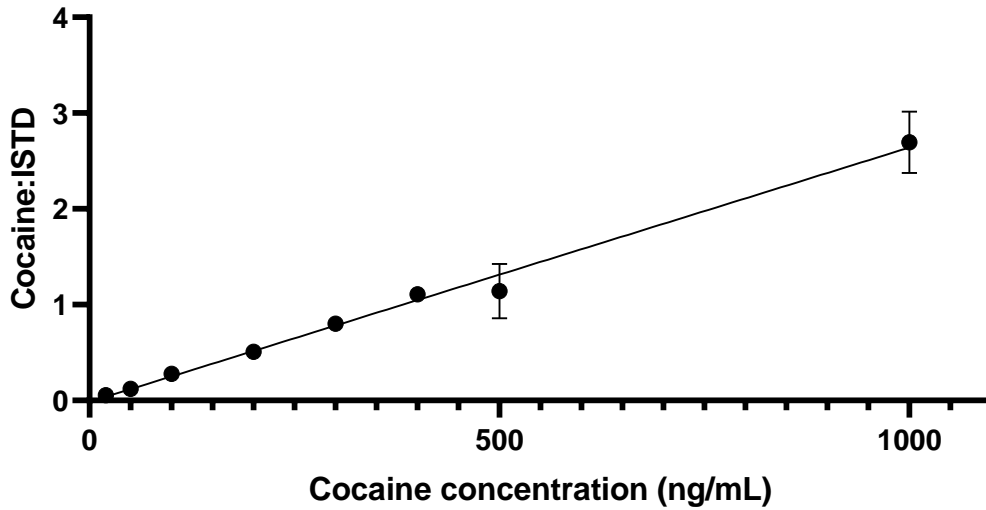


Figure 39: Quantification of cocaine in water on oxygen plasma treated mesh across a large range 20-1000ng/mL, n=5 and each error bar is equivalent to  $\pm 1$  SD.  $R^2=0.9689$

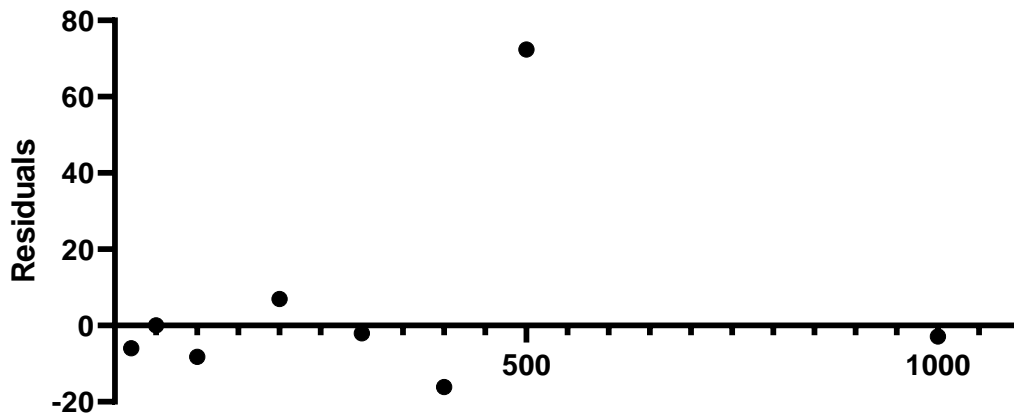


Figure 40: Residuals analysis of the linear regression of cocaine in water (20-1000ng/mL) on oxygen plasma treated mesh

Linearity across this range for cocaine on oxygen plasma treated mesh is further reduced from that of the argon and instrument cleaned plasma meshes, using the correlation coefficient as the measure (Figure 39). Visually, the fit appears better, with the point at 500ng/mL seeming to be the only point that deviates from the fit. This deviation is visible in the residuals analysis (Figure 40), which is unbiased and homoscedastic,

with most values differing little from zero. This indicates good agreement between the actual and predicted values, for all points except 500ng/mL.

The LoD and LoQ were calculated to be 14ng/mL and 25ng/mL respectively. The calculated %CV values can be seen in Table 11.

Table 11: Calculated %CV for cocaine in water across a large range on oxygen plasma treated mesh

<b>Expected concentration (ng/mL)</b>	<b>Calculated concentration (ng/mL)</b>	<b>% CV</b>
20	26	-30
50	50	0.04
100	108	-8
200	193	4
300	302	-0.7
400	416	-4
500	428	15
1000	1003	-0.3

The %CV values across this range are all quite close to zero, with the exception of the 20ng/mL and 500ng/mL points. At the lower end of the calibration the 20ng/mL point was over estimated significantly. The 500ng/mL point was under-estimated, with a response approximately equivalent to that of the 400 ng/mL point. The LoQ across this range was above the lowest value for this calibration, which explains the poor correlation between the expected and calculated values for that calibration point.

#### 3.4.2 Low range calibration of cocaine on various mesh types

The linearity of a reduced (low) range of cocaine concentrations was assessed to identify an improvement in linearity over the larger range. As with the larger range, instrument plasma treated mesh was assessed first.

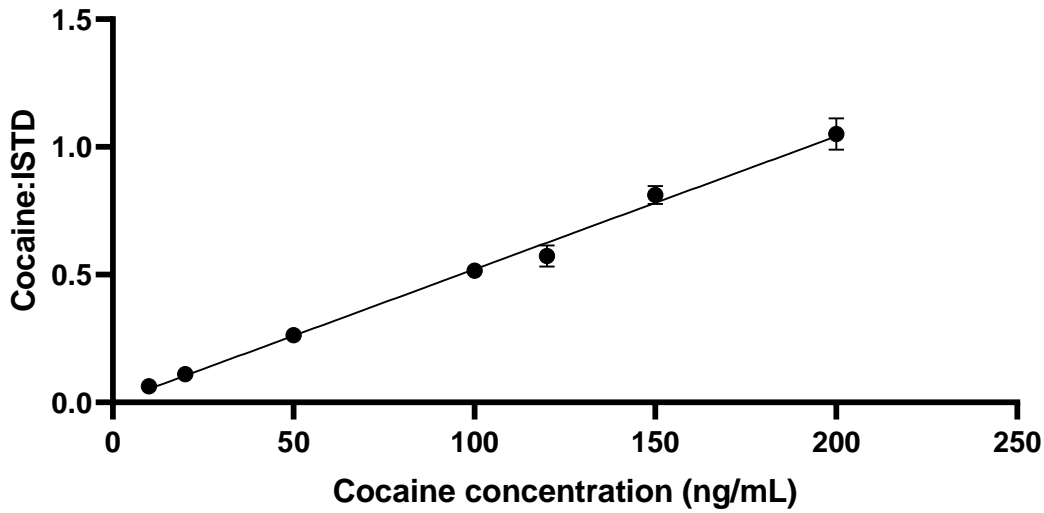


Figure 41: Quantification of cocaine in water on instrument-plasma treated mesh across a low working range 10-200ng/mL, n=5 and each error bar is equivalent to  $\pm 1$  SD.  $R^2=0.9880$

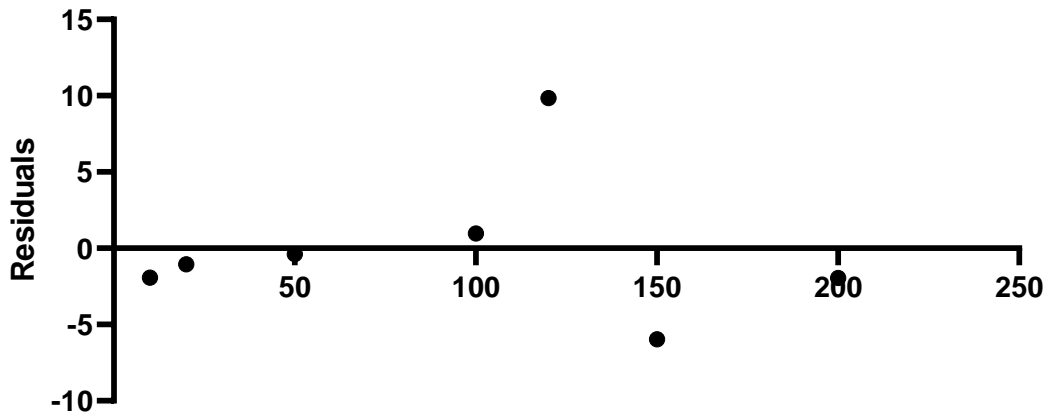


Figure 42: Residuals analysis of the linear regression of cocaine in water (10-200ng/mL) on instrument plasma treated mesh.

Comparison of the large range (Figure 34) and low range (Figure 41)  $R^2$  values show an improvement in the linearity of cocaine over reduced range on instrument plasma treated mesh. Visually the fit is improved, with little deviation from the fit for all points, with larger SDs for the 120 and 150ng/mL points. Residuals analysis shows a random distribution, with most points clustered around zero, indicating a good fit.

The LoD and LoQ for this data across this range were calculated to be 4ng/mL and 10ng/mL respectively. This represents a significant increase in sensitivity for this range when compared with the larger range on the same mesh. The calculated %CV values can be found in Table 12.

Table 12: Calculated %CV for cocaine in water across a low working range on instrument-plasma treated mesh

Expected concentration (ng/mL)	Calculated concentration (ng/mL)	% CV
10	12	-19
20	21	-5
50	50	-0.8
100	99	1
120	110	8
150	156	-4
200	202	-1

These %CV values indicate that this low calibration range is more appropriate than the larger one, as the deviations between the actual and predicted concentration values are small and close to zero, meaning that the predicted values are close to the actual concentrations.

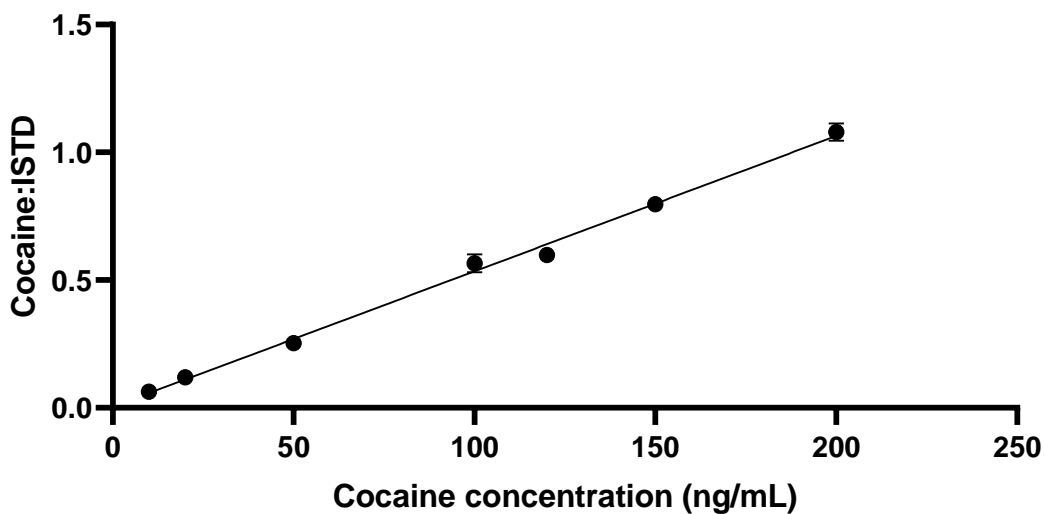


Figure 43: Quantification of cocaine in water on argon treated mesh across a low working range 10-200ng/mL, n=5 and each error bar is equivalent to  $\pm 1$  SD.  $R^2=0.9928$

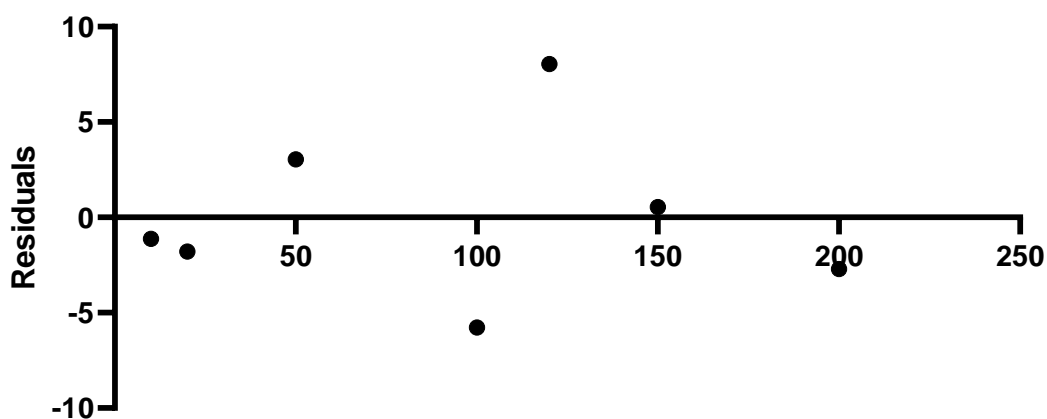


Figure 44: Residuals analysis of the linear regression of cocaine in water (10-200ng/mL) on argon plasma treated mesh

The linearity for cocaine across this range on argon plasma treated mesh (Figure 43) is far improved when compared to that of the same mesh over the larger concentration range (Figure 37) and that of the low range on instrument plasma treated mesh (Figure 41). An  $R^2$  value of above 0.99 indicates very good fit for the data presented. Residuals analysis shows a random distribution, clustered around zero (Figure 44).

The LoD and LoQ across this range were calculated to be 1ng/mL and 3ng/mL respectively. These are higher than those calculated across the larger range, despite linearity being improved. The calculated %CV values can be seen in Table 13.

Table 13: Calculated %CV for cocaine in water across a low working range on argon plasma treated mesh

<b>Expected concentration (ng/mL)</b>	<b>Calculated concentration (ng/mL)</b>	<b>%CV</b>
10	11	-11
20	22	-9
50	47	6
100	106	-6
120	112	7
150	150	0.4
200	203	-1

Although the LoD and LoQ for this range are higher than that of the larger range, the improved linearity has resulted in a substantial increase in the correlation between the predicted concentration and the expected concentration. This indicates that the lower calibration range is more suitable for quantitative analysis of cocaine on argon plasma treated mesh.

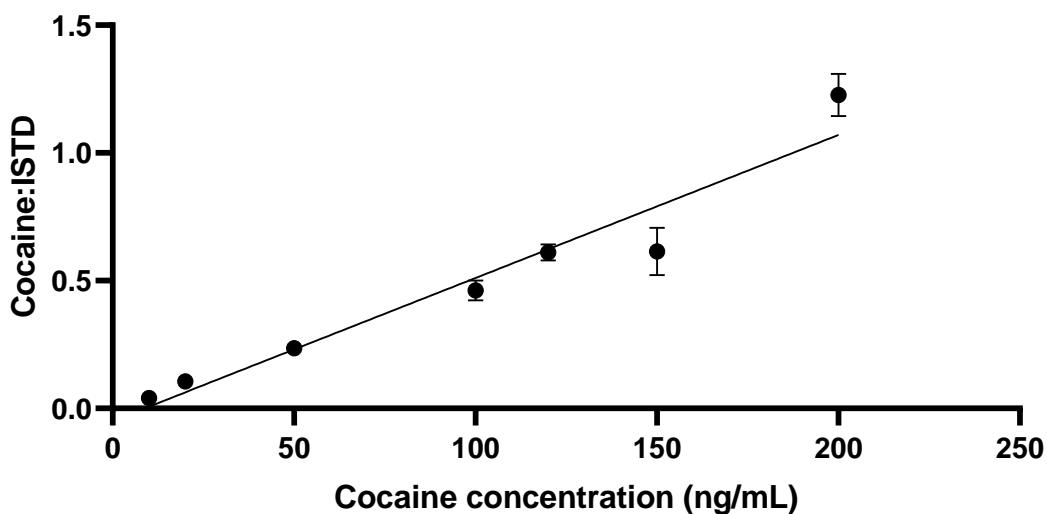


Figure 45: Quantification of cocaine in water on oxygen treated mesh across a low working range 10-200ng/mL, n=5 and each error bar is equivalent to  $\pm 1$  SD.  $R^2=0.9237$

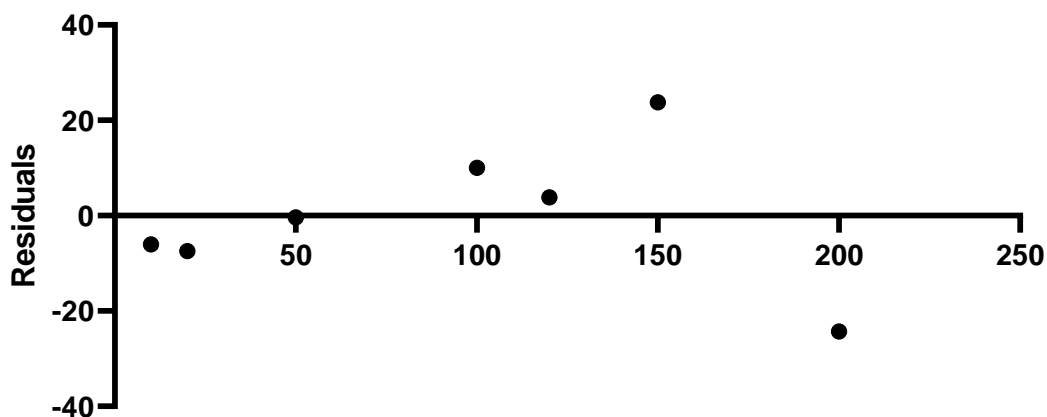


Figure 46: Residuals analysis of the linear regression of cocaine in water (10-200ng/mL) on oxygen plasma treated mesh

For oxygen plasma treated mesh, there has been a significant reduction in linearity across this range (Figure 45) when compared to the larger range (Figure 39). There is significant deviation from the fit for the 150 and 200ng/mL data points, with this reflected in the residuals analysis as outliers at these two points (Figure 46).

The LoD and LoQ across this range were calculated to be 12ng/mL and 16ng/mL respectively, a reduction from the large range on the same mesh type. The calculated %CV values can be seen in Table 14.

Table 14: Calculated %CV for cocaine in water across a low working range on oxygen plasma treated mesh

Expected concentration (ng/mL)	Calculated concentration (ng/mL)	% CV
10	16	-60
20	27	-37
50	50	-0.7
100	87	13
120	116	3.
150	126	16
200	224	-13

The calculated concentrations of the points are overestimated for 10ng/mL and 20ng/mL. As these values both fall above the LoD and LoQ across this range, this is unusual. These results show that the large calibration range is not suitable for quantification of cocaine, particularly for concentrations that fall at the lower end of this calibration.

### 3.4.3 Large range calibration of THC on various mesh types

Initial linearity assessments of THC were performed on instrument plasma treated mesh. Each mesh strip was cleaned immediately prior to use and discarded immediately following.

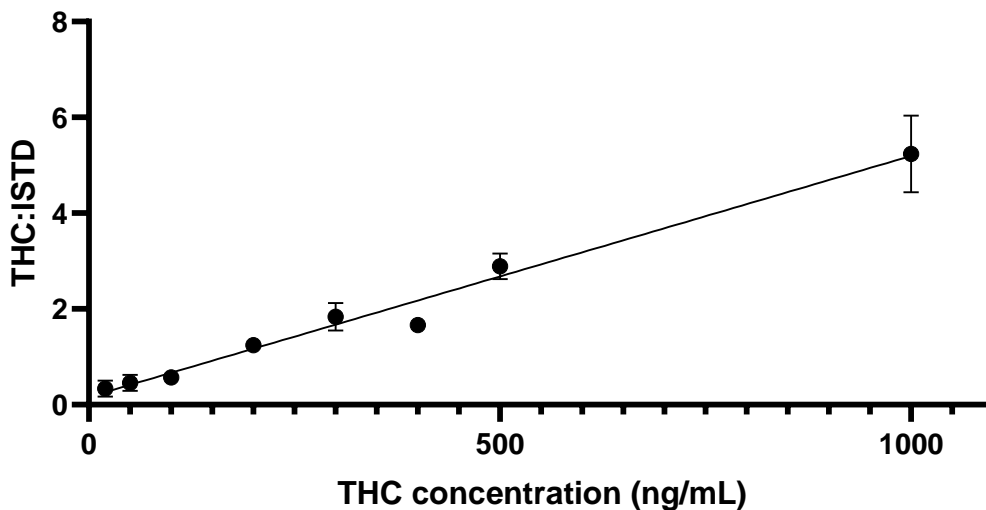


Figure 47: Quantification of THC in water on instrument plasma treated mesh across a large range 20-1000ng/mL, n=5 and each error bar is equivalent to  $\pm 1$  SD.  $R^2=0.9445$

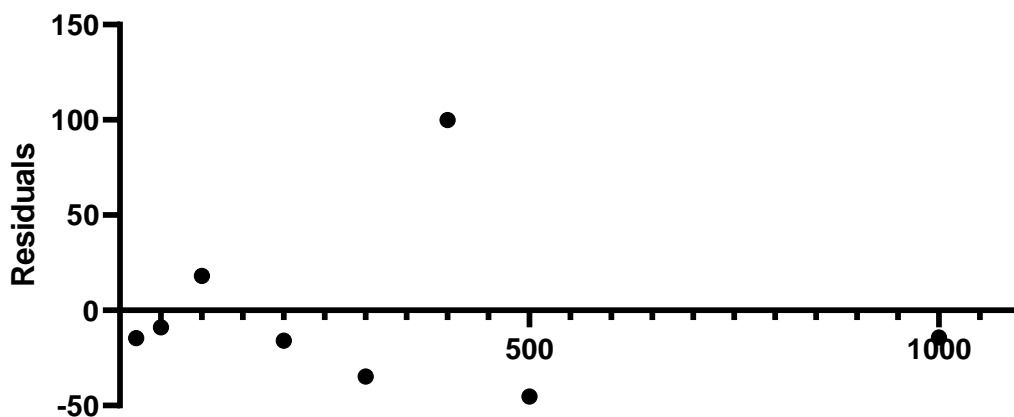


Figure 48: Residuals analysis of the linear regression of THC in water (20-1000ng/mL) on instrument plasma treated mesh

Linearity of THC across this extended range shows a linear trend, with an  $R^2$  value of 0.9445 (Figure 47). The calibration points appear to fit the linear regression applied, but the variability in the individual measurements (SD) at the higher concentration points (above 400ng/mL) affects the linearity. Residuals analysis is unbiased and homoscedastic, with one extreme outlier at 400ng/mL, and the rest of the values clustered more closely around zero (Figure 48).

LoD and LoQs across this range were calculated to be 241ng/mL and 732ng/mL. These values are very high, and do not agree with the %CV values calculated in Table 15, which show very reasonable agreement between the expected and calculated concentration for calibration points between 50-1000ng/mL. If these values were the true LoD and LoQ values, it is more likely that there would be no agreement between the expected and calculated concentrations. More likely, a large amount of background noise has falsely inflated the LoD and LoQ as a result of being unable to differentiate between isobaric interferences.

Table 15: Calculated %CV for THC in water over dynamic range on instrument-plasma treated mesh

Expected concentration (ng/mL)	Calculated Concentration (ng/mL)	% CV
20	35	-73
50	59	-18
100	82	18
200	216	-8
300	335	-12
400	300	25
500	545	-9
1000	1014	-1

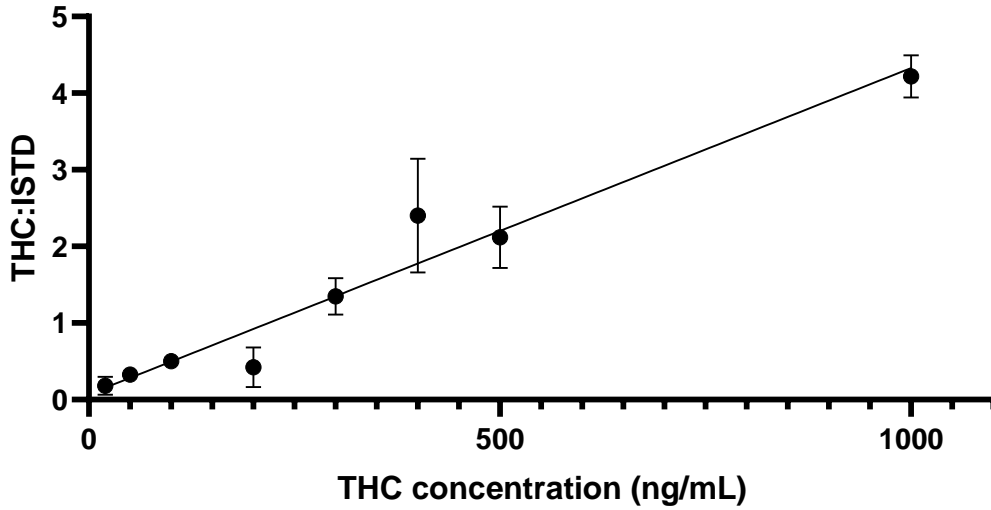


Figure 49: Quantification of THC in water on argon plasma treated mesh across a large range 20-1000ng/mL, n=5 and each error bar is equivalent to  $\pm 1$  SD.  $R^2=0.9034$

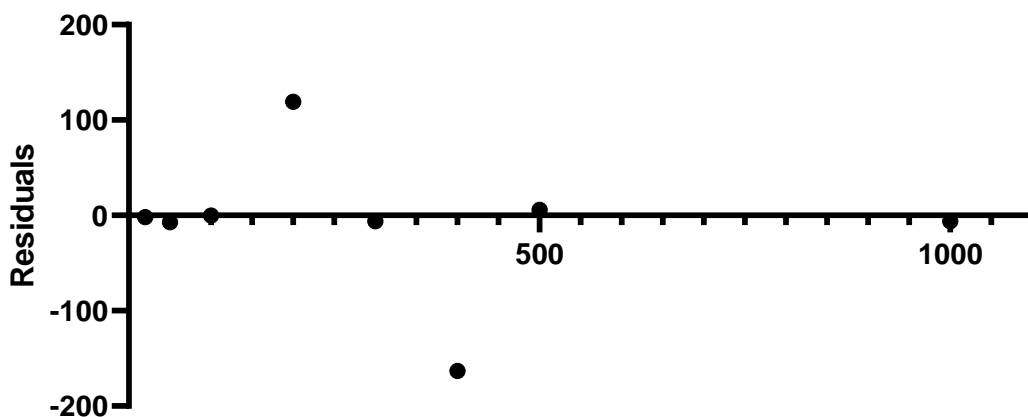


Figure 50: Residuals analysis of the linear regression of THC in water (20-1000ng/mL) on argon plasma treated mesh

The calibration across this range on argon plasma treated mesh is poor, with an  $R^2$  value of 0.9034 (Figure 49). Visually the fit of the linear regression is very poor, with larger standard deviations than have been observed for quantifications in this chapter. The residuals analysis shows most of the points are very close to zero, with the 200ng/mL and 400ng/mL the only outliers, the first being under estimated and the second being over-estimated (Figure 50).

The calculated LoD and LoQs were 182ng/mL and 498ng/mL respectively. As with the calibration on instrument plasma treated mesh, these values appear to be falsely inflated due to excessive noise in the blank. The %CV values again show reasonable agreement between the expected and calculated concentration values (Table 16).

Table 16: Calculated %CV for THC in water across a large range on argon plasma treated mesh

Expected concentration (ng/mL)	Calculated concentration (ng/mL)	% CV
20	39	-96
50	57	-14
100	100	-0.07
200	122	39
300	306	-2
400	509	-27
500	451	10
1000	1006	-0.6

The low calibration point %CV values show more deviation between the expected and calculated concentration than the higher values. This indicates that calibration across this range is not appropriate for quantification of low concentrations.

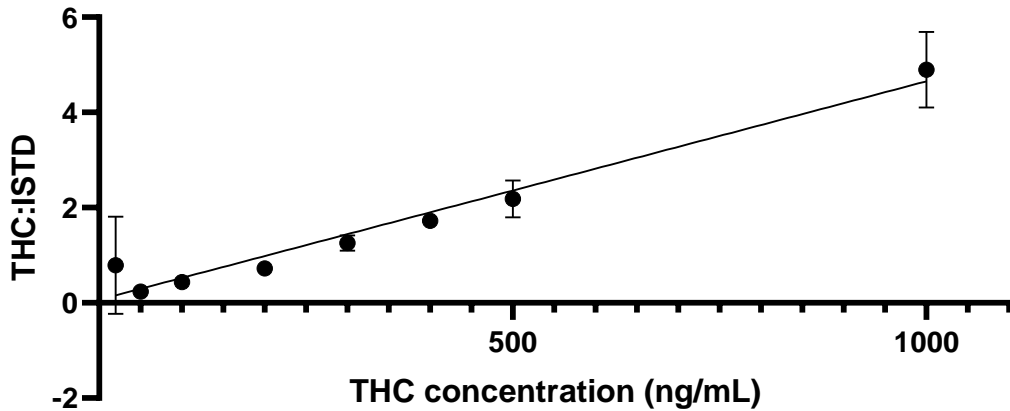


Figure 51: Quantification of THC in water on oxygen plasma treated mesh across a large range 20-1000ng/mL, n=5 and each error bar is equivalent to  $\pm 1$  SD.  $R^2=0.8920$

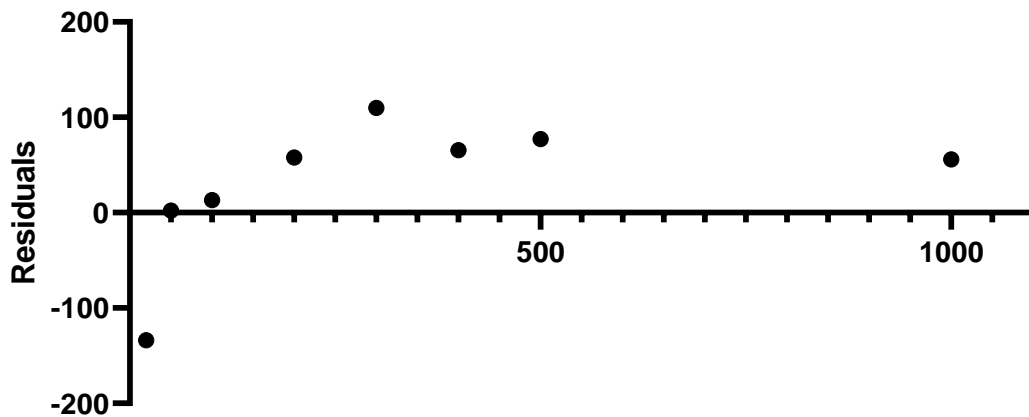


Figure 52: Residuals analysis of the linear regression of THC in water (20-1000ng/mL) on oxygen plasma treated mesh

The use of an oxygen plasma clean reduced the linearity across this range, with a decrease of the  $R^2$  value to 0.8920 (Figure 51). The calibration point at 20ng/mL was substantially higher in response than the 100ng/mL point. Residual analysis appears random, with the outlier at 20ng/mL the only negative value, due to the extreme over estimation of concentration. All other values were positive, indicating that the other points in the calibration curve are under-estimated (Figure 52). This is typical for a linear regression where there is an outlier at the low end, causing the under estimation of the remaining data.

LoD and LoQs across this range were calculated to be 50ng/mL and 142ng/mL respectively. The calculated %CV values can be seen in Table 17.

Table 17: Calculated %CV for THC in water across a large range on oxygen plasma treated mesh

<b>Expected concentration (ng/mL)</b>	<b>Calculated concentration (ng/mL)</b>	<b>% CV</b>
20	125	-527
50	77	-54
100	96	5
200	218	-9
300	216	28
400	328	18
500	411	18
1000	1080	-8

These values show reasonable agreement between the expected and calculated concentrations above 100ng/mL, which fits with the LoQ of just over 100ng/mL. The calculated concentrations also show the under estimation expected at the mid-range calibration points caused by the extreme over-estimation at the 20 ng/mL point.

#### 3.4.4 Low range calibration of THC on various mesh types

The large range THC calibrations were not suitable for quantification at low concentrations. Low range calibration was hoped to reduce these LoD and LoQs, to allow quantification of THC at low enough concentrations to be forensically useful.

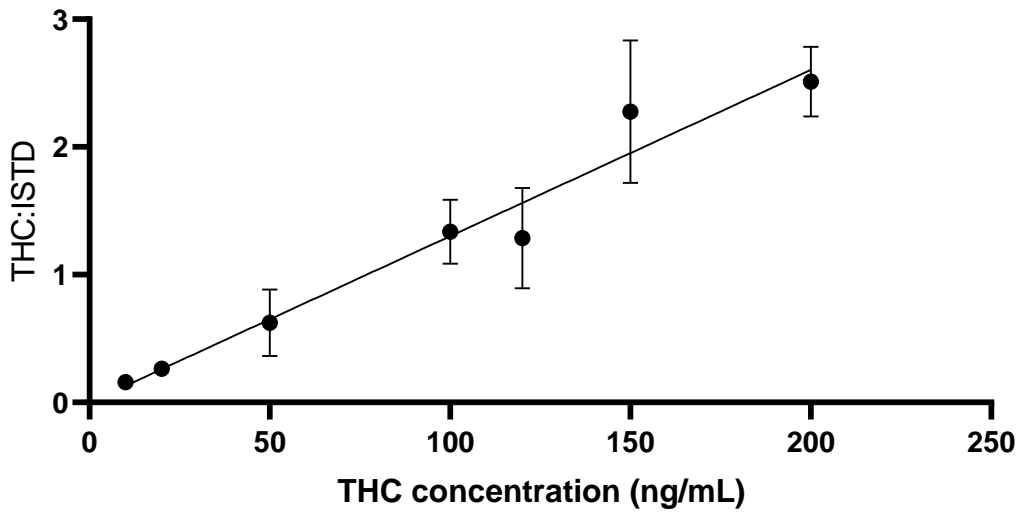


Figure 53: Quantification of THC in water on instrument plasma treated mesh across a low working range 10-200ng/mL, n=5 and each error bar is equivalent to  $\pm 1$  SD.  $R^2=0.8723$

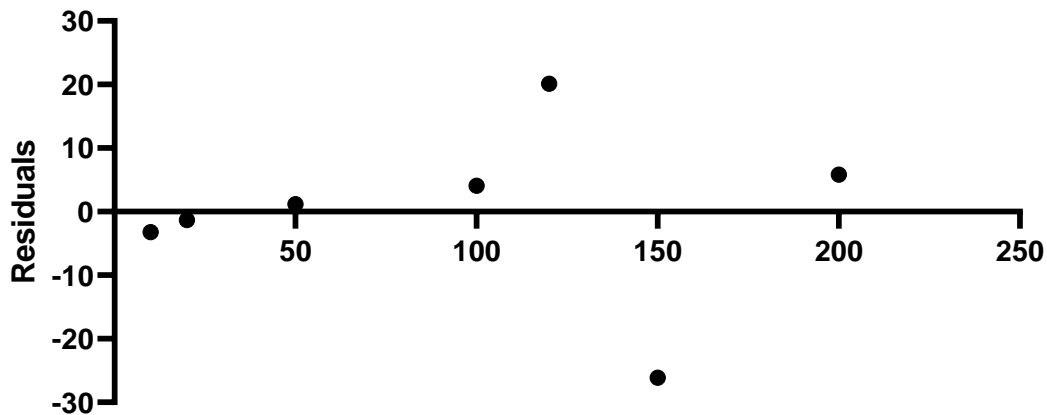


Figure 54: Residuals analysis of the linear regression of THC in water (10-200ng/mL) on instrument plasma treated mesh

Linearity of THC across this range on instrument plasma cleaned mesh was poor (Figure 53), poorer than that of the large range calibration on the same mesh type (Figure 48). The poor linearity can be attributed to large variability between replicates for each concentration, visualized as large error bars. Variations of this nature look are likely to be caused by ion interferences in the area where the target masses are located and are difficult to control with ambient mass spectrometry. Residual analysis shows a random, homoscedastic distribution, indicating no bias in the regression.

LoD and LoQs across this range were calculated to be 2ng/mL and 4ng/mL respectively. These values represent a significant drop in the LoD and LoQ from the large calibration range, despite the relatively poor linearity. Calculated %CV values can be seen in Table 18.

Table 18: Calculated %CV for THC in water across a low working range on instrument-plasma treated mesh

<b>Expected concentration (ng/mL)</b>	<b>Calculated concentration (ng/mL)</b>	<b>% CV</b>
10	13	-32
20	21	-7
50	49	2
100	96	4
120	100	17
150	176	-17
200	194	3

The calculated %CV values show good agreement between the expected and calculated concentrations, which is expected for these data where the LoD and LoQ values are below the lowest concentration calibration point. These values indicate that this lower calibration range will allow for quantification of THC at low levels.

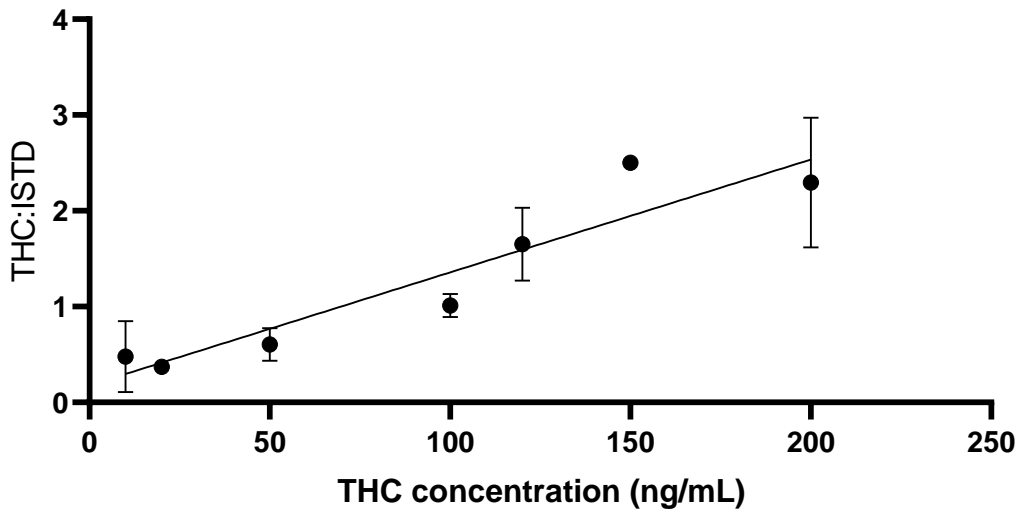


Figure 55: Quantification of THC in water on argon treated mesh across a low working range 10-200ng/mL, n=5 and each error bar is equivalent to  $\pm 1$  SD.  $R^2=0.7764$

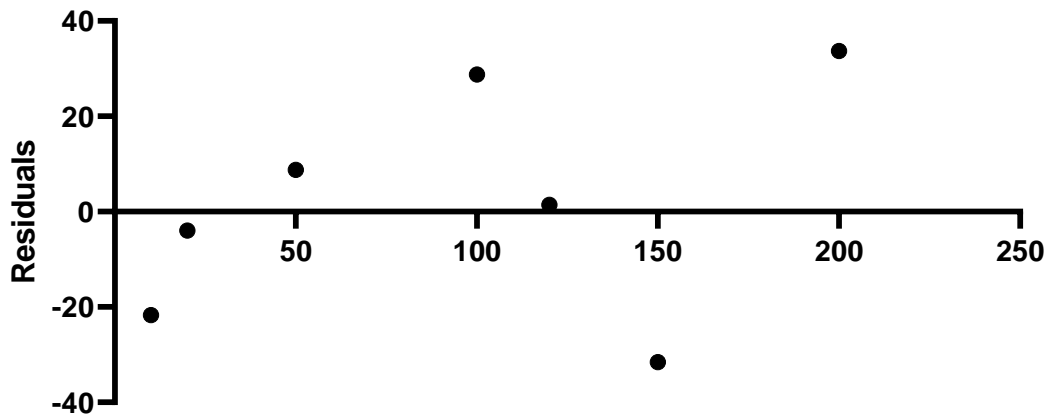


Figure 56: Residuals analysis of the linear regression of THC in water (10-200ng/mL) on argon plasma treated mesh

Linearity across the low range for argon plasma treated mesh is poor, with an  $R^2$  value of 0.7763. There appears to be a trend where the response for each calibration point falls below the line, then crosses to be above, in a wave-like pattern. This is reflected in the residuals analysis where the predicted values appear to be overestimated below 50ng/mL, under estimated between 50- 120ng/mL, with the last two points being over and under estimated respectively (Figure 55). It was not clear what was causing this pattern to be observed.

LoD and LoQs across this range were calculated to be 114ng/mL and 325ng/mL respectively.

Table 19: Calculated %CV for THC in water across a low working range on argon plasma treated mesh

Expected concentration (ng/mL)	Calculated concentration (ng/mL)	% CV
10	21	-112
20	24	-20
50	40	20
100	71	29
120	119	1
150	182	-21
200	193	4

As expected, the %CV values fluctuate in sign, following the wave-like pattern observed in both the linear and residual analysis. Ultimately, ignoring the 20ng/mL point, the deviation from the fit is not too different from the other calibrations. What makes this different is the pattern that these results seem to display, which cannot be explained.

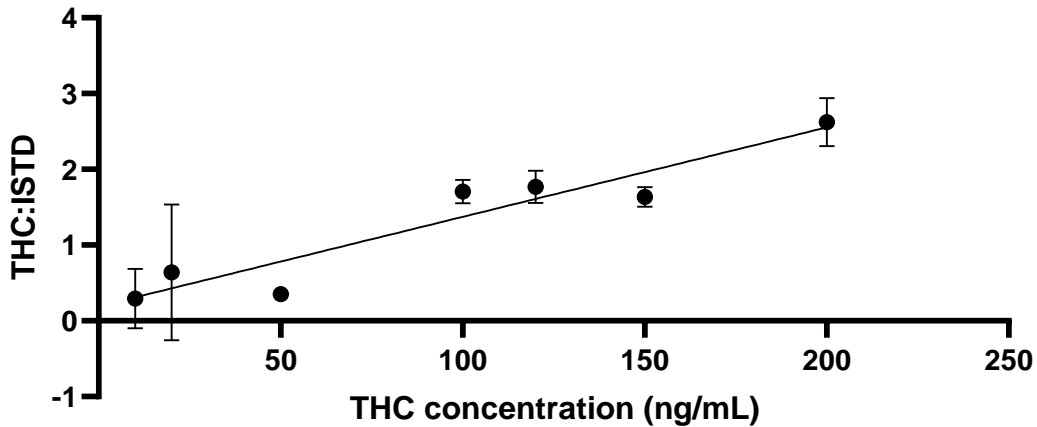


Figure 57: Quantification of THC in water on oxygen plasma treated mesh across a dynamic range 20-1000ng/mL, n=5 and each error bar is equivalent to  $\pm 1SD$ .  $R^2=0.8920$

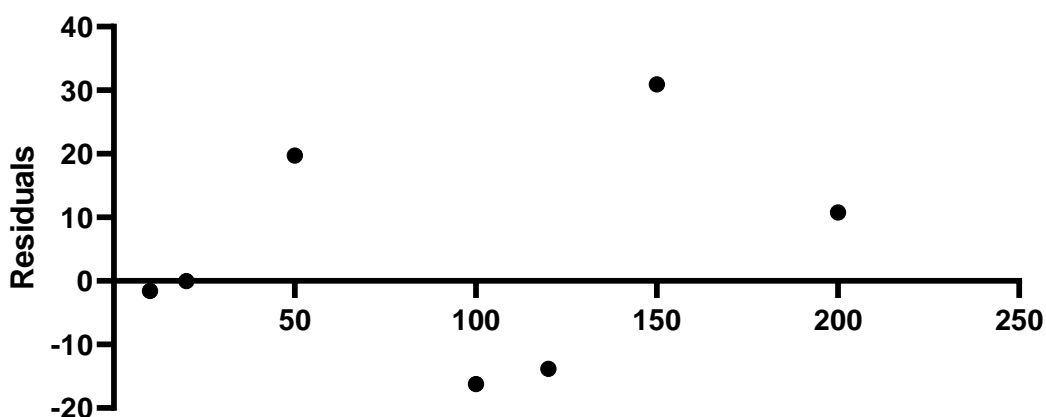


Figure 58: Residuals analysis of the linear regression of THC in water (10-200ng/mL) on oxygen plasma treated mesh

These data show the same cycling observed for the oxygen plasma treated mesh, resulting in a poor  $R^2$  value (Figure 57). High variability between replicates in the low mass range. These points above 100ng/mL don't appear to deviate as much from the line, indicating that the problems with this fit come from the lower range calibration points. This is most likely due to ion interferences in the low range, as has been observed to interfere for previous calibrations.

LoD and LoQs across this range were calculated to be 12ng/mL and 56ng/mL respectively, a substantial reduction in from the large range values. The calculated %CV values can be seen in Table 20.

Table 20: Calculated %CV for THC in water across a low range on oxygen plasma treated mesh

Expected concentration (ng/mL)	Calculated concentration (ng/mL)	% CV
20	61	-302
50	69	-38
100	111	-11
200	171	14
300	281	6
400	380	5
500	475	5
1000	1019	-2

As indicated by the residuals analysis, the %CV values indicate a good correlation between the expected and calculated concentrations above 100ng/mL. This is also in good agreement with the LoQ value of

56ng/mL, where all calculated concentrations above this level are in reasonable agreement with the expected concentrations.

Overall, for THC quantification, a low range should be used. Despite the cycling observed for argon and oxygen plasma treated mesh, the LoD and LoQs across these ranges were low enough that drugs in forensic samples would be detected.

### 3.4.5 Large range calibration of MDMA on various mesh types

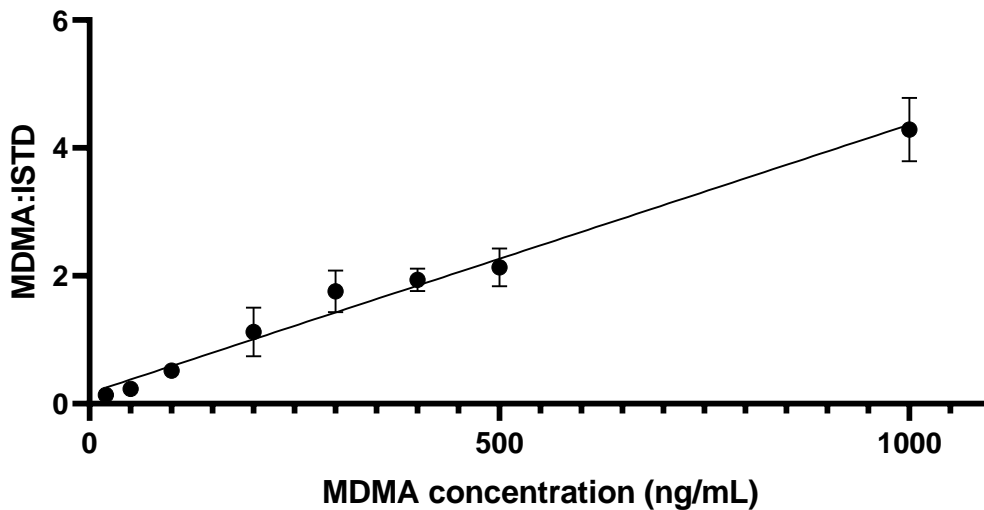


Figure 59: Quantification of MDMA in water on instrument plasma treated mesh across a large range 20-1000ng/mL, n=5 and each error bar is equivalent to  $\pm 1$  SD.  $R^2=0.9486$

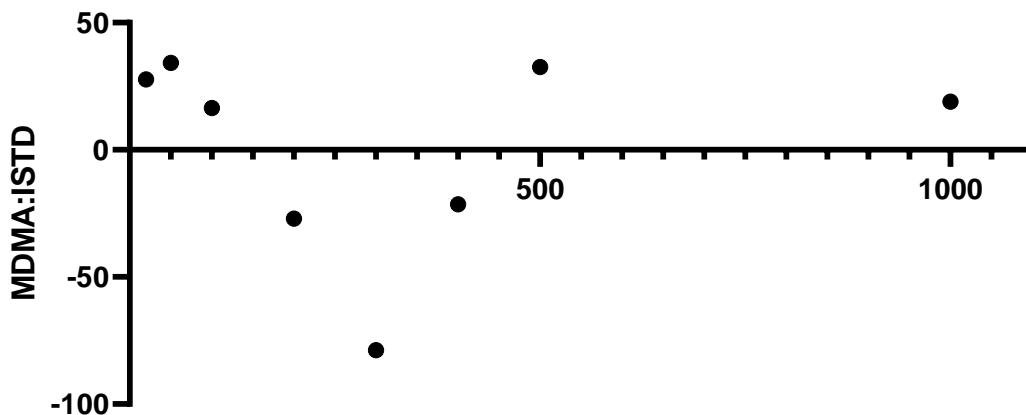


Figure 60: Residuals analysis of the linear regression of MDMA in water (20-1000ng/mL) on instrument plasma treated mesh

The MDMA calibration on instrument plasma treated mesh shows a similar cycling pattern (Figure 59) to that observed for the THC on oxygen (Figure 55) and argon (Figure 57) treated plasma mesh over the same range. The pattern observed here was not as severe and fit to the linear regression improved as the concentration increased. This pattern is repeated in the residual analysis (Figure 60), with significant variation from zero for most points.

LoD and LoQs across this range were unable to be determined due to poor linearity. The calculated values for LoD and LoQ were negative (-24ng/mL and -1ng/mL, respectively) indicating that there the regression is weighted towards the higher concentration points. This results in an under-estimation of the lower values, and in this case has resulted in a high positive y-intercept. As previously discussed, this is likely due to high background causing ion interferences in the region of interest. The calculated %CV values can be seen in Table 21.

Table 21: Calculated %CV for MDMA in water over large range on instrument plasma treated mesh

<b>Expected concentration (ng/mL)</b>	<b>Calculated concentration (ng/mL)</b>	<b>% CV</b>
20	-8	139
50	16	68
100	84	17
200	227	-14
300	379	-26
400	421	-5
500	467	7
1000	981	2

The under-estimation of low concentration calibration points can be seen in the calculated concentrations in Table 21. The fit appears to improve as the concentration increases, which fits with the assertion that the fit is skewed towards the high concentration points.

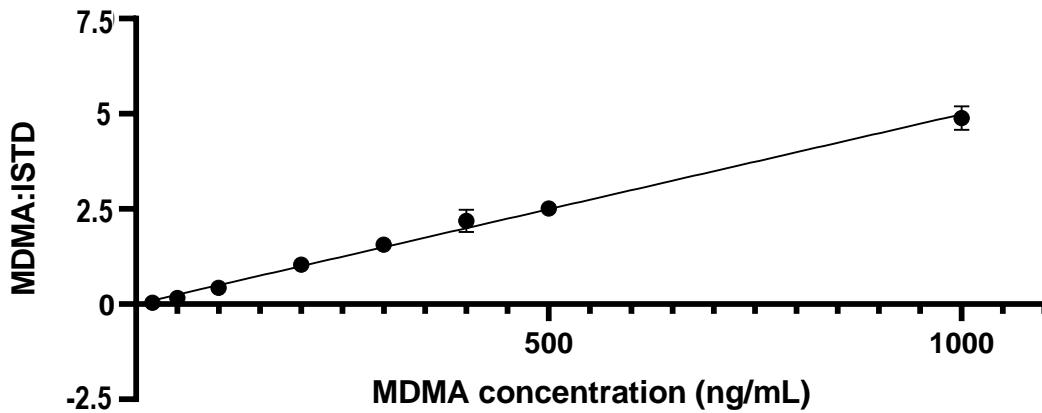


Figure 61: Quantification of MDMA in water on argon plasma treated mesh across a large range 20-1000ng/mL, n=5 and each error bar is equivalent to  $\pm 1$  SD.  $R^2=0.9858$

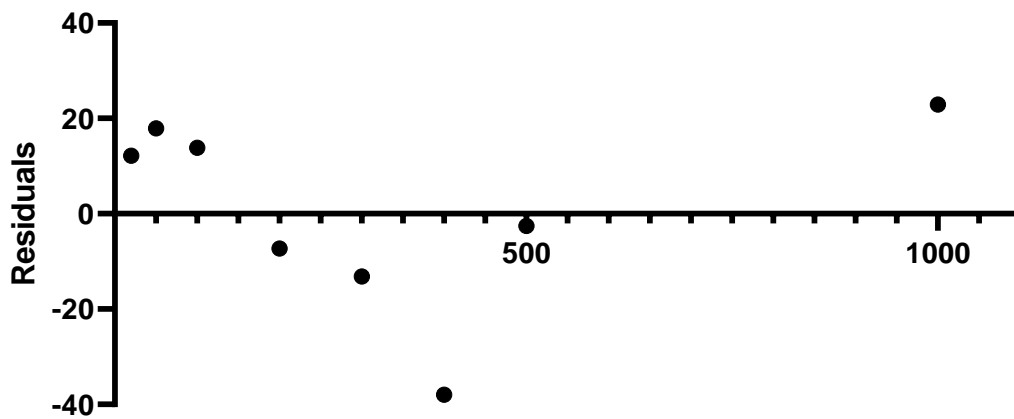


Figure 62: Residuals analysis of the linear regression of MDMA in water (20-1000ng/mL) on argon plasma treated mesh

Linearity for MDMA across this range (Figure 61) is far improved from the same range on instrument plasma treated mesh (Figure 59). Variation between replicates is low, and deviation from the line appears minimal. Residual analysis appears to show a pattern of under and over estimation as a wave (Figure 62).

LoD and LoQs across this range were unable to be calculated, due to poor linearity. The calculated %CV values can be seen in Table 22.

Table 22: Calculated %CV for MDMA in water across a large range on argon plasma treated mesh

Expected concentration (ng/mL)	Calculated concentration (ng/mL)	% CV
20	8	61
50	32	36
100	86	14
200	207	-4
300	313	-4
400	438	-10
500	503	-0.5
1000	977	2

The low concentration calibration points show poor agreement between the expected and calculated concentrations, which improves as the concentration increases. This indicates that that fit is skewed towards the high concentration calibration points. This likely means that the LoD and LoQ values calculated for this range and mesh are low only because of this weighted fit. Which would account for the poor %CV values for 20ng/mL and 50ng/mL.

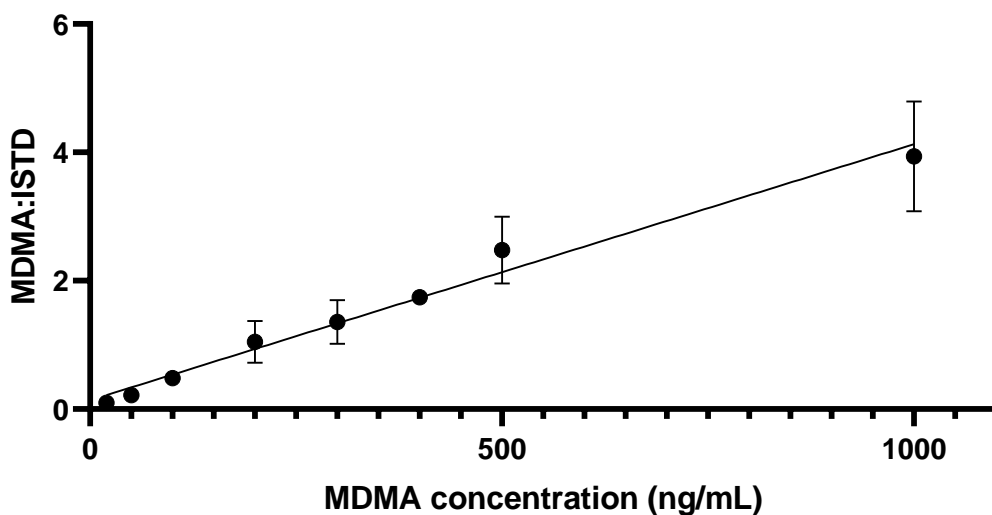


Figure 63: Quantification of MDMA in water on oxygen plasma treated mesh across a large range 20-1000ng/mL, n=5 and each error bar is equivalent to  $\pm 1$  SD.  $R^2=0.9187$

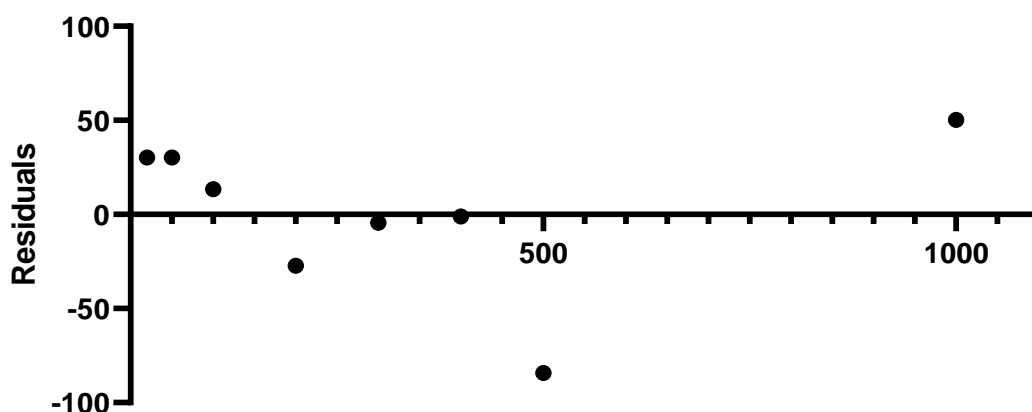


Figure 64: Residuals analysis of the linear regression of MDMA in water (20-1000ng/mL) on oxygen plasma treated mesh

Quantification of MDMA over this range on the oxygen plasma treated mesh shows increased variation between replicates (Figure 63), and decreased linearity compared to both instrument cleaned (Figure 59) and argon treated mesh (Figure 61). The residual analysis shows values clustered around for all points before 500ng/mL (Figure 64).

LoD and LOQs across this range were unable to be determined due to poor linearity (negative values of -31ng/mL & -26ng/mL were calculated). As previously discussed, the negative values here are due to the regression being weighted towards the higher calibration points. The calculated %CV values can be seen in Table 23.

Table 23: Calculated %CV for MDMA in water across a large range on oxygen plasma treated mesh

Expected concentration (ng/mL)	Calculated concentration (ng/mL)	% CV
20	-10	152
50	20	61
100	87	13
200	227	-14
300	305	-2
400	401	-0.3
500	584	-17
1000	950	5

As with the previous case where the regression was weighted towards to high points, the deviation between the expected and calculated concentration for the low concentration calibration points is high.

Deviation between the two values narrows as the concentration increases, where the fit becomes more appropriate.

### 3.4.6 Low range calibration of MDMA on various mesh types

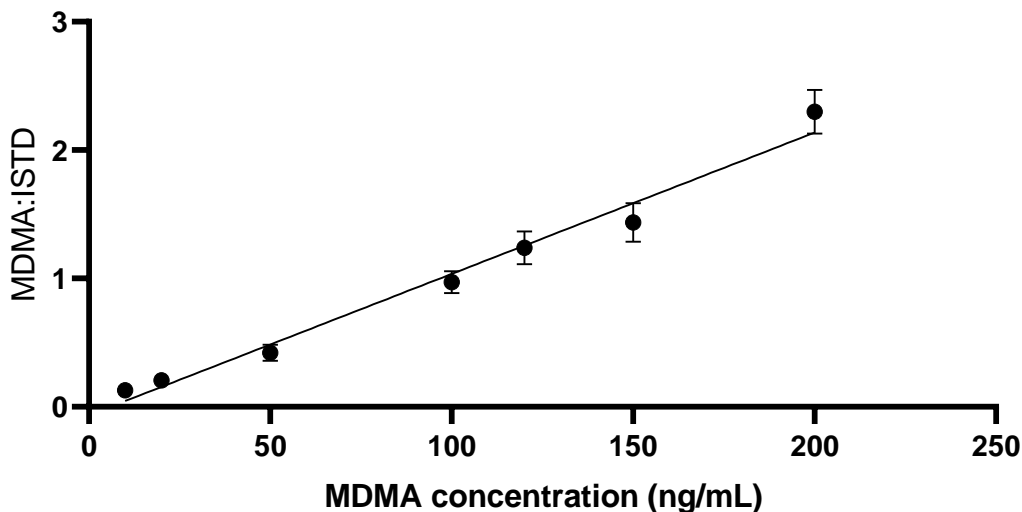


Figure 65: Quantification of MDMA in water on instrument plasma treated mesh across a low working range 10-200ng/mL, n=5 and each error bar is equivalent to  $\pm 1$  SD.  $R^2=0.9646$

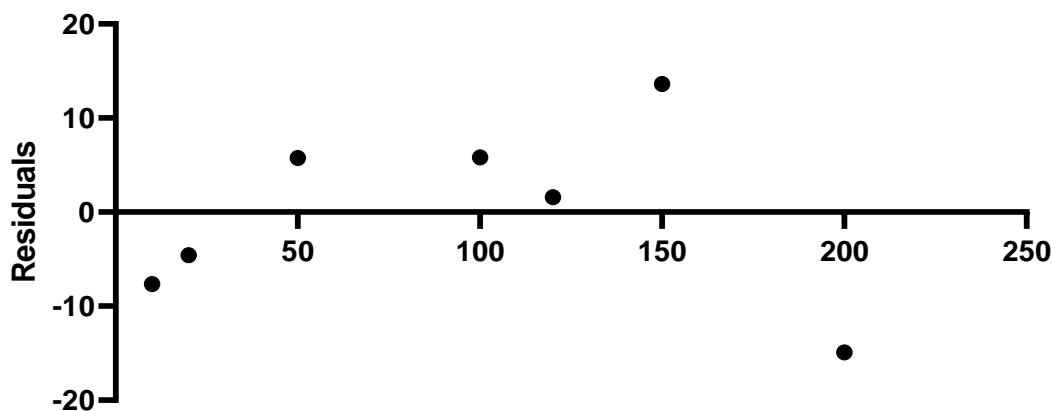


Figure 66: Residuals analysis of the linear regression of MDMA in water (10-200 ng/mL) on instrument plasma treated mesh

Calibration across this range (Figure 65) doesn't appear to show the same cycling pattern as the large range calibration (Figure 59) on the same mesh. Linearity is improved when comparing the  $R^2$  values, and residuals analysis shows a random, homoscedastic distribution, supporting the lack of pattern this this data.

LoD and LoQs across this range were calculated to be 7ng/mL and 9ng/mL respectively, with calculated %CV values in Table 24.

Table 24: Calculated %CV for MDMA in water across a low working range on instrument plasma treated mesh

Expected concentration (ng/mL)	Calculated concentration (ng/mL)	% CV
10	18	-76
20	25	-23
50	44	12
100	94	6
120	118	1
150	136	9
200	215	-8

The low concentration calibration points are overestimated, 10ng/mL quite substantially. This is unusual, as much of the previous work here indicates that deviation between the expected and calculated concentration is typically large for concentrations lower than the LoQ. Here, the LoQ is lower than both the expected concentration and the calculated concentration. This would indicate that the over-estimation at the lower end of the calibration is a random artefact, but the variation between replicates is not large, with a small standard deviation (0.0027).

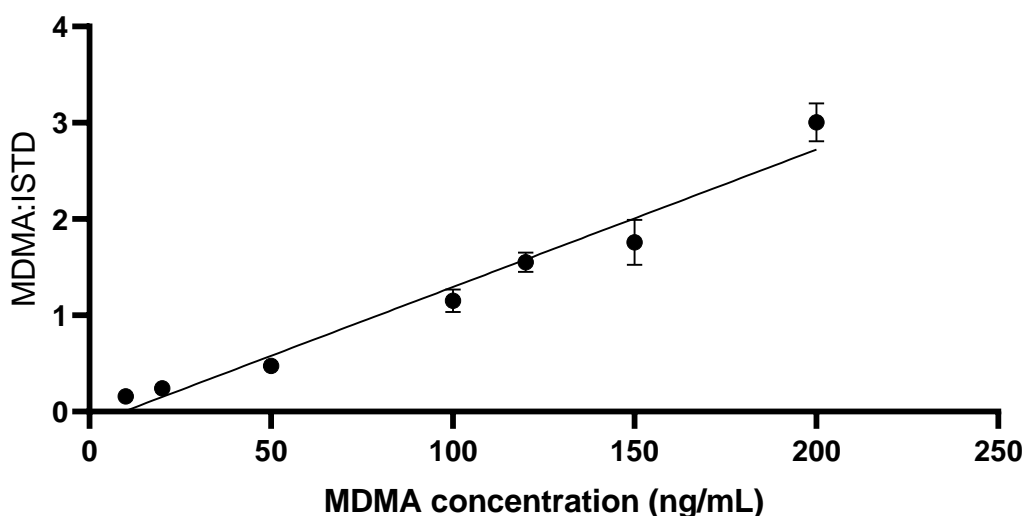


Figure 67: Quantification of MDMA in water on argon treated mesh across a low working range 10-200ng/mL, n=5 and each error bar is equivalent to  $\pm 1$  SD.  $R^2=0.9522$

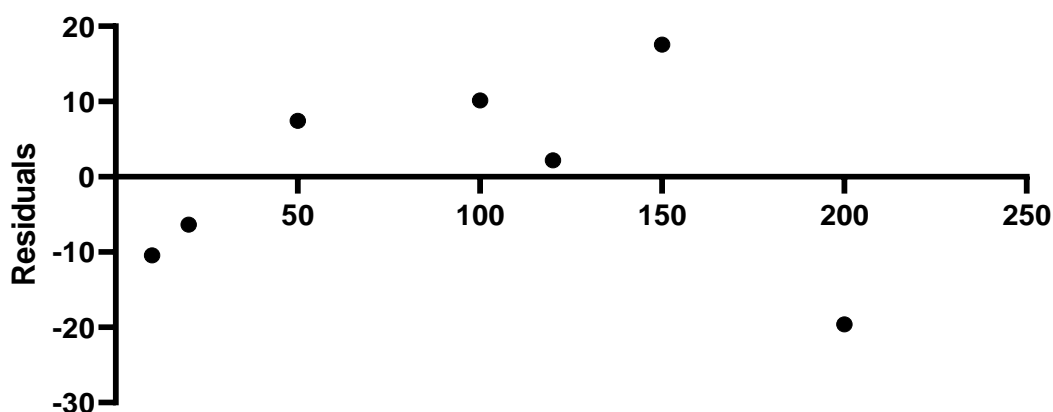


Figure 68: Residuals analysis of the linear regression of MDMA in water (10-200 ng/mL) on argon plasma treated mesh

In contrast to the shortened calibration of MDMA on instrument plasma mesh, the linearity on argon plasma treated mesh (Figure 67) is worse than the instrument plasma treated mesh (Figure 65), when comparing the  $R^2$  values. The residuals plot (Figure 68) looks very similar to that of the instrument plasma treated mesh (Figure 66), with the same outliers and same over-estimation of the low concentration calibration points.

LoD and LoQs across this range were calculated to be 10ng/mL and 11ng/mL, the calculated %CV values can be found in Table 25.

Table 25: Calculated %CV for MDMA in water across a low working range on argon plasma treated mesh

Expected concentration (ng/mL)	Calculated concentration (ng/mL)	% CV
10	20	-104
20	26	-32
50	43	15
100	90	10
120	118	2
150	132	12
200	220	-10

These low calibration points are over-estimated just like the instrument plasma treated mesh. For the 10ng/mL calibration point, this is not unexpected as this point does fall below that LoQ. The next highest calibration point is also over-estimated, but not as significantly as the lowest point.

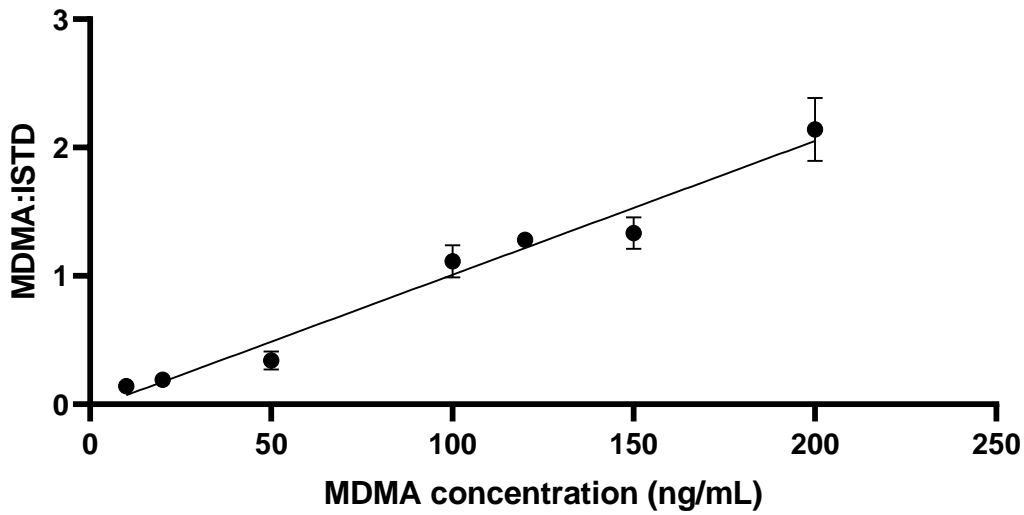


Figure 69: Quantification of MDMA in water on oxygen treated mesh across a low working range 10-200ng/mL, n=5 and each error bar is equivalent to  $\pm 1$  SD.  $R^2=0.9496$

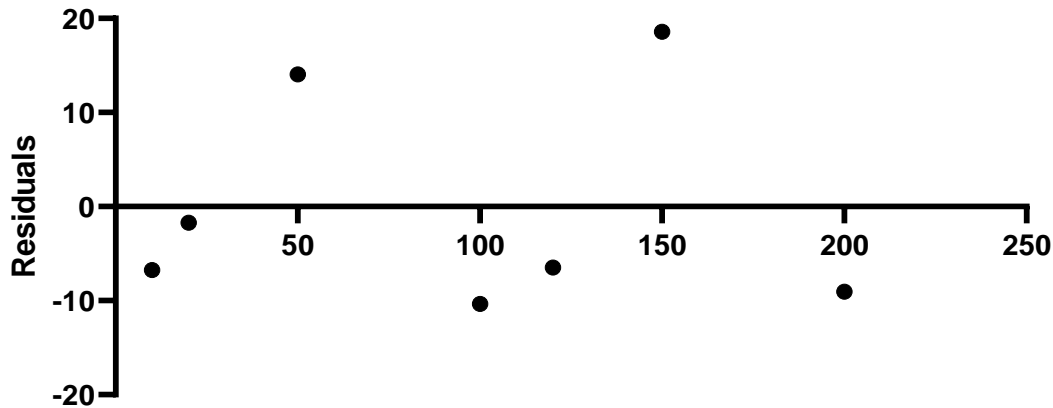


Figure 70: Residuals analysis of the linear regression of MDMA in water (10-200 ng/mL) on oxygen plasma treated mesh

On oxygen plasma treated mesh over this range (Figure 69), the  $R^2$  value is higher than that of the same mesh across the large range (Figure 63), despite appearing more linear. Residuals analysis appears more random across this range (Figure 70) on this mesh than on the instrument cleaned (Figure 66) and argon plasma cleaned mesh (Figure 68).

LoD and LoQs across this range were calculated to be 9ng/mL and 19ng/mL respectively. The calculated %CV values can be found in Table 26.

Table 26: Calculated %CV for MDMA in water across a low working range on oxygen plasma treated mesh

<b>Expected concentration (ng/mL)</b>	<b>Calculated concentration (ng/mL)</b>	<b>% CV</b>
10	17	-67
20	22	-9
50	36	28
100	110	-10
120	127	5
150	131	12
200	209	-5

Much like the two other mesh types across this range, the lower calibration points are over-estimated, however the distribution of over and under estimation on this mesh appears random.

### 3.4.7 Summary of results – linear range

Tables with the LoD and LoQ results for all three drugs, on each mesh across both the large and low ranges are included below.

Table 27: Summary of LoD and LoQ data for THC across low range and large range, on varying mesh types

<b>Mesh type</b>	<b>Low range</b>		<b>Large range</b>	
	<b>LoD (ng/mL)</b>	<b>LoQ (ng/mL)</b>	<b>LoD (ng/mL)</b>	<b>LoQ (ng/mL)</b>
<b>Instrument plasma treated</b>	2	4	241	732
<b>Argon plasma treated</b>	114	325	182	498
<b>Oxygen plasma treated</b>	12	56	50	142

Table 28: Summary of LoD and LoQ data for cocaine across low range and large range, on varying mesh types

<b>Mesh type</b>	<b>Low range</b>		<b>Large range</b>	
	<b>LoD (ng/mL)</b>	<b>LoQ (ng/mL)</b>	<b>LoD (ng/mL)</b>	<b>LoQ (ng/mL)</b>
<b>Instrument plasma treated</b>	4	10	30	32
<b>Argon plasma treated</b>	1	3	N/A	N/A
<b>Oxygen plasma treated</b>	12	16	14	25

Table 29: Summary of LoD and LoQ data for MDMA across low range and large range, on varying mesh types

Mesh type	Low range		Large range	
	LoD (ng/mL)	LoQ (ng/mL)	LoD (ng/mL)	LoQ (ng/mL)
Instrument plasma treated	7	9	N/A	N/A
Argon plasma treated	10	11	N/A	N/A
Oxygen plasma treated	9	19	N/A	N/A

It is clear from these experiments that extended ranges of calibration that push beyond one order of magnitude are not appropriate for quantification of these drugs. In practice, this means that where large ranges of concentration are encountered for samples, they either need individual calibration curves or to be diluted within the same range for accurate quantitation. This will increase the time taken for the sample analysis when quantification is required. Ultimately this means that more typical chromatography methods may be more appropriate for quantification, offering more accurate information in not much more time than it would take to prepare additional calibrations or determine sample concentration for accurate dilution into an established range.

Comparing the three drugs, cocaine response was the most linear and was detected with the most sensitivity, as cocaine ionises the most effectively of the three drugs tested. Of the three drugs THC was the least consistent, and the method was least sensitive for MDMA. Mesh-wise, there was no clear answer for which mesh facilitates optimum sensitivity, with each drug performing differently. Instrumental plasma cleaned mesh was the most consistent, across the reduced calibration range. This mesh was chosen as the optimum with which to continue analysis into the tests for intra- and inter-day consistency.

### 3.5 Inter- & intra- day consistency

To test inter- and intra-day consistency, three quantification curves were produced for each drug on the same day on instrument plasma treated mesh. Six replicates for each point were collected, across the same reduced calibration range determined to be appropriate in the previous section (10-200ng/mL). Deuterated internal standard was added to the drug solutions during preparation to a final concentration of 100 ng/mL. This was repeated on two subsequent days, with LoD and LoQ values calculated for each curve produced. For cocaine, all data were able to be collected across all replicates and all days. For MDMA three curves were produced on days one and three, sufficient data for one curve were able to be

generated only on day two. For THC even less data were able to be acquired, with day one producing three curves and day two only producing one. Data were not able to be generated on day three. This lack of data generated for THC and MDMA is indicative of the inconsistency demonstrated by this instrument and this method.

Curves generated for each drug across each day and between days can be seen in Figure 71, Figure 72, Figure 73, Figure 74, Figure 75, Figure 76, Figure 77, and Figure 78. Calculated LoD and LoQ values can be found in Table 30.

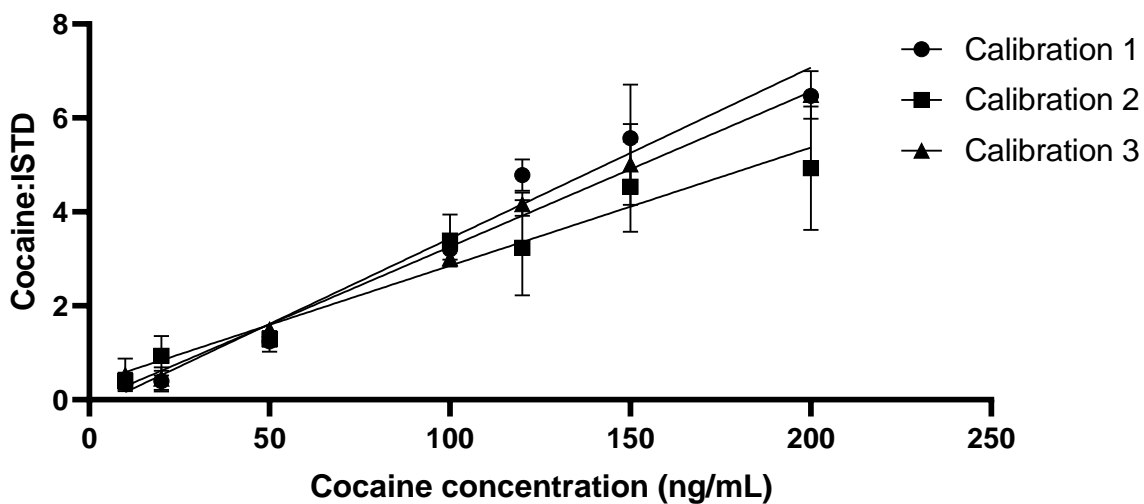


Figure 71: Comparison of calibration curves taken on day one for solutions of cocaine in water across 10-200 ng/mL (n=6), error bars are 1SD.  $R^2 = 0.9723, 0.9944$  &  $0.9951$  for calibration 1, 2 & 3 respectively.

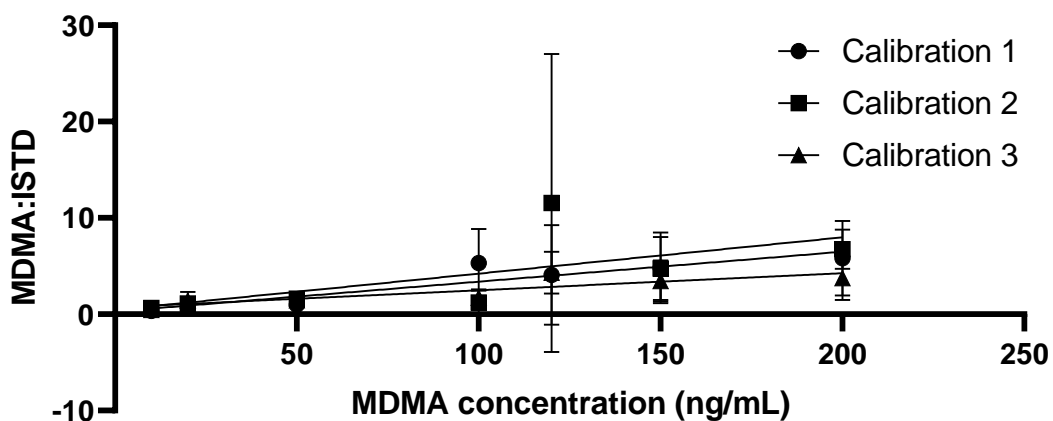


Figure 72: Comparison of calibration curves taken on day one for solutions of MDMA in water across 10-200 ng/mL (n=6), error bars are 1SD.  
 $R^2 = 0.9884, 0.931$  &  $0.9408$  for calibration 1, 2 & 3 respectively.

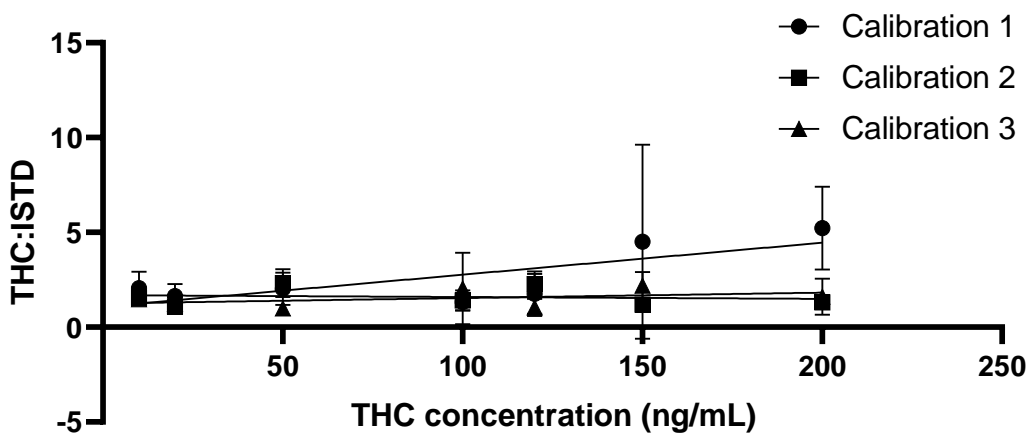


Figure 73: Comparison of calibration curves taken on day one for solutions of THC in water across 10-200 ng/mL (n=6), error bars are 1SD.  
 $R^2 = 0.5839, 0.0185$  &  $0.1823$  for calibration 1, 2 & 3 respectively.

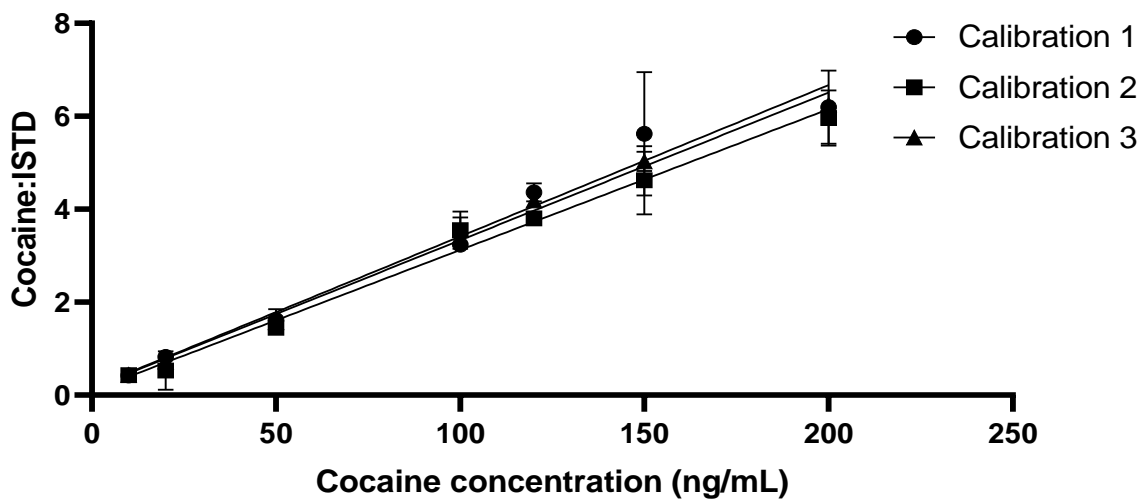


Figure 74: Comparison of calibration curves taken on day two for solutions of cocaine in water across 10-200 ng/mL (n=6), error bars are 1SD. R<sup>2</sup>= 0.9776, 0.9899 & 0.9929 for calibration 1, 2 & 3 respectively.

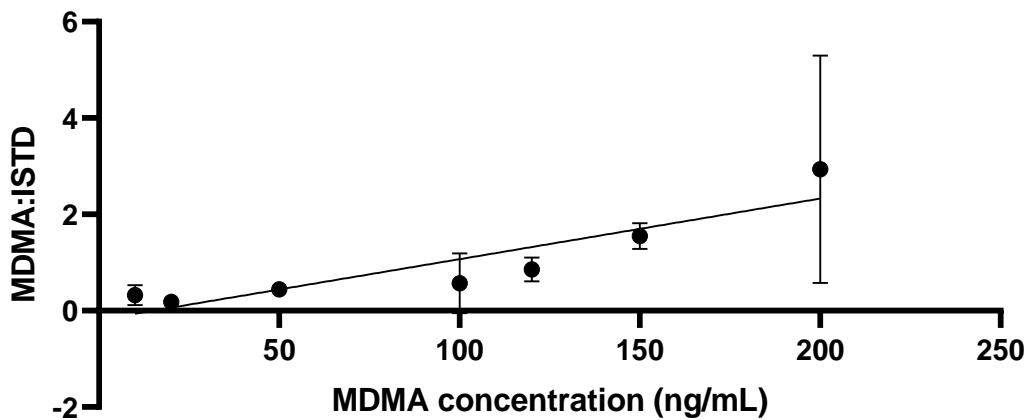


Figure 75: Calibration of MDMA in water on day two across 10-200 ng/mL (n=6), error bars are 1SD. R<sup>2</sup>= 0.821

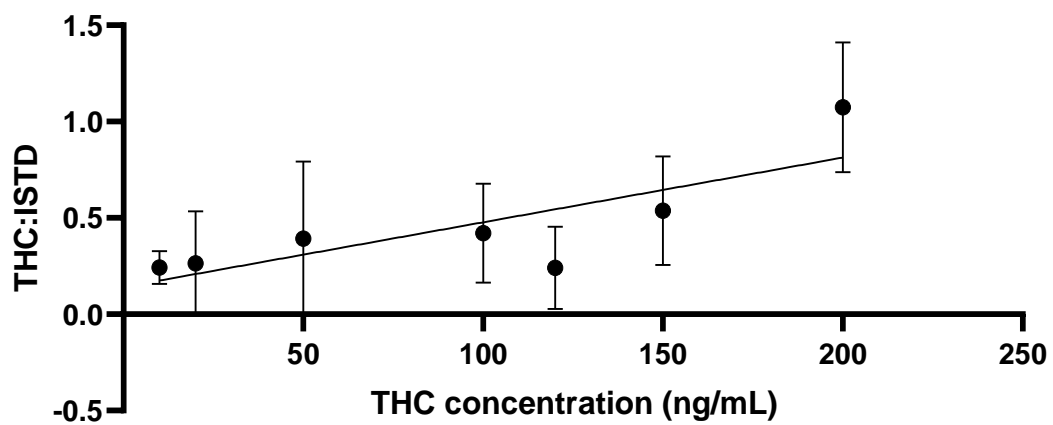


Figure 76: Calibration of THC in water on day two across 10-200 ng/mL (n=6) error bars are 1SD. R2= 0.5502

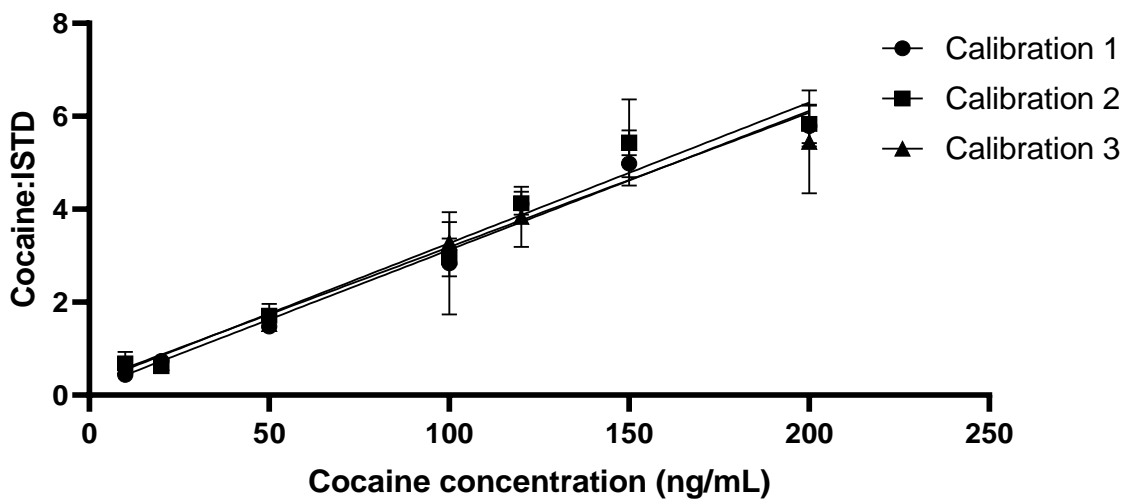


Figure 77: Comparison of calibration curves taken on day three for solutions of cocaine in water across 10-200 ng/mL (n=6), error bars are 1SD. R2= 0.9813, 0.9691 & 0.9565 for calibration 1, 2 & 3 respectively.

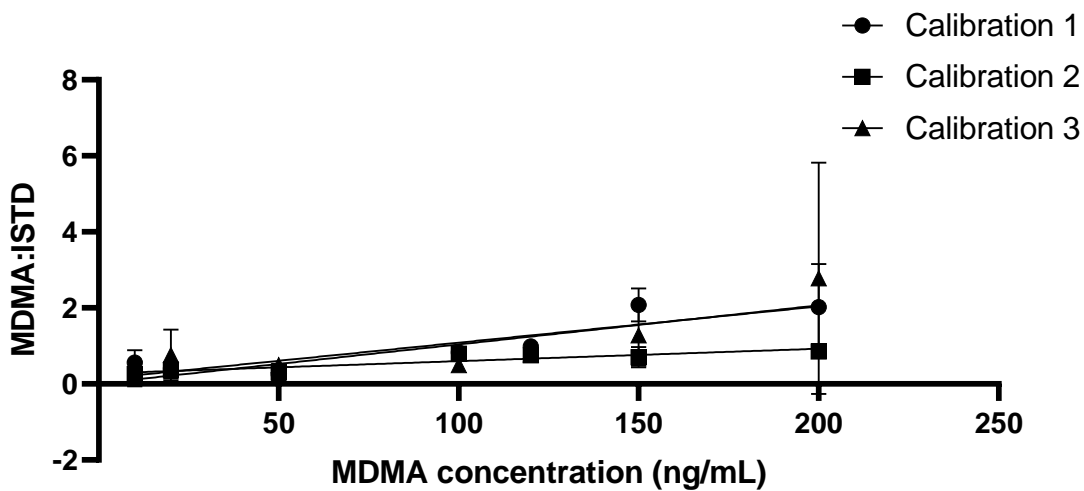


Figure 78: Comparison of calibration curves taken on day three for solutions of MDMA in water across 10-200 ng/mL (n=6), error bars are 1SD. R2= 0.803, 0.812 & 0.6902 for calibration 1, 2 & 3 respectively.

Table 30: Calculated limits of detection and quantification for cocaine, THC and MDMA for inter and intraday comparison. Where linearity was poor, values are recorded as 'N/A' in place of a negative number or zero.

Analyte	Day of collection	Curve number	LoD (ng/mL)	LoQ (ng/mL)	
Cocaine	1	1	9	16	
		2	1	25	
		3	20	53	
	2	1	22	69	
		2	N/A	N/A	
		3	4	18	
	3	1	19	59	
		2	N/A	N/A	
		3	1	21	
MDMA	1	1	40	114	
		2	29	96	
		3	25	108	
	2	1	78	174	
	3	1	110	257	
		2	281	683	
		3	51	118	
	THC	1	1	152	436
			2	4239	11338
3			878	2769	
2		1	674	1771	

LoDs and LoQs calculated on each day and across each day are highly variable. This variability is reflected in the %RSD for intra- and inter-day limits (Table 31). Intra-day %RSD was calculated using the curves calculated on that single day. Inter-day %RSD was calculated across total number of values from each curve and each day.

Table 31: %RSD for LoD and LoQs calculated for cocaine, MDMA and THC for inter and intra-day comparison. Where values are recorded as 'N/A' no data was available.

Drug	Time frame of data collection	LoD %RSD	LoQ %RSD
Cocaine	Day 1	90	62
	Day 2	152	119
	Day 3	202	97
	Overall	122	82
MDMA	Day 1	26	9
	Day 2	N/A	N/A
	Day 3	81	84
	Overall	103	95
THC	Day 1	259	279
	Day 2	N/A	N/A
	Day 3	N/A	N/A
	Overall	382	413

The inter-day consistency was generally greater than that of the intra-day, but this improvement is only valid when comparing the two. The consistency for all drugs for inter-day and intra-day is very poor. These results indicate that even with calibration on each day quantification is to be performed, the results may still be unreliable.

### 3.6 Conclusions

Quantification of the three drugs MDMA, cocaine and THC can be performed using the DSA-ToF. Linearity was observed for all three drugs over each range and on each mesh, although some performed better than others. The extended calibration range (covering two orders of magnitude) was unsuitable for quantification, with the regression being weighted towards the higher concentration calibration points. This led to over-estimation of the low calibration points and inflated limits of detection and quantification. The reduced calibration range offered lower LoDs and LoQs, and improved linearity that appeared equally weighted across the entire range. The instrument plasma treated mesh was the most consistent of the

three mesh types tested and was used for the experiments to determine the consistency of the established limits.

The intra- and inter-day consistency results showed high %RSD for both the limits of detection and the limits of quantification. These variations are too extensive to consider this method appropriate for quantification. Of most concern is that this test of ruggedness was not performed with the analyst altering any instrument parameter. The variation causing the high %RSD values are not under the control of the analyst and are likely due to changes in the environment. The implications are that quantifications performed on this instrument (regardless of the method) cannot be considered valid. The LoD values determined in this chapter demonstrate that this instrument is still very suitable for rapid screening of unknown samples and compounds, it is recommended that quantification should be performed on another, more accurate instrument.

## 4 Development of extraction methods for THC, MDMA and cocaine from saliva

### 4.1 Introduction

The movement towards less invasive sampling practices for the detection of illicit drugs in bodily fluids has resulted in saliva being one of the more popular choices for sampling. Traditional methods required blood to be drawn which has a number of implications. The first, and most obvious, is that the process of drawing blood is quite arduous and intensive for the person having blood drawn. The second, and arguably most important from a public safety perspective, is that there is a need to take a sample as soon after the initial positive result as possible. This reduces the chances of further drug elimination, making the confirmatory result more certain, and saliva is a better indicator of recent use than other biological fluids. Additionally, it has been shown that the concentration of drugs in saliva are proportional to the concentration in blood plasma [156], therefore detected concentrations in saliva can be used to approximate concentration of drugs in other biological fluids. The other major benefit for the use of saliva over other more common bodily fluids is that the collection of saliva reduces the potential for adulteration of the sample. Much like blood, the collection of saliva samples is typically observed by someone, meaning that the person being sampled is not able to substitute their sample for one that is more likely to pass.

Typical body fluid analysis for the detection of illicit substances use liquid-liquid extractions, with solvents being used to remove the analyte of interest from the matrices. This serves the dual function of removing small molecules found in the matrix that may interfere in that low molecular weight range and concentrating the analyte in a smaller volume of liquid. These extraction methods typically rely on organic solvents such as chloroform, chlorobutane or toluene. These solvents, when used in large quantities are dangerous to use, require additional controls for the analyst, including personal protective equipment and isolation controls. However, the methods discussed are very effective, and as such remain the most common method for liquid-liquid extractions to clean up samples and concentrate compounds of interest.

Solvent-free approaches have also been proven to be effective, typically involving an interaction between the sample and a substrate [157]. It's this interaction, particularly when combined with a nano-structured surface or pH manipulation of the sample can cause the analyte to move from the liquid to the stationary phase, preconcentrating the analyte and reducing matrix effects [158-160]. The concentration onto a

surface is particularly important for samples in which there is only a small amount of analyte, which is typical for body fluid samples encountered by forensic laboratories.

Pre-concentration methods have been used in the detection of both illicit substances and biomarkers in saliva using laser desorption ionisation (LDI) and desorption ionisation on porous silicon [157]. Those studies showed that the detection of these analytes was possible, with the nano-structured surfaces extracting the analyte from the saliva onto the surface, and a wash with ammonium bicarbonate buffer used to clean up the sample. The same surfaces are able to be used in the detection of the analytes from the organic layer of an extraction medium, after drying and re-suspension. Although the comparison of LDI-ToF and DSA-ToF cannot truly be made, owing to their differing ionisation methods, the concept of using these more simplified extraction methods can absolutely be transferred, as neither method relies on column separation as part of the process.

As previously discussed, one of the huge benefits of DSA-ToF is the ability to visualize all components of a sample at once, including metabolites, fragments, parent drug, and the matrix. For complicated biological samples, like saliva, this can make interpretation of the mass spectra very complicated. Although it is likely that most compounds can be detected in their matrices using ambient ionisation techniques like DSA-ToF, the large amount of background noise can reduce the sensitivity of the methods. The work in this chapter sought to identify two methods for the extraction and concentration of analytes in saliva. The first method investigated was a small-scale solvent extraction method. The second method looked to remove the use of solvents by mimicking the interaction based extraction from Guinan et al [157].

The solvent based method investigated the use of different solvents, at different volumes, and with a number of additives to the sample to improve ionisation. These experiments were all performed on mesh that had under-gone the 30 second instrument clean as described in Chapter 2. For the timed interaction experiments, the spiked saliva was buffered and the sample spot acidified. The mesh surface itself was also altered by plasma cleaning for a number of experiments.

## **4.2 Materials and Methods**

The saliva used for the experiments in this chapter was collected from the author, on the day the experiment was to be run. Saliva was collected prior to eating, but post teeth-brushing. In order to collect a reasonable amount for multiple experiments, the author took a small amount of water into their mouth and moved it around. This water-saliva mix was then collected in a 50mL falcon tube. The process was

repeated three times, with swirling after each addition to the tube to ensure homogeneity of sample. The saliva was then stored on ice for the duration of the experiments and disposed of at the end of the day.

For the preparation of spiked saliva for analysis, working solutions of MDMA, cocaine and THC were prepared to 100ng/mL concentrations, and spiked into the saliva prior to analysis. Internal standard was spiked at a concentration of 100ng/mL for quantification, from a stock solution of 10µg/mL. For the method optimisation, saliva was spiked to give a final concentration of 200ng/mL.

Borax buffer was prepared by dissolving 4.749g of Borax (Sigma Aldrich, Castle Hill, NSW) in 250mL MilliQ water, with addition of 57µL of 32% HCl to bring to pH 9.

Ammoniacal buffer was prepared by dissolving 90g of ammonium chloride (Sigma Aldrich, Castle Hill, NSW) in 375mL of 30% ammonia, and diluting to 500mL with milliQ water (pH 10). The pH of both the borax buffer and ammoniacal buffer was tested using Ajax pH sticks (ThermoFisher, Waltham, MA, USA).

Metal triflate solutions were prepared by reacting metal hydroxides with triflic acid (Sigma Aldrich, Castle Hill, NSW). For sodium triflate, 1.13mL of 1M NaOH (Sigma Aldrich, Castle Hill, NSW) was added to 100µL of triflic acid. 0.1% solution was prepared by diluting 1µL of this solution in 157µL of water. Potassium triflate was prepared by adding 1.13mL of 1M KOH (Sigma Aldrich, Castle Hill, NSW) to 100µL of triflic acid. 0.1% solution was prepared by diluting 1µL of this solution in 172µL of water. Silver triflate was supplied as is (Sigma Aldrich, Castle Hill, NSW) and diluted to 0.1% in water prior to analysis.

### **4.3 Solvent extraction of MDMA, THC and cocaine from spiked saliva**

For all analyses, drug concentrations of 100ng/mL were used, with the total volume of saliva being 200µL. The parameters investigated were: solvent type, saliva: solvent ratio, centrifugation time, volume of solvent onto mesh, acidification of sample spot and the buffering of the saliva. All data analysis was performed by comparing the signal to noise values for each drug molecular ion, across three replicates. All comparative data were collected on the same day.

Where solvent type and volume were evaluated, ratios (saliva: solvent) of 1:5, 1:4, 1:3, 1:2, 1:1, 2:1, 3:1, 4:1 & 5:1 were tested, with the final volume of solution remaining consistent (200µL). Chlorobutane, chloroform, heptane and toluene were evaluated as potential solvents. For these experiments a centrifugation time of 30sec (at 1200 rpm), and there was no buffering of the saliva or acidification of the sample spot prior to analysis. Chlorobutane, toluene and heptane were all less dense than the saliva layer

and were able to be directly removed from the Eppendorf tube with a pipette. Chloroform was denser than the saliva layer, requiring the removal of the saliva layer before sampling of the solvent could occur. This was carried out using a disposable glass pipette at the interface of the two layers, with care to ensure that the two layers were not mixed. The saliva layer was disposed of, and the remaining solvent volume was sampled by ensuring the pipette tip penetrated deep enough into the remaining volume that any mixing of the two phases would not influence the results of that analysis. Analysis was performed by pipetting 4 $\mu$ L of the solvent layer onto instrument treated mesh, allowing the solvent to evaporate, and pipetting 10 $\mu$ L of MQ water onto the dried spot immediately prior to analysis. Analysis was performed in triplicate and to reduce the likelihood of carry-over, each sample application and analysis was performed separately and on a fresh area of the mesh. That is, one of the triplicate analyses was carried out, the sample holder was removed and allowed to cool (approximately 30 sec) and the next sample volume was applied to the adjacent sampling position.

The results for each drug are presented below, with clear improvements in signal for all drugs for all ratios above 1:1.

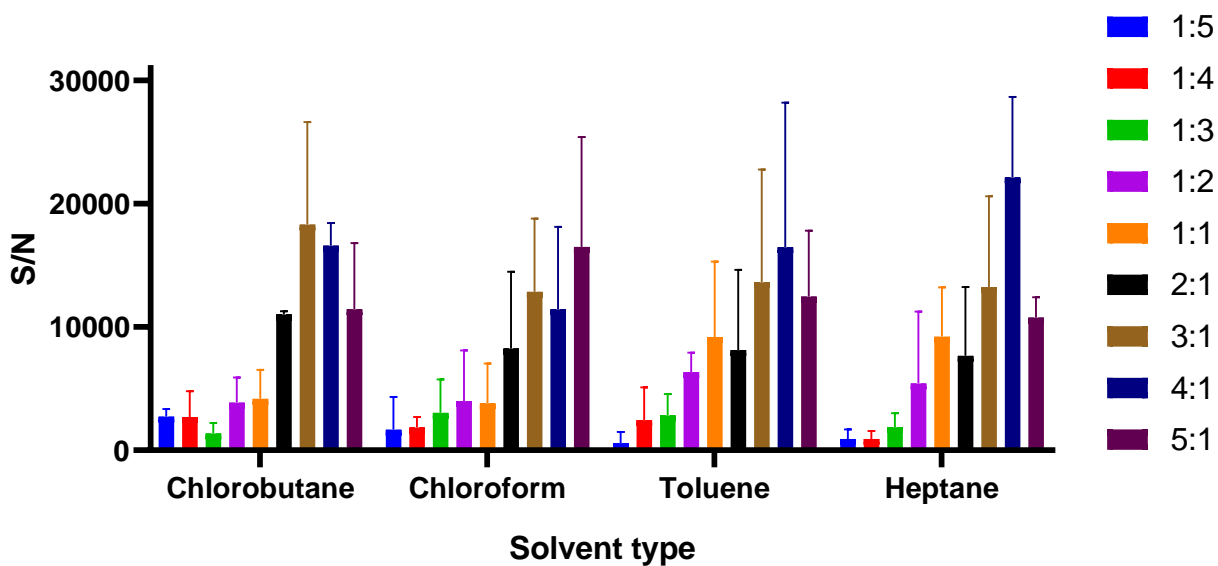


Figure 79: Comparison of solvent type and saliva: solvent ratio for extraction of cocaine from spiked saliva, n=3, error bars are 1SD

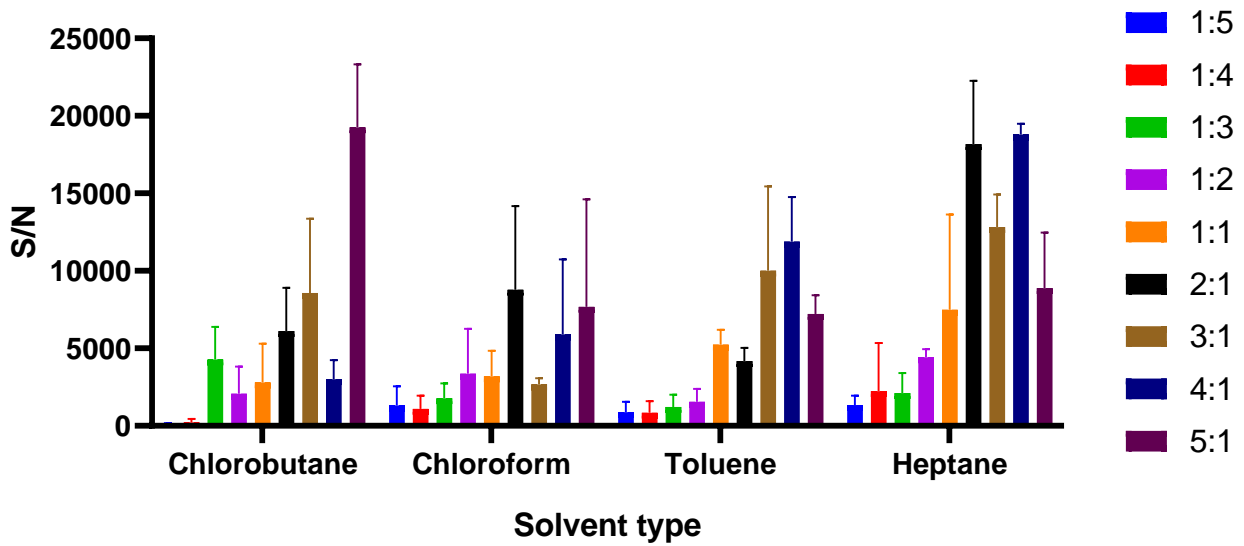


Figure 80: Comparison of solvent type and saliva: solvent ratio for extraction of THC from spiked saliva, n=3, error bars are 1SD

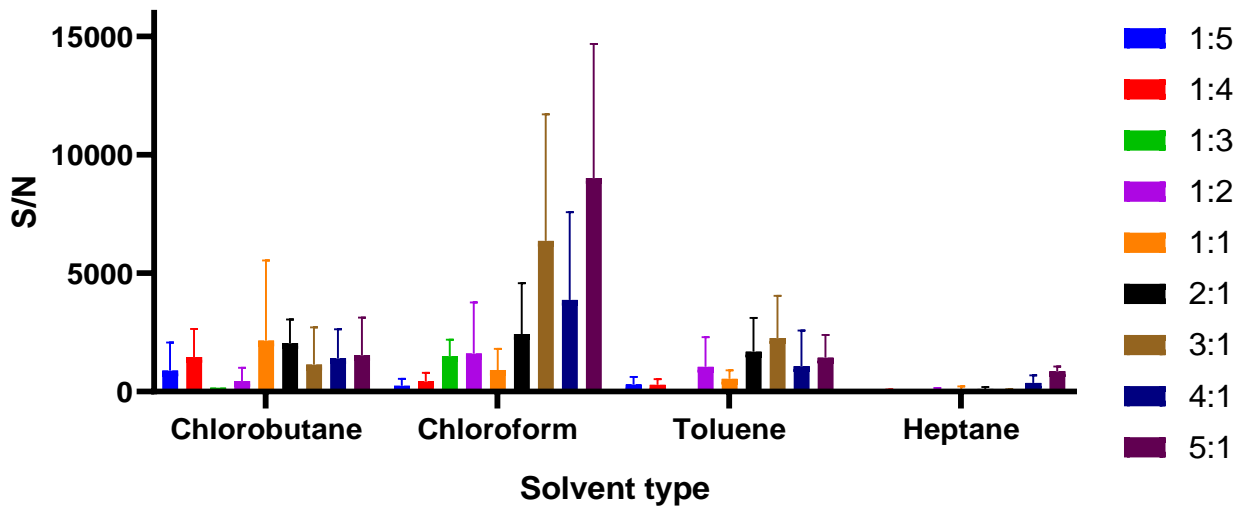


Figure 81: Comparison of solvent type and saliva: solvent ratio for extraction of MDMA from spiked saliva, n=3, error bars are 1SD

It is immediately clear that cocaine extracted well for all solvents, with no real preference visible in the data (Figure 79). For THC, heptane performed the best and both chloroform and toluene performed poorly in comparison (Figure 80). MDMA extracted poorly for all solvents except chloroform, and performed particularly poorly when heptane was used (Figure 81). For an extraction method that covers all three of these drugs, chloroform is the optimal solvent. For cocaine, the difference is negligible, but for MDMA the

poor performance of the three other solvents leaves little choice. Although THC extracts better with heptane, the signal produced from a chloroform extraction was considered acceptable for this to be the final solvent choice for a multiple drug extraction. The optimal ratio for the chloroform extraction was 5:1 saliva: solvent.

A separate method optimization was performed for a single drug extraction using heptane as the solvent for the extraction of THC. This confirmation involved the evaluation of heptane, chlorobutane and chloroform as the extraction solvent over the 3:1, 4:1 and 5:1 ratios of saliva: solvent.

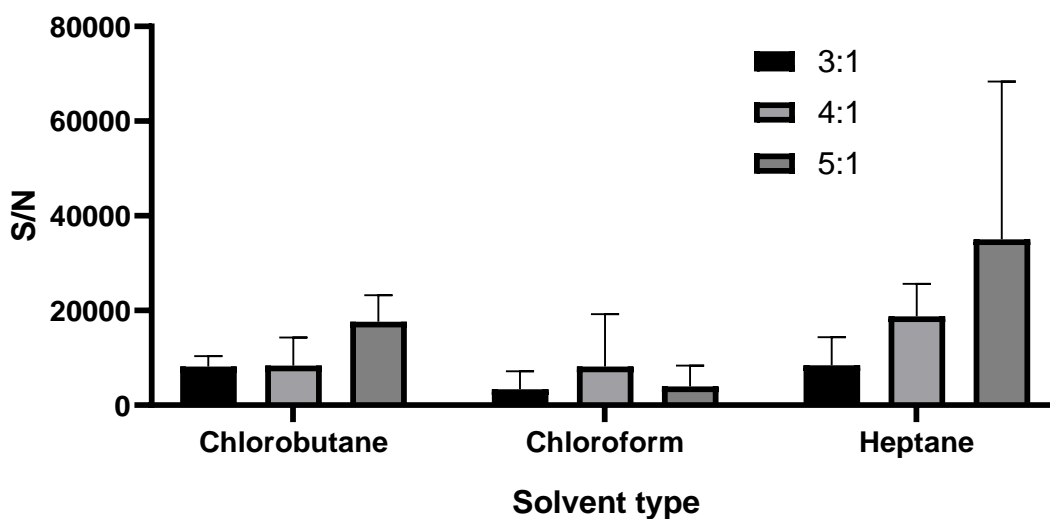


Figure 82: Comparison of solvent type and saliva: solvent ratio for the extraction of THC from spiked saliva, n=3, error bars are 1SD

These results confirmed that heptane was the most effective solvent to use for this single drug extraction, and that the 5:1 ratio was optimal, although appeared variable. This high variability resulted in the 4:1 ratio being selected, to ensure that the extractions performed would be as consistent as possible. It is interesting to note the difference in signal between the analyses, with the original comparison having a mean peak response of 10 000- 20 000 for heptane extractions at 3:1 ,4:1 and 5:1 ratios (Figure 80). The confirmation experiment in (Figure 82) shows mean peak responses of 15 000 – 40 000 for the same ratios. The only difference between these two experiments was the day on which they were performed, reinforcing the need to consider that the inter-day repeatability of this instrument is poor.

The centrifugation time was evaluated using the chloroform method for all three drugs, no buffering, no acidification of sample spot, with the same sample and water volumes for analysis. Times of 15, 30, 60, 90 and 120 seconds were tested, at a speed of 1200 rpm.

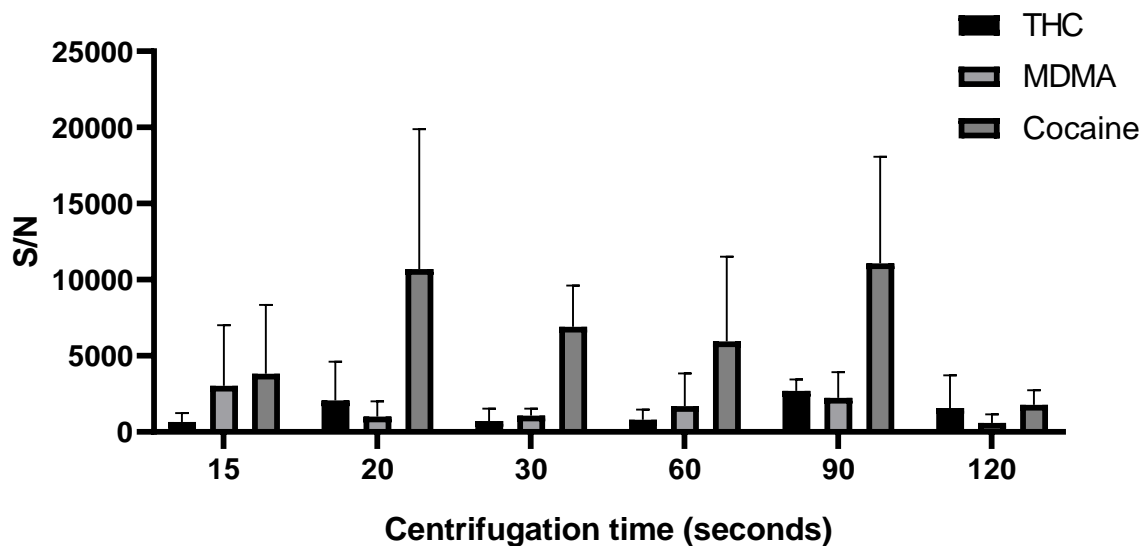


Figure 83: Comparison of centrifugation times (sec) for the chloroform extraction of THC, MDMA and cocaine from spiked saliva, n=3 and error bars are equal to 1SD

For all three drugs the optimum time of centrifugation was 90 seconds, with signal to noise dropping off for all drugs at 120 seconds (Figure 83). The centrifugation time was not optimised for the single drug heptane method, with 90 secs being considered acceptable.

The final parameter examined was the volume of solvent pipetted onto the mesh for analysis. Volumes of 2,4,6,8, and 10 $\mu$ L, with a 5:1 ratio of saliva: solvent using chloroform and a 90 second centrifugation time were compared for this experiment.

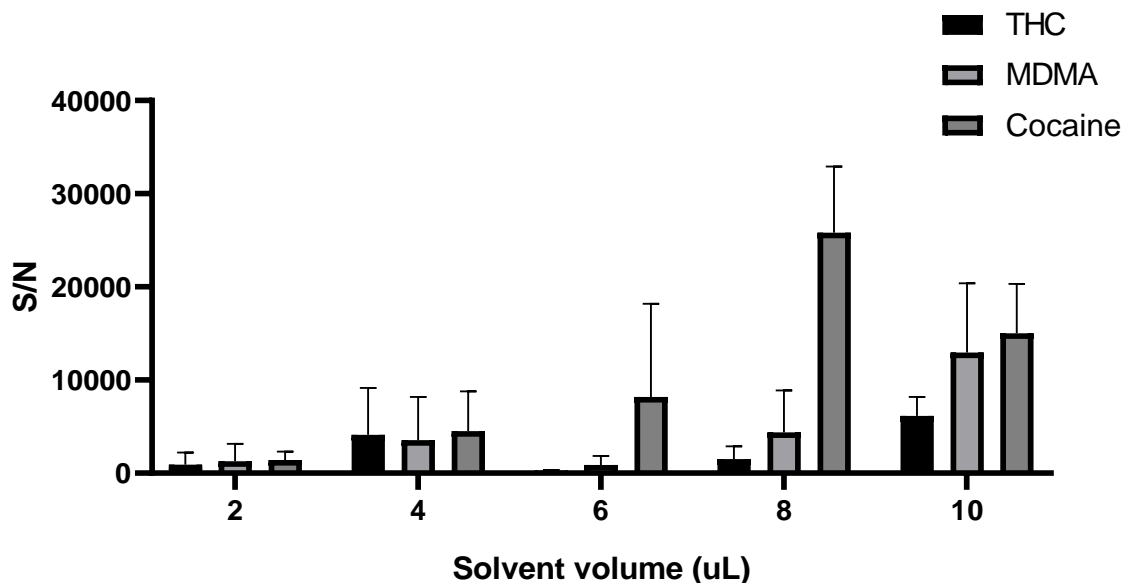


Figure 84: Comparison of solvent volumes ( $\mu\text{L}$ ) onto non-plasma treated mesh for chloroform extraction of THC, MDMA and cocaine,  $n=3$ , error bars are 1SD

The general trend is that the signal to noise increases for each drug with increasing volume of solvent (Figure 84). This is not surprising as the amount of analyte deposited onto the mesh increases, but the amount of water used to suspend the dried analyte remains consistent. This leads to a more concentrated solution being ionised and detected. Despite this, a volume of  $10\mu\text{L}$  for one analysis is very high. A sample with a large amount of analyte will likely contaminate the instrument. Additionally, the use of  $10\mu\text{L}$  of solvent will only allow one aliquot to be tested. The  $4\mu\text{L}$  volume of solvent was chosen as optimal. When considering all three drugs, this was the volume that was the most consistent, that allows for multiple replicates of the same extraction to be analysed. Taking this smaller volume initially will allow for a larger volume to be analysed if that initial aliquot was too low in concentration.

Previous work had indicated that water in system (either from the atmosphere or from the addition of the water to the top of the dried sample) was directly related to the ionisation of the analytes. This indicated that there may be benefits to the addition of acid onto dried sample spots, to provide additional protons for ionisation. Therefore, replacement of water with 0.1% trifluoroacetic acid (TFA) or 0.1% formic acid (FA) was investigated, to see if there would be potential improvement. Buffering of the saliva was also investigated to determine if there were any improvements to be made to the extraction through pH manipulation.

For this pair of experiments, the buffering was investigated first, following this the sample spot acidification was tested with the optimal buffering conditions. The buffers investigated were borax (pH 10) and ammoniacal (pH 9), as the drugs were hypothesised to extract better under basic conditions. The two acids used for the sample spot acidification were TFA and FA, two common acidic modifiers for mobile phases in chromatography.

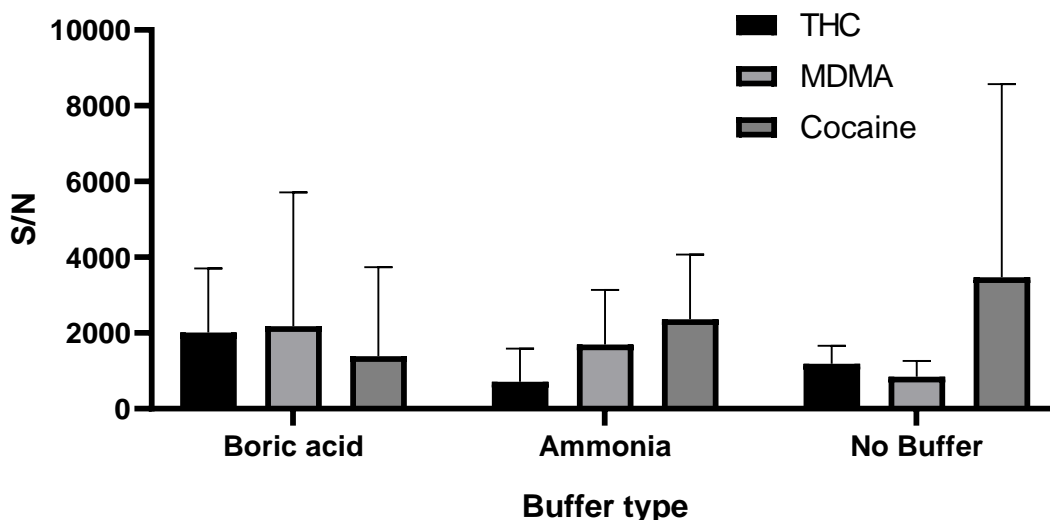


Figure 85: Comparison of buffer types for chloroform extraction of MDMA, cocaine and THC from spiked saliva, n=3, error bars are 1SD

The results showed that borax was the optimal buffer for THC and MDMA, but not for cocaine (Figure 85). The non-buffered extraction was optimal for cocaine, but the S/N was highly variable for the three replicates indicating that the higher mean value may not be totally accurate. As cocaine ionises more efficiently than MDMA and THC, the buffer that allowed the maximum extraction of these two drugs was chosen. The buffered extraction was then performed on solutions of spiked saliva, as per the optimised conditions, with

10 $\mu$ L of 0.1% TFA, 0.1% formic acid or water applied to the dried spot.

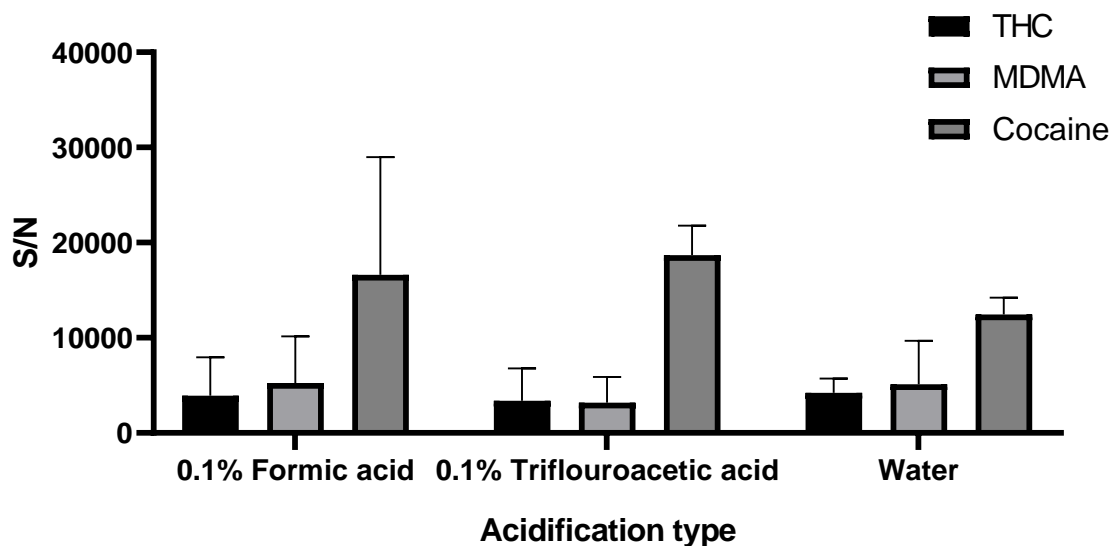


Figure 86: Comparison of acidification types for borax buffered chloroform extraction of MDMA, THC and cocaine from spiked saliva, n=3, error bars are 1SD

The addition of acid to the sample spot did not increase the ionisation of the drugs, when compared with the water only (Figure 86). The final method therefore did not involve any acidification. The final experiment looked at the impact of metal triflates on the ionisation of the three drugs, as the presence of metal ions has been shown to increase ionisation in MALDI-ToF [161]. It was thought that the presence of cations in the sample may induce adduct formation through the APCI ionisation mechanism, as anionic dopants can induce the formation of negatively charged adducts in DART [9]. Silver, potassium, and sodium triflate were used at concentrations of 0.1% in water. The metal triflate solutions were used in place of the water on top of the dried solvent spot and compared with 0.1% FA and TFA at the same time, for sample solutions of 1ng/mL and 10ng/mL concentrations.

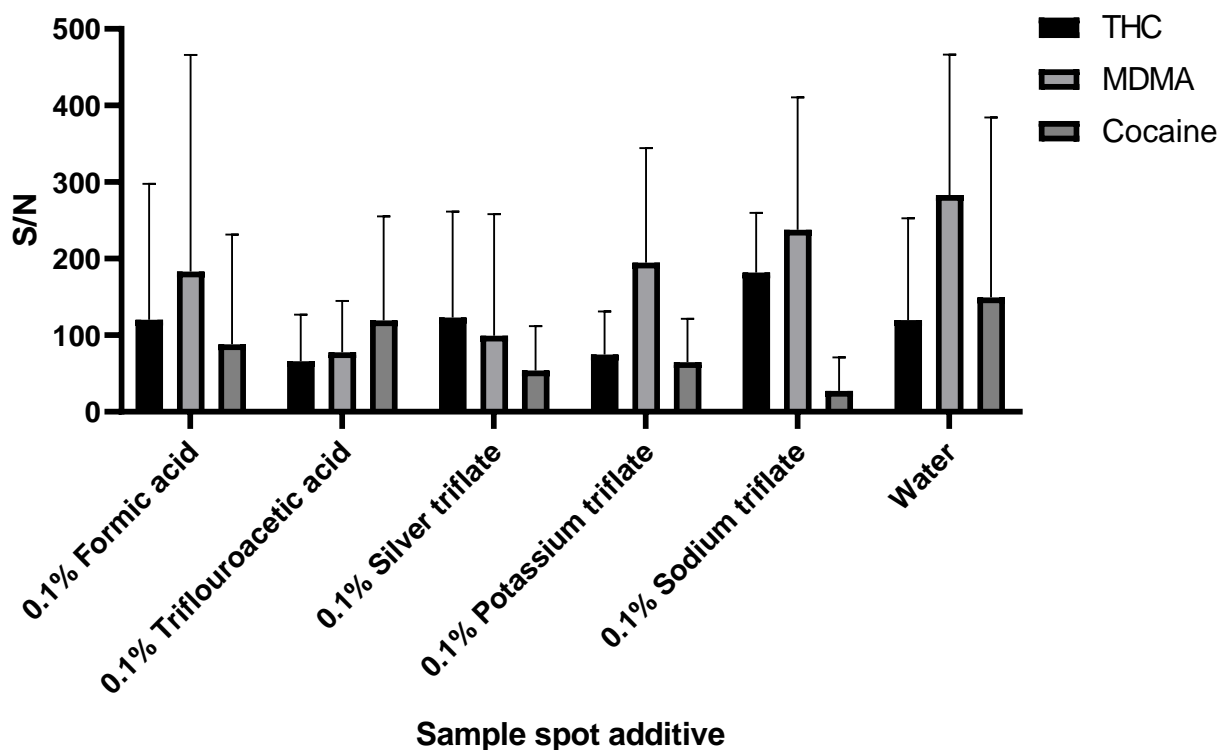


Figure 87: Comparison of sample spot treatment with 0.1% TFA, FA and metal triflates with buffered chloroform extraction of 1ng/mL MDMA, THC and cocaine from spiked saliva, n=3 and error bars are 1SD

There were no metal adducted molecular ions detected for MDMA, cocaine or THC. For the comparison above, the molecular ion signal to noise was used to determine if there were advantages to using metal triflate solutions for the molecular ion. Comparison of the SN for all dried sample spot treatments showed no increase when compared to water (Figure 87).

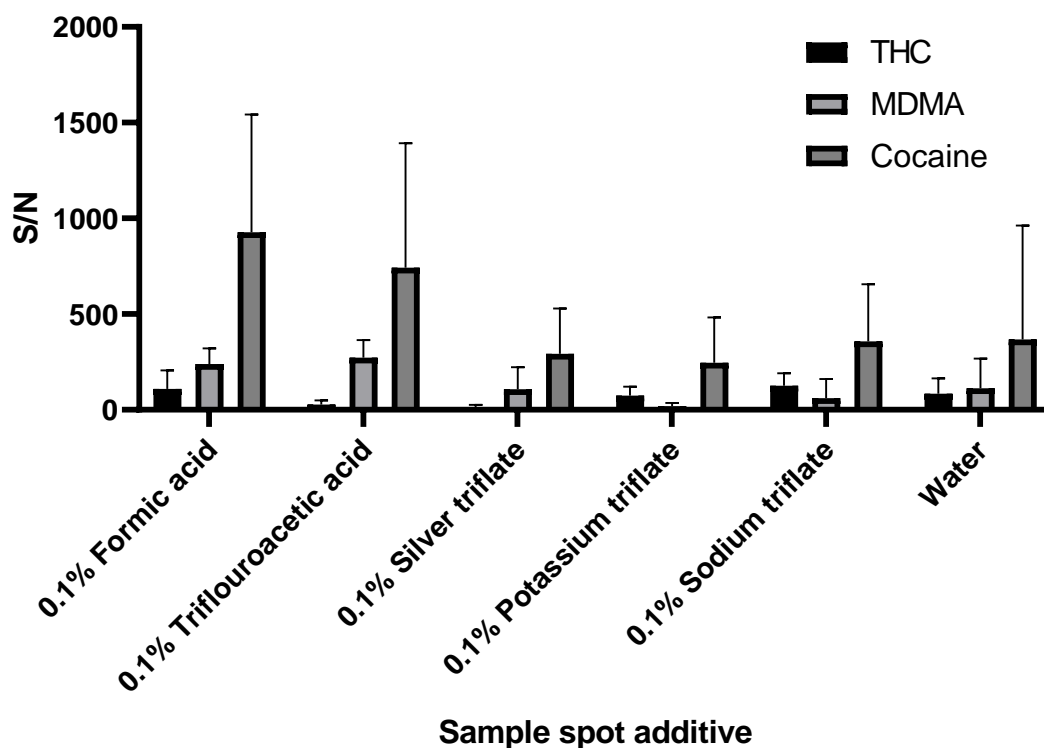


Figure 88: Comparison of sample spot treatment with 0.1% TFA, FA and metal triflates with buffered chloroform extraction of 10ng/mL MDMA, THC and cocaine from spiked saliva, n=3 and error bars are 1SD

For the 10ng/mL solution there were little differences between the sample spot treatments and the water, much like the 1ng/mL solutions (Figure 88). What is important to note is that it is clear how high the cocaine S/N is compared to MDMA and THC at the same concentration. It is a fine example of how much more efficient the ionisation of cocaine is using the DSA-ToF is compared to the other two drugs examined.

The final method optimised for the extraction of MDMA, THC and cocaine from saliva was determined to be 5:1 saliva: chloroform, using a borax buffer, 90 seconds centrifugation, 4 $\mu$ L of the solvent onto the mesh (after removal of the saliva layer), and 10 $\mu$ L of water on top of the dried solvent spot. The use of heptane in place of chloroform was determined to be optimal for the extraction of THC alone.

Following this optimisation, the linearity of the three drugs in saliva was determined. Spiked saliva was prepared at concentrations of 10-200ng/mL for each of the three drugs, and internal standard was spiked at 100ng/mL. The method optimised for all three drugs was applied and analysed, with linearity assessed using the ratio of drug to internal standard.

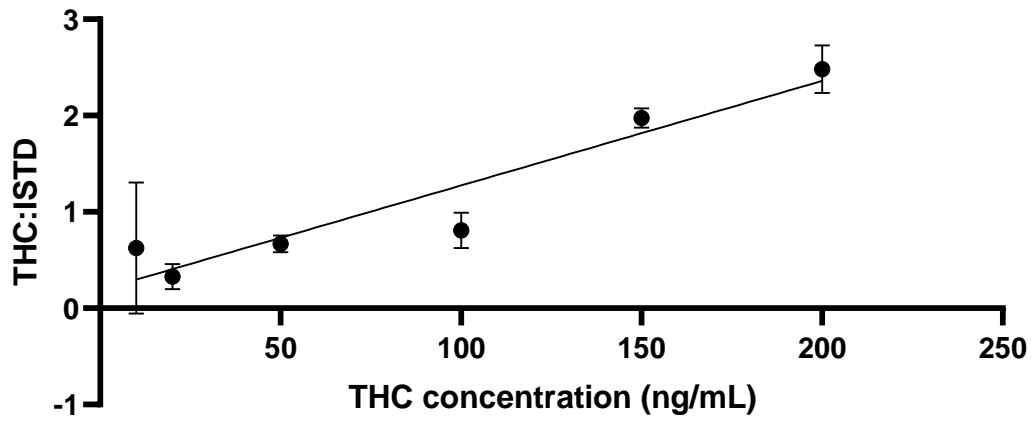


Figure 89: Ratio of THC: ISTD for THC concentrations of 10-200ng/mL, using optimised chloroform extraction method. R2= 0.9, n=3 and error bars are 1SD

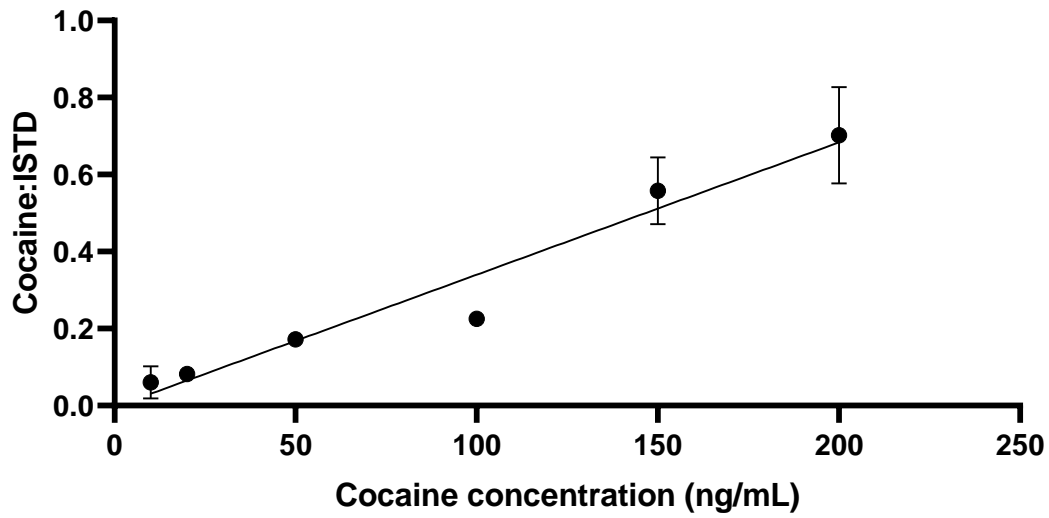


Figure 90: Ratio of cocaine: ISTD for cocaine concentrations of 10-200ng/mL, using optimised chloroform extraction method. R2= 0.9575, n=3 and error bars are 1SD

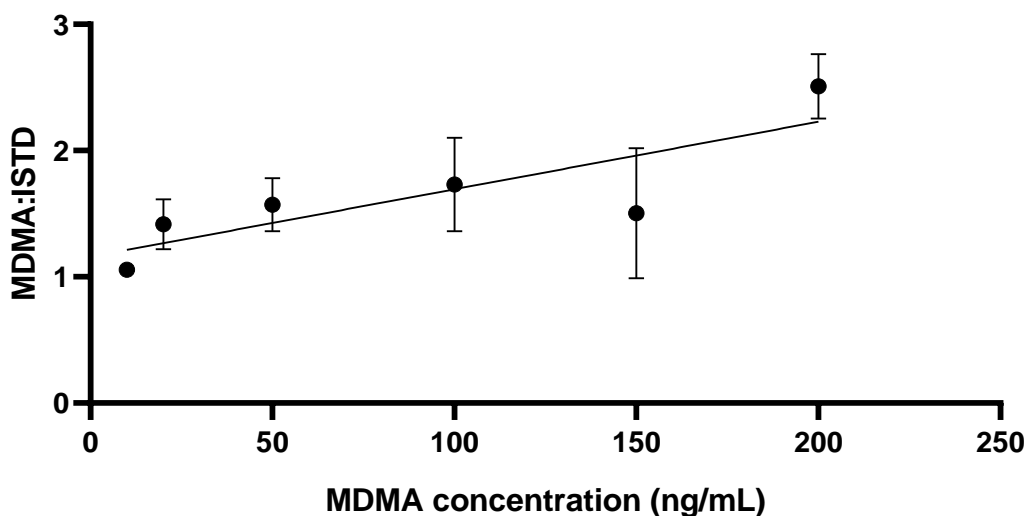


Figure 91: Ratio of MDMA: ISTD for MDMA concentrations of 10-200ng/mL, using optimised chloroform extraction method. R2= 0.9301, n=3 and error bars are 1SD

The linearity for all three drugs across this range was no less than 0.9 (Figure 89, Figure 90, & Figure 91). When compared to the linearity achieved using the drugs in water alone, the extraction exhibits more variability. For MDMA, the y-intercept also indicates that there is likely an isobaric matrix interference increasing the apparent MDMA intensity. This high y-intercept coupled with the shallow slope would indicate that there is a substantial amount of this interference being extracted from the saliva. This also indicates that the interfering compound is being extracted or ionised preferentially over the MDMA, resulting in the very small increase in ‘MDMA’:ISTD ratio across the calibration range. Limits of detection and quantification were calculated for each of the drugs using the linear regressions determined in this experiment (Table 32).

Table 32: Limits of detection and quantification for buffered chloroform extraction of THC, MDMA and cocaine from spiked saliva

Chloroform extraction	LoD (ng/mL)	LoQ (ng/mL)
THC	9	50
MDMA	186	648
Cocaine	8	18

These results further confirm that there was an issue with the extraction of MDMA in this experiment. The high limits of detection and quantification reflect the high y-intercept observed for the linear regression

calculated above. For cocaine and MDMA the limits of detection are comparable to those calculated for the same drugs in water (from Chapter 3).

The linearity of THC was also determined using heptane instead of chloroform as the extraction solvent. All other parameters of the optimised chloroform method were used. Linearity was assessed against the concentration using the ratio of THC to internal standard in the same manner as above.

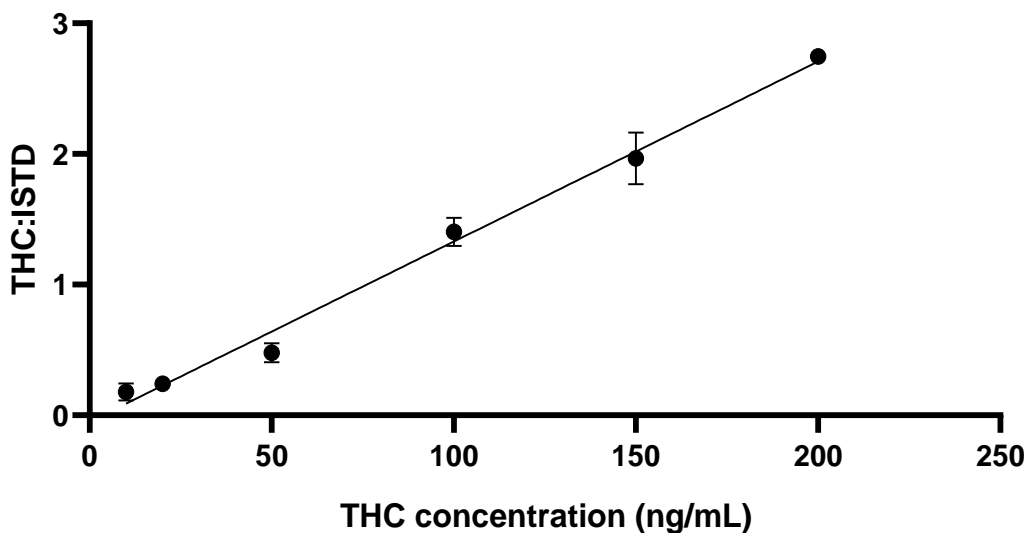


Figure 92: Ratio of THC: ISTD for THC concentrations of 10-200ng/mL, using heptane extraction method. R2= 0.9919, error bars are 1SD

Linearity for the heptane extraction of THC is far improved from that of the chloroform extraction. The variability of each set of data points is minimal, and the coefficient of variation is above 0.99, indicating a very good fit.

Table 33: Limits of detection and quantification for buffered heptane extraction of THC from spiked saliva

Heptane extraction	LoD (ng/mL)	LoQ (ng/mL)
THC	11	17

The limit of detection for the heptane extraction was higher than that of the chloroform extraction, however the limit of quantification is much lower. This further confirms that the heptane method is more appropriate than the chloroform method, although it appears that this method also extracts other compounds in the

same mass range. This is likely causing the increased limit of detection, where greater noise convolutes the mass spectrum, and the calculated limits are below the toxicological concentrations in 4.1.

#### 4.1 Timed interaction extraction of MDMA, THC and cocaine from spiked saliva

A solvent free method of extraction was also investigated, as there was the potential to further simplify this method and remove the need for solvents altogether, based on the observation that mesh became retentive of organic compounds when plasma treated. For this method, the time of interaction, mesh type (instrumental, oxygen and argon plasma cleaned), buffer and acidification of sample spot were investigated. For this method 4 $\mu$ L of spiked saliva (100ng/mL of the chosen drug) was placed onto the mesh and allowed to interact for a period of time. After that period of time, the saliva was removed and 10 $\mu$ L of water was pipetted on top immediately prior to analysis.

The initial optimisation focused on the time of the interaction on heat treated mesh (using the instrument plasma), as this was thought to be the least likely to facilitate a transfer from the saliva to the mesh. The times tested were 15, 30, 60, 90 and 120 seconds, with 4 $\mu$ L of saliva.

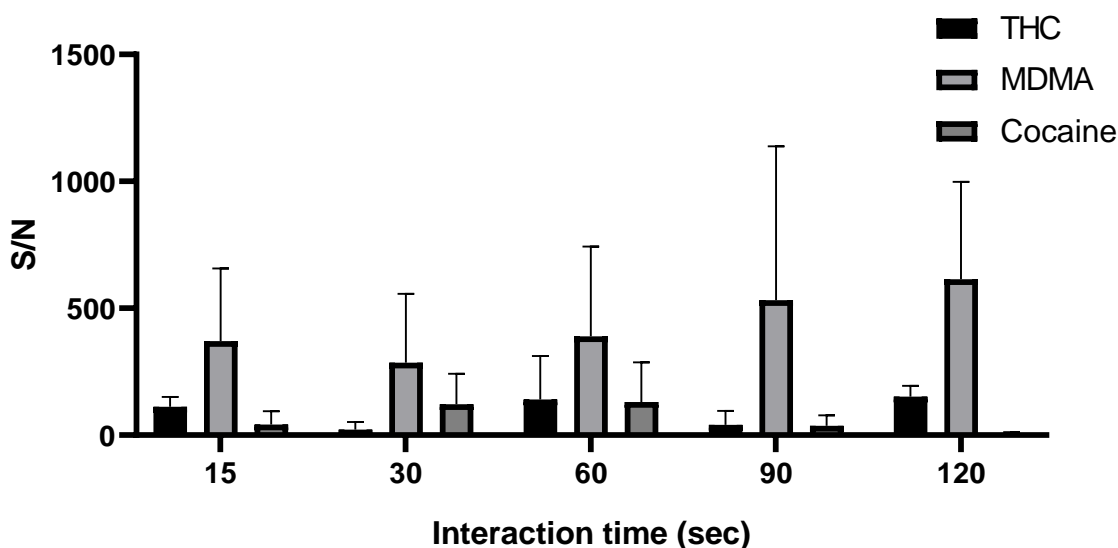


Figure 93: Comparison of interaction time on non-plasma treated mesh for extraction of THC, MDMA and cocaine from spiked saliva, n=3, error bars are 1SD

There did not appear to be any consistent increase in the amount of drug transferred (measured as the signal to noise ratio of the molecular ion peak of each drug) for the longer interaction times. That is, the changes in the S/N were seemingly random, with increases in SN at 15, 60, and 120 sec for THC, with very

minimal signal at 30 and 90 seconds. The same is true for the MDMA, where the S/N increases and decreases over the interaction times tested. Ultimately the 60 second interaction was chosen as the optimal time for this type of extraction, as this showed increases S/N values for all three drugs (Figure 93).

The mesh types investigated were instrument-treated, argon plasma treated and oxygen plasma treated meshes. These were plasma treated in the same way as the meshes investigated for the contamination improvement study (3.3.2). Although 60 seconds was chosen as the optimal interaction time for the instrument cleaned mesh, these times were also re-examined as part of this experiment, to understand the impact interaction time has on the extraction using different mesh.

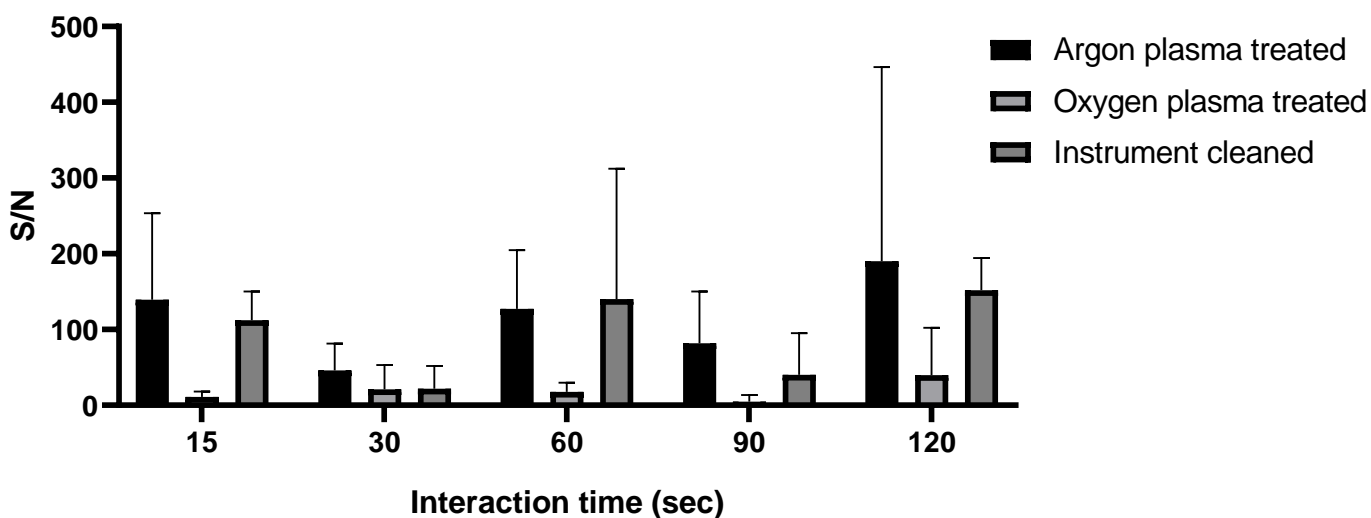


Figure 94: Comparison of plasma cleaned mesh types for the extraction of THC from spiked saliva, n=3, error bars are 1SD

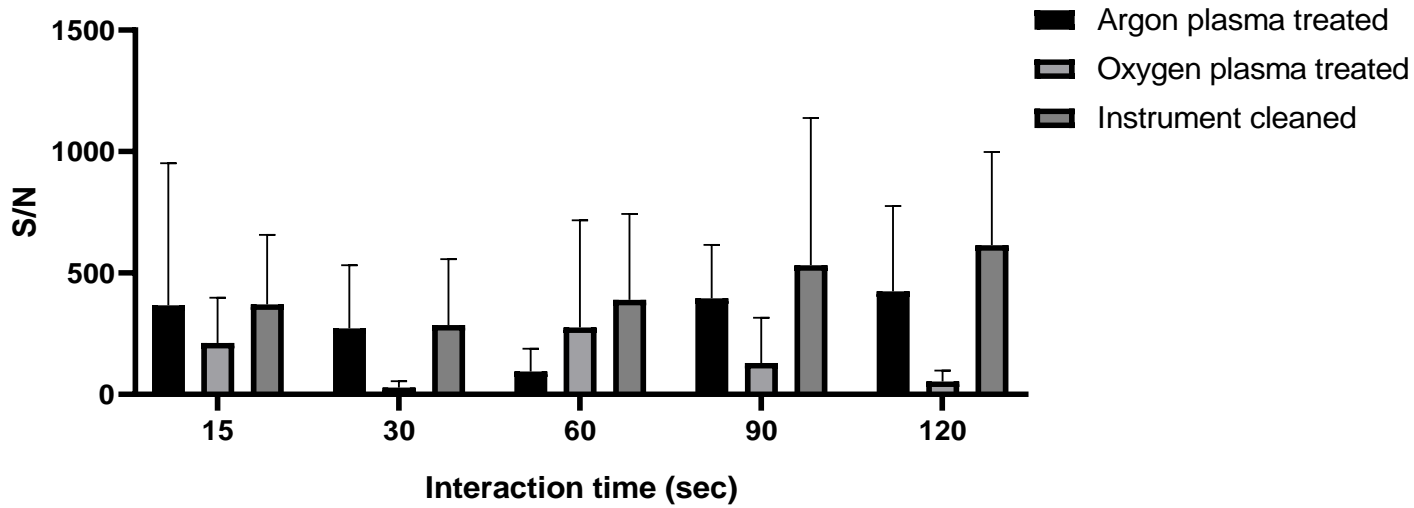


Figure 95: Comparison of plasma cleaned mesh types for the extraction of MDMA from spiked saliva, n=3, error bars are 1SD

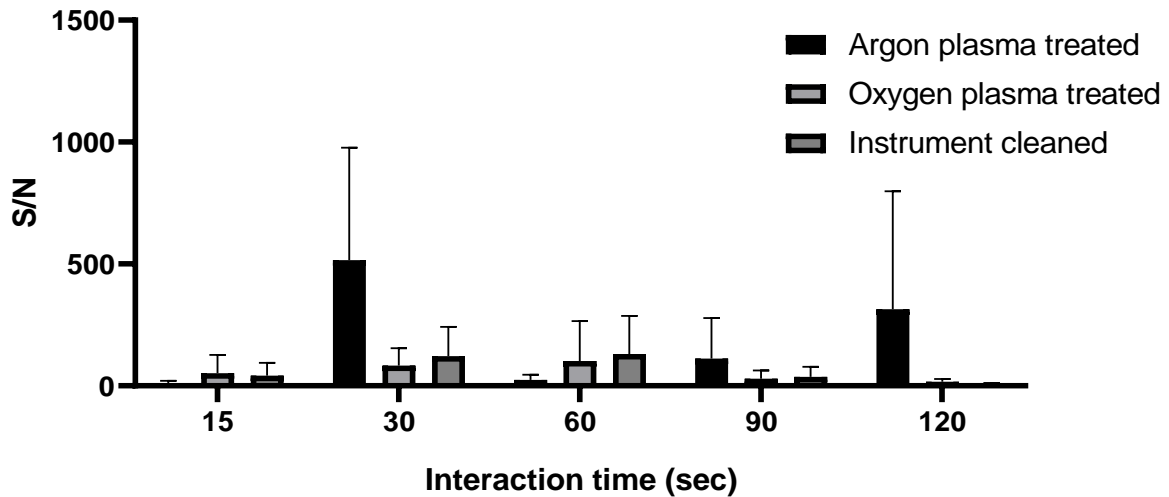


Figure 96: Comparison of plasma cleaned mesh types for the extraction of cocaine from spiked saliva, n=3, error bars are 1SD

All three drugs on each mesh type extracted most efficiently with 60 seconds interaction time (Figure 94, Figure 95, & Figure 96), confirming the previous experimental results (Figure 93). The instrument-heat treated mesh was more effective at retaining analyte than the plasma-treated mesh, and this was chosen as the optimal mesh for the timed extraction.

As with the solvent extraction, buffering was investigated as a potential avenue for increasing the extraction efficiency from the saliva, with the same buffers as the solvent extraction (ammoniacal and borax) used to buffer the saliva to pH 9 and 10 respectively. 4 $\mu$ L of saliva was allowed to interact with instrument plasma treated mesh for 60 seconds. Water was used as the sample spot wetting agent for these analyses.

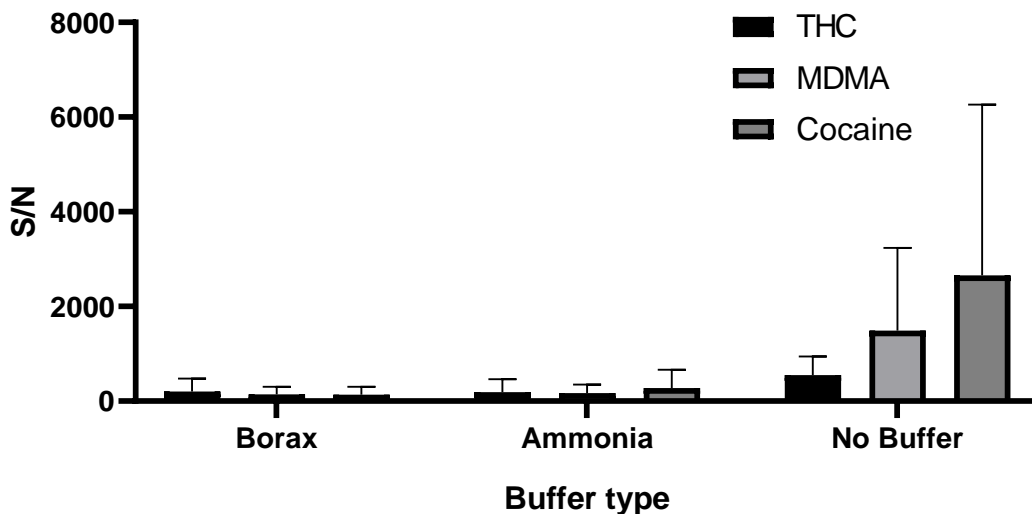


Figure 97: Comparison of buffered extraction (ammoniacal, borax and non-buffered) of THC, MDMA and cocaine from spiked saliva

The use of a buffer did not increase the retention of analyte on the mesh (Figure 97) and was not investigated further.

The final parameter investigated for this extraction type was the acidification of the sample spot, post saliva interaction, by replacing the water on top of the 'dried' spot with 0.1% TFA or 0.1% FA. According to the optimised method, 4 $\mu$ L of saliva was allowed to interact with the instrument treat mesh for 60 seconds before removal and re-wetting.

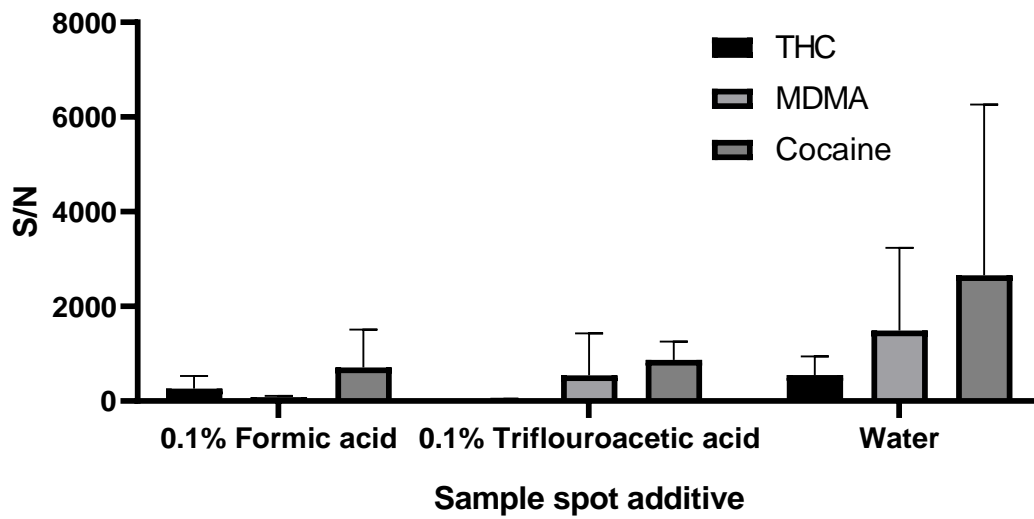


Figure 98: Comparison of acidification methods for the timed interaction extraction (60 seconds) of THC, MDMA and cocaine from spiked saliva, n=3, error bars are 1SD

Acidification of the sample spot did not improve S/N for any of the three drugs (Figure 98). Finally, the linearity of the drugs using this method was assessed, across the same range as the chloroform extraction.

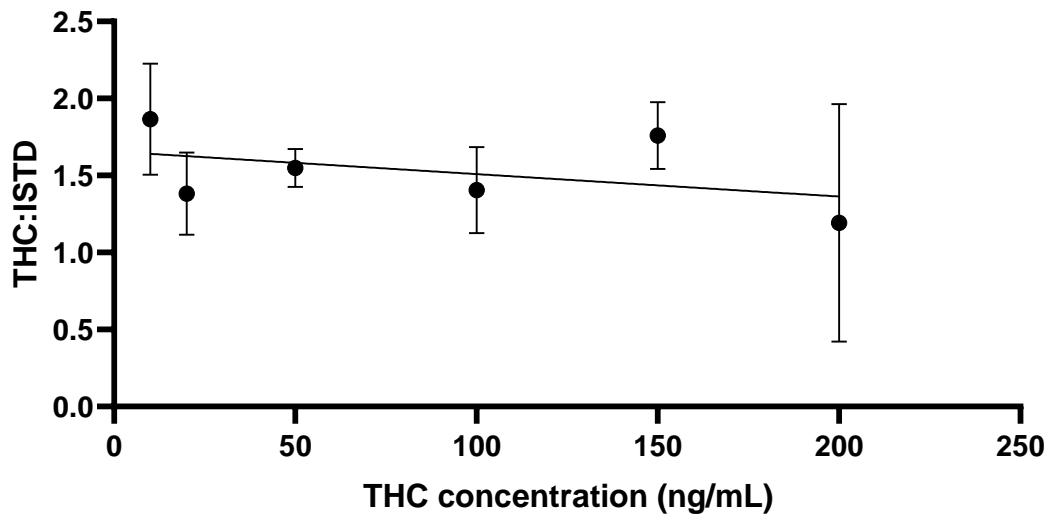


Figure 99: Ratio of THC: ISTD for THC concentrations of 10-200ng/mL in saliva, using optimised timed interaction extraction method, error bars are 1SD (n=3).  $R^2=0.0029$ .

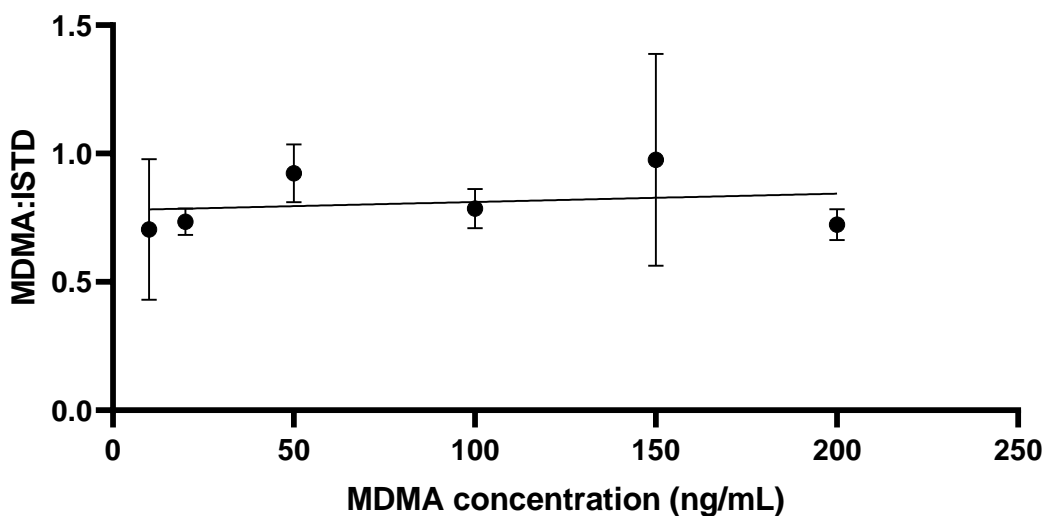


Figure 100: Ratio of MDMA: ISTD for MDMA concentrations of 10-200ng/mL in saliva, using optimised timed interaction extraction method, error bars are 1SD (n=3)  $R^2=0.0464$

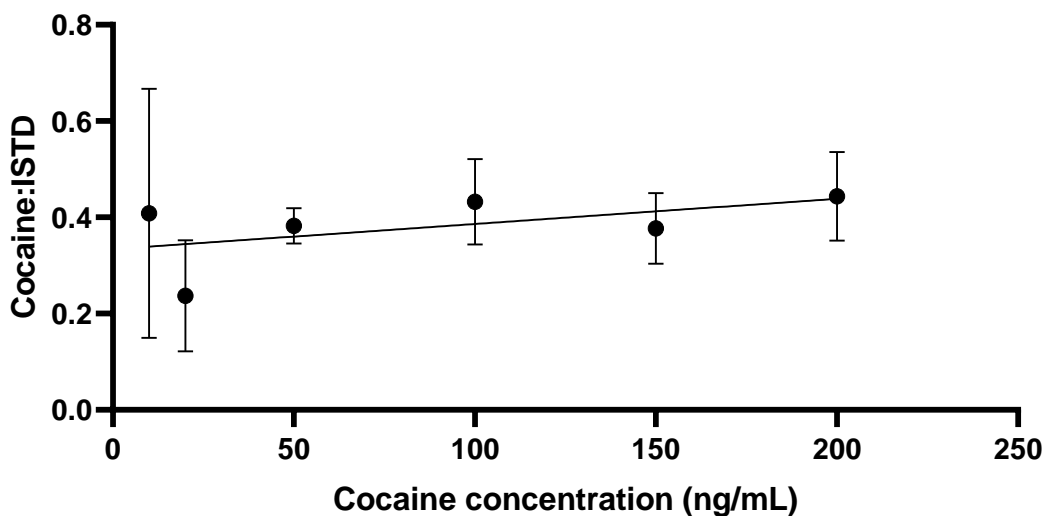


Figure 101: Ratio of cocaine: ISTD for cocaine concentrations of 10-200ng/mL in saliva, using optimised timed interaction extraction method, error bars are 1SD (n=3).  $R^2= 0.2798$

There was no linearity observed for any of the drugs, with no increased response for increased concentration. In the case of THC, the ratio of drug to internal standard was reduced over the concentration range (Figure 99). These data indicate a strong background interference compromising the detection of any

analyte transferred to the mesh. This method is therefore not suitable for quantification, but the detection itself may lend this simplified method to screening, if sample volume allows.

## 4.2 Conclusions

Two methods were developed for the detection of cocaine, MDMA and THC. A solvent extraction method using chloroform was found to extract all three drugs from spiked saliva. The same method with heptane as the extraction solvent was more effective at extracting THC, and produced a more linear response than chloroform across the same range. Limits of detection were established, and were comparable to those of the drug in water across the same range, although high y-intercepts for MDMA indicated that there may be specificity issues. Ultimately, this method will be quite suitable for rapid qualitative analysis of saliva samples. Quantitation is possible, but should not be relied on, as it's highly likely that the variability in limits of detection and quantification is just as pronounced as that observed for the drug solutions in water. Additionally, high y-intercepts observed for MDMA indicated that the specificity of the method was not adequate to ensure reliable estimations of content in saliva.

A secondary extraction involving no solvents was developed, involving a period of saliva interaction and subsequent removal. This method was shown to extract small amounts of analyte, but quantification was not at all possible, as no linearity was observed for any of the three drugs. Mesh alterations in the form of plasma treatment to encourage adherence of analyte to the mesh were investigated but showed no increase in S/N for any of the drugs tested. This method would be suitable for rapid screening of drugs in saliva, but ultimately the solvent extraction would offer more quality results with little increase in time and effort from the analyst.

These results show that the qualitative detection of drugs in saliva is very possible using this instrument. There is real potential here for application of the solvent extraction method to be used for screening of drugs in a forensic lab (or otherwise). More work will need to be done on the method to identify and improve the selectivity of the solvent extraction. This may allow the method to be used for rudimentary quantification with more certainty than the method in its current state would offer. For the timed interactions, modifications to the physical properties of the mesh may improve transfer from the saliva to the mesh. These may include increasing the surface area of the mesh, using radical oxygen sites (from plasma exposure) to introduce chemical functionality to the surface for more effective and targeted partition of analyte from the saliva.

Ultimately, further work in this space may pave the way for significantly reduced analysis time for screening of saliva samples. This will have huge benefits for public safety, allowing rapid identification of exogenous compounds in saliva. As discussed in earlier chapters, the benefits of DSA-ToF are that targeted and non-targeted analysis can be run at the same time, without any adjustments to the method. For saliva analysis, this means that there is practically no limit to the number of drugs that can be detected, something that cannot be said for techniques such as immunochromatography or immunoassays development of different antibodies is required whenever a new kit for a new drug is required. For use of the methods described in this chapter, the only limiting factor will be the extraction method, which can be altered to suit very rapidly. The vast amount of literature using ambient mass spectrometry for the detection of a huge number of drugs supports that these techniques are the future of screening, to provide a rich amount of data to improve public health and safety.

## 5 DSA-ToF for breath analysis of nicotine, pseudoephedrine and caffeine

### 5.1 Introduction

Exhaled breath is made up of aerosol particles formed from the epithelial lining fluid (ELF) of the oesophagus. These aerosol particles also contain saliva, and other compounds from the gas exchange process, including volatile organic compounds and biomarkers for disease [162-164]. Breath analysis has recently found favour as it is a non-invasive and non-adulterable sample collection method that has been shown to offer comparable chemical information to other biological matrices often used for testing such as blood, urine and saliva [165]. It is well known that in order for drugs to be found on the ELF that there must be some transfer across the alveolar epithelial cells, but that they must travel through the cells themselves, as the junctions between the cells are too tight to facilitate this transition [166]. This is important as the types of drugs that transition in this manner are more likely to be smaller and more lipophilic in order to pass through the cell membranes successfully. This lipophilic character is also likely to increase the concentration in the aerosol particles formed, as they are more likely to accumulate on the surface of liquids and assist in the formation of such particles [167]. It should be noted however, that the formation of these aerosols is strongly dependent on the breathing mode of an individual and that these generalisations do not always apply.

Due to these benefits, breath testing remains an emerging field outside of the medical industry. Quantifying compounds from exhaled breath presents a range of problems, largely due to the physiology involved. Although detectable compounds in breath are contributed from multiple points in the gas exchange cycle, approximately one third of the volume of an exhaled breath is classed as 'physiological dead space', as it has not undergone gas exchange at the alveoli [167]. This complicates the interpretation of breath analysis results, as not all compounds detected have come from the gas exchange process and may be due to the saliva in the aerosol particles, or similar. The question must be asked: how confident can we be in the analysis of breath analysis results if we are not certain of the origin of the components? Furthermore, standardising breath analysis is incredibly difficult, as the parameters that dictate the composition of breath are highly individualised and are dependent on the health status and breathing mode of the individual [167]. The humidity, temperature, alveolar space, dead space and volume must be taken into account when considering and attempting to develop and standardise methods. Logic dictates that these conditions should be constant in order to produce meaningful results, but this simply cannot be achieved using human

subjects. Breath analysis methods must therefore be considered qualitative at best where these conditions are not standardised, allowing rapid screening tests and little more at this point in time.

Breath analysis sampling techniques can be divided into two categories: off-line and real-time. Off-line analysis involves a twostep process where the breath collection and analysis are completed separately. The benefit of off-line analysis is that the analyst is able to treat the sample and pre-concentrate it prior to analysis, leading to a more sensitive method. The drawback is that off-line sampling offers limited real-time pharmacokinetic information. Within off-line sampling there are three major strategies: adsorption, extraction and condensation (Figure 102). Adsorption relies on a material to trap analytes of interest as breath is exhaled. Adsorption was initially used to detect volatile organic compounds (VOCs) in the early stages of breath research and was improved with the invention of SPME and sorbent tubes, allowing prolonged exhalation and concentration of analytes onto the material. There is sufficient variety in the number and type of sorbents that methods can be altered to increase both sensitivity and selectivity [168]. Adsorption is a difficult method to validate, as there is the potential for degradation of the analyte on the sorbent, and the recoveries for these methods are not known and not able to be determined with a great deal of accuracy. In addition, it is quite difficult to achieve accurately known vapour phase concentrations of standards for quantitation purposes.

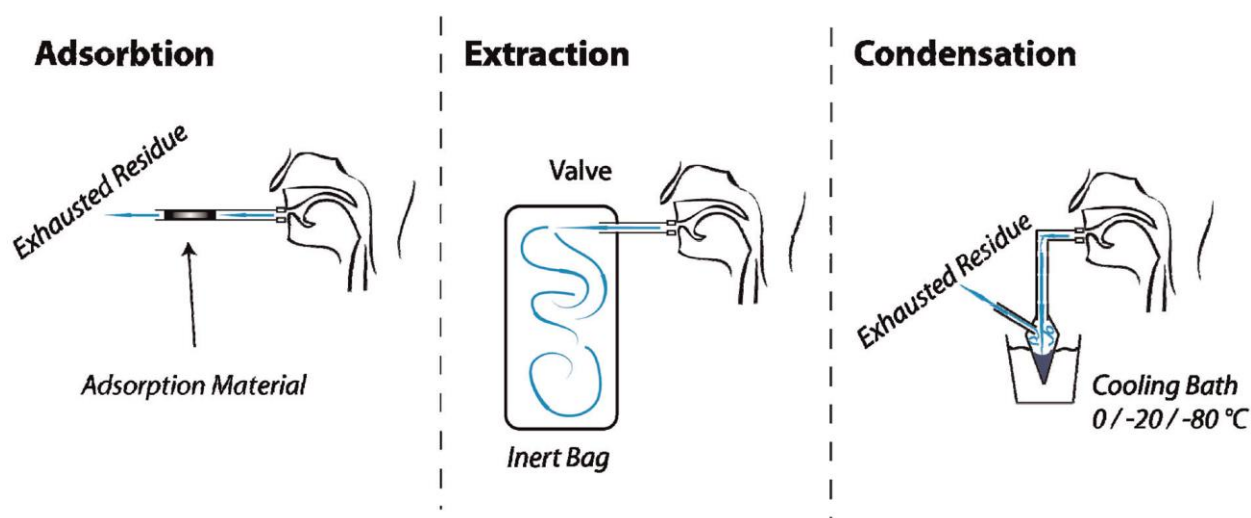


Figure 102: Off-line method for sampling breath. Reproduced from [167]

The use of a container of defined size for breath collection is termed extraction [169]. The trapped breath can then be injected straight from the container into the instrument for analysis or pre-concentrated through solvent extraction prior to analysis [170]. The use of containers with a defined volume standardises

the collection process somewhat, in that distinct and defined concentration factors can be determined to offer some version of a semi-quantitative analysis. In this manner, extraction sampling methods offer the best opportunity to achieve quantitation, particularly when the person exhaling is able to fill the sampling container fully, and the recovery of the components through solvent extractions and concentration steps is well known. The difficulty with this method is that the selectivity is non-existent. All compounds exhaled into the bag are extracted and concentrated, which can lower the sensitivity of the technique.

Condensation is the method most commonly employed when compounds of low volatility require testing. The breath is condensed in a container at low temperatures, producing a breath concentrate made up of water and compounds of low volatility. The use of condensation sampling allows for high sensitivity analysis to be achieved through extensive pre-concentration of large volumes of breath [171]. This condensate can be injected directly into an instrument, much like extracted breath in the previous example, or it can be pre-concentrated through a solvent extraction step. Ultimately, the choice of sampling method for off-line sampling should be made with the type of analyte in mind. As with all sampling methods for analytical chemistry, there is no 'one size fits all' technique, and while adsorption methods are optimal for VOC collection the detection of non-VOC compounds will not be facilitated by these methods.

Real-time analysis marries the sampling and analysis steps to allow rapid data regarding the presence of and concentration of analytes to be determined. Techniques used in this manner must be validated extensively in order to compete with other well known (and sometimes preferred) diagnostic methods. Parameters such as sensitivity, selectivity and robustness in particular must be well researched and understood to ensure that the best information is being provided, especially for use in a point of care diagnostic capacity. The real-time methods most commonly used can be categorized by the type of detection technique used: vacuum ionisation and ambient ionisation.

Vacuum ionisation for breath analysis includes Electron Impact (EI), Selected Ion Flow Tube Mass Spectrometry (SIFT-MS) and Proton Transfer Reaction Mass Spectrometry (PTR-MS). EI is an excellent tool for identifying unknown compounds, but is limited for use with VOCs as the molecules must be in the gas phase before they can be bombarded with electrons and ionised [172]. Additionally, EI induces fragmentation which can be problematic for breath analysis, which already has a complicated matrix to investigate. This issue can be addressed by coupling EI-MS with a GC to separate out components of the breath sample to make analysis of the spectra produced much easier. SIFT-MS is a chemical ionisation technique that is also well suited to VOCs, particularly headspace analysis [173]. It is highly sensitive and

can be integrated into existing ventilator set-ups to facilitate real-time breath analysis for patients who are not breathing naturally or who may be sedated, particularly with propofol [174]. Finally, PTR-MS, another chemical ionisation method using proton transfer. Like EI and SIFT-MS, PTR-MS is not suitable for the analysis of non-volatile compounds, as all three operate below atmospheric pressure and therefore require the sample molecules to be transported into the vacuum before any ionisation can take place, a process that is not conducive to the movement of non-volatile compounds [175].

Atmospheric ionisation for real-time breath analysis covers both atmospheric pressure chemical ionisation (APCI) and extractive electrospray ionisation (EESI)/secondary electrospray ionisation (SESI). APCI is, as described previously, a chemical ionisation method that produces both molecular ions and fragments and is suitable for the analysis of non-volatile compounds. APCI is considered robust and reliable but is prone to inducing thermal degradation in some molecules, due to the ionisation process itself, which tends to make use of a heated plasma.

EESI/SESI involves the mixing of the breath sample with an ion cloud formed from an electrospray ionisation (ESI) source, where charge transfer then takes place. Also suitable for non-volatile compounds [176], EESI/SESI are highly sensitive without enhancements to the instrument, but sensitivity can also be enhanced with instrumental changes such as a funnel to direct the breath flow into a smaller area for improved charge transfer in the ESI ion cloud [177, 178]. These methods also have the benefit of being a soft-ionisation technique, and producing primarily molecular ions, which is ideal for breath analysis with no separation component. Much like the off-line sampling methods for breath analysis, the target analytes should be considered when deciding which real-time technique will be employed. Volatile compounds will perform best with vacuum ionisation methods, whereas non-volatile compounds will only be detected using atmospheric ionisation.

Further emerging research is occurring in the space of pharmacokinetics, where real-time tracking of pharmaceutical concentration is used to improve safety where drugs have narrow therapeutic ranges. This is directly linked to the increased interest around personalised medicine, where differences in individual patient metabolisms are being considered when administering drugs, leading to customised patient treatment plans [179]. Differences in drug metabolism between patients are influenced by a patient's Body Mass Index, current health status, any addictions present and even the genes of the patient [180]. These are complex factors, and can have dramatic impacts on the safety of treatments such as anaesthetic and opioids where the concentration in plasma changes rapidly. Therapeutic drug monitoring (TDM) allows

adjustment of drug dosage based on the real-time concentrations in plasma, ensuring that the patient is comfortable and safe at all time during treatment. TDM has been used for the detection and monitoring of propofol, methadone, and nicotine already, with the potential for the monitoring of fentanyl. Propofol requires continuous infusion for a patient to maintain appropriate levels of sedation, and studies have shown that the concentration in breath is consistent and the relationship between the concentration in breath and plasma is relatively well understood [181]. Propofol in exhaled breath has been detected using both real-time (SIFT-MS & PTR-MS), as well as off-line using SPME [181]. Methadone is exhaled in relatively high concentrations in breath [182], and tends to be administered on a frequent and continuous schedule at quite high doses [183]. Off-line adsorption methods have been used in conjunction with GC-MS to capture, extract and analyse the breath of volunteers taking regular doses of the drug, with great success, with the potential for breath analysis as a compliance tool [182]. The pharmacokinetics of nicotine have also been successfully monitored using breath analysis, using EESI [184] and APCI [185] methods to model this characteristic kinetic behaviour quite easily without quantifying. Finally, the potential for the detection of fentanyl in breath has been examined, with studies that show the contamination of ventilators in hospitals with fentanyl, where it is only used intravenously [186, 187]. Although the detection of fentanyl (a non-volatile drug) in breath is yet to be achieved, the potential to monitor such a dangerous and widespread drug in a rapid and accurate way such as breath analysis would be a huge benefit for both the medical and regulatory space.

The field of breath analysis for disease detection is constantly evolving, and while the mechanisms for the exhalation of many of these compounds is still under investigation, the presence of the biomarkers has been shown to be an excellent indicator of disease. The presence of ketones, particularly acetone, in the breath has long been known as a marker of diabetes, and can easily be detected through breath analysis [188, 189]. Stomach ulcers can be detected through the presence of urea in the breath, an indicator of *Helicobacter pylori* infection [190]. Monitoring nitric oxide in breath is used for asthma therapy [191], and exhaled hydrogen can be a marker for lactose intolerance [192]. More complex diseases can be diagnosed too, such as chronic obstructive pulmonary disease (COPD) [193] and cancers of the head and neck [194], and lungs [195]. With a better understanding of the mechanisms behind the exhalation of compounds such as this, as well as more exploratory breath analysis to identify further compounds of interest, this field of diagnostic breath analysis will only grow in the years to come.

It is little wonder then, that the use of breath analysis has moved into the regulatory space.

Breath testing for alcohol at the roadside is globally accepted, and recently the detection of illicit drugs in breath was demonstrated by Stephanson et al. [196], where nine common drugs of abuse (DoA) were detected using LC-MS. This was achieved through off-line sampling using a filter to remove micro-particles from exhaled breath, and a collection vessel of 30L to standardise the volume of sample obtained for all participants. Further work has since shown the detection of 28 drugs of abuse in a single method, using the same filter and bag collection, with limits of detection down to picograms per filter [197]. Many other methods have been developed targeting certain classes of drugs alone, such as amphetamines, methadone and THC. The DoA shown to be present and detectable in breath are listed in Table 34 below.

Table 34: Detectable drugs of abuse in the breath

<b>Analyte</b>	<b>Reference</b>
Amphetamine	[165, 196-199]
Methamphetamine	[165, 196-198]
6-acetylmorphine	[165, 197, 200]
Morphine	[165, 196, 197]
Cocaine	[165, 196, 197]
Benzoylceognine	[165, 196, 197, 201]
Diazepam	[165, 196, 197]
Oxazepam	[165, 196, 197]
THC	[165, 196, 197, 202, 203]
EDDP (methadone metabolite)	[197]
Alprazolam	[165, 197]
Ritalinic acid	[197]
Methadone	[165, 168, 182, 197, 204, 205]
7-amino flunitrazepam	[197]
Methylphenidate	[197, 199]
Nitrazepam	[197]
Flunitrazepam	[197]
OH-alprazolam	[197]
7-amino clonazepam	[197]
Buprenorphine	[165, 197]

Hydromorphone	[197]
7-amino nitrazepam	[197]
Norbuprenorphine	[197]
DM-Tramadol	[197]
Tramadol	[197]
Nicotine	[206]

These works demonstrate the utility of breath analysis for criminal justice, workplace testing or compliance reasons, for rapid data collection of profiling that cannot be performed using more traditional sample types.

Although there are significant advances in the field of breath testing, both for real-time and off-line sampling, there is still a need for a sampling method that combines the speed of real-time analysis with the sensitivity and sample storage capability of off-line analysis. A paper by Guinan et al. demonstrated a sensitive and rapid technique for the detection of nicotine in the breath of a smoker using matrix assisted laser desorption ionisation time of flight mass spectrometry (MALDI-ToF), and desorption ionisation on porous silicon (DIOS) [206]. MALDI-ToF is a highly sensitive soft-ionisation technique. The method described involved no extraction, derivatisation or rinsing protocols, with a direct sample acquisition from the volunteer, either by exhalation directly onto the DIOS substrate or by exhaling into an Eppendorf tube for suspension in water and deposition onto the DIOS substrate. This paper formed the basis of the work discussed in this chapter, replacing DIOS and MALDI-ToF with DSA-ToF.

The benefit of using direct MS methods (like DIOS-MALDI and DSA-ToF) in place of chromatography-MS techniques for breath analysis is that MS produced contain analyte, matrix and fragment ions all together, giving a fully comprehensive and very rapid overview of the sample. This chapter details three experiments: the detection of pseudoephedrine, caffeine and theobromine after oral ingestion in the breath of a volunteer, and the detection of nicotine in a regular smoker over a period of 2 hours, after using an e-cigarette using both an exhaled breath collection method and a simplified direct analysis method. All methods discussed within this chapter had a total sample collection and analysis time of less than five minutes.

## 5.2 Materials and methods

### 5.2.1 Standards and solvents

Nicotine standard was provided by Forensic Science South Australia (Adelaide, SA), no deuterated internal standard was available.

### 5.2.2 Sample collection

This work involved three volunteers. Two were non-smokers (and non- 'vapers'), one was a regular 'vaper'. Control samples were provided by the two non-vaping volunteers, for the nicotine study. One non-vaping volunteer also provided samples for the caffeine and pseudoephedrine detection study, with the control sample being provided by the same volunteer.

The initial experiments utilised the off-line collection method developed by Guinan et al. [206]. Briefly, two volunteers exhaled into Eppendorf tubes (Eppendorf, Hamburg, Germany) for 15 seconds through a piece of plastic straw, cut to approximately 5cm in length. Suspension took place by pipetting 5µL of milliQ water to the Eppendorf immediately following the exhalation, and vortex mixing for 30 seconds.

For the detection of nicotine, the volunteer withheld from vaping for 8 hours prior to the collection of the blank (t=0 min). Following that, the volunteer vaped (honeydew flavour, with added nicotine. No further details about the vaping procedure were provided by the volunteer) and samples were collected at 10, 20, 30, 60 & 120 minutes. Samples were collected by the volunteer exhaling through a 5cm length of straw into an Eppendorf tube. Analysis was conducted in triplicate.

The second experiment had the vaping volunteer exhale directly onto the mesh for 15 seconds, through the same straw length as previous. Suspension of the exhaled breath was done by pipetting 1µL of milliQ water directly onto the mesh itself, immediately following the exhalation.

For the detection of pseudoephedrine and caffeine, the volunteer consumed a coffee (single shot, milk based) and 60mg of pseudoephedrine as prescribed, after contributing a blank sample. Samples were collected at 10, 20, 30, 60 & 120 minutes after consumption of analytes, by breathing into an Eppendorf tube for 15 seconds through a 5cm straw and suspending the material in the Eppendorf in 5µL water.

### 5.3 Results and discussion

DSA-ToF identification of nicotine was established through accurate mass using a standard, with an average ppm error of -1.16 (n=6). The representative spectrum for nicotine standard solution (10 $\mu$ g/mL) can be seen in Figure 103, with the molecular ion peak for nicotine present at m/z 163.12352.

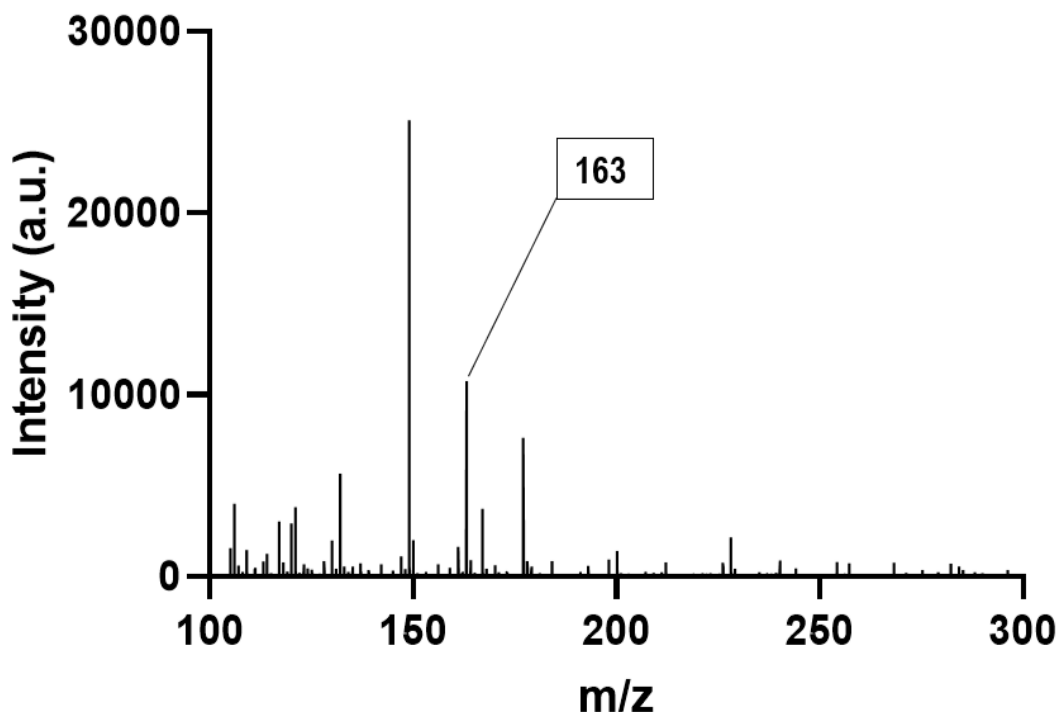


Figure 103: Representative spectrum of nicotine standard (10 $\mu$ g/mL) acquired by DSA-ToF analysis, showing nicotine detection at m/z 163

Initial method development was conducted to determine the optimal sample suspension volume. In optimising this volume, two parameters were considered: the need to not dilute the target analyte, and the need to perform replicate analysis. For the MALDI method discussed earlier, the technique is so sensitive that only 1 $\mu$ L of suspension was required for analysis [206]. This allowed the suspension volume to be small (5 $\mu$ L), allowing for maximum saturation of the solution with the breath analytes, and still allowing for replicate analysis (n=3) of the samples for a robust technique. It was initially thought that this sample volume may be too low for translation to the DSA-ToF. As previously discussed, the amount of analyte that travels into the mass spectrometer inlet is far less than that present on the mesh in the first place, such is the nature of APCI. Thus, it would be better to have more sample on the mesh in the first place, to mitigate this issue.

The vaping volunteer was asked to provide three samples, by exhaling into an Eppendorf tube through a short length of straw (approximately 5cm). These exhalations were then re-suspended in 5, 10 and 20 $\mu$ L of ultra-pure water and centrifuged for 1 minute at 2500rpm. Analysis was conducted in triplicate, using 1 $\mu$ L of the suspension onto the mesh, which had been heat treated at 350 $^{\circ}$ C for 5 minutes prior to use (in the nitrogen plasma of the DSA). The results showed that the 5 $\mu$ L suspension gave the highest signal to noise ratio for the molecular ion peak (Figure 104), and that despite the volunteer not having vaped immediately prior to the experiment, they had done so only 2-3 hours prior to sampling, ensuring some nicotine remained in the body for detection. .

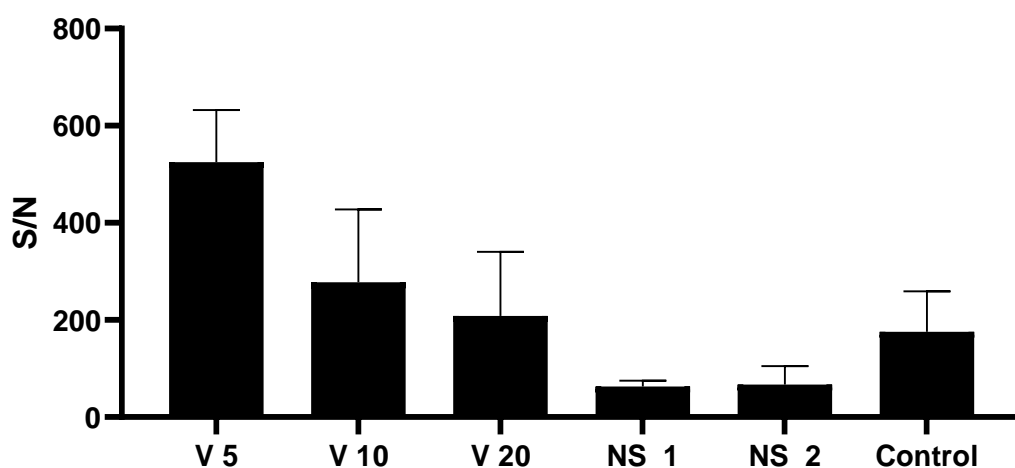


Figure 104: Comparison of nicotine signal to noise for varying suspension volumes, using Eppendorf based method. Volumes investigated were 5, 10 & 20 $\mu$ L. Non-smoking comparison data collected with 5 $\mu$ L volume

Firstly, S/N is used here in place of signal intensity as there is no internal standard, without which the signal cannot be used reliably as a measure of response (as discussed in Chapters 2 & 3). Of note is that the S/N of nicotine is far higher in any of the vaper's samples than the two non-smokers who contributed their samples to this experiment. The signal for these two non-smokers and for the control (water only) is due to an isobaric interfering peak present at  $m/z$  163.04, and unable to be fully differentiated from any nicotine peak. It is possible that some of the response recorded for the vaping volunteer's breath samples is due to the interfering peak being unresolved from the nicotine peak, however nicotine was positively identified in the breath of the vaping volunteer using accurate mass. During this experiment, the calibrant was not run through the system during acquisition, although it was calibrated prior. Due to this interfering peak, all

further nicotine work was performed with the calibrant running during acquisition, so that lockmass calibration could be retrospectively performed in order to differentiate this peak from any nicotine found.

#### 5.4 Detection caffeine, caffeine metabolites and pseudoephedrine in breath

Initially though, the method was tested on one of the non-smoking volunteers, who had consumed a coffee and a pseudoephedrine tablet at approximately the same time. A blank sample was taken prior to consumption of these items, and samples were then taken 10, 20, 30, 60 and 120 minutes following that, using the Eppendorf suspension method. Calibrant was run through the system, as the first round of nicotine samples were tested within the same timeframe.

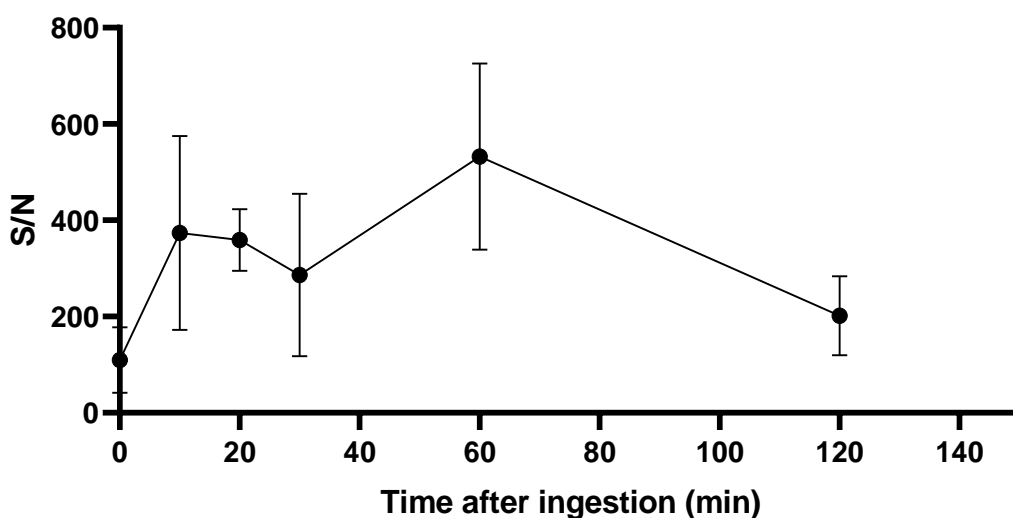


Figure 105: Average S/N of caffeine (m/z 195) in exhaled breath of a volunteer from DSA-ToF analysis. Error bars represent one SD from n=3

For caffeine, the signal to noise ratio for the blank was significant (Figure 105), as the volunteer was a regular coffee drinker, and had already consumed one approximately two hours previous to the sample acquisition. This was not unexpected, as it was thought that the caffeine would be both on the breath and in the saliva of the volunteer, and that there would be an amount of caffeine consistently present for someone who was a regular consumer of high levels of caffeine. Literature reports that for regular coffee drinkers, the baseline concentration is between 2-10mg/mL [207]. There was a clear spike after the blank sample, culminating in the maxima at 60 minutes. The absorption time of caffeine into the blood is 45 minutes [208], correlating nicely with these data. The literature states that the peak concentration in blood is seen between 1-2 hours after consumption [209]. After 120 minutes, the levels drop substantially, almost to the levels seen in the blank. The half-life of caffeine is 3-7 hours [210], however this can vary significantly between

individuals, based on their age, general health and interactions with other drugs, which may explain the accelerated elimination seen here. Factors such as smoking can halve the half-life, and oral contraception can double it [211]. This volunteer was a non-smoker, but no further medical information was known as to further explain the seemingly rapid metabolism seen here.

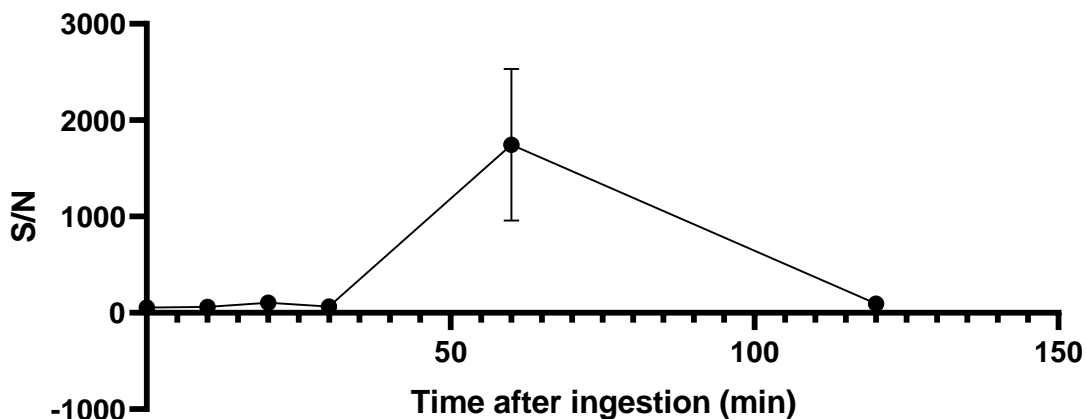


Figure 106: Average S/N (m/z 180) of caffeine metabolites in exhaled breath of a volunteer from DSA-ToF analysis. Error bars represent one SD from n=3

The metabolism of caffeine produces three compounds, in the following percentages: paraxanthine (84%), theobromine (12%) and theophylline (4%) [212]. These three compounds have the same molecular weight and cannot be distinguished from one another using the molecular ion formed from DSA-ToF analysis. Tracking of the signal to noise of m/z 180 (which is present in the spectrum of paraxanthine, theophylline and theobromine) shows a large peak 60 minutes after consumption of caffeine, coinciding with the peak concentration of caffeine in the breath of the subject (Figure 106). It is interesting to note that the signal intensity values for the m/z 180 graph as above are far higher than those of the caffeine. This could be due to the three molecules contributing to the signal (likely if the metabolic rate of the volunteer was sufficiently high) or could be related to increased fragmentation of the caffeine ions relative to the metabolites. The caffeine ionisation efficiency may also be reduced when compared to that of its metabolites, contributing to diminished S/N in comparison.

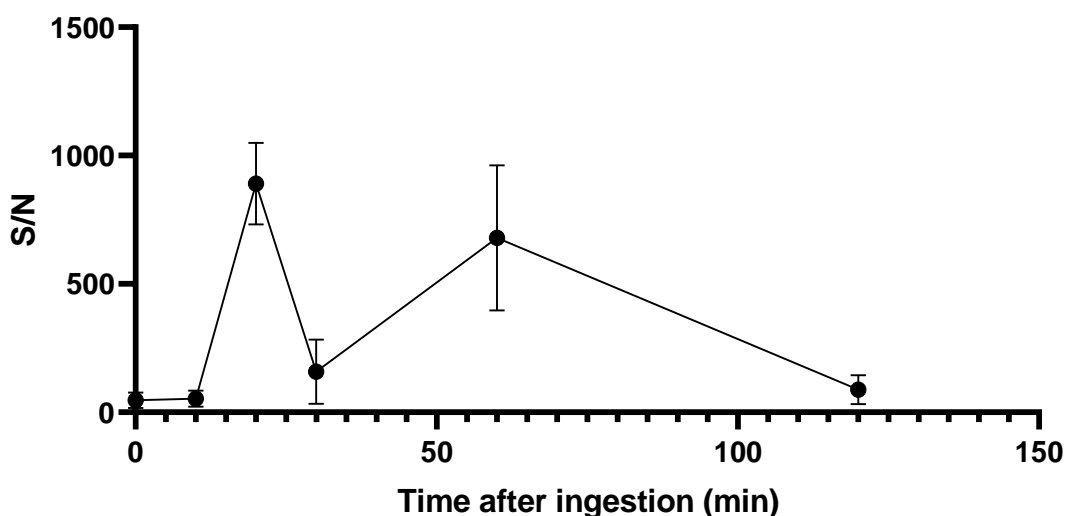


Figure 107: Average SN of pseudoephedrine in exhaled breath of a volunteer from DSA-ToF analysis. Error bars represent one SD from n=3

The pseudoephedrine also showed clear uptake and elimination, but two spikes were observed 20 and 60 minutes after consumption (Figure 107). The blank showed no presence of pseudoephedrine prior to the volunteer taking the tablet, and levels returned to those of the blank after 2 hours. It is not clear why there are two spikes present, metabolism or partitioning may be the reason for this, but this phenomenon has not been described previously. Alternatively, the low value for 30 minutes may simply be due to a low sample collection efficiency, resulting a reduced collection of breath and therefore pseudoephedrine.

Pseudoephedrine is absorbed entirely and almost immediately into the gastrointestinal tract after oral administration [213], likely leading to the early increase in signal. The peak concentration in plasma is reached between 1-3 hours after administration, depending on the individual and the dosage type received [213, 214]. The half-life of the drug is between 3-6 hours, again depending on the dosage type and individual metabolic rate [214].

This experiment shows the utility of DSA-ToF for qualitative breath testing only, with a lack of internal standard not allowing for quantification to be attempted. One simple test showed the presence of at least three compounds and allowed the uptake and elimination curves of these compounds to be produced, highlighting the similarity of breath content to that of blood or saliva. With these results alone, it is easy to see how this method could be extended to other compounds of interest, including illicit drugs and biomarkers for disease. Additionally, the method can be simplified further, as demonstrated in the following.

## 5.5 Detection of nicotine from breath using Eppendorf collection and direct exhalation

The vaping volunteer provided their breath samples while they were confined to a cleanroom. For this reason, it was not possible to analyse samples immediately after they were taken. Instead, all samples were received in bulk at the conclusion of the two-hour time period. Although the Eppendorf tubes were sealed, and the samples were prepared in the same manner as the volume optimization experiment, there was no detection of nicotine, and certainly no discernible trend over the two-hour period (Figure 108).

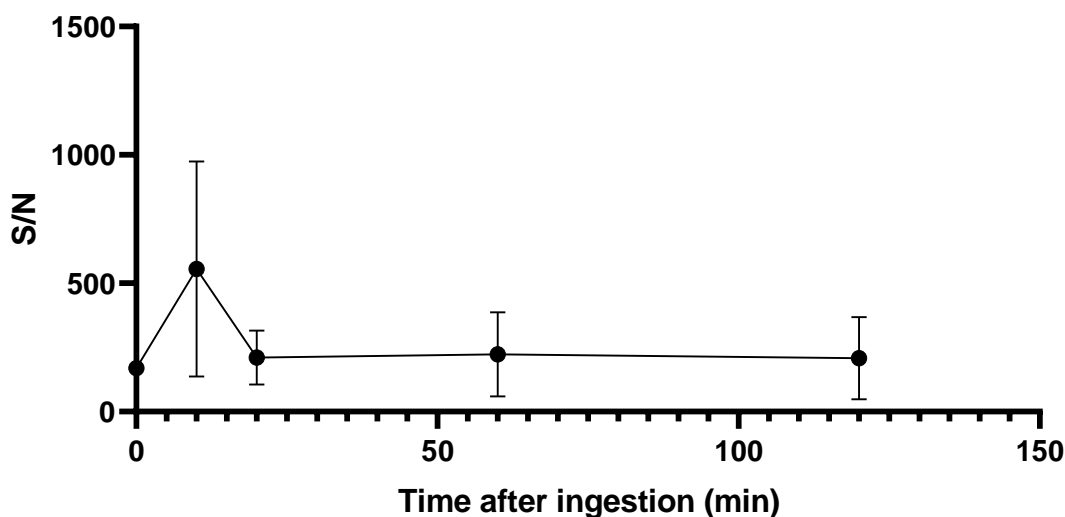


Figure 108: Average S/N of nicotine in exhaled breath of a smoker from DSA-ToF analysis using Eppendorf sample collection method. Error bars represent one SD from n=3

It is likely that over the two hours where the samples were in storage in the clean room area, that the breath vapour escaped from the Eppendorf tubes without immediate suspension. In an ideal scenario, immediate suspension would take place, but if there is any chance of analyte loss if a delay is encountered, this suspension protocol should be avoided. A more direct approach was conceived, as the nature of the ionisation and design of the instrument allowed for a more direct deposition of breath onto the mesh itself. The same volunteer abstained from smoking for the same period of time, with samples collected at the same interval as the previous experiment. Samples were collected by having the volunteer exhale through a straw directly onto the mesh for 15 seconds. The suspension was then performed on the mesh immediately prior to the analysis, which occurred immediately following the suspension, ensuring minimal time delays between sampling and analysis. This method produced an uptake and elimination curve

(Figure 109) that replicates that produced from MALDI-ToF MS, which in turn replicates that of the nicotine concentration profile reported for blood plasma over the same period of time [206].

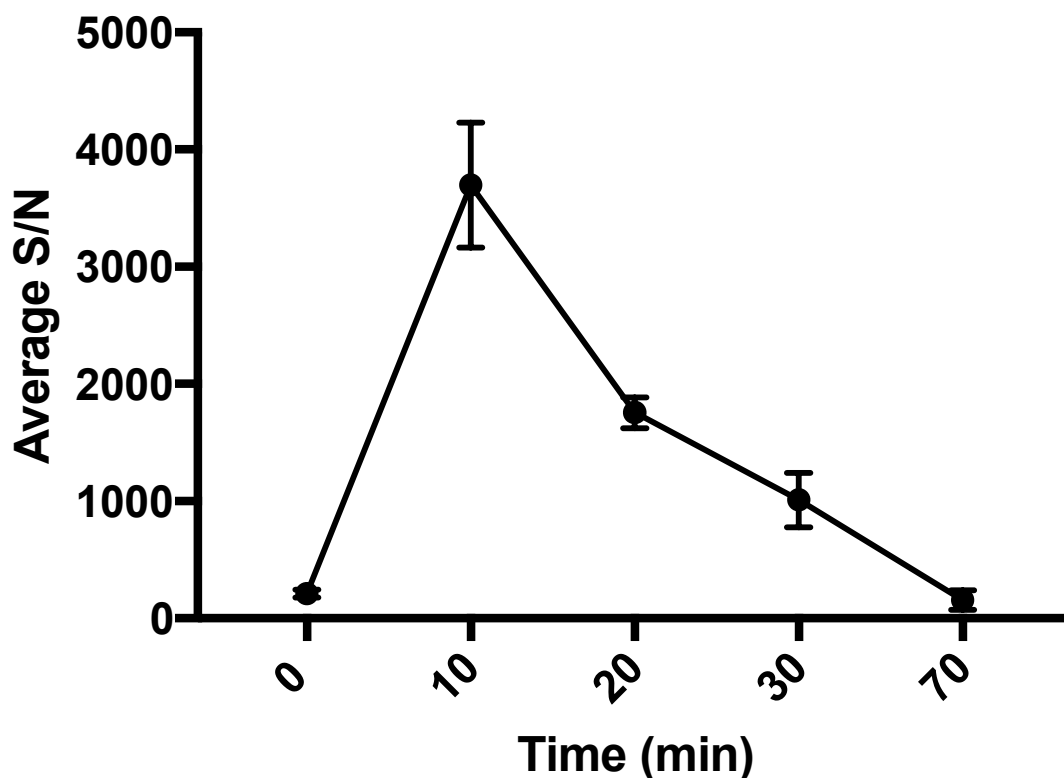


Figure 109: Average SN of nicotine in exhaled breath of a smoker from DSA-ToF analysis using modified sample collection method. Error bars represent one SD , n=3

This direct method removes a number of steps where there was the potential to lose analyte. The exhalation through a straw into the Eppendorf tube initially removes analyte through condensation on the interior of the straw, and through a lack of seal on the tube itself during the exhalation. The suspension requires the opening of the tube, potentially resulting in another loss. The suspension and centrifugation did not guarantee that all the analyte made it into the solution ready, or that the suspension was homogenous when sampling. Direct deposition onto the mesh ensures that as much of the analyte as possible makes it onto the mesh. The suspension method also has another drawback, in that the total amount of analyte exhaled in 15 seconds is divided into three volumes for analysis. In the direct deposition method, the volunteer exhales three separate times, but concentrates the analyte from each, resulting in a higher S/N to noise ratio, and potentially increasing the sensitivity of the technique.

The uptake and elimination curve produced with this method compares directly to that produced by MALDI-ToF and other more sophisticated techniques [206]. Nicotine crosses the blood-brain barrier within just a few minutes of consuming the substance [215], and is therefore likely to cross the lung barrier within the same timeframe. This is represented in the curve (Figure 109), with the peak maxima occurring just 10 minutes after the volunteer consumed nicotine, a level substantially above that of the  $t=0$  minute measurement. The nicotine S/N returned to pre-vape levels after the two-hour period, consistent with the known half-life of nicotine of approximately two hours.

An aliquot of the vape liquid used by the volunteer was also taken and analysed, to assess spectral similarity between compounds found in the liquid and those exhaled after consumption. Studies have shown that vape liquids and their associated vapours contain any number of toxic compounds, including carbonyl compounds, volatile organic compounds, various particulate matter, and heavy metals [216-219]. The major constituent is propylene glycol, which although deemed 'food safe', has not been subject to any long-term safety studies for human consumption when consumed in this manner [217, 220]. The liquid used by the volunteer in this experiment was honeydew flavoured, and was not purchased with nicotine already present, rather it was added in by the volunteer. Thus, any compounds of interest in the mixed liquid may have come from either source. The liquid was analysed neat on the mesh (after heat treatment) and produced a relatively clean spectrum. There was a large nicotine peak (Figure 110), but other compounds produced peaks that were too small to identify with confidence. It is likely that these small molecules at low concentration are related to the flavour and aroma compounds present in the mixture, but this was unable to be confirmed.

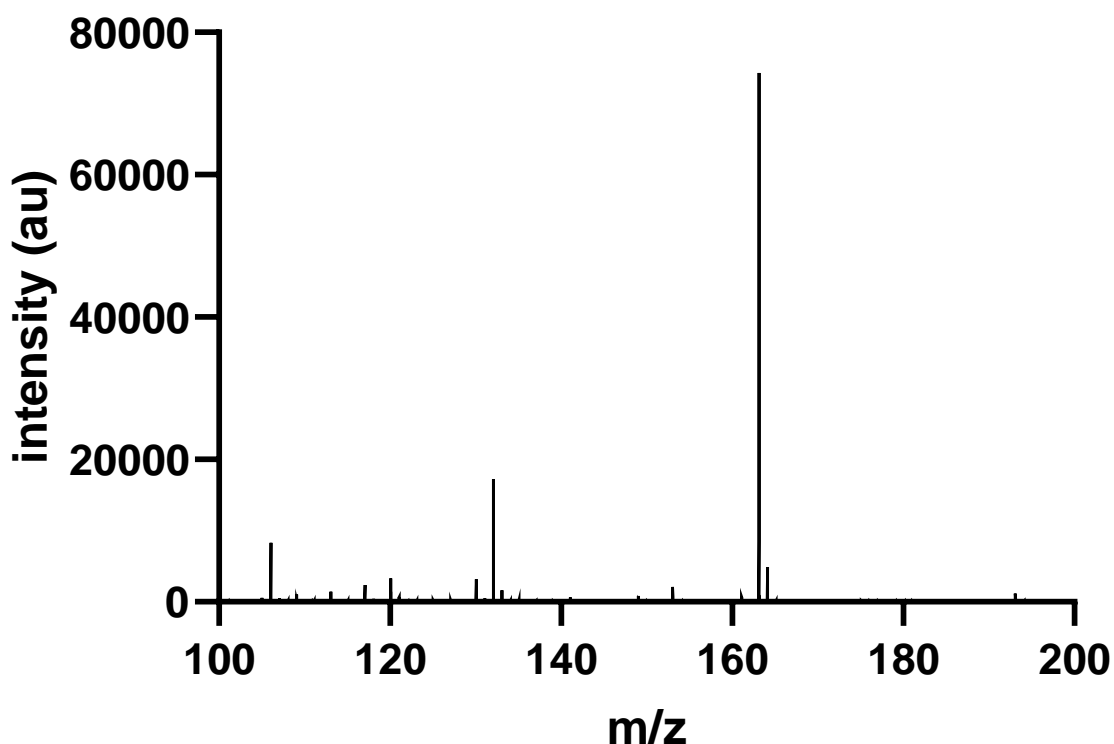


Figure 110: Representative spectrum of neat vape-liquid, provided by the volunteer. A nicotine peak can be seen at  $m/z$  163.

Peaks in breath were not consistent with those seen in the vape liquid, besides the nicotine. Any flavour compounds associated with the ‘honeydew’ flavour were not able to be visualized in the breath or the vape liquid itself. This is not surprising, as studies on the toxic compounds in the vapour produced from e-cigarettes have shown that the levels are much lower than those within the liquid, and far lower when compared to the levels seen in tobacco cigarette smoke [216, 217].

## 5.6 Conclusions

This work demonstrates the utility of the DSA-ToF for the screening of compounds in breath. It details two methods for the sample collection of breath, one modelled from MALDI-ToF work in the detection of nicotine in breath, and one further simplified method.

The first experiment demonstrated the value of DSA-ToF as a broad screening method, with the detection of caffeine & its three major metabolites, and pseudoephedrine within the same sample collection and analysis. Sharp increase in the S/N of these compounds were seen immediately following consumption, with gradual decreases over the two-hour experimental period.

The second experiment demonstrated that the breath collection method developed by Guinan et al. [206] was able to be applied to the detection of nicotine in the breath of an e-cigarette user. Method optimisation showed detection of the nicotine molecular ion for the 'vaping' subject, with no nicotine seen in the breath of the two non-smoking subjects. However, when the method was applied to nicotine detection where there was a delay in suspension, a serious loss of analyte from the sampling process was seen, due to a time delay between sample collection and sample analysis.

The final experiment demonstrated a far simplified method for the direct exhalation onto the DSA-ToF mesh followed by suspension. The time taken for sample collection and analysis was far reduced, without compromising the results. The uptake and elimination curve seen across two hours of sample collection is comparable to that produced using MALDI-ToF, a far more sensitive instrument. Additionally, this also corresponds to the curve known to be produced when nicotine levels in blood plasma are monitored.

This work demonstrates the potential of DSA-ToF, and other ambient ionisation techniques for the detection of drugs and metabolites in breath. DSA-ToF (and other ambient ionisation techniques) are capable of broad, non-targeted analysis to identify a range of compounds and metabolites, as demonstrated by the caffeine detection in this chapter. Further work should be performed to confirm that the method is selective enough to allow confirmation of identification for any parent drugs and metabolites present in the breath. This would allow for application of this method to pharmacokinetics and real time drug monitoring. This chapter has shown this method is capable of detecting a number of drugs and metabolites in one single, rapid and simplified analysis. Screening of breath samples in this way would provide a huge volume of information for diagnoses, drug concentration, and identification where appropriate.

## 6 Towards the combined detection of organic and inorganic gunshot residues

### 6.1 Introduction

One area of interest for the application of ambient ionisation mass spectrometry is the detection of organic gunshot residue (oGSR). GSR refers to the by-products of a firearm discharge and comprises an organic component (oGSR) and an inorganic component (iGSR). Typically, forensic analysis has focussed purely on the iGSR, which is formed from an ammunition's primer. For this type of analysis, the focus is on both the chemical composition of the particle and the morphology, from an individual particle and population perspective. The current gold-standard technique for the detection of iGSR has been Scanning Electron Microscopy coupled with energy dispersive x-ray analysis (SEM-EDS) since the 1980's. International standards from ASTM define the particle types considered most likely to be associated with the discharge of firearm [221]. The standard dictates that particles containing lead, barium and antimony, or lead, barium, calcium, silicon and tin within the same particle are the most probative. Thus far, this has been effectual in the establishment of firearm discharge and the involvement of those with these particles on their person. The same standard also details other particle composition and the related association with the discharge of a firearm, which has led to concern that these other 'less probative' particles may have external, environmental sources, reducing their overall evidentiary value from a forensic perspective.

For this reason, the organic components ejected from a firearm during discharge can also be considered as a valuable source of evidence where firearms are concerned. Moreover, the rise of Pb-free primers will reduce the likelihood of encountering traditional primer residues ('characteristic' PbBaSb particles [221]), and increase the prevalence of GSR particles containing Sb and Al [222]. These elements have non-firearm sources and would therefore be considered of less probative value. The organic components of GSR are due to the propellant or primer, and other compounds added to increase the performance of the ammunition. The list of compounds associated with oGSR is extensive, but is by no means exhaustive, as many reviews have highlighted [223-225]. Although the list of potential target compounds is large, analytes consistently targeted in method development are ethyl centralite (EC), methyl centralite (MC), dinitrotoluenes (DNT), diphenylamine (DPA), and its nitrated derivatives, as well as nitroglycerine (NG) and nitrocellulose (NC) [223].

There has been a multitude of methods evaluated for oGSR detection, from presumptive to confirmatory. At this point in time, there is no 'gold-standard' method for the detection of oGSR, as there is with SEM-EDS for iGSR. Approaches evaluated include colorimetric testing, FTIR spectroscopy, electrochemical detection, ion mobility spectrometry, HPLC and GC, and multiple applications of mass spectrometry, as outlined by Goudsmits et al. [226]. Despite this, there are a number of techniques that show promise, including the use of solid-phase microextraction (SPME) sampling, coupled with GC-MS. This technique is popular with the analysis of volatile organic compounds, which lends itself well to those same compounds present in smokeless powders and firearm discharge residues [227, 228]. The downside to this technique lies in the high temperatures required for GC separations, which have been shown to degrade key components of oGSR (N-NDPA & NG) [229, 230], potentially reducing the overall value of this technique. Other chromatography methods such as LC-MS offer more sensitivity, without the compound degradation seen in GC [231]. The sensitivity offered by these methods allows work to be performed assessing the transfer and activity level questions associated with forensically relevant compounds, allowing for the importance of presence and concentration of oGSR compounds to be interpreted [232]. Despite the strides being made in this research space, chromatographic methods often rely on the destruction of a sample in order to extract, concentrate or digest compounds of interest. This is of concern, as the probative value of GSR evidence should be greatly increased when oGSR and iGSR results are presented in parallel, and the sample preparation techniques employed for the aforementioned methods may destroy or compromise any iGSR present.

The following question forms the basis for the research presented in this chapter: how can iGSR and oGSR be analysed in parallel, without collection of one compromising the other. The difference in chemical composition between the two types of GSR is stark, demonstrated by the difference in collection methods. For iGSR, collection is facilitated by application of an adhesive tape mounted on an aluminium SEM stub, or by a swab wet with solvent. The adhesive tape option has been shown to be more effective for the collection of iGSR particles [233], and allows the transition from collection to testing to be as seamless as possible. Initial efforts to combine the two required the use of multiple sampling platforms, using both the adhesive stub and incorporating a second swabbing step for oGSR [234]. This is problematic, as the collection of one GSR type before the other in this manner has the potential to remove or degrade the other type prior to sampling. That is, swabbing for oGSR may dislodge any iGSR particles, of which there already may be very few. Conversely, the collection of iGSR may remove oGSR compounds, leading to a reduction in recoverable oGSR when swabbing. More recent methods have sought to circumvent this issue by

developing a singular sampling device, or by incorporating oGSR testing into already established procedures [233, 235, 236]. Some methods have involved the removal of the organic components from the surface of the stub using solvent extractions [235], or the detection of these analytes on the surface of the stub itself, using non-destructive beam techniques [231, 236]. One such UHPLC-MS method utilised a solvent extraction method that sonicated the pin stub in a solvent, and filtered out the inorganic particles suspended in solution [233]. Modified carbon adhesive stubs for simultaneous collection of oGSR and iGSR have been shown to outperform swabbing in the recovery of oGSR, while also decreasing the interference from extraneous organic components typically encountered in these swabbing methods [235]. However, the use of independent sampling sectors on the stub in this method reduces the total amount of both iGSR and oGSR able to be collected, by about half. Alternate analysis methods propose analysing the two types of GSR within the same run. A study in 2014 showed separation of 11 organic and 10 inorganic GSR compounds using capillary electrophoresis [237]. This method lacked sensitivity, and required significant sample preparation, making it unsuitable for the application to real shooting samples. Earlier, cyclic and square wave voltammetry had been shown to concurrently detect antimony, lead, DN & NG, or antimony, lead, zinc & DPA. The limitations of this work lie within the requirement to use clean standards, with no effort to determine whether the technique is suitable for use with samples that would typically be obtained for forensic analysis [238]. Furthermore, both of these methods require the sample to be dissolved and gives only results for the bulk properties of the resulting solution. This eliminates the nuance of individual particle morphology and composition and opens the methods for criticism when considering any external sources of these elements and compounds.

While these proposed methods show some promise, the widespread acceptance of SEM-EDS as the preferred iGSR analysis technique means that it is preferable to integrate any oGSR method into this workflow. This would allow analysts to maintain the depth of knowledge SEM-EDS offers, while adding an extra layer of information in the form of oGSR. This combination is also the most likely to be adopted by forensic practitioners, which should be a high priority when designing and testing parallel detection methods. Non-chromatographic based techniques are ideal for this space, enabling theoretically non-destructive detection of oGSR components. One such technique is the use of micro-Raman spectroscopy with laser-ablation Inductively Coupled Plasma Mass Spectrometry (ICP-MS), which was able to complete testing of iGSR and oGSR from a single sampling platform within two hours [236]. Micro-Raman mapping has also been used to demonstrate the possibility of an automated mapping program for the detection of oGSR particles, in a manner similar to the particle mapping used for iGSR [239]. Despite the analytical

successes, these two methods have practical downsides. The use of laser ablation ICP-MS required the tuning of the laser, as it was found to burn through the carbon adhesive on the surface of the stub, calling into question the 'non-destructiveness' of this method. The micro-Raman mapping software was not tested on actual samples, which doesn't bode well for its sensitivity in a forensic setting, despite the detection of appropriately sized particles (3.4 μm) [239]. Vibrational spectroscopy may simply not be sensitive enough to detect the extremely low quantities of oGSR compounds typically encountered in a casework situation, particularly for more minor components of formulations.

In recent years, colorimetric testing has been tested as a feasible alternative to more comprehensive examination of oGSR. In 2018, a test involving the use of sodium borohydride to screen for common oGSR compounds such as DPA and mono- and poly-nitro diphenylamines was developed [240]. This colour change reaction proved to be accurate and sensitive in the detection of these compounds, under laboratory conditions. In order to determine the effects of this test on iGSR components, EDS was performed on an substitute for iGSR, before and after exposure to the sodium borohydride reagent. No degradation of the composition was observed, but particle morphology was not considered in this experiment, nor was the suitability of this test in the field, on the surface of carbon adhesive stubs. Without thorough validation of these methods under 'field' and 'casework' conditions, it is difficult to get a true sense of the utility for forensic casework.

Ideally, as a goal for the research described in this thesis, a method was to be developed for oGSR analysis that combined the specificity and sensitivity of mass spectrometry with the speed and ease of colorimetric testing. One solution to this is the use of ambient ionisation mass spectrometry, reaping the specificity benefits of MS analysis without the arduous and destructive sample preparation required for chromatography. There has already been movement in this area, with a 2017 study demonstrating the detection of MC, EC, DPA & NC using DART [221]. These compounds were detected from cartridge cases and from SEM stub extracts used to sample a cotton surface, showing that the method has the potential to be integrated into current processing. The authors even went so far as to demonstrate that an iGSR particle could be identified on the surface of the stub following the extraction procedure. What was not investigated though, was the overall effect of solvent extractions on the number and positioning of any iGSR particles present on the surface of the stub at the time of extraction, nor were they able to show the effects of SEM-EDS sample treatment on the amount of recoverable oGSR [221]. For this reason, this cannot be considered as a method fully developed for the seamless integration into current iGSR sampling and

analysis techniques. DESI-MS has also been investigated as a method for oGSR detection directly from stubs. Morelato et al. [28] demonstrate the detection of MC, EC and DPA from adhesive GSR stubs spiked with standard solutions of those compounds. This work also analysed the neat propellant powders and was able to detect EC, MC and DPA in most of these samples. When it came to detecting the same compounds from stubs used to collect GSR after shooting only EC was able to be detected, despite the successful detection in smokeless powders harvested from the same ammunition as those being discharged [28]. Although this method was highly appropriate for direct integration into the current GSR methods (same sampling device), the paper does not demonstrate successful application to 'case-work' samples with the same success as the neat propellant or spiked stubs.

Ambient ionisation is rich enough in data that chemometrics have also been used to correctly identify and group smokeless powders based on oGSR associated compounds [142]. Although this has also not been demonstrated on stubs themselves, and under casework conditions, identification type assessment of these groups of compounds represents an important step forward in this space. The idea that smokeless powders, and potentially oGSR residues, could be analysed in this way and produce more than just an action-type association is huge, demonstrating the power of ambient mass spectrometry in this field. In addition, ambient ionisation MS gives a rapid snapshot of the bulk material, allowing for non-targeted screening of many compounds. This is beneficial in the analysis of oGSR, as the list of compounds that may be present is large and ever changing, based on manufacturer formulations and purpose.

This chapter details the development of an oGSR extraction and detection method that utilises the current iGSR sampling platforms (carbon adhesive pin stubs). The method developed within this chapter is shown to integrate into current SEM-EDS sampling and analysis, without disturbing or removing iGSR particles, delivering a comprehensive and data-rich set of results. The work herein also demonstrates the applicability of this method for use in casework, through the incorporation of real samples into the validation process.

## **6.2 Materials and methods**

### **6.2.1 Standards and solvents**

Reference standards chosen for validation of the extraction and analysis method were ethyl centralite, methyl centralite (as an internal standard), a mixed GSR surveillance standard containing various oGSR associated compounds as shown in Table 1 (Accustandard, New Haven, CT). EC was added by the analyst to a concentration of 100µg/mL. Blank stubs (Tri-Tech Forensics, North Caroline, USA) were used and spiked with the mixed GSR standard using an Eppendorf air-displacement pipette (Eppendorf,

Hamburg, Germany). Solvents evaluated were acetonitrile, methanol, ethanol and a mixture of methanol, acetone and acetonitrile (Sigma Aldrich, St Louis, MO).

Table 35: oGSR associated compounds contained in Accustandard GSR surveillance standard (Accustandard, New Haven, CT)

Analyte	CAS Number	Target Concentration
Dimethyl phthalate	131-11-3	200µg/mL
2,4'-Dinitrodiphenylamine	612-36-2	50µg/mL
2,4-Dinitrodiphenylamine	961-68-2	50µg/mL
2-Nitrodiphenylamine	119-75-5	50µg/mL
4-Nitrodiphenylamine	836-30-6	50µg/mL
2,2'-Dinitrodiphenylamine	18264-71-6	50µg/mL
4,4'-Dinitrodiphenylamine	1821-27-8	50µg/mL
Diphenylamine	122-39-4	200µg/mL
N-Nitrosodiphenylamine	86-30-6	75µg/mL

### 6.2.2 Sample collection

Samples were collected from the hands of a shooter after separately firing both 0.40 calibre and 0.22 calibre ammunitions. A sample of 0.22LR Winchester XTR ammunition (Batch No. 1DTM62) was discharged from a Smith and Wesson Model 63 revolver. The shooter thoroughly washed their hands, and a blank sample was collected using a single GSR stub to sample from both hands. Six rounds were discharged into a bullet recovery tank., Immediately following, the hands of the shooter were sampled using GSR stubs, first from the right hand, then the left. Two stubs were used for each hand. The samples were labelled RH1 and RH2, and LH1 and LH2 respectively. This firing-collection process was then repeated two more times, totalling 18 rounds of ammunition discharged and 12 samples collected.

The shooter then thoroughly washed and dried their hands, before a second blank sample was collected. Six rounds of 0.40 S&W Federal Premium Law Enforcement ammunition (Batch No. V42Z458) were discharged from a 0.40 calibre Smith and Wesson M&P (Military and Police) semi-automatic pistol into a bullet recovery tank. The sampling protocol and replicate procedure was then repeated as above, until 18 rounds of ammunition had been discharged, and 12 samples collected.

Samples were stored at 4°C until analysis by either technique, and between analysis types. Extracts were analysed within two hours of extraction, with analysis consuming all extract and no further storage being required.

### 6.2.3 Equipment

Inorganic GSR analysis was conducted using a FEI Inspect F50 SEM system with EDAX elemental analysis capability. Particle identification was performed using GSR Magnum automated particle analysis software. The brightness and contrast settings of the particle analysis system were calibrated using a Au/Nb/Ge/Si/C calibration standard (Eastern Analytical). A Synthetic Particle Standard (PLANO W. Plannet GmbH, Wetzlar, Germany, SPS-5P-2a-X02-Y03) was analysed at the start and end of each run as a positive control. Further SEM operating and analysis parameters can be seen in Table 36.

Table 36: Set-up and Operating Conditions for SEM-EDS analysis

<b>Parameter</b>	<b>Setting</b>
Accelerating Voltage	25kV
Working Distance	10mm
Emission Current	~110µA
Magnification	486x
Min. Particle Size	0.5µm
Dwell Time	10µs

DSA-ToF MS analysis was performed as per the protocol describe in the materials and methods chapter, with no changes to instrument parameters made.

### 6.2.4 Data analysis

Particles were classified as “characteristic” of firearms origin or “consistent” with firearms origin in accordance with ASTM E1588-17 [221].

Following the automated system’s classification, all GSR classifications were verified by an operator prior to further data treatment. Multiple hits on the same particles were excluded from further particle counts, and exemplar spectra and particle images were collected where appropriate.

Mass spectrometry data analysis was performed on ToF Driver software for all calibration (Perkin Elmer), with image exportation taking place using mMass open source software. All accurate mass data were obtained after lockmass calibration between m/z 121 and 322 calibration peaks and after manual averaging over peaks in TIC by the analyst.

### 6.3 Evaluation of DSA -ToF for detection of GSR compounds

With the end application in mind, four compounds were chosen for validation of the solvent extraction and analysis method. The four compounds were ethyl centralite (EC), methyl centralite (MC), diphenylamine (DPA) and N-nitrosodiphenylamine (N-NDPA). These compounds were chosen as their presence is indicative of firearm discharge, particularly the presence of N-NDPA, which forms under the conditions of ammunition storage from the reaction between nitrocellulose compounds and DPA present within the propellant formulations [241]. The initial stage of method development was to determine if the DSA-ToF could detect these compounds, via accurate mass. As detailed in other chapters, the details of the DSA-ToF acquisition method remain largely the same, as there are limited options for altering the delivery of the ions to the mass spectrometer, and accurate mass identification will benefit from the lack of fragmentation for increased amounts of molecular ion. The mesh was cleaned according to Perkin Elmer's recommended heat treatment protocol, with 30 seconds in the plasma stream prior to addition of the analyte. All four of the analytes of interest were able to be detected, as well as deuterated DPA and N-NDPA. The accurate mass ppm error is shown in Table 37 below, for six replicates.

Table 37: Accurate mass error (ppm) for targeted oGSR compounds (n=6)

<b>Compound</b>	<b>Mass added to mesh (ng)</b>	<b>Molecular ion mass (amu)</b>	<b>Accurate mass ppm error (n=6)</b>
Ethyl Centralite (1ug/mL)	5	269.1654	-2.80
Methyl Centralite (1ug/mL)	5	241.1341	-2.67
Diphenylamine (DPA) (10ug/mL)	50	170.0970	2.33
N-Nitrosodiphenylamine (N-NDPA) (10ug/mL)	50	199.0871	1.19

These results demonstrate the sensitivity of DSA-ToF for oGSR analysis, with very low amounts of these compounds being successfully detected. There is a consensus within the community that the amount of oGSR on the hands of someone who has recently discharged a firearm is below 1ug [235, 242], which falls within the range of the proposed limits of this analysis technique.

## 6.4 Quantification of EC

Throughout this thesis, the ability of the DSA-ToF to quantify analytes has been demonstrated, but with reservations. Although there is the potential for DSA-ToF to quantify compounds with the presence of an internal standard, inter- and intra-day variation is sufficient to cause significant uncertainty. Nonetheless, the quantification of EC was investigated, as other forms of ambient mass spectrometry have been shown to provide sufficient data to classify smokeless powder residues by ammunition type and manufacturer [142].

Quantification of EC was performed using MC as the internal standard. The working range was 0-200  $\mu\text{g/mL}$ , with solution concentrations of 10, 20, 50, 100, 120, 150 & 200  $\text{ng/mL}$  and 1  $\text{ng}$  of MC deposited onto the dried solvent spot prior to re-wetting. DSA settings were consistent with those listed in the materials and methods chapter, and analysis was performed on instrument-treated DSA mesh.

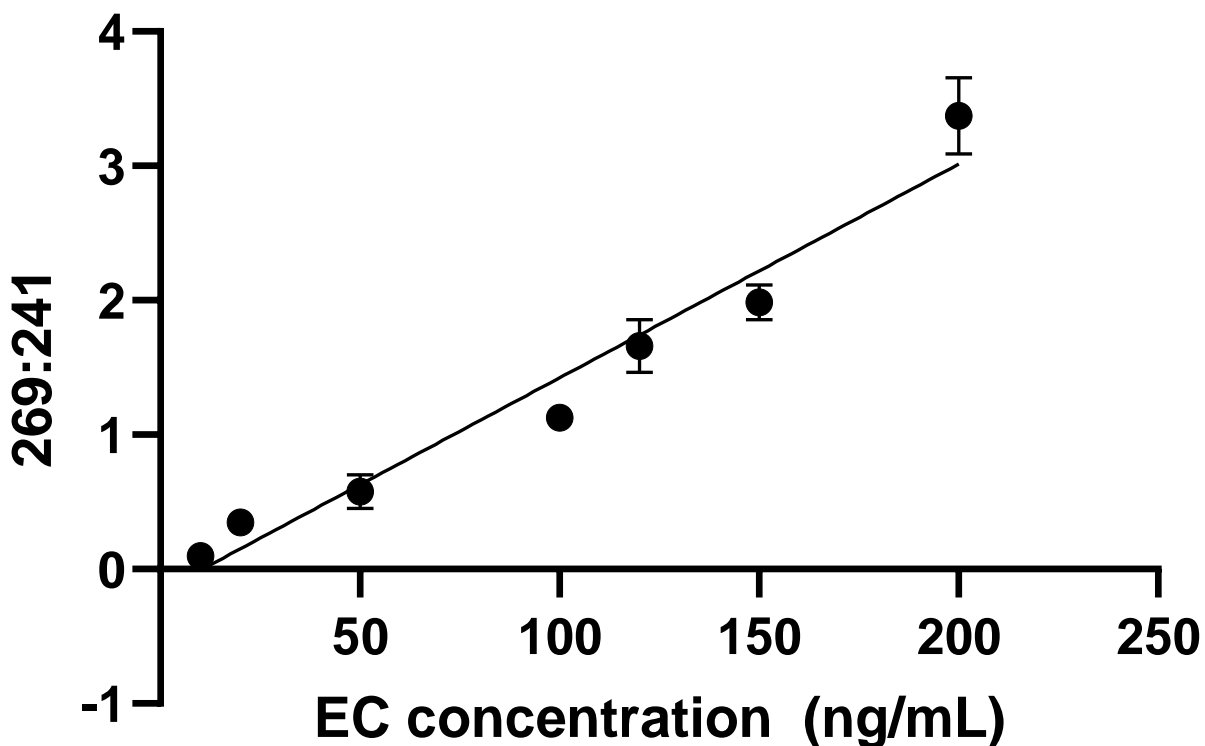


Figure 111: Calibration curve for Ethyl Centralite, using Methyl Centralite as the internal standard. Response is given as the ratio between the molecular ion peaks of EC and MC,  $n=3$  & error bars are 1SD ( $R^2= 0.9577$ ).

This work demonstrates that the detection and quantification of EC is possible across a wide working range, and with little variation from that linear trend when MC is used as the internal standard. As with all quantification performed on the DSA-ToF, the use of the area or height alone as a measure of response is not appropriate. For this work, EC and MC are close enough in structure and should therefore be matrix matched. Where non-matched internal standards are used (as is true in this case) it is important that the chosen ISTD is not present in the broader sample community. In this case, MC is not common in ammunition but should be used with caution in case MC was ever found to be present in a GSR sample with EC. This would not stop EC being detected, but if MC was present in the sample the concentration of EC would be underestimated, and the any MC present would be mistakenly attributed to the ISTD than the sample. The limits of detection and quantification as determined from this experiment were 11.6ng/mL and 13.7ng/mL respectively, which corresponds to 2.3ng and 2.7ng when the volume of analyte solution applied is considered. These results are promising, as despite the fact that the amount of oGSR deposited onto the hands of someone discharging a firearm is in the  $\mu\text{g}$  range, it is highly likely that these compounds would disappear rapidly, either through use of the hands (or hand-washing) or through vaporisation of these volatile organic compounds. As demonstrated in previous chapters, the sensitivity of the instrument varies day to day, and this will need to be taken into account when applying this method to samples, if quantification is required.

## 6.5 Extraction and Analysis

With the DSA-ToF's ability to detect the compounds of interest established, the next stage of the process was the development of a method for the extraction of these compounds from the surface of the GSR stubs. Two approaches were initially considered: a solvent extraction, and a physical transfer of components from the stubs to the stainless-steel mesh. The stub was spiked with 10ng of EC, and allowed to evaporate to dryness. Analyte concentration was strongest in the middle of the stub, as this was where the spiking solution was placed. In an evidentiary situation, the concentration of the analytes of interest is likely to be distributed across the entire surface of the stub, whether homogenously or otherwise. This was taken into account when developing the method for the extraction, to ensure that that maximum amount of analyte was removed from the stub no matter what the distribution was.

Initially, the physical transfer was considered as the sample holder is composed of 13 round sample areas in which a continuous piece of stainless-steel mesh is placed for sample deposition. A physical transfer would have been quick, solvent-free and simple. However, the diameter of the GSR stubs (12.5mm)

exceeded that of the sample holder (9.5mm). Nonetheless, an attempt was made to facilitate the physical transfer of EC to the mesh by cutting the mesh into small squares and pressing these to the surface of a blank and a spiked stub. These were analysed by re-wetting with 10 $\mu$ L of water and the addition of 1ng MC to determine the amount of EC transferred. At the same time, solvent extractions were performed using methanol (MeOH), Ethanol (EtOH) and Acetonitrile (AcCN). An arbitrary volume of solvent (50 $\mu$ L) was applied to the surface of the spiked and blank stubs, as the solvent volume had yet to be optimised. After 10 second of interaction with the surface of the stub, the solvent was removed by tipping the stub slightly and allowing it to pool at one edge of the surface. An auto-pipette was used to remove the solvent remaining and transfer it to an Eppendorf tube to await analysis. As volatile organic solvents were being used for the extraction, the volume remaining after the elapsed interaction time was significantly lower than the original 50 $\mu$ L pipetted onto the surface. This is also due to the recovery method, which cannot possibly remove all solvent from the surface of the stub. For this reason also, the stubs were allowed to dry completely before their lids were replaced and returned to storage.

Analysis of these extracts was performed by pipetting 4 $\mu$ L of the solvent onto the surface of the mesh and allowing evaporation to dryness. Once the solvent had evaporated, 10 $\mu$ L of water was placed over the area where the solvent had been, and 1ng of internal standard (MC) was added to allow for approximation of recovery. All solvent extractions were performed in triplicate and analysed in triplicate where solvent volume allowed. The physical transfer and analysis was performed only once for the blank and spiked stubs.

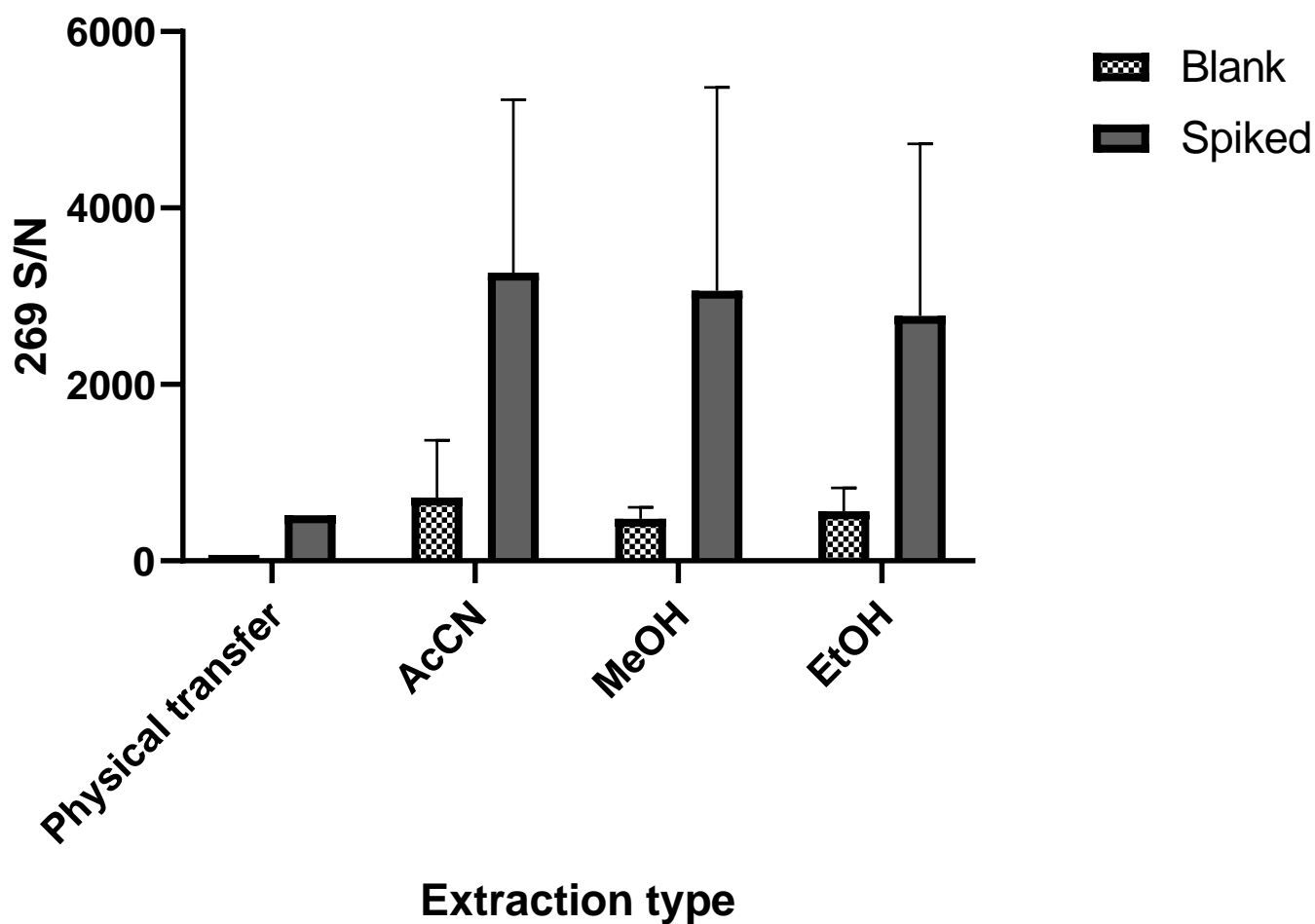


Figure 112: Comparison of extraction solvents and methods for EC spiked onto an adhesive GSR stub

For the purposes of comparing the solvents (and methods) to one another, the EC molecular ion ( $m/z$  269.16538) S/N was compared. It is clear from the graph above that the physical transfer cannot compare to a solvent extraction method. This was expected, and not entirely unwelcome, as the method itself would have been more difficult to execute for large sample numbers than a solvent extraction. It is also noteworthy that there is a clear difference in S/N for the blank and spiked samples. This indicates that the extraction method is removing EC from the stub. The responses recorded for the blank stubs are likely due to an isobaric interference, unable to be differentiated from the EC peak. The error bars do indicate that there is a large amount of variability in the amount removed, and this is not unexpected. With a method such as this, where more than half of the solvent is not recovered from the surface of the stub, it stands to reason that some EC would remain on the stub as well, leading to inconsistent recoveries. Regardless of

this variability, the percentage recovery was estimated using calibration curves generated on the day of analysis. Although the signal to noise for the spiked samples did not differ much between the solvent types, the amount recovered was significantly different and showed that EtOH and MeOH outperformed AcCN substantially (Table 38).

Table 38: Comparison of solvent type for Ethyl Centralite recoveries from spiked SEM stub surface

<b>Solvent type</b>	<b>EC concentration detected (ng/mL)</b>	<b>Amount detected (ng)</b>	<b>% recovery</b>
Acetonitrile	108	5	53
Methanol	223	11	111
Ethanol	225	11	111

As there was no discernible difference between the EtOH and MeOH extractions, the rest of the method development continued with the use of MeOH as the solvent, as this was the solvent the standards were made up in. The calculated recoveries of over 100% all but confirm the presence of an isobaric interference for EC, contributing some of the signal response for that peak.

MeOH was used throughout the method development, until a literature article highlighted the benefits of a mixed solvent approach [243], and this was trialled as an alternative against MeOH and AcCN. This mixed solvent was made up of 40%:40%:20% MeOH: Acetone: AcCN (referred to as 2:2:1 from here), and outperformed MeOH and AcCN alone when compared for the recovery of EC from the surface of spiked stubs (Figure 113). These results were obtained after the remainder of the method was finalised, and as such the solvents were evaluated using the optimised solvent volumes, interaction times and analysis volumes. When considering the remainder of the method development discussed in this chapter, it is worthwhile keeping in mind that these experiments were conducted using MeOH as the solvent, and not the mixed solvent. Even though the mixed solvent was shown to offer benefits there was not time available to repeat experiments using the mixed solvent.

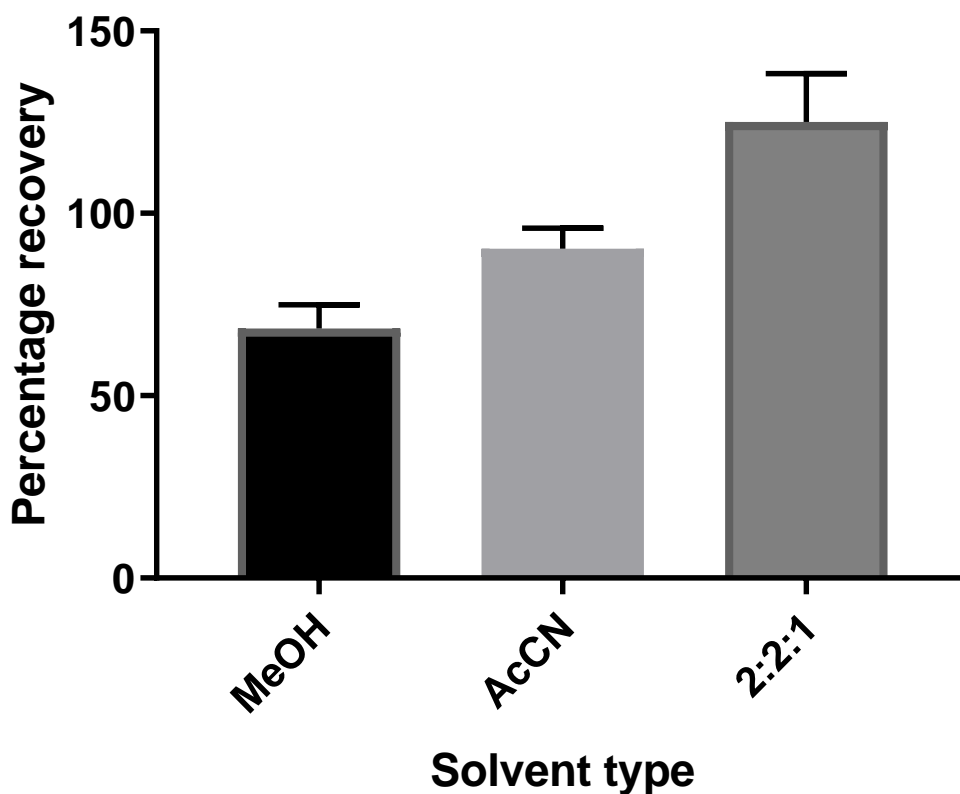


Figure 113: 50 $\mu$ L solvent recovery (%) comparison for EC from adhesive GSR stubs

Following on from this solvent optimisation, the volume of solvent was investigated. In order to maximise the amount of analyte extracted from the surface of the stub, the volume of solvent needed to cover the entire surface of the stub for all (if not most) of the interaction time. For the purposes of this experiment, the interaction time was kept to 10 seconds, as this parameter was yet to be optimised. Volumes of 10, 50, 100 and 150 $\mu$ L were considered, as 50 $\mu$ L had already been shown to extract detectable amounts of analyte. A reduction in the volume may have resulted in more concentrated analyte extraction, whereas a larger volume may have diluted the analyte, but ultimately increased the extraction recovery through a reduction in evaporation.

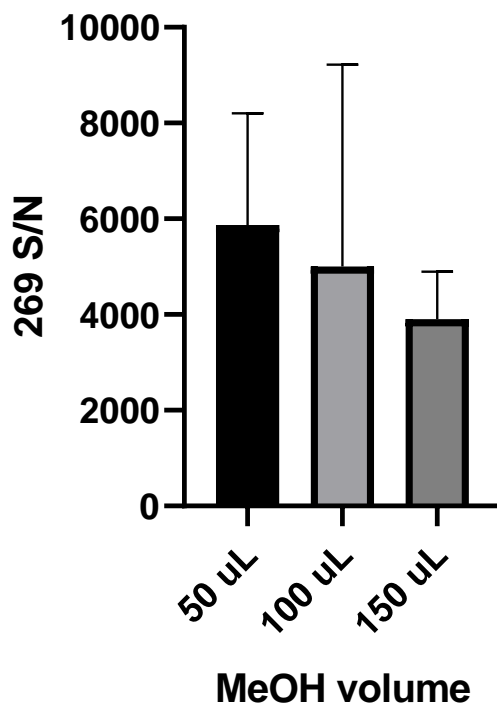


Figure 114: Comparison of MeOH volume for extraction of EC from GSR stubs

Ultimately, 10 $\mu$ L was deemed unsuitable due to a low recovery volume. The solvent evaporated significantly in the time spent interacting with the surface of the stub, resulting in such a low volume of solvent being recovered that analysis was not possible. Signal to noise for the 100 $\mu$ L extraction was reduced through over-dilution and was also deemed unsuitable (Figure 114). Finally, the 150 $\mu$ L volume was also considered not fit-for-purpose due to decreased S/N values, although this volume showed the most consistency. The 100% recovery for use of 50 $\mu$ L solvent (Figure 113, Table 38) suggests that this volume of solvent is sufficient to remove all (if not most) of the analyte on the surface, and this is not improved with a higher volume of solvent. Thus, all further experimentation was performed with 50 $\mu$ L solvent volume, which covers the surface of the stub comfortably, allows for three replicate measurements, and extracts the greatest amount of analyte.

Once the ability to extract EC from the surface of stubs was established, and a method optimised, this method was applied to stubs spiked with the mixed oGSR standard. Stubs were spiked with sufficient GSR surveillance standard for compound deposition amounts to be in the range of 0.0375ng-1ng (Table 39).

Table 39: Deposition amounts (ng) for oGSR associated compounds in mixed GSR surveillance standard

<b>Compound name</b>	<b>Amount deposited onto surface of stub (ng)</b>
Dimethyl phthalate	1
2,4'-Dinitrodiphenylamine	0.25
2,4-Dinitrodiphenylamine	0.25
2-Nitrodiphenylamine	0.25
4-Nitrodiphenylamine	0.25
2,2'-Dinitrodiphenylamine	0.25
4,4'-Dinitrodiphenylamine	0.25
Diphenylamine	1
N-Nitrosodiphenylamine	0.0375
Ethyl Centralite	0.5

Although the deposited amounts are low, the instrument has been demonstrated to reliably detect very low amounts of these compounds when this mixed standard was initially tested. This experiment sought to mimic the sub-microgram amounts of oGSR expected to be encountered on a person following the discharge of a firearm [235, 242]. The spectra produced showed detection of DPA (m/z 170), dimethyl phthalate (m/z 195), EC (m/z 269), but not N-NDPA (m/z 199) (Figure 115).

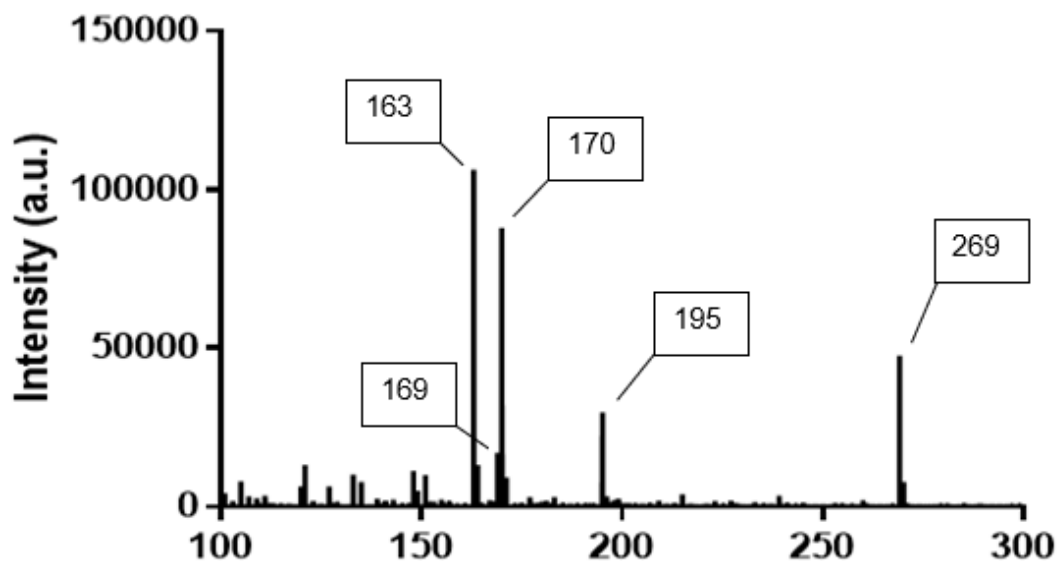


Figure 115: Representative spectra for 2:2:1 solvent recovery of mixed GSR surveillance standard from surface of SEM stub

Although all the other oGSR standards were detected as their protonated molecular ions as expected, N-NDPA yielded a peak at  $m/z$  169 rather than 199 under these conditions. N-NDPA is prone to forming radical fragments during heating or ionisation [244]. Therefore the peak at  $m/z$  169 most likely arises from N-NDPA as a result of homolysis of the N-N bond, which forms the diphenylamidogen radical that then becomes protonated (Figure 116).

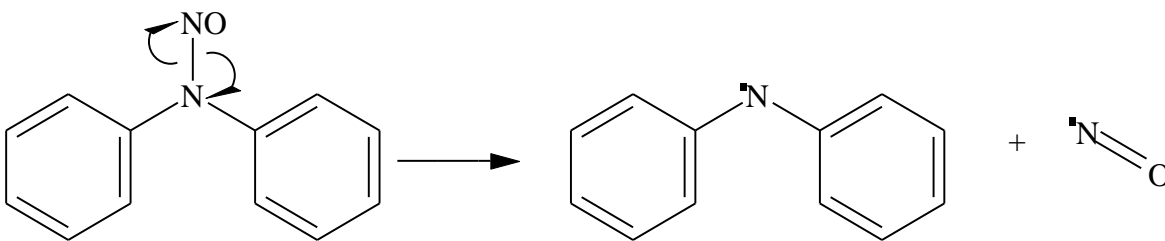


Figure 116: Reaction scheme for decomposition of N-NDPA (left) to diphenylamidogen (right)

Therefore, although the N-NDPA molecular ion cannot be detected under these conditions, N-NDPA can nevertheless be reliably detected and differentiated from DPA. N-NDPA is highly indicative of smokeless powder, as it forms when the stabiliser DPA scavenges nitric oxides released through the degradation of nitrate ester propellants in storage. The ratio of DPA/N-NDPA has therefore found use in the estimation of

propellant age [140], although it is not known whether this ratio is translated in a predictable manner during ambient ionisation.

Finally, to assess the suitability of this method to the analysis of stubs used to collect GSR from shooters, a number of extracts from stubs provided by research group members who had carried out test firings were analysed. These stubs were analysed previously using SEM-EDS analysis of iGSR particles from varying ammunition types and had been sitting in ambient conditions for at least one year. These extractions predated the discovery of the mixed solvent's superior extracting properties, and as such were performed using MeOH. Initially, it was thought that the elapsed time between sampling and extraction, as well as the exposure to the SEM vacuum, would have significantly reduced the amount of EC on the surface of the stub. Happily, the analysis not only showed detection of EC, but also showed that these ammunition types were consistent amongst replicates and stubbing replicates, but may be dissimilar between ammunition types (Figure 117) which is to be expected as smokeless powder compositions vary between ammunition manufacturers and sometime within types from the same manufacturer.

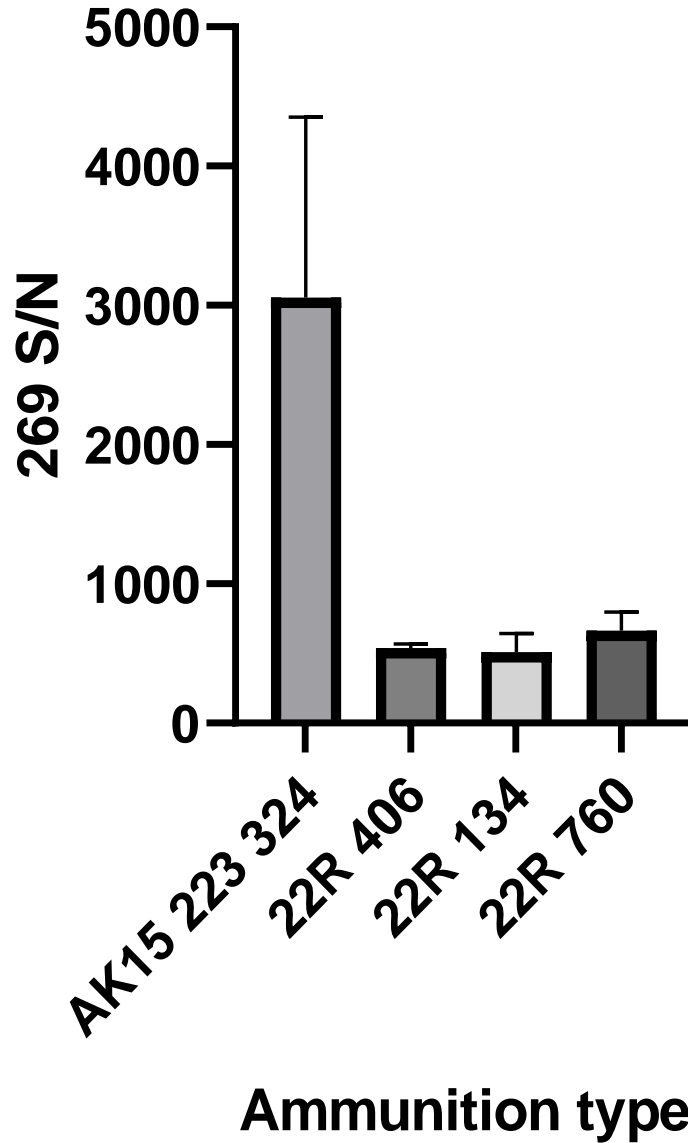


Figure 117: Comparison of EC S/N for aged, field used stubs using MeOH extraction method

The AK sample shows the detection of EC very convincingly, however the consistently low response for the other three ammunition types may not be EC detected, but be a product of the isobaric interference seen in the earlier experiments. Regardless of the origin of the S/N response for the three 22R samples, the detection of EC from the AK sample indicates that detection of these volatile oGSR compounds may be possible with long time delays between sampling and analysis. Whether the 22R response is an artefact of an interference or a truly low EC amount, the implication is that ammunition manufacturers may be

discriminated based on their differing oGSR marker compositions (if known), as other work has shown that it is possible to differentiate between smokeless powder samples originating from different sources [142]. Combining this with iGSR evidence, which has also demonstrated the ability to differentiate between ammunition manufacturers [245] would vastly increase the probative value of GSR evidence.

Following on from these unexpected results, a stability study for EC on the surface of GSR stubs was performed. Stubs were spiked with 10ng of EC, and were stored, in their tubes, in a cardboard box at room temperature. Blank stubs were also stored with the spiked stubs. Extractions of the spiked and blank stubs were performed on days 0, 1, 7 & 30 to determine if there was any loss of EC from the surface of the spiked stubs. This experiment was also for the purpose of determining isobaric interferences that may interfere with the detection or quantification of EC. On each testing day, samples were removed from storage and extracted using MeOH (this experiment also pre-dates the use of the mixed solvent) and analysed with 1ng of MC for semi-quantitation. It was hypothesised that there would be a reduction in the amount of EC present on the stubs. However, based on the ability to detect EC from year old stubs stored at room temperature (Figure 117), the loss was not expected to render EC un-detectable. Additionally, when the final day of testing was reached, the instrument was suffering heavily from contamination of the nitrogen supply. This had a detrimental impact on the results obtained on this day. For this reason, the 30 day data was discarded. Taking into account the trend without the 30 day data, the amount of EC recovered from the initial spike to the one week point did not change (Figure 118).

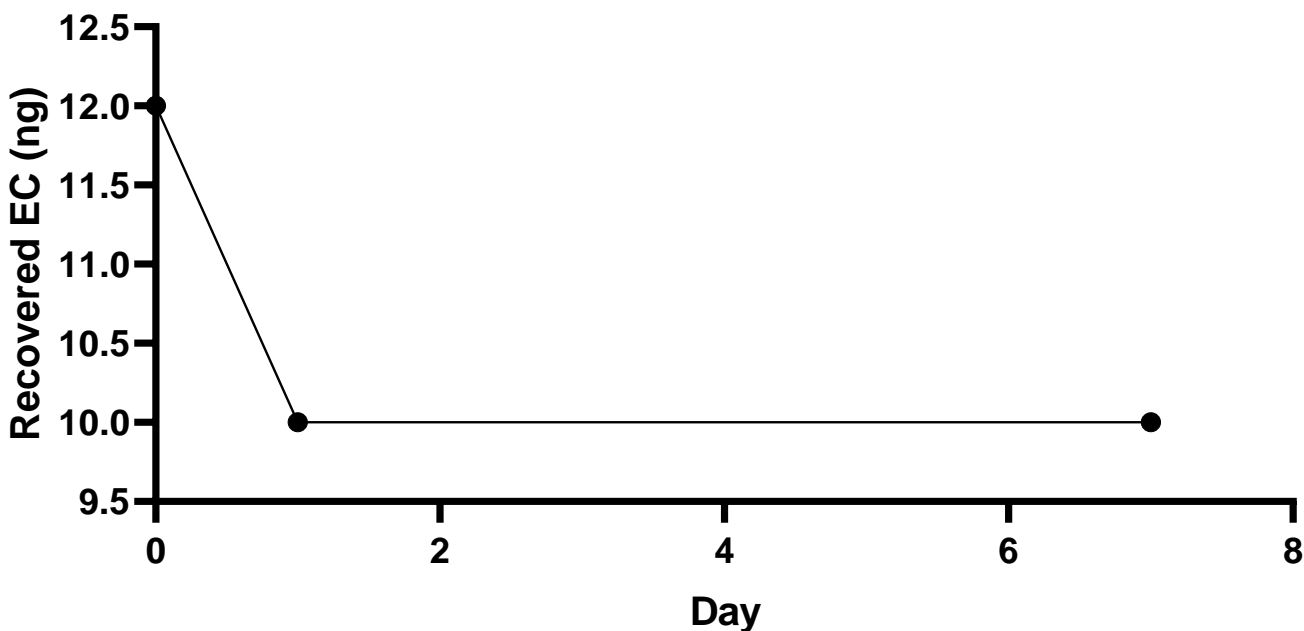


Figure 118: Recovered EC (ng) across seven-day period for GSR stubs stored at room temperature

It would appear that EC was only detected on day zero, with consistent low values on days one and seven being due to the isobaric interference discussed numerous times in this chapter. Although calibration curves were constructed on the day of analysis, the ionisation potential of the instrument on the day of analysis may have impacted the final recovered amounts of EC being presented. The optimal way to perform this analysis would have been to extract all solutions and analyse on the same day, which may have revealed a trend.

As it is, the previous experiment showed that EC peak was still detectable after being stored at room temperature for approximately one year. This qualitatively demonstrates that storing GSR stubs at room temperature for may still allow for oGSR detection, although this is highly dependent on how much was present on the stub initially. To ensure that there was minimal loss of oGSR for the remaining experiments, all samples were stored at 4°C as soon as practicable and were only removed from refrigeration for analysis.

## 6.6 SEM-EDS impacts on solvent recovery - organic GSR compound analysis

In order to finalise the method optimisation, samples from test firings were required to determine whether SEM-EDS or solvent extraction would be the best first step. Essentially, an investigation was carried out to

determine whether there is movement or loss of iGSR if solvent extraction was carried out first, and whether there is loss of oGSR from the surface of the stub if SEM-EDS is carried out first. Additionally, it was important to determine which part of the SEM process would be more detrimental to the recovery of oGSR from the surface of the stub, the EDS beam, or the vacuum.

The samples collected were designated RH1, RH2, LH1 & LH2, where LH is equivalent to 'left-hand' and RH is equivalent to 'right-hand'. The number following refers to the order in which the sample was taken. So, RH1 refers to the first stub taken from the right-hand of the volunteer at each firing event. For each calibre of ammunition one full set of RH1, RH2, LH1 & LH2 stubs were used for the following analyses. LH1 samples underwent solvent extraction and DSA-ToF analysis one day after the sampling had taken place to ensure that the maximum levels of recoverable oGSR were available. LH2 samples were analysed one month after receipt in the same manner as the LH1 samples. These LH2 samples were used to determine loss of oGSR over the period of storage. RH1 samples were extracted and analysed after exposure to the SEM vacuum, but not the electron beam. Finally, the RH2 samples were extracted and analysed following exposure to the SEM vacuum and electron beam. This was performed for both types of ammunition fired, leading to a total of 8 samples being tested.

DSA-ToF analysis failed to detect the three targeted compounds (MC, EC, and DPA) on any of the stubs and for both the .22 calibre and .40 calibre ammunition. Peaks in the areas expected were not able to be positively identified using accurate mass, as the calculated ppm error values were 200 or more. The DSA-ToF had demonstrated its sensitivity for the analysis of these compounds, and the samples being analysed were a 'best-case scenario', wherein the shooter had been swabbed immediately after an extended firing event. It was therefore deemed unlikely that the targeted compounds were present but not detectable. Rather, the formulations of the primer and propellant in the ammunitions used were not known, and it seemed possible that the compounds of interest simply were not in the formulations in the first place.

A representative spectrum acquired from a solvent extract of the stub used to collect residue from firing .40 calibre ammunition is shown in Figure 119. Small peaks in the region of interest for oGSR were present, but as discussed above, the accurate mass measurements were not consistent with MC, EC, DPA or N-NDPA. The inset shows a peak with the mass  $m/z$  227, which could possibly originate from akardite (AK-II), a well-recognised component of propellant powders [226]. However, accurate mass measurements were not very close to the expected mass for this compound, and the identity was therefore not unambiguously verified for the 'real-life' samples.

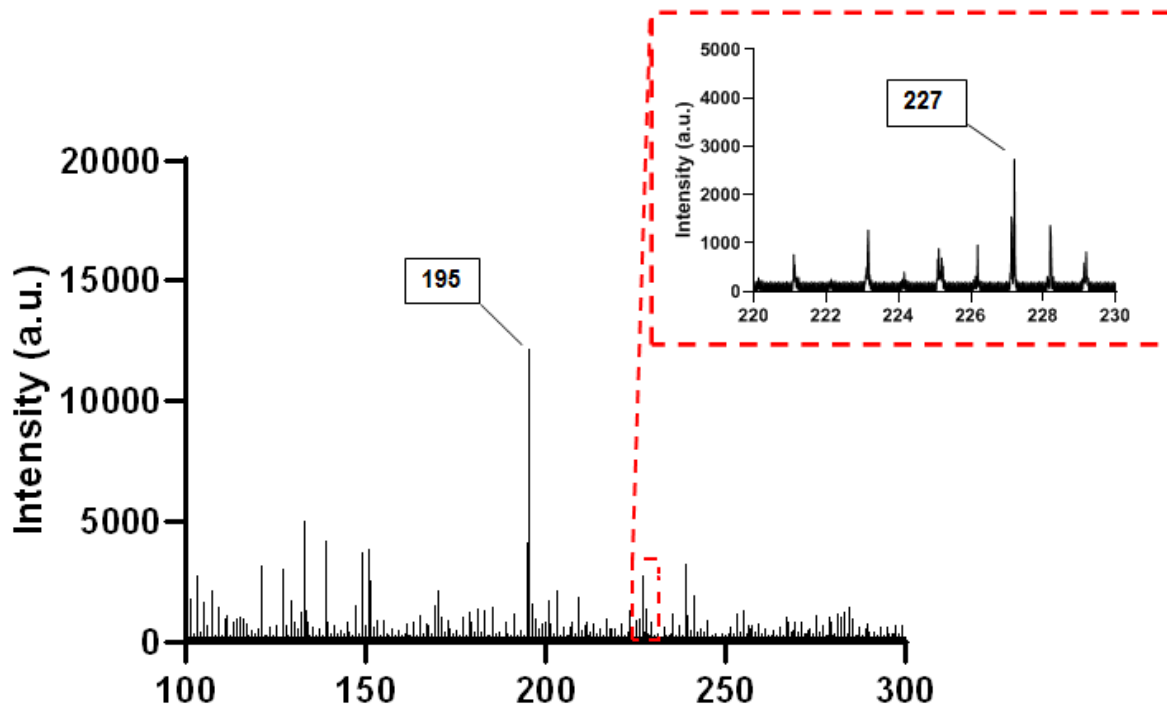


Figure 119: Representative spectrum from right hand of volunteer, after discharge of a firearm, using 0.40 calibre ammunition. Inset shows peak at m/z 227. Dimethylphthalate is shown at m/z 195.

To confirm that the lack of targeted compounds detected from the stub was due to the absence of them in the ammunition, an extraction of the smokeless powder was performed. A small volume of dichloromethane (300 $\mu$ L) was used to extract 10mg of the smokeless powder from the 0.40 calibre ammunition, with deuterated N-NDPA as an internal standard. An aliquot of this extract was further diluted 1:100 in AcCN and analysed in triplicate by DSA-ToF.

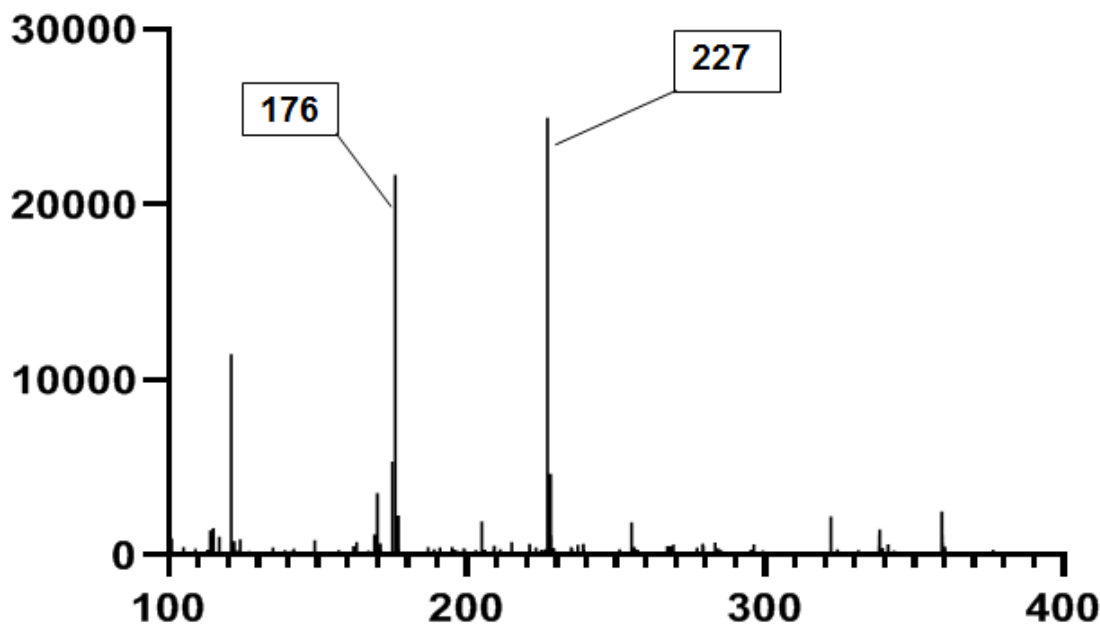


Figure 120: Extract of smokeless powder from 0.40 ammunition used in test firing, showing akardite at m/z 227 and deuterated N-NDPA standard at m/z 176

The resulting spectrum (Figure 120) confirms that EC, MC, and DPA were not present, and that the powder contains a compound with an accurate mass of 227.1994, corresponding to AK-II (-4.13ppm). The most likely explanation for the positive result in the smokeless powder and the lack of positive result in the 'real-life' sample is that the amount of AK-II in the real samples was too low to be properly resolved from the interference. This led to a split peak at this mass, as seen in the inset of Figure 119, which resulted in the lack of positive ID for AK-II. These results reinforce the need for an oGSR method to be flexible regarding the compounds it is able to detect. Propellant formulations change, and compositions are not always publicly available, so any method that is designed to detect them must be broad and non-specific, as DSA-ToF is. The application of an ambient ionisation high resolution MS technique to samples such as these allows accurate mass identification of non-targeted compounds, in a rapid, 'real-time' acquisition that shows all components of a complex mixture at once.

Without peaks for targeted compounds present on the stubs, the peak at m/z 227, presumed to be AK-II, was used as a measure of the response for comparison of analysis order.

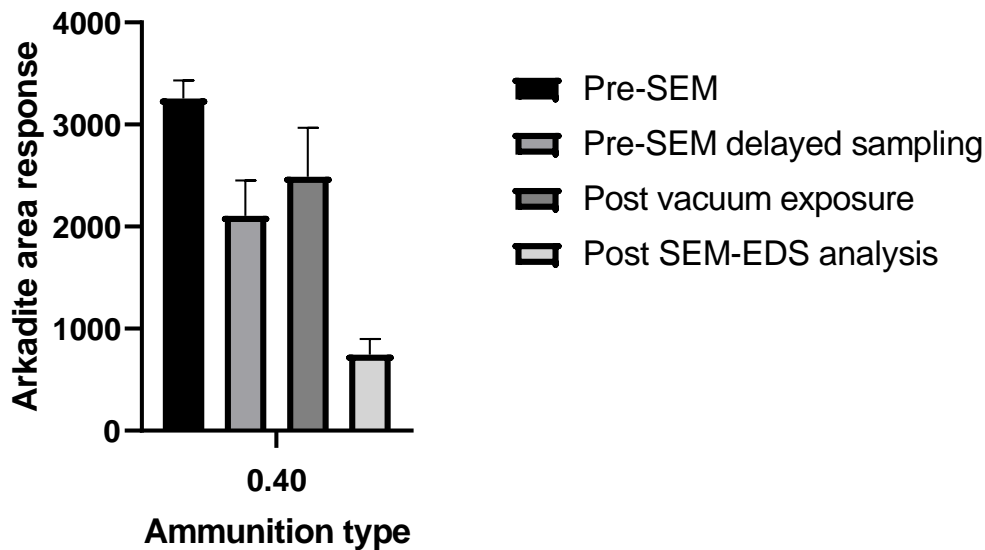


Figure 121: Comparison of analysis order based on the area response of peak with m/z 227 recovered from and 0.40 stubs

These experiments indicate that there is some loss of oGSR from the surface of the stub during SEM-EDS analysis (Figure 121). The highest response came from the stubs that were analysed prior to exposure to the SEM vacuum chamber, although there were no cases where detection was not at all possible. As these experiments were conducted using a 'best-case scenario' approach, where collection occurred immediately following firearm discharge, it is likely that these levels are higher than would be seen in a 'real-life' shooting investigation. Therefore, it is recommended that solvent extraction take place prior to any SEM-EDS analysis.

### 6.7 Solvent recovery impacts on SEM-EDS analysis - Inorganic GSR trace detection

The stubs that were analysed by SEM-EDS first, and subsequently re-analysed after solvent extraction were compared as a measure of the disruptiveness of the solvent extraction on the iGSR present. It was vital to determine if the solvent would disrupt particles of probative value on the stub surface, or alter the stub surface itself. Gross differences in the adhesive appearance and presence of non-oGSR surface debris (skin cells, hair, dust etc) were used to compare visually between the area of a single stub pre- and post-solvent exposure.

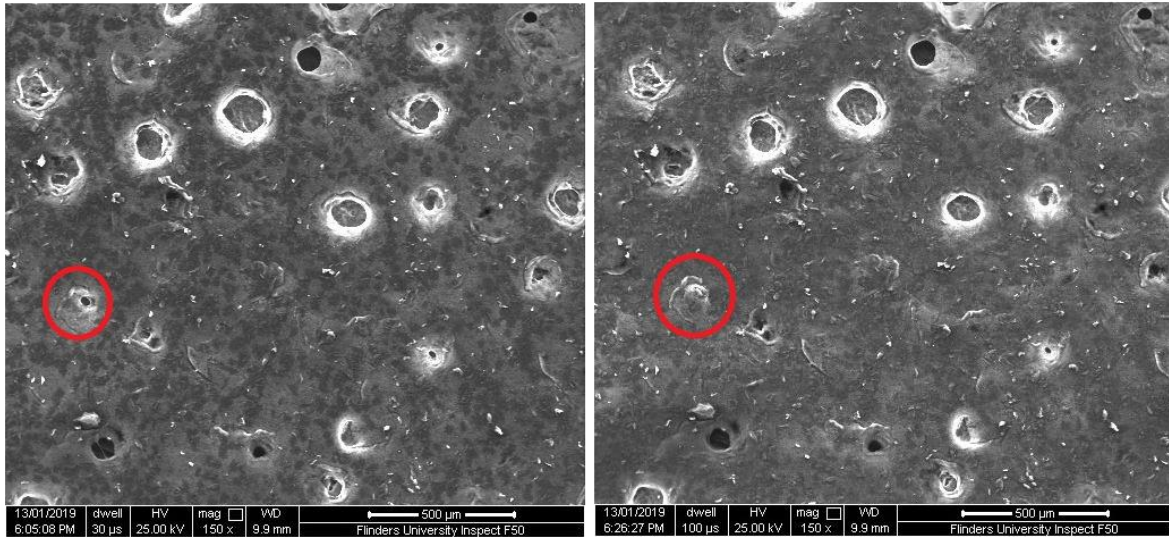


Figure 122: Secondary electron image of 0.22 calibre ammunition sample stub, both pre-solvent (left) and post-solvent (right). Red circle indicates a slight visible change to the stub, attributable to solvent contact

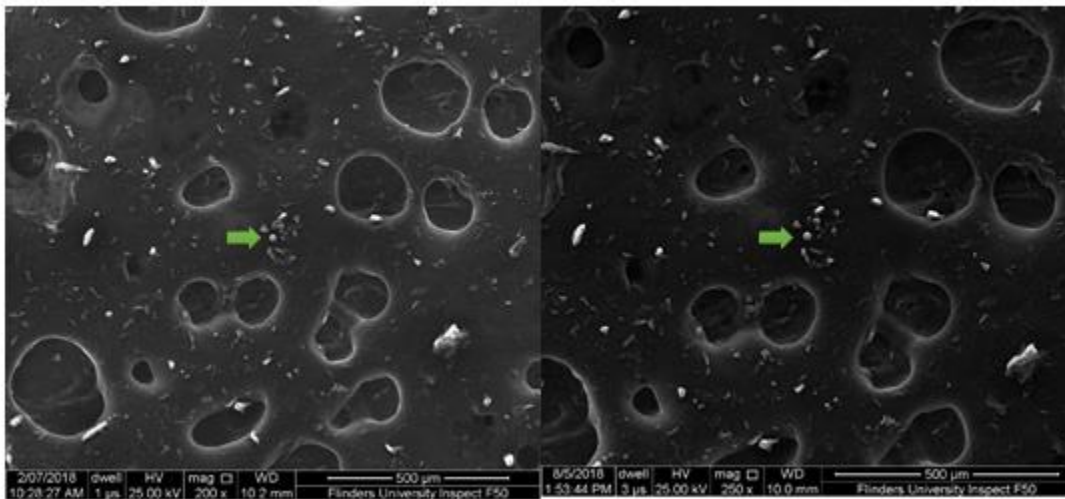


Figure 123: Secondary electron image of 0.40 calibre ammunition sample stub, both pre-solvent (left) and post-solvent (right).

The 0.22 calibre ammunition has an area of change (as indicated by the red circle), where a pitted area has been filled, presumably by solvent contact (Figure 122). This change in surface morphology did not impact the analysis in any way. The 0.40 calibre ammunition shows no gross visual differences when comparing pre and post solvent contact images (Figure 123).

In addition to the gross visual comparison, automated particle analysis software (GSR Magnum) results were compared for the same pre- and post-solvent extraction stubs. The results showed heavy particle

loadings, which is to be expected for stubs taken under immediate post-firing conditions. For this reason, the entire surface of the stub was not searched with an eight-hour search time limit being imposed. The total particle counts for 0.22 and 0.40 calibre ammunition, pre and post solvent exposure, can be seen below (Table 40 and Table 41)

Table 40: Pre- and post- solvent particle counts for 0.22 calibre ammunition from the dominant hand of the shooter

<b>Composition</b>	<b>Pre-solvent count</b>	<b>Post-solvent count</b>
PbBaSb	38	40
BaSb	45	45
PbSb	70	63
BaCaSi	4	4
BaAl	18	19
Pb	523	626
Total particle count	3529	3650

Table 41: Pre- and post- solvent particle counts for 0.40 calibre ammunition from the dominant hand of the shooter

<b>Composition</b>	<b>Pre-solvent count</b>	<b>Post-solvent count</b>
PbBaSb	341	256
BaSb	439	429
PbSb	191	245
BaCaSi	7	10
BaAl	2	6
Pb	2075	1268
Total particle count	4586	5320

Comparison of the particle counts shows good correlation between the two for both calibres. Those cases where the particle counts do change (for better or worse) can be explained by the instrument error in classifying the composition of particles of this size (sub 0.5µm in size). Despite it being clear that the number of iGSR particles on the stubs are not impacted by the solvent extraction, the positioning of 'characteristic' particles [221] on the 0.22 calibre stub pre- and post- solvent extraction was also evaluated.

### 0.22 LH2\_2 "characteristic" classification

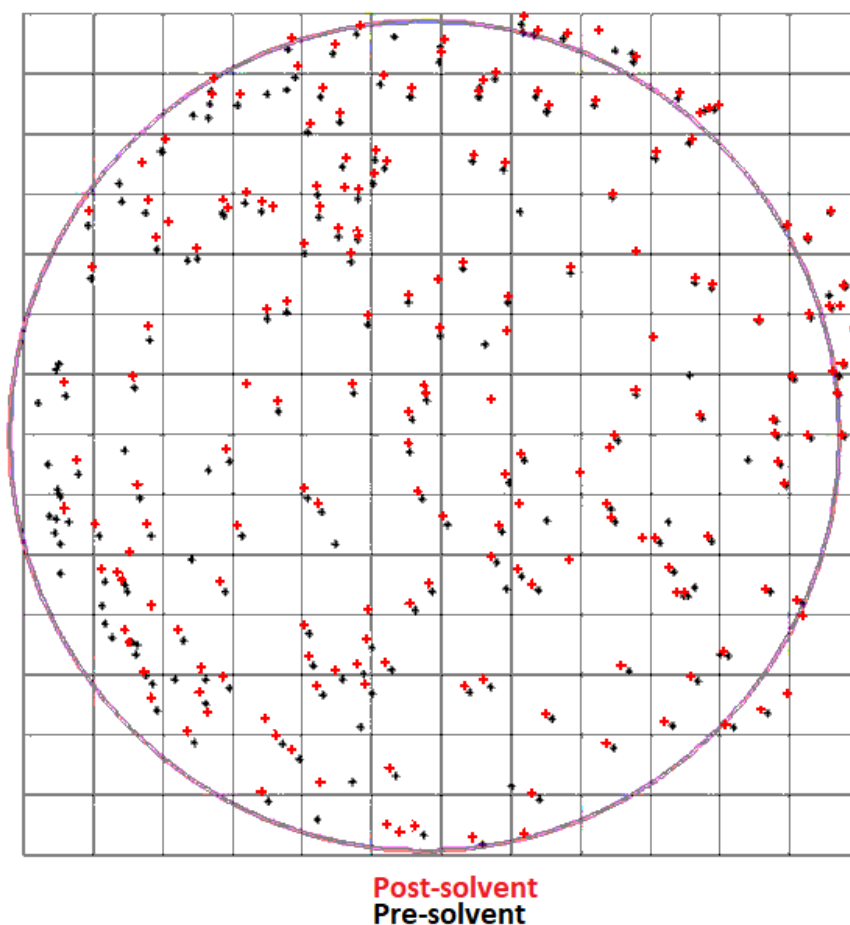


Figure 124: Particle distribution map of sample stub from the shooter's left-hand following discharge of 6x 0.22LR rounds from a revolver. Pre-solvent (black) and Post-solvent (red, offset).

The map shows that the pre- and post- solvent positions of characteristic particles are practically unchanged (Figure 124). Particles being classified as 'characteristic' by GSR Magnum are being re-detected in their same positions after solvent exposure. For additional confirmation of nil-impact solvent exposure, a number of individual particles had their morphology and compositions analysed pre- and post- solvent exposure. No change was observed for any of these particles.

These data directly support the conclusion that solvent extraction should take place prior to SEM-EDS analysis of GSR stubs. Detection of oGSR compounds is maximised prior to exposure to the vacuum chamber, and exposure to solvent does not impact the number of or positioning of iGSR particles.

## 6.8 Conclusions

This chapter details the development of a method to detect oGSR from the surface of existing iGSR adhesive stubs, allowing tandem detection of both types of residues, using DSA-ToF and SEM-EDS.

The initial experiments demonstrated that DSA-ToF is capable of detecting volatile oGSR compounds at levels very similar to what would be expected on the hands of someone who has recently discharged a firearm. This initial work also demonstrated the semi-quantitative analysis of ethyl centralite, indicating that it may be possible to approximately quantify other oGSR compounds where a suitable internal standard is available. Quantitative data may allow the age and provenance of smokeless powders and oGSR residues, where appropriate.

Application of this method to 'real' samples did not detect the targeted compounds, but a peak at  $m/z$  227 in the 0.40 calibre samples was thought to be akardite, which is often used in place of EC in propellant powders. Although the ID of this peak was not possible in the 'real' samples, analysis of the corresponding powder confirmed the presence of AK-II through accurate mass (-4.13ppm). Analysis of this smokeless powder also confirmed the absence of EC, MC and DPA from the ammunition.

The order of analysis experiments indicated that solvent extraction was able to take place prior to SEM-EDS analysis of iGSR particles, without any movement or net loss of those particles of probative value. This order of analysis was confirmed through the evaluation of peak response for stubs exposed to SEM vacuum, and SEM vacuum and electron beam prior to solvent extraction. These data showed a reduction in the peak response for  $m/z$  227 when solvent extraction was not performed immediately following collection.

This method shows promise for rapid, comprehensive identification of complex mixtures extracted from the surface of GSR adhesive stubs. The broad and non-specific nature of the method will allow targeted and non-targeted analysis simultaneously, providing much needed analytical flexibility. The varied and constantly changing compositions of propellant formulations demand this level of fluidity in detection methods, and the analysis of these samples will only benefit from advances and improvements in ambient mass spectrometry into the future.

## 7 Conclusions and Future Work

The work detailed in this thesis sought to evaluate the DSA-ToF for forensic applications. These applications included the qualitative and quantitative detection of illicit drugs both in solution and in saliva, the detection of nicotine, caffeine, caffeine metabolites, and pseudoephedrine in breath and the detection of organic GSR from the surface of collection stubs.

**Chapter one** gave a comprehensive background regarding the use of ambient ionisation in forensic science. It outlined the issues facing forensic science, and in particular, forensic toxicology, where a rapid, accurate and high-throughput method would be of use. Lastly, the current scope of research surrounding the DSA-ToF was discussed. The ultimate aims of the work were established, to evaluate the suitability of this new instrument for forensic work, and to develop a number of methods that would demonstrate this suitability.

**Chapter two** developed the methods for the detection of illicit drugs, namely cocaine, MDMA and THC in water. An optimal method was developed for the use of the DSA-ToF, not just for the detection of the drugs in question, but for all further use. Environmental factors were identified for consideration in the analysis of results, including temperature and humidity, which may influence the mass spectra produced.

**Chapter three** investigated the quantitative detection of cocaine, MDMA and THC in solution, and the use of mesh cleaning techniques to improve the sensitivity of these analyses. The results showed that the instrument is better suited to qualitative analysis. Limits of detection were shown to be within acceptable ranges for forensic sensitivity, for all three drugs of interest. Ultimately, inter- and intra-day variation in limits of detection and quantification were inappropriately high, with the recommendation that the DSA-ToF method should be used only for screening purposes, to be followed with more accurate and reliable methods of confirmation.

**Chapter four** detailed the development of two methods for the detection of cocaine, MDMA and THC in saliva. Firstly, a time-based method using neat saliva on the surface of the mesh was shown to allow for the detection of all three drugs. Following this simple method, a solvent extraction was optimised using a small amount of chloroform. Both methods demonstrated the qualitative detection of all three drugs of interest, and further investigation of showed that a rough quantitation was possible, although not recommended.

**Chapter five** demonstrated the detection of nicotine in breath, using a simplified collection and analysis method. Nicotine was able to be detected in the breath of a volunteer who uses e-cigarettes, through

exhalation through a straw positioned on the mesh, over a two-hour period. The uptake and elimination of nicotine was observed via this method, which mimicked that for blood plasma. This method was also used to demonstrate the detection of pseudoephedrine, caffeine and caffeine metabolites in breath. This demonstrates the potential of DSA-ToF for the analysis of a broad range of compounds in complex matrices, through the application of non-targeted analysis.

**Chapter six** was concerned with the application of the DSA-ToF to the detection of organic GSR. The chapter details the method development, and application thereof to the parallel detection of organic and inorganic GSR. It was shown that the solvent extraction method did not influence the presence, number or position of inorganic GSR, and was able to remove organic components from the surface of GSR stubs, both from those stubbed and from those field sampled. These results show proof-of-principle for the parallel detection of the two component classes to improve the probative value of GSR evidence.

Ultimately, DSA-ToF was shown to have forensic potential for the screening of biological and chemical samples. Qualitative analysis is easily achieved, however reliable quantitative analysis cannot be achieved with this instrument, and any data relating to quantitation should be treated carefully and with consideration of the laboratory and instrument conditions for the day on which it was taken. Despite this, the work contained within this thesis does demonstrate that DSA-ToF has the potential to contribute to many fields of forensic science, and beyond. The instrument does not offer any advantages over other ambient ionisation methods (such as DART or DESI), with the biggest point of difference being that the DSA cannot be integrated into existing MS systems. The instrument still suffers from the same poor reproducibility, lack of differentiation between isobaric compounds, and poor sensitivity in the same manner as other ambient ionisation methods.

Despite this, the potential for high-throughput, non-specific screening of forensic samples is huge. As demonstrated multiple times in this thesis, the ability to identify a broad range of compounds, across multiple classes, allowed the detection of GSR compounds, illicit drugs, and pharmaceutical drugs without any changes to the acquisition method. In addition, the flexibility of this approach suits the analysis of samples where the composition is unknown, which is so often the case for forensic samples. The limited sample preparation and short analysis times cannot be matched by the other currently available methods, and may reduce analysis times once the active ingredient is determined through screening processes like those discussed in this thesis.

Future work should seek to develop further qualitative methods for the detection of small molecules within complex matrices, such as body fluids. Work might also seek to continue improving the instrument interface itself, through the focusing of the plasma into a smaller surface area, allowing for

more accurate and less contaminated analysis. DSA-ToF has the capacity to analyse solid samples, and future work would do well to investigate this, and should not be limited to forensic analysis. To combat the isobaric interference problems encountered repeatedly throughout this thesis, comprehensive investigations into derivatisation should be performed. Movement of the mass of interest away from these interfering peaks would improve both the selectivity and sensitivity of these methods.

Ambient ionisation in all of its forms should be looked upon as a future direction for presumptive testing that delivers more accurate and reliable results, without compromising on the speed and high-throughput nature of current methods.

## 8 References

1. El-Aneed, A., A. Cohen, and J. Banoub, *Mass Spectrometry, Review of the Basics: Electrospray, MALDI, and Commonly Used Mass Analyzers*. Applied Spectroscopy Reviews, 2009. **44**(3): p. 210-230.
2. Awad, H., M.M. Khamis, and A. El-Aneed, *Mass Spectrometry, Review of the Basics: Ionization*. Applied Spectroscopy Reviews, 2015. **50**(2): p. 158-175.
3. Ifa, D.R., et al., *Desorption electrospray ionization and other ambient ionization methods: current progress and preview*. Analyst, 2010. **135**(4): p. 669-681.
4. Winter, G.T., J.A. Wilhide, and W.R. Lacourse, *Characterization of a Direct Sample Analysis (DSA) Ambient Ionization Source*. Journal of the American Society for Mass Spectrometry, 2015. **26**(9): p. 1502-1507.
5. Pavlovich, M.J., B. Musselman, and A.B. Hall, *Direct analysis in real time—Mass spectrometry (DART-MS) in forensic and security applications*. Mass spectrometry reviews, 2018. **37**(2): p. 171-187.
6. Marshall, A.G., C.L. Hendrickson, and G.S. Jackson, *Fourier transform ion cyclotron resonance mass spectrometry: a primer*. Mass spectrometry reviews, 1998. **17**(1): p. 1-35.
7. Ifa, D.R., et al., *Forensic applications of ambient ionization mass spectrometry*. Analytical and Bioanalytical Chemistry, 2009. **394**(8): p. 1995-2008.
8. Green, F., et al., *Ambient mass spectrometry: advances and applications in forensics*. Surface and Interface Analysis: An International Journal devoted to the development and application of techniques for the analysis of surfaces, interfaces and thin films, 2010. **42**(5): p. 347-357.
9. Gross, J.H., *Direct analysis in real time—a critical review on DART-MS*. Analytical and bioanalytical chemistry, 2014. **406**(1): p. 63-80.
10. McEwen, C.N., R.G. McKay, and B.S. Larsen, *Analysis of Solids, Liquids, and Biological Tissues Using Solids Probe Introduction at Atmospheric Pressure on Commercial LC/MS Instruments*. Analytical Chemistry, 2005. **77**(23): p. 7826-7831.
11. Chen, H., Z. Ouyang, and R.G. Cooks, *Thermal Production and Reactions of Organic Ions at Atmospheric Pressure*. Angewandte Chemie International Edition, 2006. **45**(22): p. 3656-3660.
12. Takáts, Z., et al., *Direct, trace level detection of explosives on ambient surfaces by desorption electrospray ionization mass spectrometry*. Chemical Communications, 2005(15): p. 1950-1952.
13. Haapala, M., et al., *Desorption Atmospheric Pressure Photoionization*. Analytical Chemistry, 2007. **79**(20): p. 7867-7872.
14. Takáts, Z., et al., *Mass Spectrometry Sampling Under Ambient Conditions with Desorption Electrospray Ionization*. Science, 2004. **306**(5695): p. 471.
15. Haddad, R., et al., *Easy Ambient Sonic-Spray Ionization-Membrane Interface Mass Spectrometry for Direct Analysis of Solution Constituents*. Analytical Chemistry, 2008. **80**(3): p. 898-903.
16. Na, N., et al., *Development of a dielectric barrier discharge ion source for ambient mass spectrometry*. Journal of the American Society for Mass Spectrometry, 2007. **18**(10): p. 1859-1862.
17. Cody, R.B., J.A. Laramée, and H.D. Durst, *Versatile New Ion Source for the Analysis of Materials in Open Air under Ambient Conditions*. Analytical Chemistry, 2005. **77**(8): p. 2297-2302.
18. Shiea, J., et al., *Electrospray-assisted laser desorption/ionization mass spectrometry for direct ambient analysis of solids*. Rapid Communications in Mass Spectrometry, 2005. **19**(24): p. 3701-3704.
19. Chen, H., A. Venter, and R.G. Cooks, *Extractive electrospray ionization for direct analysis of undiluted urine, milk and other complex mixtures without sample preparation*. Chemical Communications, 2006(19): p. 2042-2044.
20. Shieh, I.F., C.-Y. Lee, and J. Shiea, *Eliminating the Interferences from TRIS Buffer and SDS in Protein Analysis by Fused-Droplet Electrospray Ionization Mass Spectrometry*. Journal of Proteome Research, 2005. **4**(2): p. 606-612.
21. Andrade, F.J., et al., *Atmospheric Pressure Chemical Ionization Source. 2. Desorption-Ionization for the Direct Analysis of Solid Compounds*. Analytical Chemistry, 2008. **80**(8): p. 2654-2663.
22. Nemes, P. and A. Vertes, *Laser Ablation Electrospray Ionization for Atmospheric Pressure, in Vivo, and Imaging Mass Spectrometry*. Analytical Chemistry, 2007. **79**(21): p. 8098-8106.
23. Harper, J.D., et al., *Low-Temperature Plasma Probe for Ambient Desorption Ionization*. Analytical Chemistry, 2008. **80**(23): p. 9097-9104.
24. Chen, H., et al., *Neutral Desorption Sampling of Living Objects for Rapid Analysis by Extractive Electrospray Ionization Mass Spectrometry*. Angewandte Chemie International Edition, 2007. **46**(40): p. 7591-7594.
25. Ratcliffe, L.V., et al., *Surface analysis under ambient conditions using plasma-assisted desorption/ionization mass spectrometry*. Analytical chemistry, 2007. **79**(16): p. 6094-6101.
26. Takáts, Z., J.M. Wiseman, and R.G. Cooks, *Ambient mass spectrometry using desorption electrospray ionization (DESI): Instrumentation, mechanisms and applications in forensics, chemistry, and biology*. Journal of Mass Spectrometry, 2005. **40**(10): p. 1261-1275.
27. Morelato, M., et al., *Forensic applications of desorption electrospray ionisation mass spectrometry (DESI-MS)*. Forensic science international, 2013. **226**(1-3): p. 10-21.
28. Morelato, M., et al., *Screening of gunshot residues using desorption electrospray ionisation-mass spectrometry (DESI-MS)*. Forensic Science International, 2012. **217**(1-3): p. 101-106.

29. Chen, H.-W., B. Hu, and X. Zhang, *Principle and Application of Ambient Mass Spectrometry for Direct Analysis of Complex Samples*. Chinese Journal of Analytical Chemistry, 2010. **38**(8): p. 1069-1088.
30. Chipuk, J.E., M.H. Gelb, and J.S. Brodbelt, *Surface-Enhanced Transmission Mode Desorption Electrospray Ionization: Increasing the Specificity of Ambient Ionization Mass Spectrometric Analyses*. Analytical Chemistry, 2010. **82**(1): p. 16-18.
31. Rummel, J.L., et al., *The coupling of direct analysis in real time ionization to Fourier transform ion cyclotron resonance mass spectrometry for ultrahigh-resolution mass analysis*. Rapid Communications in Mass Spectrometry, 2010. **24**(6): p. 784-790.
32. Song, L., et al., *Ionization Mechanism of Positive-Ion Direct Analysis in Real Time: A Transient Microenvironment Concept*. Analytical Chemistry, 2009. **81**(24): p. 10080-10088.
33. Newsome, G.A., I. Kayama, and S.A. Brogdon-Grantham, *Direct analysis in real time mass spectrometry (DART-MS) of discrete sample areas without heat damage*. Analytical Methods, 2018. **10**(9): p. 1038-1045.
34. Dalmia, A., *Rapid Detection of Vanilla Bean Extract Adulteration with Tonka Bean Extract with No Chromatography or Sample Preparation*. Perkin Elmer Application Note, 2013.
35. Elliot, N.M., Dalmia, A., Schwarz, C., Leffler, A. M. & Dorman, F., *Analysis of Cathinones in Bath Salts by Direct Sample Analysis TOF MS*. Perkin Elmer Application Note, 2013.
36. Thompson, R.D. and T.J. Hoffmann, *Determination of coumarin as an adulterant in vanilla flavoring products by high-performance liquid chromatography*. Journal of Chromatography A, 1988. **438**(C): p. 369-382.
37. Elmer, P., *Milk Adulteration with Melamine- Screening, Testing and Real-Time Detection*. Perkin Elmer Case Study, 2013.
38. Elmer, P., *Milk Authenticity- Organic vs Non-organic*. Perkin Elmer Case Study, 2012.
39. Vetter, W. and M. Schröder, *Concentrations of phytanic acid and pristanic acid are higher in organic than in conventional dairy products from the German market*. Food Chemistry, 2010. **119**(2): p. 746-752.
40. Carpio, A., et al., *Differentiation of organic goat's milk based on its hippuric acid content as determined by capillary electrophoresis*. Electrophoresis, 2010. **31**(13): p. 2211-2217.
41. Dalmia, A., *Rapid Screening of Adulteration in Pomegranate Juice Using DSA/TOF with Minimal Sample Preparation*. Perkin Elmer Application Note, 2013.
42. Dalmia, A., *Rapid Measurement of Extra Virgin Olive Oil Adulteration with Olive Pomace Oil with No Sample Preparation Using DSA/TOF*. Perkin Elmer Application Note, 2013.
43. Dalmia, A., *Rapid Measurement of Olive Oil Adulteration with Seed Oils with Minimal Sample Preparation Using DSA/TOF*. Perkin Elmer Application Note, 2013.
44. Pérez-Camino, M.D.C., et al., *Alkyl esters of fatty acids a useful tool to detect soft deodorized olive oils*. Journal of Agricultural and Food Chemistry, 2008. **56**(15): p. 6740-6744.
45. Cooks, R.G., et al., *Ambient mass spectrometry*. Science, 2006. **311**(5767): p. 1566-1570.
46. Cotte-Rodríguez, I., et al., *Desorption electrospray ionization of explosives on surfaces: sensitivity and selectivity enhancement by reactive desorption electrospray ionization*. Analytical chemistry, 2005. **77**(21): p. 6755-6764.
47. Cotte-Rodríguez, I., et al., *In situ trace detection of peroxide explosives by desorption electrospray ionization and desorption atmospheric pressure chemical ionization*. Analytical Chemistry, 2008. **80**(5): p. 1512-1519.
48. Cotte-Rodríguez, I., H. Chen, and R.G. Cooks, *Rapid trace detection of triacetone triperoxide (TATP) by complexation reactions during desorption electrospray ionization*. Chemical Communications, 2006(9): p. 953-955.
49. Wells, J.M., et al., *Implementation of DART and DESI ionization on a fieldable mass spectrometer*. Journal of the American Society for Mass Spectrometry, 2008. **19**(10): p. 1419-1424.
50. Cotte-Rodríguez, I. and R.G. Cooks, *Non-proximate detection of explosives and chemical warfare agent simulants by desorption electrospray ionization mass spectrometry*. Chemical Communications, 2006(28): p. 2968-2970.
51. Talaty, N., et al., *Fabric analysis by ambient mass spectrometry for explosives and drugs*. Analyst, 2008. **133**(11): p. 1532-1540.
52. Mulligan, C.C., N. Talaty, and R.G. Cooks, *Desorption electrospray ionization with a portable mass spectrometer: in situ analysis of ambient surfaces*. Chemical Communications, 2006(16): p. 1709-1711.
53. Sanders, N.L., et al., *Detection of explosives as negative ions directly from surfaces using a miniature mass spectrometer*. Analytical chemistry, 2010. **82**(12): p. 5313-5316.
54. Bianchi, F., et al., *Micro-solid-phase extraction coupled to desorption electrospray ionization-high-resolution mass spectrometry for the analysis of explosives in soil*. Analytical and Bioanalytical Chemistry, 2015. **407**(3): p. 931-938.
55. Laramée, J., et al., *Forensic Applications of DART (Direct Analysis in Real Time) Mass Spectrometry*, in *Forensic analysis on the cutting edge*. 2007, Wiley: New Jersey.
56. Nilles, J.M., et al., *Explosives detection using direct analysis in real time (DART) mass spectrometry*. Propellants, Explosives, Pyrotechnics, 2010. **35**(5): p. 446-451.
57. Sisco, E., J. Dake, and C. Bridge, *Screening for trace explosives by AccuTOF™-DART®: an in-depth validation study*. Forensic science international, 2013. **232**(1-3): p. 160-168.
58. Swider, J.R., *Optimizing Accu Time-of-Flight/Direct Analysis in Real Time for Explosive Residue Analysis*. Journal of forensic sciences, 2013. **58**(6): p. 1601-1606.

59. Newsome, G.A., L.K. Ackerman, and K.J. Johnson, *Humidity affects relative ion abundance in direct analysis in real time mass spectrometry of hexamethylene triperoxide diamine*. Analytical chemistry, 2014. **86**(24): p. 11977-11980.
60. Rowell, F., et al., *Detection of nitro-organic and peroxide explosives in latent fingerprints by DART-and SALDI-TOF-mass spectrometry*. Forensic Science International, 2012. **221**(1-3): p. 84-91.
61. Clemons, K., et al., *Trace analysis of energetic materials via direct analyte-probed nanoextraction coupled to direct analysis in real time mass spectrometry*. Forensic science international, 2013. **231**(1-3): p. 98-101.
62. Sisco, E. and T.P. Forbes, *Rapid detection of sugar alcohol precursors and corresponding nitrate ester explosives using direct analysis in real time mass spectrometry*. Analyst, 2015. **140**(8): p. 2785-2796.
63. Weston, D.J., et al., *Direct analysis of pharmaceutical drug formulations using ion mobility spectrometry/quadrupole-time-of-flight mass spectrometry combined with desorption electrospray ionization*. Analytical chemistry, 2005. **77**(23): p. 7572-7580.
64. Leuthold, L.A., et al., *Desorption electrospray ionization mass spectrometry: direct toxicological screening and analysis of illicit Ecstasy tablets*. Rapid Communications in Mass Spectrometry: An International Journal Devoted to the Rapid Dissemination of Up-to-the-Minute Research in Mass Spectrometry, 2006. **20**(2): p. 103-110.
65. Ricci, C., et al., *Combined Fourier-transform infrared imaging and desorption electrospray-ionization linear ion-trap mass spectrometry for analysis of counterfeit antimalarial tablets*. Analytical and bioanalytical chemistry, 2007. **387**(2): p. 551-559.
66. Rodriguez-Cruz, S.E., *Rapid analysis of controlled substances using desorption electrospray ionization mass spectrometry*. Rapid Communications in Mass Spectrometry: An International Journal Devoted to the Rapid Dissemination of Up-to-the-Minute Research in Mass Spectrometry, 2006. **20**(1): p. 53-60.
67. Kauppila, T.J., et al., *Direct analysis of illicit drugs by desorption atmospheric pressure photoionization*. Rapid Communications in Mass Spectrometry, 2008. **22**(7): p. 979-985.
68. Cotte-Rodríguez, I., C.C. Mulligan, and R.G. Cooks, *Non-proximate detection of small and large molecules by desorption electrospray ionization and desorption atmospheric pressure chemical ionization mass spectrometry: instrumentation and applications in forensics, chemistry, and biology*. Analytical chemistry, 2007. **79**(18): p. 7069-7077.
69. Keil, A., et al., *Ambient Mass Spectrometry with a Handheld Mass Spectrometer at High Pressure*. Analytical Chemistry, 2007. **79**(20): p. 7734-7739.
70. Lin, Z., et al., *Rapid screening of clenbuterol in urine samples by desorption electrospray ionization tandem mass spectrometry*. Rapid Communications in Mass Spectrometry: An International Journal Devoted to the Rapid Dissemination of Up-to-the-Minute Research in Mass Spectrometry, 2008. **22**(12): p. 1882-1888.
71. Kauppila, T.J., et al., *Rapid analysis of metabolites and drugs of abuse from urine samples by desorption electrospray ionization-mass spectrometry*. Analyst, 2007. **132**(9): p. 868-875.
72. Huang, G., et al., *Rapid screening of anabolic steroids in urine by reactive desorption electrospray ionization*. Analytical chemistry, 2007. **79**(21): p. 8327-8332.
73. Nielen, M., et al., *Feasibility of desorption electrospray ionization mass spectrometry for rapid screening of anabolic steroid esters in hair*. Analytica chimica acta, 2011. **700**(1-2): p. 63-69.
74. Daugherty, S.C., H., *Automated Direct Sample Analysis (DSA/TOF) for the Rapid Testing of Drug Compounds*. Perkin Elmer Application Note, 2013.
75. Lesiak, A.D., et al., *Direct analysis in real time mass spectrometry (DART-MS) of "bath salt" cathinone drug mixtures*. Analyst, 2013. **138**(12): p. 3424-3432.
76. LaPointe, J., et al., *Detection of "bath salt" synthetic cathinones and metabolites in urine via DART-MS and solid phase microextraction*. Journal of the American Society for Mass Spectrometry, 2015. **26**(1): p. 159-165.
77. Team, M.A., *Analysis of Phosphodiesterase Type 5 Inhibitors Extracted from Herbal Preparations by DSA/TOF MS*. Perkin Elmer Application Note, 2013.
78. Crighton, E., et al., *Exploring the Application of the DSA-TOF, a Direct, High-resolution Time-of-Flight Mass Spectrometry Technique for the Screening of Potential Adulterated and Contaminated Herbal Medicines*. Journal of the American Society for Mass Spectrometry, 2019: p. 1-7.
79. Khine, A.A., et al., *Identifying the composition of street drug Nyaope using two different mass spectrometer methods*. African Journal of Drug and Alcohol Studies, 2015. **14**(1): p. 49-56.
80. Wolf J, B.K., McGowan J, Edirisinghe M, *Investigation of Direct Sample Analysis - Time of Flight mass spectrometry (DSA-TOF) for the forensic analysis of seized drugs*, in ANZFSS 23rd International Symposium on the Forensic Sciences. 2016: Auckland, New Zealand.
81. Moore, A., et al., *Rapid screening of opioids in seized street drugs using ambient ionization high resolution time-of-flight mass spectrometry*. Forensic Chemistry, 2019. **13**: p. 100149.
82. Chen, H., et al., *Desorption electrospray ionization mass spectrometry for high-throughput analysis of pharmaceutical samples in the ambient environment*. Analytical Chemistry, 2005. **77**(21): p. 6915-6927.
83. D'Aloise, P. and H. Chen, *Rapid determination of flunitrazepam in alcoholic beverages by desorption electrospray ionization-mass spectrometry*. Science & Justice, 2012. **52**(1): p. 2-8.
84. Sun, X., et al., *Coupling of single droplet micro-extraction with desorption electrospray ionization-mass spectrometry*. International Journal of Mass Spectrometry, 2011. **301**(1-3): p. 102-108.

85. Van Berkel, G.J., M.J. Ford, and M.A. Deibel, *Thin-layer chromatography and mass spectrometry coupled using desorption electrospray ionization*. Analytical Chemistry, 2005. **77**(5): p. 1207-1215.
86. Ifa, D.R., et al., *Quantitative analysis of small molecules by desorption electrospray ionization mass spectrometry from polytetrafluoroethylene surfaces*. Rapid Communications in Mass Spectrometry: An International Journal Devoted to the Rapid Dissemination of Up-to-the-Minute Research in Mass Spectrometry, 2008. **22**(4): p. 503-510.
87. Hu, Q., et al., *Desorption electrospray ionization using an Orbitrap mass spectrometer: exact mass measurements on drugs and peptides*. Rapid Communications in Mass Spectrometry: An International Journal Devoted to the Rapid Dissemination of Up-to-the-Minute Research in Mass Spectrometry, 2006. **20**(22): p. 3403-3408.
88. Nyadong, L., et al., *Desorption electrospray ionization reactions between host crown ethers and the influenza neuraminidase inhibitor oseltamivir for the rapid screening of Tamiflu®*. Analyst, 2008. **133**(11): p. 1513-1522.
89. Rodriguez-Cruz, S., *Rapid screening of seized drug exhibits using desorption electrospray ionization mass spectrometry (DESI-MS)*. Microgram J, 2008. **6**(1-2): p. 10-15.
90. Kauppila, T.J., et al., *Desorption electrospray ionization mass spectrometry for the analysis of pharmaceuticals and metabolites*. Rapid Communications in Mass Spectrometry, 2006. **20**(3): p. 387-392.
91. Stojanovska, N., et al., *Analysis of amphetamine-type substances and piperazine analogues using desorption electrospray ionisation mass spectrometry*. Rapid Communications in Mass Spectrometry, 2014. **28**(7): p. 731-740.
92. Stojanovska, N., et al., *Presumptive analysis of 4-methylmethcathinone (mephedrone) using desorption electrospray ionisation-mass spectrometry (DESI-MS)*. Australian Journal of Forensic Sciences, 2014. **46**(4): p. 411-423.
93. Bailey, M.J., et al., *Rapid detection of cocaine, benzoylecgonine and methylecgonine in fingerprints using surface mass spectrometry*. Analyst, 2015. **140**(18): p. 6254-6259.
94. Stojanovska, N., et al., *Qualitative analysis of seized cocaine samples using desorption electrospray ionization-mass spectrometry (DESI-MS)*. Drug testing and analysis, 2015. **7**(5): p. 393-400.
95. Roscioli, K.M., et al., *Desorption electrospray ionization (DESI) with atmospheric pressure ion mobility spectrometry for drug detection*. Analyst, 2014. **139**(7): p. 1740-1750.
96. Musah, R.A., et al., *Direct analysis in real time mass spectrometry with collision-induced dissociation for structural analysis of synthetic cannabinoids*. Rapid Communications in Mass Spectrometry, 2012. **26**(19): p. 2335-2342.
97. Musah, R.A., et al., *Rapid identification of synthetic cannabinoids in herbal samples via direct analysis in real time mass spectrometry*. Rapid Communications in Mass Spectrometry, 2012. **26**(9): p. 1109-1114.
98. Dunham, S.J., P.D. Hooker, and R.M. Hyde, *Identification, extraction and quantification of the synthetic cannabinoid JWH-018 from commercially available herbal marijuana alternatives*. Forensic science international, 2012. **223**(1-3): p. 241-244.
99. Wenjie, L., et al., *Rapid and Direct Analysis of Sibutramine Hydrochloride Illegally Added in Weight-loss Healthy Food by DART-MS/MS Method [J]*. Chinese Pharmaceutical Affairs, 2012. **2**.
100. Duvivier, W.F., et al., *Rapid analysis of Δ-9-tetrahydrocannabinol in hair using direct analysis in real time ambient ionization orbitrap mass spectrometry*. Rapid Communications in Mass Spectrometry, 2014. **28**(7): p. 682-690.
101. Jacobs, A.D. and R.R. Steiner, *Detection of the Duquenois–Levine chromophore in a marijuana sample*. Forensic science international, 2014. **239**: p. 1-5.
102. Lesiak, A.D., et al., *DART-MS as a Preliminary Screening Method for “Herbal Incense”: Chemical Analysis of Synthetic Cannabinoids*. Journal of forensic sciences, 2014. **59**(2): p. 337-343.
103. Vaclavik, L., A.J. Krynitsky, and J.I. Rader, *Mass spectrometric analysis of pharmaceutical adulterants in products labeled as botanical dietary supplements or herbal remedies: a review*. Analytical and bioanalytical chemistry, 2014. **406**(27): p. 6767-6790.
104. Lesiak, A.D., et al., *Rapid detection by direct analysis in real time-mass spectrometry (DART-MS) of psychoactive plant drugs of abuse: The case of Mitragyna speciosa aka “Kratom”*. Forensic science international, 2014. **242**: p. 210-218.
105. Easter, J.L. and R.R. Steiner, *Pharmaceutical identifier confirmation via DART-TOF*. Forensic science international, 2014. **240**: p. 9-20.
106. Musah, R.A., et al., *DART–MS in-source collision induced dissociation and high mass accuracy for new psychoactive substance determinations*. Forensic science international, 2014. **244**: p. 42-49.
107. Kuki, Á., et al., *Detection of nicotine as an indicator of tobacco smoke by direct analysis in real time (DART) tandem mass spectrometry*. Atmospheric Environment, 2015. **100**: p. 74-77.
108. Lim, A.Y., et al., *Detection of drugs in latent fingerprints by mass spectrometric methods*. Analytical Methods, 2013. **5**(17): p. 4378-4385.
109. Gómez-Ríos, G.A. and J. Pawliszyn, *Solid phase microextraction (SPME)-transmission mode (TM) pushes down detection limits in direct analysis in real time (DART)*. Chemical Communications, 2014. **50**(85): p. 12937-12940.
110. Lesiak, A.D., et al., *DART-MS for rapid, preliminary screening of urine for DMAA*. Drug testing and analysis, 2014. **6**(7-8): p. 788-796.
111. Nilles, J.M., T.R. Connell, and H.D. Durst, *Quantitation of chemical warfare agents using the direct analysis in real time (DART) technique*. Analytical chemistry, 2009. **81**(16): p. 6744-6749.

112. Bevilacqua, V.L., et al., *Ricin activity assay by direct analysis in real time mass spectrometry detection of adenine release*. Analytical chemistry, 2010. **82**(3): p. 798-800.
113. D'agostino, P., et al., *Liquid chromatography electrospray tandem mass spectrometric and desorption electrospray ionization tandem mass spectrometric analysis of chemical warfare agents in office media typically collected during a forensic investigation*. Journal of Chromatography A, 2006. **1110**(1-2): p. 86-94.
114. D'Agostino, P.A., et al., *Desorption electrospray ionisation mass spectrometric analysis of chemical warfare agents from solid-phase microextraction fibers*. Rapid Communications in Mass Spectrometry, 2007. **21**(4): p. 543-549.
115. Rummel, J.L., et al., *Structural elucidation of direct analysis in real time ionized nerve agent simulants with infrared multiple photon dissociation spectroscopy*. Analytical chemistry, 2011. **83**(11): p. 4045-4052.
116. Harris, G.A., C.E. Falcone, and F.M. Fernández, *Sensitivity "hot spots" in the direct analysis in real time mass spectrometry of nerve agent simulants*. Journal of the American Society for Mass Spectrometry, 2012. **23**(1): p. 153-161.
117. Harris, G.A., M. Kwasnik, and F.M. Fernández, *Direct analysis in real time coupled to multiplexed drift tube ion mobility spectrometry for detecting toxic chemicals*. Analytical chemistry, 2011. **83**(6): p. 1908-1915.
118. Hagan, N.A., et al., *Detection and identification of immobilized low-volatility organophosphates by desorption ionization mass spectrometry*. International Journal of Mass Spectrometry, 2008. **278**(2-3): p. 158-165.
119. Song, Y. and R.G. Cooks, *Reactive desorption electrospray ionization for selective detection of the hydrolysis products of phosphonate esters*. Journal of mass spectrometry, 2007. **42**(8): p. 1086-1092.
120. Weyermann, C., et al., *Differentiation of blue ballpoint pen inks by laser desorption ionization mass spectrometry and high-performance thin-layer chromatography*. Journal of forensic sciences, 2007. **52**(1): p. 216-220.
121. Ifa, D., et al., *Forensic analysis of inks by imaging desorption electrospray ionization (DESI) mass spectrometry*. Analyst, 2007. **132**(5): p. 461-467.
122. Van Berkel, G.J. and V. Kertesz, *Automated sampling and imaging of analytes separated on thin-layer chromatography plates using desorption electrospray ionization mass spectrometry*. Analytical Chemistry, 2006. **78**(14): p. 4938-4944.
123. Yu, S., et al., *Bioanalysis without sample cleanup or chromatography: the evaluation and initial implementation of direct analysis in real time ionization mass spectrometry for the quantification of drugs in biological matrixes*. Analytical chemistry, 2008. **81**(1): p. 193-202.
124. Jones, R.W. and J.F. McClelland, *Analysis of writing inks on paper using direct analysis in real time mass spectrometry*. Forensic science international, 2013. **231**(1-3): p. 73-81.
125. Drury, N., R. Ramotowski, and M. Moini, *A comparison between DART-MS and DSA-MS in the forensic analysis of writing inks*. Forensic science international, 2018. **289**: p. 27-32.
126. Houlgrave, S., et al., *The Classification of Inkjet Inks Using Accu TOF™ DART™(Direct Analysis in Real Time) Mass Spectrometry—A Preliminary Study*. Journal of forensic sciences, 2013. **58**(3): p. 813-821.
127. Pfaff, A.M. and R.R. Steiner, *Development and validation of AccuTOF-DART™ as a screening method for analysis of bank security device and pepper spray components*. Forensic science international, 2011. **206**(1-3): p. 62-70.
128. Musah, R.A., et al., *Direct analysis in real time mass spectrometry for analysis of sexual assault evidence*. Rapid communications in mass spectrometry, 2012. **26**(9): p. 1039-1046.
129. Jones, R.W., R.B. Cody, and J.F. McClelland, *Differentiating Writing Inks Using Direct Analysis in Real Time Mass Spectrometry*. Journal of Forensic Sciences, 2006. **51**(4): p. 915-918.
130. Zhou, Z. and R.N. Zare, *Personal information from latent fingerprints using desorption electrospray ionization mass spectrometry and machine learning*. Analytical chemistry, 2017. **89**(2): p. 1369-1372.
131. Chen, T., Z.D. Schultz, and I.W. Levin, *Infrared spectroscopic imaging of latent fingerprints and associated forensic evidence*. Analyst, 2009. **134**(9): p. 1902-1904.
132. Ifa, D.R., et al., *Latent Fingerprint Chemical Imaging by Mass Spectrometry*. Science, 2008. **321**(5890): p. 805.
133. Justes, D.R., et al., *Detection of explosives on skin using ambient ionization mass spectrometry*. Chemical Communications, 2007(21): p. 2142-2144.
134. Maric, M. and C. Bridge, *Characterizing and classifying water-based lubricants using direct analysis in real time® time of flight mass spectrometry*. Forensic Science International, 2016. **266**: p. 73-79.
135. Baumgarten, B., et al., *Preliminary classification scheme of silicone based lubricants using DART-TOFMS*. Forensic Chemistry, 2018. **8**: p. 28-39.
136. Maric, M., et al., *Chemical discrimination of lubricant marketing types using direct analysis in real time time-of-flight mass spectrometry*. Rapid Communications in Mass Spectrometry, 2017. **31**(12): p. 1014-1022.
137. Bridge, C. and M. Marić, *Temperature-Dependent DART-MS Analysis of Sexual Lubricants to Increase Accurate Associations*. Journal of The American Society for Mass Spectrometry, 2019. **30**(8): p. 1343-1358.
138. Proni, G., et al., *Comparative analysis of condom lubricants on pre & post-coital vaginal swabs using AccuTOF-DART*. Forensic Science International, 2017. **280**: p. 87-94.
139. Zhao, M., et al., *Desorption electrospray tandem MS (DESI-MSMS) analysis of methyl centralite and ethyl centralite as gunshot residues on skin and other surfaces*. Journal of Forensic Sciences, 2008. **53**(4): p. 807-811.
140. Venter, A., et al., *A Desorption Electrospray Ionization Mass Spectrometry Study of Aging Products of Diphenylamine Stabilizer in Double-Base Propellants*. Propellants, Explosives, Pyrotechnics, 2006. **31**(6): p. 472-476.

141. Li, F., et al., *A method for rapid sampling and characterization of smokeless powder using sorbent-coated wire mesh and direct analysis in real time - mass spectrometry (DART-MS)*. *Science & Justice*, 2016. **56**(5): p. 321-328.
142. Lennert, E. and C. Bridge, *Analysis and classification of smokeless powders by GC-MS and DART-TOFMS*. *Forensic Science International*, 2018. **292**: p. 11-22.
143. Lennert, E. and C.M. Bridge, *Rapid screening for smokeless powders using DART-HRMS and thermal desorption DART-HRMS*. *Forensic Chemistry*, 2019. **13**: p. 100148.
144. Williamson, R., et al., *The coupling of capillary microextraction of volatiles (CMV) dynamic air sampling device with DART-MS analysis for the detection of gunshot residues*. *Forensic Chemistry*, 2018. **8**: p. 49-56.
145. McCullough, B.J. and C.J. Hopley, *Results of the first and second British Mass Spectrometry Society interlaboratory studies on ambient mass spectrometry*. *Rapid Communications in Mass Spectrometry*, 2019.
146. Davey, J., K. Armstrong, and P. Martin, *Results of the Queensland 2007-2012 roadside drug testing program: The prevalence of three illicit drugs*. *Accident Analysis and Prevention*, 2014. **65**: p. 11-17.
147. Drummer, O.H., et al., *Drugs in oral fluid in randomly selected drivers*. *Forensic Science International*, 2007. **170**(2-3): p. 105-10.
148. Verstraete, A., *The Results of the Roadside Drug Testing Assessment Project*, in *Drugs of Abuse*, R. Wong and H. Tse, Editors. 2005, Humana Press. p. 271-292.
149. Boorman, M. and K. Owens, *The victorian legislative framework for the random testing drivers at the roadside for the presence of illicit drugs: An evaluation of the characteristics of drivers detected from 2004 to 2006*. *Traffic Injury Prevention*, 2009. **10**(1): p. 16-22.
150. Grossman, G., *Solar-powered systems for cooling, dehumidification and air-conditioning*. *Solar energy*, 2002. **72**(1): p. 53-62.
151. Molina, D.K., *Handbook of Forensic Toxicology for Medical Examiners*. Practical Aspects of Criminal and Forensic Investigators Series, ed. V.J. Geberth. 2010, Boca Raton: CRC Press.
152. Shun'ko, E.V. and V. Belkin, *Cleaning properties of atomic oxygen excited to metastable state  $2s\ 2\ 2\ p\ 4\ (S\ 1\ 0)$* . *Journal of Applied Physics*, 2007. **102**(8): p. 083304.
153. Izdebska-Podsiady, J., *Application of Plasma in Printed Surfaces and Print Quality*, in *Non-Thermal Plasma Technology for Polymeric Materials*. 2019, Elsevier. p. 159-191.
154. Keller, B.O., et al., *Interferences and contaminants encountered in modern mass spectrometry*. *Analytica chimica acta*, 2008. **627**(1): p. 71-81.
155. NATA, *Guidelines for the validation and verification of quantitative and qualitative test methods*. 2012, NATA Australia.
156. Idowu, O.R. and B. Caddy, *A Review of the Use of Saliva in the Forensic Detection of Drugs and Other Chemicals*. *Journal of the Forensic Science Society*, 1982. **22**(2): p. 123-135.
157. Guinan, T., et al., *Rapid detection of illicit drugs in neat saliva using desorption/ionization on porous silicon*. *Talanta*, 2012. **99**: p. 791-798.
158. Miyaguchi, H., et al., *Microchip-based liquid-liquid extraction for gas-chromatography analysis of amphetamine-type stimulants in urine*. *Journal of Chromatography A*, 2006. **1129**(1): p. 105-110.
159. Jiang, Y., et al., *Integrated plastic microfluidic devices with ESI-MS for drug screening and residue analysis*. *Analytical chemistry*, 2001. **73**(9): p. 2048-2053.
160. Ma, M. and F.F. Cantwell, *Solvent microextraction with simultaneous back-extraction for sample cleanup and preconcentration: preconcentration into a single microdrop*. *Analytical Chemistry*, 1999. **71**(2): p. 388-393.
161. Moule, E.C., et al., *Silver-assisted development and imaging of fingermarks on non-porous and porous surfaces*. *International Journal of Mass Spectrometry*, 2017.
162. Grote, C. and J. Pawliszyn, *Solid-phase microextraction for the analysis of human breath*. *Journal of Analytical Chemistry* 1997. **69**(4): p. 587-596.
163. Phillips, M., et al., *Variation in volatile organic compounds in the breath of normal humans*. *Journal of Chromatography B*, 1999. **729**(1-2): p. 75-88.
164. Phillips, M., *Breath tests in medicine*. *Scientific American*, 1992. **267**(1): p. 74-79.
165. Beck, O., et al., *Detection of drugs of abuse in exhaled breath using a device for rapid collection: comparison with plasma, urine and self-reporting in 47 drug users*. *Journal of Breath Research*, 2013. **7**(2): p. 026006.
166. Kiem, S. and J.J. Schentag, *Interpretation of antibiotic concentration ratios measured in epithelial lining fluid*. *Journal of Antimicrobial agents*, 2008. **52**(1): p. 24-36.
167. Berchtold, C., et al., *Real-time monitoring of exhaled drugs by mass spectrometry*. *Mass Spectrometry Reviews*, 2014. **33**(5): p. 394-413.
168. Beck, O., et al., *Determination of methadone in exhaled breath condensate by liquid chromatography-tandem mass spectrometry*. *Journal of Analytical Toxicology*, 2011. **35**(3): p. 129-133.
169. Di Francesco, F., et al., *Breath analysis: trends in techniques and clinical applications*. *Microchemical Journal*, 2005. **79**(1-2): p. 405-410.
170. Beauchamp, J., et al., *On the use of Tedlar® bags for breath-gas sampling and analysis*. *Journal of Breath Research*, 2008. **2**(4): p. 046001.

171. Horvath, I., J. Hunt, and P. Barnes, *Exhaled breath condensate: methodological recommendations and unresolved questions*. *European Respiratory Journal*, 2005. **26**(3): p. 523-548.
172. Risby, T.H., *Critical issues for breath analysis*. *Journal of Breath Research*, 2008. **2**(3): p. 030302.
173. Smith, D., et al., *Quantification of acetaldehyde released by lung cancer cells in vitro using selected ion flow tube mass spectrometry*. *Rapid Communications in Mass Spectrometry*, 2003. **17**(8): p. 845-850.
174. Boshier, P.R., et al., *On-line, real time monitoring of exhaled trace gases by SIFT-MS in the perioperative setting: a feasibility study*. *Analyst*, 2011. **136**(16): p. 3233-3237.
175. Cristescu, S., et al., *Screening for emphysema via exhaled volatile organic compounds*. *Journal of Breath Research*, 2011. **5**(4): p. 046009.
176. Gu, H., et al., *Rapid analysis of aerosol drugs using nano extractive electrospray ionization tandem mass spectrometry*. *Analyst*, 2010. **135**(6): p. 1259-1267.
177. Meier, L., et al., *Extractive Electrospray Ionization Mass Spectrometry • Enhanced Sensitivity Using an Ion Funnel*. *Analytical Chemistry*, 2012. **84**(4): p. 2076-2080.
178. Meier, L., et al., *Sensitive detection of drug vapors using an ion funnel interface for secondary electrospray ionization mass spectrometry*. *Journal of Mass Spectrometry*, 2012. **47**(5): p. 555-559.
179. Crews, K.R., et al., *Pharmacogenomics and individualized medicine: translating science into practice*. *Clinical Pharmacology & Therapeutics*, 2012. **92**(4): p. 467-475.
180. Mayer, P. and V. Höllt, *Pharmacogenetics of opioid receptors and addiction*. *Pharmacogenetics genomics*, 2006. **16**(1): p. 1-7.
181. Kamysek, S., et al., *Drug detection in breath: effects of pulmonary blood flow and cardiac output on propofol exhalation*. *Analytical Bioanalytical Chemistry*, 2011. **401**(7): p. 2093.
182. Beck, O., et al., *Study on the sampling of methadone from exhaled breath*. *Journal of Analytical Toxicology*, 2011. **35**(5): p. 257-263.
183. Joseph, H., S. Stancliff, and J. Langrod, *Methadone maintenance treatment (MMT): a review of historical and clinical issues*. *The Mount Sinai Journal of Medicine*, 2000. **67**(5-6): p. 347-364.
184. Ding, J., et al., *Development of extractive electrospray ionization ion trap mass spectrometry for in vivo breath analysis*. *Analyst*, 2009. **134**(10): p. 2040-2050.
185. Berchtold, C., L. Meier, and R. Zenobi, *Evaluation of extractive electrospray ionization and atmospheric pressure chemical ionization for the detection of narcotics in breath*. *International Journal of Mass Spectrometry*, 2011. **299**(2-3): p. 145-150.
186. Gold, M.S., N.A. Graham, and B.A. Goldberger, *Second-hand and third-hand drug exposures in the operating room: a factor in anesthesiologists' dependency on fentanyl*. 2010, Taylor & Francis.
187. Gold, M.S., et al., *Fentanyl abuse and dependence: further evidence for second hand exposure hypothesis*. *Journal of Addictive Diseases*, 2006. **25**(1): p. 15-21.
188. Buszewski, B., et al., *Human exhaled air analytics: biomarkers of diseases*. *Biomedical Chromatography*, 2007. **21**(6): p. 553-566.
189. Španěl, P., K. Dryahina, and D. Smith, *Acetone, ammonia and hydrogen cyanide in exhaled breath of several volunteers aged 4–83 years*. *Journal of Breath Research*, 2007. **1**(1): p. 011001.
190. Kim, K.-H., S.A. Jahan, and E. Kabir, *A review of breath analysis for diagnosis of human health*. *Trends in Analytical Chemistry*, 2012. **33**: p. 1-8.
191. Risby, T.H. and S. Solga, *Current status of clinical breath analysis*. *Journal of Applied physics B*, 2006. **85**(2-3): p. 421-426.
192. Oberacher, M., et al., *Diagnosing lactase deficiency in three breaths*. *European Journal of Clinical Nutrition*, 2011. **65**(5): p. 614.
193. Cazzola, M. and G. Novelli, *Biomarkers in COPD*. *Pulmonary Pharmacology Therapeutics*, 2010. **23**(6): p. 493-500.
194. Hakim, M., et al., *Diagnosis of head-and-neck cancer from exhaled breath*. *British Journal of Cancer*, 2011. **104**(10): p. 1649.
195. Mazzone, P.J., et al., *Diagnosis of lung cancer by the analysis of exhaled breath with a colorimetric sensor array*. *Thorax*, 2007. **62**(7): p. 565-568.
196. Stephanson, N., et al., *Method validation and application of a liquid chromatography-tandem mass spectrometry method for drugs of abuse testing in exhaled breath*. *Journal of Chromatography B: Analytical Technologies in the Biomedical and Life Sciences*, 2015. **985**: p. 189-196.
197. Ullah, S., S. Sandqvist, and O. Beck, *A liquid chromatography and tandem mass spectrometry method to determine 28 non-volatile drugs of abuse in exhaled breath*. *Journal of Pharmaceutical and Biomedical Analysis*, 2018. **148**: p. 251-258.
198. Beck, O., et al., *Amphetamines detected in exhaled breath from drug addicts: a new possible method for drugs-of-abuse testing*. *Journal of Analytical Toxicology*, 2010. **34**(5): p. 233-237.
199. Beck, O., et al., *Determination of amphetamine and methylphenidate in exhaled breath of patients undergoing attention-deficit/hyperactivity disorder treatment*. *Therapeutic Drug Monitoring*, 2014. **36**(4): p. 528-534.
200. Stephanson, N., et al., *Method validation and application of a liquid chromatography-tandem mass spectrometry method for drugs of abuse testing in exhaled breath*. *Journal of Chromatography B*, 2015. **985**: p. 189-196.

201. Ellefsen, K.N., et al., *Quantification of cocaine and metabolites in exhaled breath by liquid chromatography-high-resolution mass spectrometry following controlled administration of intravenous cocaine*. Analytical Bioanalytical Chemistry, 2014. **406**(25): p. 6213-6223.
202. Beck, O., et al., *Detection of  $\Delta^9$ -tetrahydrocannabinol in exhaled breath collected from cannabis users*. Journal of Analytical Toxicology, 2011. **35**(8): p. 541-544.
203. Himes, S.K., et al., *Cannabinoids in exhaled breath following controlled administration of smoked cannabis*. Clinical Chemistry, 2013. **59**(12): p. 1780-1789.
204. Beck, O., et al., *Method for determination of methadone in exhaled breath collected from subjects undergoing methadone maintenance treatment*. Journal of chromatography B, 2010. **878**(24): p. 2255-2259.
205. Beck, O., S. Sandqvist, and J. Franck, *Demonstration that methadone is being present in the exhaled breath aerosol fraction*. Journal of Pharmaceutical and Biomedical Analysis, 2011. **56**(5): p. 1024-1028.
206. Guinan, T.M., H. Abdelmaksoud, and N.H. Voelcker, *Rapid detection of nicotine from breath using desorption ionisation on porous silicon*. Chemical Communications, 2017. **53**(37): p. 5224-5226.
207. Baselt, R.C., *Disposition of toxic drugs and chemicals in man*. Vol. 59. 2000: Chemical Toxicology Institute.
208. Liguori, A., J.R. Hughes, and J.A. Grass, *Absorption and subjective effects of caffeine from coffee, cola and capsules*. Pharmacology Biochemistry Behavior, 1997. **58**(3): p. 721-726.
209. Blanchard, J. and S. Sawers, *The absolute bioavailability of caffeine in man*. European Journal of Clinical Pharmacology, 1983. **24**(1): p. 93-98.
210. Drugbank. *Caffeine*. 2005 13 Feb 2019 [cited 2019 16 Feb 2019]; Available from: <https://www.drugbank.ca/drugs/DB00201#pharmacology>.
211. Fredholm, B.B., et al., *Actions of caffeine in the brain with special reference to factors that contribute to its widespread use*. Pharmacological Reviews, 1999. **51**(1): p. 83-133.
212. Committee on Military Nutrition, R., et al., *Caffeine for the Sustainment of Mental Task Performance : Formulations for Military Operations*. 2001, Washington: Washington, D.C.: National Academies Press.
213. Kanfer, I., R. Dowse, and V. Vuma, *Pharmacokinetics of oral decongestants*. The Journal of Human Pharmacology, 1993. **13**(6P2): p. 116S-128S.
214. Simons, F.E.R., et al., *Pharmacokinetics of the orally administered decongestants pseudoephedrine and phenylpropanolamine in children*. The Journal of Pediatrics, 1996. **129**(5): p. 729-734.
215. Le Houezec, J., *Role of nicotine pharmacokinetics in nicotine addiction and nicotine replacement therapy: a review*. The International Journal of Tuberculosis, 2003. **7**(9): p. 811-819.
216. Goniewicz, M.L., et al., *Levels of selected carcinogens and toxicants in vapour from electronic cigarettes*. Tobacco Control, 2014. **23**(2): p. 133-139.
217. McAuley, T.R., et al., *Comparison of the effects of e-cigarette vapor and cigarette smoke on indoor air quality*. Inhalation Toxicology, 2012. **24**(12): p. 850-857.
218. Romagna, G., et al., *Cytotoxicity evaluation of electronic cigarette vapor extract on cultured mammalian fibroblasts (ClearStream-LIFE): comparison with tobacco cigarette smoke extract*. Inhalation Toxicology, 2013. **25**(6): p. 354-361.
219. Schivo, M., M.V. Avdalovic, and S. Murin, *Non-cigarette tobacco and the lung*. Clinical Reviews in Allergy Immunology, 2014. **46**(1): p. 34-53.
220. Cobb, N.K. and D. Abrams, *E-cigarette or drug-delivery device*. New England Journal of Medicine, 2011. **365**(3): p. 193-195.
221. ASTM, *E1588-17 Standard practice for gunshot residue analysis by scanning electron microscopy/energy dispersive X-ray spectrometry*. 2017, ASTM International: West Conshohocken, PA.
222. Tucker, W., et al., *Gunshot residue and brakepads: Compositional and morphological considerations for forensic casework*. Forensic Science International, 2017. **270**: p. 76-82.
223. Dalby, O., D. Butler, and J.W. Birkett, *Analysis of gunshot residue and associated materials - A review*. Journal of Forensic Sciences, 2010. **55**(4): p. 924-943.
224. O'Mahony, A.M. and J. Wang, *Electrochemical detection of gunshot residue for forensic analysis: A review*. Journal of Electroanalysis, 2013. **25**(6): p. 1341-1358.
225. Taudte, R.V., et al., *Detection of Gunshot Residues Using Mass Spectrometry*. BioMed Research International, 2014. **2014**: p. 16.
226. Goudsmits, E., G.P. Sharples, and J.W. Birkett, *Recent trends in organic gunshot residue analysis*. TrAC - Trends in Analytical Chemistry, 2015. **74**: p. 46-57.
227. Dalby, O. and J.W. Birkett, *The evaluation of solid phase micro-extraction fibre types for the analysis of organic components in unburned propellant powders*. Journal of Chromatography A, 2010. **1217**(46): p. 7183-7188.
228. Sauzier, G., et al., *Optimisation of recovery protocols for double-base smokeless powder residues analysed by total vaporisation (TV) SPME/GC-MS*. Talanta, 2016. **158**: p. 368-374.
229. Stevens, B., S. Bell, and K. Adams, *Initial evaluation of inlet thermal desorption GC-MS analysis for organic gunshot residue collected from the hands of known shooters*. Forensic Chemistry, 2016. **2**: p. 55-62.
230. Pigou, P., et al., *An investigation into artefacts formed during gas chromatography/mass spectrometry analysis of firearms propellant that contains diphenylamine as the stabiliser*. Forensic Science International, 2017. **279**: p. 140-147.

231. Taudte, R.V., C. Roux, and A. Beavis, *Stability of smokeless powder compounds on collection devices*. Forensic Science International, 2017. **270**: p. 55-60.
232. Maitre, M., et al., *Thinking beyond the lab: organic gunshot residues in an investigative perspective*. Australian Journal of Forensic Sciences, 2018: p. 1-7.
233. Taudte, R.V., et al., *The development and comparison of collection techniques for inorganic and organic gunshot residues*. Analytical Bioanalytical Chemistry, 2016. **408**(10): p. 2567-2576.
234. Meng, H. and B. Caddy, *Gunshot residue analysis—a review*. Journal of Forensic Science, 1997. **42**(4): p. 553-570.
235. Benito, S., et al., *Characterization of organic gunshot residues in lead-free ammunition using a new sample collection device for liquid chromatography–quadrupole time-of-flight mass spectrometry*. Forensic Science International, 2015. **246**: p. 79-85.
236. Abrego, Z., et al., *A novel method for the identification of inorganic and organic gunshot residue particles of lead-free ammunitions from the hands of shooters using scanning laser ablation-ICPMS and Raman micro-spectroscopy*. Analyst, 2014. **139**(23): p. 6232-6241.
237. Morales, E.B. and A.L.R. Vázquez, *Simultaneous determination of inorganic and organic gunshot residues by capillary electrophoresis*. Journal of Chromatography A, 2004. **1061**(2): p. 225-233.
238. Vuki, M., et al., *Simultaneous electrochemical measurement of metal and organic propellant constituents of gunshot residues*. Analyst, 2012. **137**(14): p. 3265-3270.
239. Bueno, J. and I.K. Lednev, *Raman microspectroscopic chemical mapping and chemometric classification for the identification of gunshot residue on adhesive tape*. Analytical and Bioanalytical Chemistry, 2014. **406**(19): p. 4595-4599.
240. Gandy, L., et al., *A novel protocol for the combined detection of organic, inorganic gunshot residue*. Forensic Chemistry, 2018. **8**: p. 1-10.
241. Bergens, A., *Decomposition of diphenylamine in nitrocellulose based propellants—II. Application of a numerical model to concentration-time data determined by liquid chromatography and dual-wavelength detection*. Talanta, 1995. **42**(2): p. 185-196.
242. Moran, J.W. and S. Bell, *Skin permeation of organic gunshot residue: implications for sampling and analysis*. Analytical Chemistry, 2014. **86**(12): p. 6071-6079.
243. Ali, L., et al., *A Study of the Presence of Gunshot Residue in Pittsburgh Police Stations using SEM/EDS and LC-MS/MS*. Journal of Forensic Sciences, 2016. **61**(4): p. 928-938.
244. Ho, J.S., et al., *Distinguishing diphenylamine and N-nitrosodiphenylamine in hazardous waste samples by using high-performance liquid chromatography/thermospray/mass spectrometry*. Environmental Science Technology, 1990. **24**(11): p. 1748-1751.
245. Seyfang, K.E., et al., *Analysis of elemental and isotopic variation in glass frictionators from 0.22 rimfire primers*. Forensic science international, 2018. **293**: p. 47-62.